Dispersion of air pollution in the Christchurch area

A thesis submitted in fulfilment of the requirements
for the degree of
Doctor of Philosophy in Environmental Science

by

Stanley van den Assem

Department of Geography
University of Canterbury
New Zealand
October 1997

Acknowledgement

This research is supported by many, which is greatly appreciated. First of all, I would like to thank my partner Alma, for her patience and for the sacrifices she endured. I would also like to thank the Canterbury Regional council and NIWA for their financial and practical help. Dr. Jose Restrepo of Civil Engineering helped with designing the instrumented towers. Very important and greatly appreciated was the technical input of Gary Smith, technician of the Department of Geography. Many thanks to Chris Brady, Burnside High School, South Power at Packe Street, the Christchurch City Council Water Services Unit at Beckenham and the Polytechnic at Sullivan Avenue, who allowed an instrumented tower to be erected on their properties. Adventurous assistance has been provided by Fiona Young and Ed Butler by frequently climbing the 21 m high tower with the eddy correlation equipment. Dr. Rachel Spronken-Smith has also been very helpful with setting up the eddy correlation equipment. The nocturnal assistance of Andrew Roozen with handling the tethered balloon is especially very much appreciated. Important meteorological data were provided by Dave Somerville, Christchurch City Council, Dr. Neil Cherry, Lincoln University and Dr. Peter Knudsen from the Met. Service. James Guard was very helpful with the installation of RAMS and he provided excellent computer customer services. Last, but not least, many thanks to my supervisor Dr. Andy Sturman and to all the people not explicitly named, who helped me with this project. Thank you all, very much.

Abstract

Christchurch, New Zealand, has a serious air pollution problem during the winter season, due to frequently occurring stagnant air masses and strong inversions, combined with increased emissions caused by burning wood and coal for domestic heating. During this research project an investigation was made of the role of meteorological processes affecting the dispersion of air pollution in the Christchurch environment. At the smaller end of the scale, analysis was conducted of the relationships between surface layer fluxes and land use in the Christchurch area, while at the larger scale drainage flows and interactions with advection were studied. A data collection system was established during the winter of 1995 to obtain a three dimensional picture of the atmosphere, being most detailed near the surface and in the Christchurch area. Two 10.5 m, two 21 m towers and two mobile weather stations were deployed in the area, combined with a network of existing weather stations. Tethered balloon flights with a sonde provided detailed profiles of temperature, humidity and wind up to 500 m, while pilot balloon soundings gave information of wind profiles up to 6000 m. Air pollution data were provided by the Canterbury Regional Council. Analysis of the heat fluxes in the Christchurch area indicated that during fine days in winter, the Bowen ratios over the urban areas were much higher than over the surrounding rural environment, which could have implications for dispersion of air pollution. Drainage flows from the Port Hills and the Canterbury Plains were observed together with their impact on the dispersion of air pollution in Christchurch. During clear nights very stable thermal conditions developed up to an elevation of 100 to 200 m. Above these stable layers strong low level jets were observed. Atmospheric waves occurred frequently and at times they had a dramatic impact on dispersion of air pollution. Simulations using the three dimensional prognostic model RAMS, version 3b, have shown that drainage flows can still develop under clear sky conditions with advection at a synoptic scale, due to decoupling. Verification of two case study days showed that simulated airflow patterns agreed reasonably well with observations, although some significant deviations occurred also. Dispersion of CO was simulated by using a Eulerian mode, and the results agreed reasonably well at the general level, although the results were less accurate at the detailed level. It is suggested that the overall performance of the simulations will be improved by adjusting and refining model settings and boundary conditions, and by the applications of inhomogeneous initialization procedures, cloud physics, an improved surface flux routine and dispersion studies using a Lagrangian or hybrid mode.

Contents

List of symbols

Latin

a empirical parameter used for the relationship between GS and Rn
a_1 empirical parameter used for the relationship between GS and Rn
a_2 empirical parameter used for the relationship between GS and Rn
a_3 empirical parameter used for the relationship between GS and Rn
A advective heat flux
b empirical parameter used for the relationship between GS and Rn
b_1 water availability
b_2 water advection and entrainment parameter
c_1 empirical parameter to obtain z_o
c_2 empirical parameter to obtain z_o
c_k empirical parameter relating K_H to K_M
c_p heat capacity of air at constant pressure
c_v heat capacity of air at constant volume
d displacement height log-wind profile
f Coriolis parameter
F anthropogenic heat flux
$F_{x,y,z}$ friction forces in x, y or z direction
g gravitation force
GS ground storage heat flux
h height of canopy or vegetation
H sensible heat flux
k Von Karman constant
K_H eddy diffusivity for sensible heat
K_M eddy diffusivity for momentum
L Monin-Obukhov length
LE latent heat flux
L_v latent heat of vaporation
p pressure
q specific humidity
R gas constant
Rn net radiation
s change of the saturation of specific humidity with temperature
S total surface area of buildings
t time
T temperature
u horizontal wind speed in x direction
u_* friction velocity
v horizontal wind speed in y direction
w vertical wind speed
z geopotential height
z_o roughness length
z_g height of local topography
z_i depth of the inertial sublayer
z^* terrain following height

Greek

β Bowen ratio
γ psychrometric value
ρ density of air
ε mixing ratio of air
θ potential temperature
τ surface stress
ψ_H stability correction function for heat
ψ_M stability correction function for momentum

Special symbols

$\overline{}$ time averaging operator
$'$ deviation from average
∂ partial derivative operator
Δ discrete difference
∇ nabla operator
$\bullet$ dot vector operator
$\rightarrow$ vector symbol

List of Tables

List of Figures

List of Plates

1. The air pollution problem

1.1 Introduction

The goal of this research project is to obtain a much better understanding of the meteorological processes involved in the dispersion of atmospheric pollutants in an environment where significant air pollution and strong geographic effects are present. The study area is Christchurch, New Zealand, where atmospheric pollution is a serious problem. Topographic effects enhance the complexity of the atmospheric processes and dispersion of pollutants. The focus of the project is on atmospheric processes ranging from local to meso-scale, which includes the influence of surface characteristics at a suburban scale through to the effects of the Southern Alps.

So far, knowledge about dispersion of atmospheric pollution in an environment with strong topographic effects is limited. Standard dispersion models are often very inaccurate in these conditions, while previous research has failed so far to resolve the details of dispersion in the Christchurch area. An intensive field campaign and model applications conducted during this study have provided the information desperately needed to enhance knowledge of the air pollution problem. This should provide a sound basis for developing air pollution management tools in the area.

Geographical and meteorological conditions combine in Christchurch to create an air pollution potential, which is unlike that of any other New Zealand city. Stagnant air masses and strong inversions frequently occur during wintertime. Recirculation situations have a potential to occur, due to the effects of the sea breeze and topographically induced local winds. The winter period coincides with the heaviest usage of coal and wood for domestic heating. Following the passing of the Resource Management Act (1991), there has been renewed interest in appropriate management of environmental quality, including air pollution. Further improvement in air quality in the Christhchurch area requires measures to be taken, which must be politically, economically and scientifically acceptable.

The remainder of this chapter will cover a general background of air pollution, the phases of the air pollution problem, an outline of existing numerical dispersion models, the situation of air pollution in Christchurch and the objectives of this project. Finally, the format of the thesis will be discussed.

1.2 General background

During pre-historic times the human race experienced air pollution problems, such as the nuisance of smoke from campfires, which at times was made more serious by natural disasters such as forest fires and volcanic activity. Later, when civilization gained momentum and people started to live in cities and began working with metals, pollution problems arose, even as early as the biblical and classical times. However, a dramatic increase in air pollution occurred during the 19th century industrialization, when pollutants were freely emitted in the air. During the pre-world war II period this century, uncontrolled

emissions increased even further with expanding industrialization, and notorious smog events were recorded in London, Glasgow and Liege. Soon after the second world war, serious attempts were made to reduce emissions in western countries by changing to different types of fuel and the introduction of control technology (Griffin, 1994). Unfortunately, the post world war II economic boom changed the nature and the number of the emission sources, which had a detrimental effect on ambient air quality, as can be demonstrated by the dramatic increased usage of motor vehicles. The phenomenon of secondary pollutants due to photochemical reactions emerged, as firstly recorded in Los Angeles, and now a widespread problem. In several cities, such as Los Angeles, Mexico City, New York, Singapore and Tokyo, measures are taken to slow the rate at which the air quality deteriorates, by promoting public transport and car pooling, and introducing cleaner cars (The Economist, 1996). In many countries problems caused by primary pollutants, such as smoke and sulphur dioxide, are diminished. However, in general the air quality associated with secondary pollutants in or downstream of big cities appears not to have stabilized or even started to improve (Lefohn *et al.*, 1992; Wagner, 1990).

The pollution problems in the former Soviet block countries are enormous, and are not expected to be solved in the short term due to the economical struggle these countries are experiencing (Elsom, 1992; Feshback and Friendly, 1992; Shahgedanova and Burt, 1994). In addition, extreme air pollution problems exist or are expected to emerge in many developing countries, as increased industrialization occurs, combined with urbanization and strong population growth (WHO, 1992). Due to economic pressure cheap fuels are frequently used and often no or limited emission control technology is applied (Schwela, 1995). According to Elsom (1996), quoting GEMS (Global Environmental Monitoring System) for the 1988-1992 period, the highest ambient levels of one-hour ozone were recorded in Mexico City, Los Angeles and New York City. The highest values of annual average total suspended particulate matter were recorded in Cairo, Calcutta and Mexico City, while the highest annual average sulphur dioxide levels occurred in Mexico City (again), Rio de Janeiro and Seoul.

In 1992, the first Earth Summit was held in Rio de Janeiro, where targets were set to preserve the environment for future generations, followed by a second summit in June 1997 in New York, where the decisions which were taken at the first summit were evaluated. However, so far the situation is almost at a stalemate, due to developing countries criticising the rich countries for not fulfilling promised aid to improve the environment (The Press, 1997a). The USA, the world's largest polluter, is criticised by European countries for not doing enough to reduce emissions of the so-called greenhouse gases (particularly CO_2) (The Press, 1997b). A positive development is the fact that the environment is now being recognized as an asset worth preserving, although several organisations such as Greenpeace argue that the measures which are taken, are not going far enough. The heart of the pollution problem is population growth (Elsom, 1996) and continuing world wide economic expansion. However, influential organisations such as the Catholic Church still oppose birth control. Speakers at the WHO summit in Rome in 1996 argued for *another green revolution* (referring to large scale introduction of more productive crops and breeds and the application of pesticides during the sixties) to feed the growing populations in third world countries. As long as expansion of the populations and economy is seen as the ultimate destiny, the situation of the global environmental looks rather gloomy.

1.3 What is air pollution?

Air pollution can be defined as '*the presence in the atmosphere of substances or energy in such quantities and of such duration liable to cause harm to human, plant or animal life, or damage to human-made materials and structures, or changes in the weather and climate, or interference with the comfortable enjoyment of life or property or other human activities*' (Elsom, 1992, page 3). Although many other definitions can be given, a common feature of these definitions is that air pollution generates a negative impact, either physically or psychologically. The scales in time and space in which atmospheric pollutants manifest themselves in the environment range from decameters and minutes (local), tens of kilometers and hours (regional), up to global and milennia (e.g. CO_2 enrichment of the atmosphere). The air pollution process can be said to go through several stages, as described in the following sections.

1.3.1 Emissions

Emission is the process of discharging pollutants into the atmosphere. Emitted pollutants can be gases or suspended particulate matter. The size of the particulates ranges from less than 0.1 μm to larger than 10 μm. The chemical structure of atmospheric pollutants varies from very simple (inorganic) molecules, such as O_3, CO, SO_2, NO and NO_2 to complicated organic structures. An emissions inventory provides information about the types and amounts of pollutants being emitted over certain periods of time and the spatial distribution of sources in an area. The emissions can be deduced from industrial processing rates, fossil fuel consumption, traffic density, etc. However, obtaining accurate emission data over short averaging scales in time and space may be very difficult (Fujita *et al*, 1992; Pilinis *et al.*, 1993). Often, the emission inventories do not take into account variations by day of the week, which can be substantial, as described by Broennimann and Neu (1997) and Simmonds and Keay (1997). Several factors can influence the emission rates on a day to day basis, such as weather conditions (heating of buildings, decision to travel by motor vehicle), social activities and industrial processing levels. Semi-empirical models can be used to simulate emissions, such as traffic emission models (Matzoros and Van Vliet, 1992; Bellasio, 1997).

Most of the emissions occur relatively close to the Earth's surface. Major sources of emission are industry, traffic and domestic heating. The relative importance of these sources depends on location and time. Emission sources can also be classified by their spatial structure, as point sources (single chimney stack), line sources (highway) and area sources (city) (Oke, 1978).

1.3.2 Atmospheric chemistry

After emission the pollutants have become ambient, and occur as *primary* pollutants. However, the emitted materials can undergo chemical reaction, leading to *secondary* pollutants. Very complicated reaction chains have been recognised and described (Harrison and Perry, 1986; Seinfeld, 1986; Sloane and Tesche, 1991). Several models are constructed to quantify these reaction chains, especially with respect to ozone formation (Zanetti, 1990; Zlatev *et al.*, 1992; Yamartino *et al.*, 1992; Gong and Cho, 1993; Scheffe and Morris, 1993). The complexity and non-linearity of atmospheric flow dynamics, coupled with the non-linear and multiphase character of atmospheric chemistry, make air quality modelling a particularly challenging problem, according to Saylor and Fernandes (1993). However, during this project not much attention will be paid to the formation of secondary pollutants, since they appear to play a minor role in the Christchurch area

(Canterbury Regional Council, 1993) due to the fact that Christchurch's air pollution is mainly a winter problem, when photochemistry can be neglected.

1.3.3 Dispersion

Once pollutants are emitted into the air, they are subject to ambient airflow. Dispersion of atmospheric pollutants occurs by advection, atmospheric turbulence, which can be considered as the perturbation part of the mean flow, molecular diffusion, which is several orders of magnitude less effective at transporting quantities than is turbulence (Stull, 1988), and gravitational settling of particulate matter. The fine particulates are considered most important with respect to their impact (Elsom, 1992), but their fall velocity is small and can be neglected for many applications. During this project, attention is focused on advective and turbulent processes of the atmosphere. These processes determine the dispersion of the air pollutants, which is particularly important in the boundary layer. Stull (1988) defined the boundary layer as *'that part of the troposphere that is directly influenced by the presence of the earth's surface, and responds to surface forcings with a timescale of about an hour or less'*. It is in the boundary layer that we live, but also emit most of the atmospheric pollutants. The height of the boundary layer is variable and often shows a diurnal cycle, particularly during clear sky conditions. Atmospheric pollutants are mixed throughout the boundary layer, mainly by turbulent processes, which are generated by forced convection or free convection or both. Forced convection is created by advection and surface roughness, which creates aerodynamic stress, while free convection is created by buoyancy forces due to thermal instability of the air (Oke, 1978; Stull, 1988; Garratt, 1992). Obviously, high air pollution concentrations can be encountered near the surface when accumulation of pollutants occurs. This happens when the boundary layer height is low and the pollutants are emitted below this level, when there are low wind speeds causing low ventilation in the affected area and reduced mechanic turbulent forcing, and persistence of these unfavourable atmospheric conditions. Complications can occur due to recirculations of pollutants or by fumigation, when polluted air aloft is mixed downwards to the surface. More general information about dispersion of air pollution can be found in WMO (1972), Oke (1978), Stern *et al.* (1984), Venkatram and Wyngaard (1988).

1.3.4 Deposition

Air pollutants can be removed from the atmosphere by chemical conversion or by either dry or wet deposition. Dry deposition is the absorption or adsorption of pollutants at the surface by objects (vegetation, animals, humans, buildings, soil, etc.). The flux to the surface is given by the product of the surface concentration and the deposition velocity (Harrison, 1990). The deposition rate is generally different from fall velocity of particulate matter. Wet deposition occurs when atmospheric pollutants form droplets by hygroscopic activity (rainout) or when pollutants are absorbed by falling raindrops (washout). During the project, deposition will be neglected, since firstly the modelling of dispersion is restricted to CO, which has low deposition rates. Secondly, deposition rates are relatively low compared to uncertainties in emission rates, while thirdly, a limited period of time is considered, and finally, washout processes are neglected.

1.3.5 Impact

The final stage of the pollution problem is the impact it causes. The impact may vary from reduced visibility of the atmosphere to even human mortality. The impact of a particular pollutant on an object like a human, is dependent on concentrations and duration. The impact on the global climate system by the so-called greenhouse gases, takes a long time to become significant, but it could well be irreversible and this is a cause of

serious concern (Wyman, 1991; Bouma *et al.*, 1996). Climate change is currently a major topic of international research.

Quite often it is very difficult to establish a qualitative relationship between a particular pollutant or group of pollutants and a certain impact, such as a disease. Many factors may be involved, complicating matters dramatically. Collier and Hardaker (1995) discuss possible relationships between diseases and climate, weather and air quality conditions, although they note that *'much of the published work over the years lacks scientific credibility'*. Several attempts to quantify the economic impact of air pollution have been made, as is demonstrated by Curtiss and Rabl (1996). The impact of atmospheric pollutants is outside the scope of this project, although indirectly the reason for its existence.

1.4 Numerical dispersion models

Numerical models have become important tools for describing the dispersion of air pollution. The dispersion models can be classified into several categories: diagnostic versus prognostic, statistical versus deterministic, Eulerian versus Lagrangian, and models handling only primary pollutants versus models containing atmospheric chemistry (Air Quality Models). A brief overview of a few of these different types of model is given below.

1.4.1 Statistical methods

When an extensive database of meteorological and ambient air pollution data is available, statistical methods can be very useful. The statistical approach can provide stochastic data, such as probabilities, distributions and confidence limits of certain events. Although statistical methods do not provide direct physical relationships, they can provide empirical functions and indications of phenomena which are important for particular air pollution events. Common methods are multiple regression, principal component analysis and more recently, 'neural network methods' (Bose and Liang, 1996; Hagan *et al.*, 1996). The empirical models which result from statistical methods are especially useful in a complicated environment and they can be used as a tool for forecasting. However, the approach may not perform well during extreme conditions, and generally it will be completely inadequate when circumstances are changing, for example after the introduction of new emission sources in an area. The models and methods discussed in the following paragraphs have basically a deterministic, instead of a statistical, approach.

1.4.2 Diagnostic models

Diagnostic atmospheric dispersion models use an atmospheric field, based on observations at a certain time. The model lacks the ability of a time integration which provides a new field at a later time. However, the dispersion itself is integrated in time, based on the analysed atmospheric field. The complexity of the methods used to analyse the atmospheric field range from extremely simple, such as zero dimensional (data at one point only, e.g. data derived from one surface station), to a full three dimensional atmospheric field. The atmospheric fields can be obtained by the combination of observations and an interpolation technique or by objective analysis (Sasaki, and Lewis, 1970; Goodin *et al.*, 1980; Sashegyi and Madala, 1994). This is a technique which calculates the atmospheric field as it should be according to physical relations, using observations which can be nudged when their

deviation is too much from the atmospheric field. Information such as topography and surface characteristics can be incorporated. The objective analysis technique can be applied also in prognostic models and forms part of Four Dimensional Data Analysis (FDDA) (Stauffer and Seaman, 1990; Fast, 1995), a complicated procedure which allows the incorporation of observations into the model which vary over three spatial dimensions and time.

The advantage of dispersion models which use a diagnostic atmospheric field, is that they are computationally less demanding, but their disadvantage is that they are not able to cope properly with changing atmospheric conditions. Later in this thesis, two case days are discussed qualitatively, and the atmospheric fields were then obtained simply by interpolation of the available observations. However, no dispersion modelling is undertaken using these atmospheric fields.

1.4.3 Plume models

This type of dispersion model is generally run using diagnostic atmospheric data and it has become very popular, due to it's simple concept and relatively low demand on computer resources. Plume models can be attractive tools when the number of simulated emissions sources is limited and the assumptions being made are not seriously violated. The plume models simulate the dispersion of atmospheric pollutants from an individual source. The basic model uses generally a diagnostic atmospheric field (wind, thermal stability), which is assumed to be homogeneous and stationary. Semi-empirical formulations are constructed for evaluating the plume rise after leaving the stack, as reviewed by Briggs (1975) and Hanna *et al.* (1982). Plume rise based on more physical relations is described by Golay (1982) and Nieuwstadt and De Valk (1987). The vertical and horizontal diffusion of the plume is often based on the concept of a Gaussian distribution, where the vertical deviation is generally different from the horizontal. At this point the assumption of negligible effects of vertical wind shear is introduced. The parameters of the Gaussian distribution are derived from the intensity of atmospheric turbulence and plume travel time. Gaussian plume models are described in most standard books on atmospheric pollution and many publications (Benarie, 1980; Hanna *et al.* 1982; Hanna *et al.* 1987; Nieuwstadt and Van Dop, 1982; Venkatram and Wyngaard, 1988; Lyons and Scott, 1990; Turner, 1994). However, as Zanetti (1990) points out, the simple concept gives rise to serious limitations. These include the fact that advection terms often produce unrealistic diffusion. K-theory is sometimes applied to simulate vertical plume growth, but it is often inappropriate for turbulent flows, while the relationship of the diffusion coefficients to standard atmospheric measurements is often difficult to establish. Another severe limitiation of plume models is the assumption of homogeneous and stationary conditions. However, segmented plume models (Hales *et al.* (1977) and puff models (Roberts *et al.* 1970) were developed, which allow changing wind directions. Puff models have also been improved by allowing wind shear and other effects (Hanna *et al.* 1982).

It has been widely acknowledged that atmospheric vertical stability can cause processes such as fumigation and lofting, which are not incorporated in the original Gaussian plume models, and adaptations were introduced later to simulate these phenomena. Other adaptations were developed to cope with vertically unstable conditions, plume height in complex terrain, and deposition and reflection of pollutants near the surface. Several modelling groups have developed hybrid models, which activate different modules, depending on circumstances (Oleson, 1988; Carruther *et al.* 1992; Weil, 1992; Hanna and Chang, 1993). Despite their sometimes ingeneous complexity, Gaussian plume models do not perform well in conditions such as complex terrain, near coasts with sea breeze, as

demonstrated by Lyons *et al.* (1995), and during strong vertical wind shear (Pielke and Uliasz, 1993). Boznar *et al.* (1993) described a complete failure of their Gaussian plume model in complex terrain during particular circumstances and proved the superior performance of their neural network system.

1.4.4 Prognostic models

Prognostic atmospheric models are able to forecast atmospheric fields at later times by time integration. A wide range of models are developed, with space and time scales varying from global and centuries (climate models), global and 1-2 weeks (weather forecasting) to meso-scale and 1-2 days to local scale and hours. During this project meso to local scale features are studied, and the three dimensional prognostic model RAMS is used extensively, as described in more detail in Chapter 2.

1.4.5 Eulerian dispersion models

Eulerian models use a fixed reference system, i.e. the coordinate system is not moving with respect to the earth. The Eulerian air pollution approach is based on conservation of mass of the pollutant. The local change of concentration of the pollutant is equal to advection plus turbulent transport plus input from sources or output to sinks, generally neglecting molecular diffusion. Eulerian dispersion models are receptor oriented, so that the grid points represent receptors of pollutants. A disadvantage of the Eulerian approach is the grid discretization of the volume containing atmospheric pollutants, which can be a particular problem near emission sources, where sub-grid variations are most likely to occur. Each grid point can be located in the centre of a cell, which produces a single box model when only one cell is used (Oke 1978), or a multiple box model, which has many cells.

Eulerian dispersion models can be two or three dimensional and the wind field can be diagnostic or prognostic. The turbulent closure technique applied is an important feature of the models and relates directly to the diffusion of the pollutants. Stokes and Tyson (1981) simulated dispersion of smoke over Christchurch, using K-theory in a diagnostic windfield; Pielke *et al.* (1992) described the three dimensional prognostic RAMS model, based on 1st order turbulent closure, although higher order closures are often introduced by its users. Scheffe and Morris (1993) presented their *Eulerian* urban airshed model, which requires a given three dimensional wind field, is based on K-theory, and includes an atmospheric chemistry module.

1.4.6 Lagrangian models

Lagrangian models use a moving reference system, in contrast to the Eulerian models. However, Lagrangian models (modules) can be nested inside a Eulerian model, which provides the wind field. Two types of Lagrangian model can be distinguished, the Lagrangian box model and the Lagrangian particle model. The Lagrangian box models are sometimes used for atmospheric chemistry and simulate a box of air, also called an airshed, which moves along the trajectory. The Lagrangian particle models simulate particles, which move along the mean trajectories and are combined with a stochastic component, resembling diffusion by turbulence. The particles may represent an individual or an ensemble of air pollutants. The stochastic component is often created by random walk algorithms using Monte Carlo techniques, where the parameters are derived from atmospheric characteristics. Parameterizations of random walk models are described by Smith (1968) for homogeneous turbulent flow, and for inhomogeneous flow by Wilson *et al.* (1981a and 1981b), Van Dop *et al.* (1985) and Luhar and Britter (1989).

A Lagrangian model can be applied by using a diagnostic or a prognostic atmospheric field, although prognostic three dimensional fields tend to be used. A Lagrangian particle model has the advantage of providing sufficient resolution close to an emission source, in contrast to the Eulerian approach. Like the Gaussian plume model, it is source oriented, and in homogeneous conditions it should create similar results to the plume model. However, the Lagrangian model has the advantage of not being restricted by the list of assumptions associated with the Gaussian plume model, and it should therefore be able to create realistic dispersion patterns in complex terrain, non-stationary conditions, sea-breezes, as demonstrated by Lyons *et al.* (1995) for lake/sea breezes, Bossert and Poulos (1995) for an exit jet, and Pielke and Moran (1996) for dispersion over The Great Plains. The Lagrangian particle model has the disadvantage of becoming computationally expensive when many particles are released over a longer time interval. A solution to this problem can be achieved by treating the older particles, which are generally further from its source and more diffuse, in a Eulerian mode. Uliasz (1993) describes the successful application of such a hybrid model. During this project no Lagrangian dispersion studies were undertaken, since this approach is computationally not very efficient when an area source, such as the city of Christchurch, is considered and many particles must be simulated. Therefore, the dispersion studies were initiated using the Eulerian approach.

1.5 The Christchurch situation

1.5.1 History

Christchurch has a history of air pollution, which goes back many decades. As early as the 1930s, the wintertime air pollution became a major local issue and the Christchurch City Council attempted to control industrial and domestic smoke emissions, but it was not very effective with respect to domestic sources (Moody, 1983). During the 50s and 60s it was recognised that Christchurch had the worst air pollution problem in New Zealand (Sparrow, 1968) and that domestic heating was an important contributor to smoke and sulphur dioxide emissions (Christchurch Regional Planning Authority, 1966). The Clean Air Act 1972 was introduced, giving local authorities legal power to control emissions, and in 1977 Clean Air Zones were declared in Christchurch (Moody, 1983). Within these zones only approved heating devices can be installed.

The composition of the prevalent air pollutants has gradually changed over time. Sulphur dioxide is no longer a major issue, since the ambient concentrations are generally within acceptable limits. Smoke is still a severe problem and carbon monoxide has emerged as a contaminant of present concern, because of the extent to which both exceed the Ambient Air Quality Guidelines. While nitric oxide concentrations are substantial, nitrogen dioxide, which is the principle species of human health concern, is within acceptable concentrations (Canterbury Regional Council, 1993).

Christchurch's air quality continues to be a matter of public debate. Technically, a substantial reduction of the air pollution problem can be obtained easily by banning all solid fuel heating within a fixed term. This does not solve the emissions by traffic, which are becoming increasingly important, according to subsequential emission inventories (Kennedy *et al.*, 1974; Brady and Pullen, 1985; Canterbury Regional Council, 1997). Politically the situation seems to be rather sensitive, and after complaints, meetings and

reports for more than half a century, progress towards good air quality in Christchurch appeared to be rather slow. However, during the winter of 1997 the Canterbury Regional Council adopted a scheme to ban open fires and phase out older types of wood burners under stricter regulations.

1.5.2 Atmospheric pollutants in Christchurch

Monitoring of smoke, CO, SO_2 and NO_x has been carried out at different sites in Christchurch on a daily basis and at even shorter time intervals. Ozone and hydrocarbons are not monitored on a regular basis, but Paterson (1981) suggested that high concentrations are not likely in the Christchurch area, which is confirmed by a short period of observations during the summer of 1997 in Lincoln, about 20 km from Christchurch (Stephens, pers. com.). The air pollution sites and methods of analysis have changed several times in the past. This makes interpretation of the data sometimes difficult. Emission inventories were undertaken for Christchurch by Kennedy *et al.* (1974), Brady and Pullen (1985) and Canterbury Regional Council (1997). An emission inventory is useful for distinguishing different sources of air pollution and providing a general pattern of emissions, but it does not generate accurate information of actual emissions on a daily or even a hourly basis. Stokes and Tyson (1981) recognised a clear diurnal pattern in air pollution concentrations, which can be related to variations in emissions and atmospheric conditions. Smoke is considered the most important atmospheric pollutant in Christchurch, caused mainly by domestic heating; followed by CO, which is mostly emitted by motor vehicles, but to some extent also by domestic fires. Sulphur dioxide is released mainly by burning coal from industrial and domestic sources, while NO is mainly emitted by motor vehicles.

1.5.3 The physical setting of Christchurch

Christchurch is a mid-latitude city and is situated on the eastern edge of the gently sloping Canterbury Plains, near the coast. The city is surrounded by contrasting environments: the sea to the east, the Port Hills to the south, the Canterbury Plains in southwest to northerly directions, and further westwards the Southern Alps. Therefore, meteorological conditions at local (suburban) scale in Christchurch can be quite complex. For example, Heathcote is located in a valley on the southern fringe of the city and it will often experience different airflow patterns than Woolston or Linwood, which are at open, flat locations, close to the sea. In contrast, suburbs on the western fringes of the city are likely to experience stronger influences from the rural Canterbury Plains.

Sea breezes appear to occur in all seasons, but are most pronounced during the summer, according to Sturman and Tyson (1981). Interactions between different types of air flow are evident. McKendry *et al.* (1986, 1988) described three major scales of factors influencing air flow in Canterbury and Christchurch. Firstly, there are dynamic orographic effects of the Southern Alps, which perturbate the predominantly westerly flow, causing localized antitriptic air flow, which is from the northeast in Christchurch. Secondly, thermo-topographic effects, caused by regional and land-sea thermal contrasts and slope heating or cooling, are superimposed on this. Thirdly, there are boundary layer stability variations. Frequently, strong vertical wind shear (in speed and direction) occurs in the Christchurch area below the 850 hPa level (Surridge, 1980). Ryan (1980) investigated nocturnal northwest drainage flow from the Canterbury Plains, which is clearly affected by the Port Hills and sometimes the shallow flow from the Canterbury Plains does not reach Christchurch. An explanation might be the decreased slope of the Canterbury Plains further eastwards, increased surface roughness close to Christchurch or the urban heat island effect (Tapper, 1990). So far, research has been mostly restricted to observations

where the physical cause of the processes could only partly be explained or quantified. Obviously, complicated airflow patterns occur in the Christchurch area with interaction of flows at different scales, including drainage flow from the Canterbury Plains and the Port Hills, sea breezes and possibly re-circulations. This makes quantifying dispersion of atmospheric pollutants a challenging task.

1.5.4 Dispersion of air pollution in Christchurch

Air pollution in Christchurch is a typical winter phenomenon, due to reduced atmospheric mixing and increased domestic emissions. Owens and Tapper (1977) classified synoptic weather conditions and related these classes to observed ambient air pollution concentrations. Their highest ranking class was *northwest flow, undeveloped at lower levels.* During this situation strong thermal inversions are likely to occur at both low and higher elevations, severely reducing vertical mixing of polluted air. Other synoptic conditons favouring the development of high air pollution events are *a high pressure system, generally associated with a weak geostrophic flow,* which covers the South Island and *southwest flow, following the passage of a cold front.* During this project two case studies were conducted, one during southwest flow (C2728) and another during weak geostrophic flow (C3031), respectively. The case studies are discussed in detail in Chapter 4.

Detailed statistical analysis by Sturman (1982, 1985) revealed that the spatial distribution of pollution is largely controlled by local airflow patterns, a process also described by Kristensen *et al.* (1982). Light drift, associated with high air pollution concentrations causes complex airflow patterns over Christchurch. Accurate measurements of these light and spatially variable airflows are difficult. Several models were constructed to predict 24 hour ground level air pollution concentrations with limited success (Brown, 1974; Kennedy and Tolley, 1978; Stokes and Tyson, 1981). Several reasons for these results include insufficient or inadequate input data, coarseness of the models, application of the models in an environment which does not satisfy their assumptions, for example, of homogeneous terrain and atmospheric stability criteria, and inability of the models to describe certain phenomena, such as sea breezes, katabatic flow and influences of topography. However, in recent years dramatically increased computer power has become available and sophisticated atmospheric models are developed, based on a large set of actual physical relations. This provides the possiblity to investigate the atmospheric processes in the Christchurch area with much more detail and reliability then undertaken before.

1.6 Objectives and approaches

The broad aim of this project is to improve knowledge of atmospheric behaviour in the Christchurch area in such a way that more effective regional air pollution policy can be developed. The downstream objective is the improvement of environmental quality in the region.

Particularly, the behaviour of the atmospheric boundary layer in the Christchurch area needs further investigation. It is the boundary layer where people live and where most air pollution is emittted. Features such as surface characteristics and topography influence the development of the boundary layer and dispersion of air pollution. Using a numerical model to quantify the dispersion of atmospheric pollutants, its performance could be

improved dramatically, when detailed information about these influences is incorporated into the model settings and boundary conditions. Consequently, such an adjusted model could reach the phase where it is applied as an air quality management tool, leading to improved decision making.

This project has taken a relatively broad approach, because the environment of Christchurch is rather complex, promoting significant contributions to the dispersion of air pollution due to atmospheric processes operating at different scales. At the smaller end of the scale, research is conducted on surface characteristics in the Christchurch area, while at larger scales airflow patterns are investigated in the Canterbury Region together with the interactions of advection at synoptic scales with flow at smaller scales.

So, the objectives of this project are formulated:
a. to provide a description of surface characteristics and their spatial variations in the Christchurch area, and their significance for dispersion studies.

b. to provide a description of observed local airflow perturbations which can be related to variations in surface characteristics, local topography and urban heat island effects.

c. to obtain knowledge about the evolution of the boundary layer in the Christchurch area during periods of high air pollution concentrations or during intervals with a high air pollution potential.

d. to provide a description of the interaction between different scales of wind regime and the resulting local dispersion of atmospheric pollutants.

e. to demonstrate the ability to simulate airflow patterns and dispersion of air pollution in the Christchurch area with an acceptable accuracy.

Other important factors of the Christchurch air pollution problem, which are outside the scope of this project, but need further investigation, include firstly a detailed statistical analysis of the relationship between ambient air pollution concentrations and meteorological variables or other relevant factors. Secondly, qualitative and quantitative analysis of spatial and temporal variations of emissions is required, especially at relatively small scales (e.g. 2-4 km, 0.5-2 hr), although larger scales are useful as well. This has been partly resolved by the recent emissions inventory work (Canterbury Regional Council, 1997). Thirdly, the application of extensive dispersion modelling to a wide range of case study situations is needed. However, this study aims to provide the basis for this more extensive modelling.

The approach taken to achieve the above mentioned objectives is:

- to make observations of wind, temperature and humidity profiles close to the surface (< 30 m) in the Christchurch area, so that heat and momentum fluxes can be derived. These fluxes provide the information for quantifying the surface characteristics, and their likely influence on dispersion processes.
- to make surface observations which illustrate the spatial structure of the wind field and temperature pattern in the Christchurch area at a high resolution. The spatial structure outside this area requires less detail.
- to obtain a three dimensional picture of atmospheric conditions over the South Island, with most detail in the boundary layer and in the Christchurch area.
- to use a three dimensional prognostic model for simulations, primarily based on physical relationships.

The approaches taken will be discussed throughout the thesis, while the structure of the thesis will be outlined in the next section.

1.7 Structure of the thesis

The aims and objectives of the research project are discussed in this chapter, together with the general background of the air pollution problem, as well as the specific context of the Christchurch area.

Chapter 2 deals with materials and methods, the instruments and the locations of the observations. It also provides a description of the numerical model which was used as a tool for simulations.

In Chapter 3, attention is focussed on the examination of surface characteristics in the Christchurch area. The reader is given a description of the different methods used to obtain momentum and heat fluxes at various sites. The results were subsequently partly implemented in model settings during simulations of case studies.

In Chapter 4, two case studies are presented when high air pollution concentrations occurred in Christchurch. Time series of ambient pollutants, wind and temperature are presented, as well as spatial patterns of wind and vertical profiles in the boundary layer. This provides the reader a four dimensional (three spatial, one temperal) picture of the boundary layer in the area during both case studies. The analysis of the cases is provided mainly in a qualitative way.

In Chapter 5, katabatic flows are described and results of two dimensional simulations of the flows developed on the Port Hills and Canterbury Plains are presented The numerical studies also include a sensitivity analysis comprising soil moisture content, soil type, vertical grid size, and thermal stratification of the ambient air.

In Chapter 6, a third spatial dimension is added and a discussion of airflow in complex terrain is given. Results of three dimensional simulations are presented over 24 hour intervals under various conditions of synoptic scale advection.

In Chapter 7, the reader is presented with the results of simulations of the two case studies discussed earlier in Chapter 4. The verification of the model contains extensive statistical analysis.

Chapter 8 reviews the objectives stated in Chapter 1, and continues with the final discussion and conclusions of the project. Finally, recommendations are given for further research.

Appendix A contains detailed descriptions of calibration procedures followed, while Appendix B contains several additional figures and output products of the simulations.

2. Sites, observations and tools

2.1 Introduction

A data collection system was established in the Christchurch area, which was designed to provide a three dimensional picture of the processes in the lower part of the atmosphere, as detailed as the available equipment allowed. It is the lower part of the atmosphere which directly influences the horizontal and vertical dispersion of air pollutants, so that it was the major focus of the measurement programme. A second objective of the measurement programme is to gain an understanding of the influence of surface characteristics in the area, including vegetation cover and the height and spacing of buildings. These characteristics are considered to have an influence on air pollution mixing. Since local atmospheric conditons are influenced by larger (synoptic) scale phenomena, data were also collected from stations over the South Island of New Zealand and information was retrieved from weather maps.

2.2 The Christchurch area

Christchurch is situated on the coast at the eastern edge of the Canterbury Plains, just north of the Port Hills, which are part of Banks Peninsula. The Southern Alps are important orographic features with peaks over 3000 m to the west and north-west of Canterbury, as is Banks Pensinsula with hills to almost 1000 m. The height of the Port Hills varies between 250 and 500 m. The Canterbury Plains are predominantly rural, and mostly covered with grassland, although horticulture and forestry do exist as well. Christchurch city covers roughly 20 km in the east-west direction and 12 km in the north-south direction, covering about 225 km^2. Christchurch's landuse can be divided into 75% residential, 10% industrial, 5% recreational (e.g. parks and playgrounds) and 10% commercial.

2.2.1 Landuse details of Christchurch

In 1995, the residential areas of Christchurch consisted mainly of single 1 or 2 storey buildings surrounded by a significant area of pavement and garden space. The gardens consist of lawns, shrubs, bushes and trees. Variations between suburbs do exist with regard to the areas covered by houses, pavement and gardens, as well as in the composition of the gardens, the number of trees per given area and type and height of the trees. However, these variations are neglected in this study.

Christchurch has basically light industry, with buildings and structures generally 5 to 10 m high. Vegetation in the industrial areas is almost absent, while most of the area is covered by buildings, structures and pavement. In contrast, the recreational areas are mainly covered by grass, bushes and trees. Again, for both of these landuse types, local variations are discarded for purposes of this study. The commercial areas are mostly covered by buildings, often multi-storey, partly covered by pavement and to a minor extend with vegetation. Due to this definition, the campus of the university at Ilam is classified as 'commercial landuse', although it is not a commercial area in the true sense.

Table 2.1. Area coverage (%) of vegetation, buildings and pavement for different types of land use, defined for the Christchurch area.

Landuse	Area	Vegetation	Buildings	Pavement
Residential	75	30	45	25
Industrial	10	2	58	40
Recreational	5	83	2	15
Commercial	10	5	75	20

The data shown in Table 2.1 are based upon maps, aerial photographs and information from the Christchurch City Council (CCC).

2.3 Data collection in 1995

During the winter of 1995 a number of different forms of data were collected in the Christchurch area, and a summary is given below.

- *Instrumented towers.* Two 10.5 m and two 21 m towers were deployed for monitoring low level atmospheric characteristics, using a profile method and the eddy correlation technique. Data collection started at the end of June 1995 and continued until the beginning of September 1995 (see Figure 2.1). Data were stored every 10 minutes, but during some periods even more frequently.
- *Mobile weather stations.* One mobile weather station was located at Cashmere, providing windspeed, wind direction, temperature of the soil at 0.05 m depth, air temperature at the surface, and humidity and temperature at 2.5 m from the surface, soil heat flux, net and global solar radiation and precipitation. The station was operational from mid June until the end of August 1995. Another mobile station was located at the instrumented tower at Beckenham in order to provide additional data at this site. This mobile station was similar to the other at Cashmere, except that no wind direction, precipitation and soil heat flux were recorded. It was operational from 20 July to 29 August 1995, with data being stored at 10 minute intervals.
- *Tethered balloon (blimp) flights.* A tethered balloon with a sonde attached provided profiles of temperature, humidity and wind up to 300 - 500 m above the surface. One flight (ascent and descent) generally took about 30 to 45 minutes. The blimp was transported on a trailer, so that soundings at different sites could be undertaken within 1 to 2 hours. During the winter of 1995, 76 successful flights were undertaken on calm days at various locations in the Christchurch area (see Figure 2.2, Plate 2.9, and Table 2.2 for more details).
- *Pilot balloon/radiosonde soundings.* A pilot balloon or radiosonde sounding was performed on most of the days when blimp flights were made. The balloons were tracked using a theodolite and provided profile measurements of wind speed and direction (pilot balloon) and temperature and humidity (radiosonde) up to altitudes between 1500 and 6000 m.
- *Eddy correlation.* Eddy correlation equipment was used at the Beckenham site for 180 hours in August, providing latent and sensible heat fluxes over the urban surface. These fluxes are compared with the heat fluxes derived from the profile method at the same site.

• *Additional observations.* Soil samples were taken at various sites in the area, while a log book has been kept throughout the winter, containing observations of clouds and other relevant phenomena.

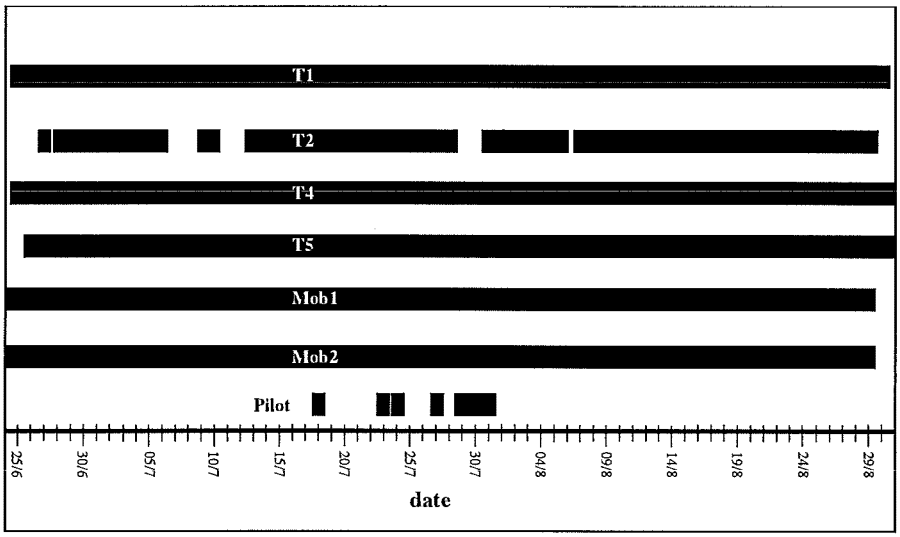

Figure 2.1 Time distribution and status of operational measurement platforms. T1: tower at Burnside High; T2: tower at Beckenham; T4: tower at Marshland; T5: tower at Ensors Gardens; Mob1: mobile weather station at Cashmere; Mob2: mobile weather station at Beckenham; Pilot: pilot balloon flights performed. Solid bar indicates period of equipment operation.

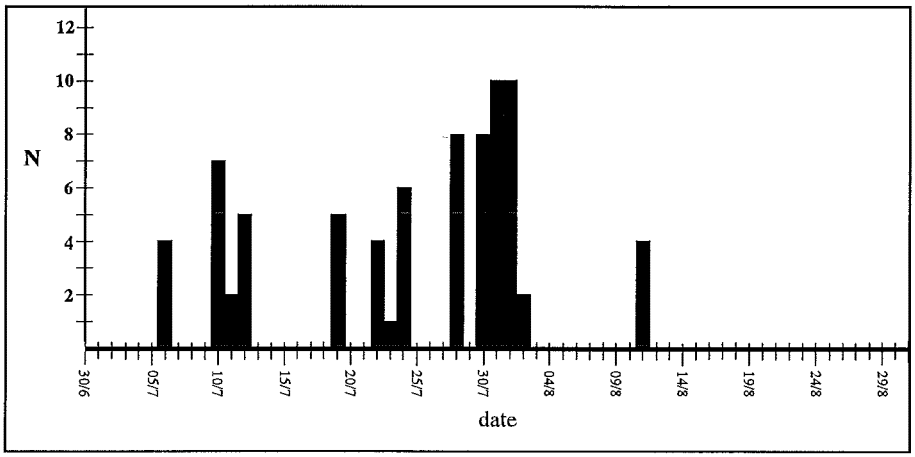

Figure 2.2 Distribution of the number of blimp flights (N) per evening-morning period during the 1995 winter season.

The above described data set is supplemented by:

- *Weather stations.* A network of weather stations already existed in the area: Christchurch Airport (MetService), Bromley (CCC), Hornby (CRC), St Albans (CRC) and Opawa (CRC). Notation: '(CCC)' means operated by Christchurch City Council and '(CRC)' is operated by the Canterbury Regional Council.
- *Synoptic weather maps.* Weather maps have been collected for mean sea level and upper levels (850, 700 and 500hPa).
- *Radar wind balloon/radiosonde soundings.* Soundings from Invercargill, Hokitika and Paraparaumu were included in the data set.
- *ECMWF gridded atmospheric analysis data and Australian radiosonde soundings* were available for model initialization and Four Dimensional Data Analysis (defined earlier), but not applied.
- *Sea surface temperatures.* Sea surface temperatures around the South Island were obtained from NIWA Christchurch.
- *Air pollution data.* These data were provided by the Canterbury Regional Council from various locations in Christchurch.

2.4 Sites

The sites for the instrumented towers and mobile stations were chosen to cover possible spatial variability of atmospheric phenomena near the surface (see Figure 2.3). Since the resources were limited, and because both spatial distribution and simultaneous profile measurements were performed, only 5 sites for the towers and the mobile stations were used. One mobile weather station was located at Cashmere, 1 km from the tower at Beckenham at a height of 150m above sea level, one tower was in a rural area, just outside Christchurch, while the other three towers were located in different suburbs of the city. The second mobile station was located at the Beckenham tower to provide additional data for flux measurements. The locations for the blimp flights were selected so that they were close to an instrumented tower or weather station, or covered a spatial contrast (e.g. urban - rural, land - sea, open flat area - Port Hills). The pilot balloon observations were performed on the roof of the Department of Geography building at Ilam for practical reasons. This can be justified because upper air flow is much less affected by local conditions, and the reason for these observations was to relate surface processes to airflow aloft.

Local conditions are likely to have a major impact on the observations close to the surface (less than 50 m) and possibly to higher elevations. In the following sections the sites of the instrumented towers, the mobile station at Cashmere and the blimp flights are described in some detail.

2.4.1 Burnside

A 21m tower was erected in the playgrounds of the Burnside High School, Greers Road. The High School is located in a residential area, while the tower was located in a reasonably open area, covered with short grass, although a few 10 to 12 m high deciduous trees were situated about 50 m away to the northeast, a cricket yard with a metal wire fence was located 15 m to the east, and a few bushes less than 2 m high existed 15 to 20 m to the north and northwest. A 2 m high dyke started 10 m to the northwest of the tower, stretching westwards. Buildings were located 60 m south, 92 m to the northwest and at 160 m to the northeast from the tower. The buildings were predominantly 1 or 2 storey

structures, being less than 10m high. For further details see Figure 2.4 and Plates 2.1 and 2.2.

Orientation. In plan view, the main poles with the instruments pointed towards 17° (NNE) away from the tower, the net radiometer towards 77° (ENE). The net radiometer experienced no shading caused by the tower, but the recorded wind speed may have been influenced by the tower with the anemometers on the leeward side (wind direction about 197°), or even with the anemometers on the wind ward site (wind direction about 17°, although the latter effects were probably neglectible.

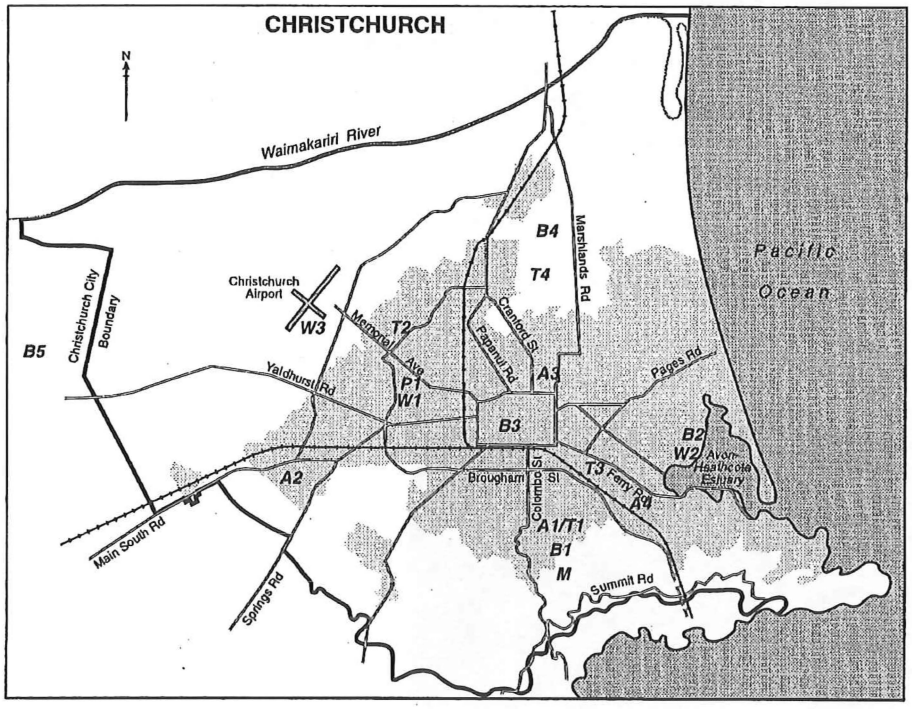

Figure 2.3 Map of the Christchurch area displaying the locations of the instrumented towers (T), mobile weather station (M), blimp sites (B), pilot balloon sounding location (P), weather stations in the area (W) and air pollution observations sites (A). Sites: T1: Beckenham; T2: Burnside; T3: Ensors Gardens; T4: Marshland; W1: Campus Univ. of Canterbury; W2: Bromley; W3: Christchurch. International Airport; A1: Beckenham; A2: Hornby; A3: St. Albans; A4: Opawa; B1: Beckenham; B2: Bromley; B3: Hagley Park; B4: Marshland; B5: West Melton; M: Cashmere.

2.4.2 Beckenham

A 21 m tower and a mobile station were established in the yard of the Christchurch City Council Water Services Unit, 54 Colombo Street in Beckenham. The Beckenham site is located in a residential area and surrounded by deciduous trees to the south, southeast, northeast and north within a distance of 50 m from the tower. Directly around the tower was short grass, while about 30 m west of the tower were stored materials, generally with a height less than 2 m. Single or two storey buildings existed at distances over 60 m. For further details see Figure 2.5 and Plate 2.3.

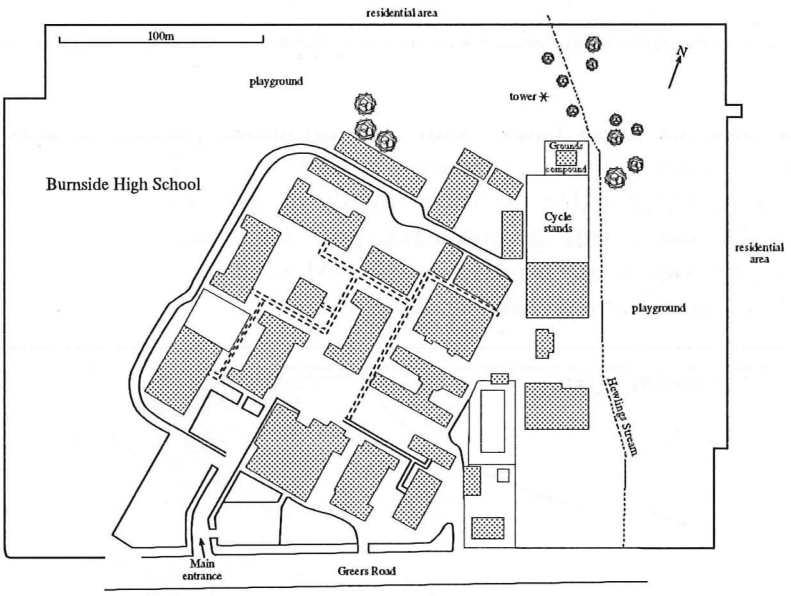

Figure 2.4 Map of the Burnside site.

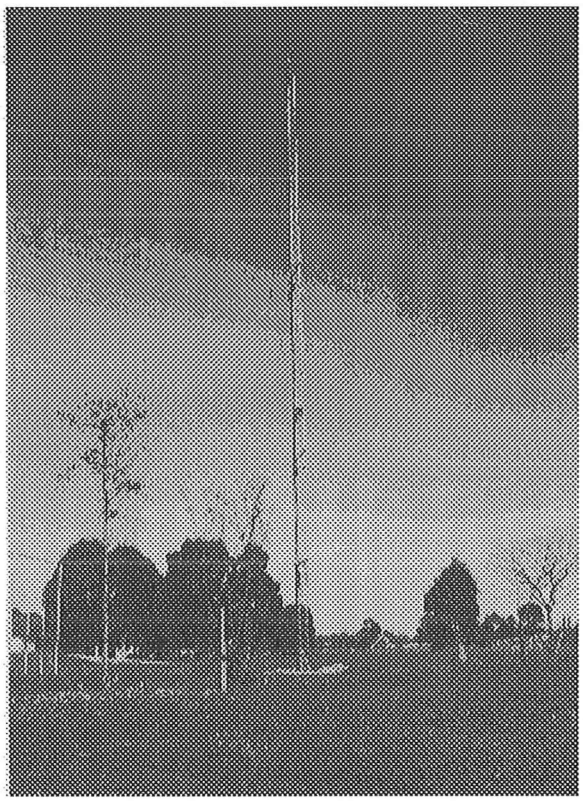

Plate 2.1 Instrumented tower at Burnside High looking south.

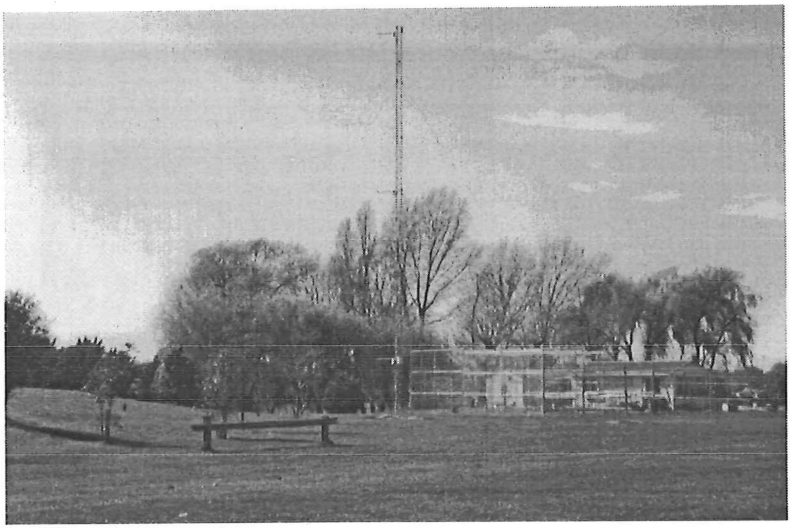

Plate 2.2 Instrumented tower at Burnside High looking northeast.

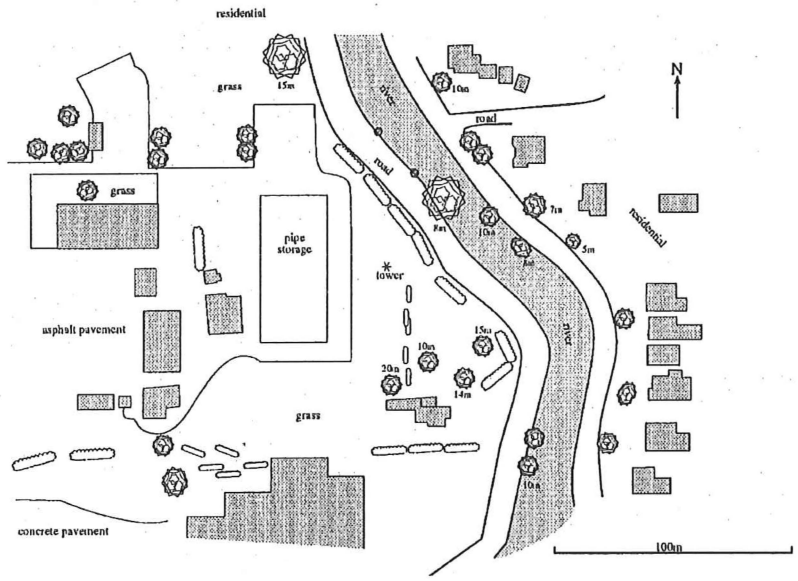

Figure 2.5 Map of the Beckenham site.

Orientation. In plan view, the main poles with the instruments, as well as the net radiometers pointed towards 39° (NE) away from the tower. The anemometers may have been influenced when on the leeward side of the tower and theoretically to some extent when being directly on the windward side.

2.4.3 Cashmere

A mobile weather station was installed on the slopes of the Port Hills at 150m above sea level. The station was installed on a ridge at the end of Hollis Avenue in an open area. Houses were located within 250 m of the site, while the vegetation around the station was short to medium long grass. (see Plates 2.4 and 2.5).

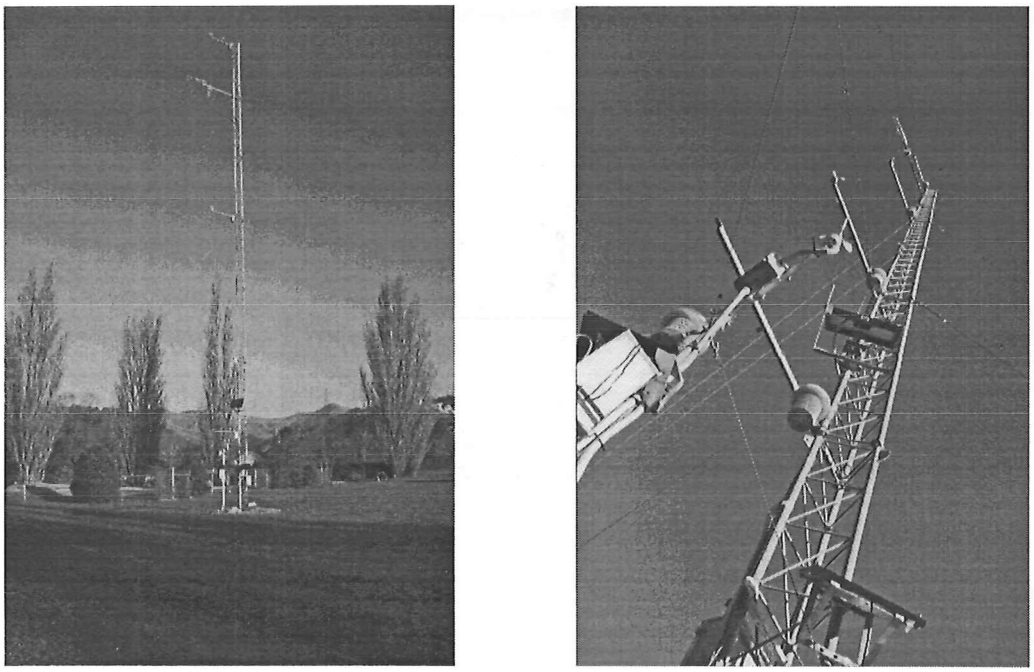

Plate 2.3 Instrumented tower plus mobile station at Beckenham looking southeast (left) and looking upwards (right).

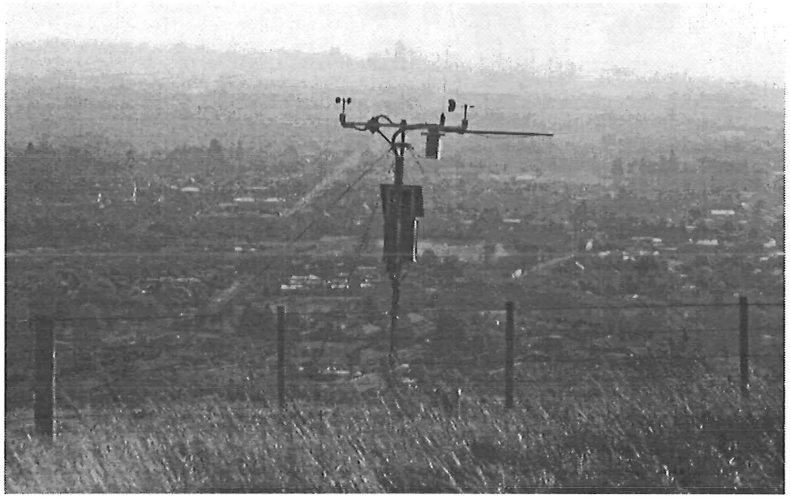

Plate 2.4 Mobile weather station at Cashmere looking north.

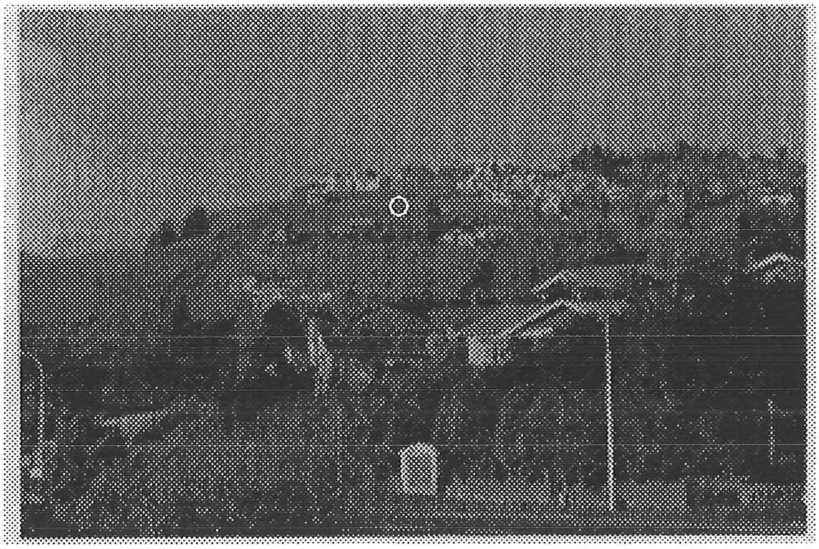

Plate 2.5 Mobile weather station at Cashmere, located in circle.

2.4.4 Ensors Garden

A 10.5 m high tower was erected at Ensors Garden, the recreation area near the Polytech in Sullivan Avenue. South, east and north of the Ensors Garden are residential areas, but to the west the area is industrial. The tower was located on the eastern side of the playgrounds. Single storey houses existed within 25 m to the east and a 8 m high floodlight was at a distance of 7 m in a south southeast direction from the tower (see Figure 2.6 and Plate 2.6). The poles on which the instruments were mounted were directed towards 330° (NNW), away from the tower.

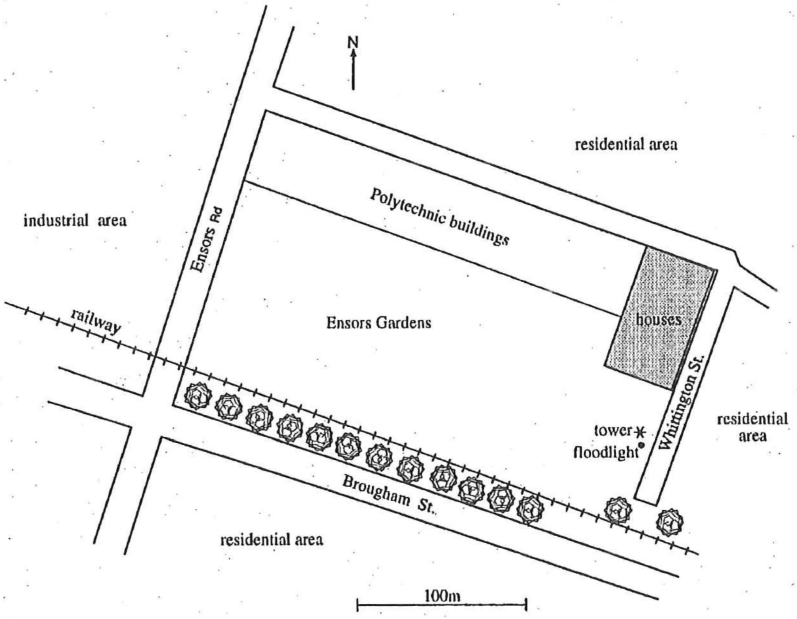

Figure 2.6 Map of the Ensors Garden site.

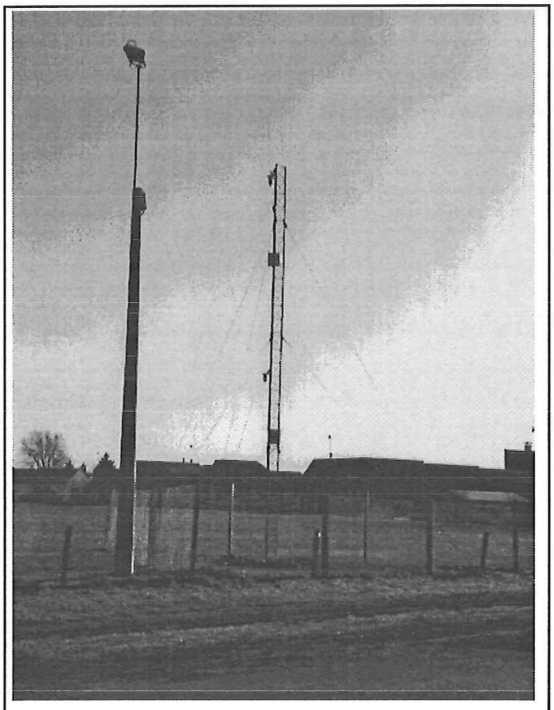

Plate 2.6 Instrumented tower at Ensors Garden.

2.4.5 Marshland

A 10.5 m tower was erected at 711 Hills Road in Marshland, about 2 km north of Christchurch. The Marshland site was in a rural area with a grass land use, although at distances over 500 m (short) crops existed as well. A few houses were located at distances over 70 m. A 1 m high hedge was 15 m south of the tower, and 25 m to the south 10 m high non-deciduous trees were located. These trees are expected to have influenced wind speed observations with wind directions from $180^{o} \pm 15^{o}$ (see Figure 2.7 and Plates 2.7 and 2.8). The instrumented poles were pointing towards 300^{o} (WNW) away from the tower.

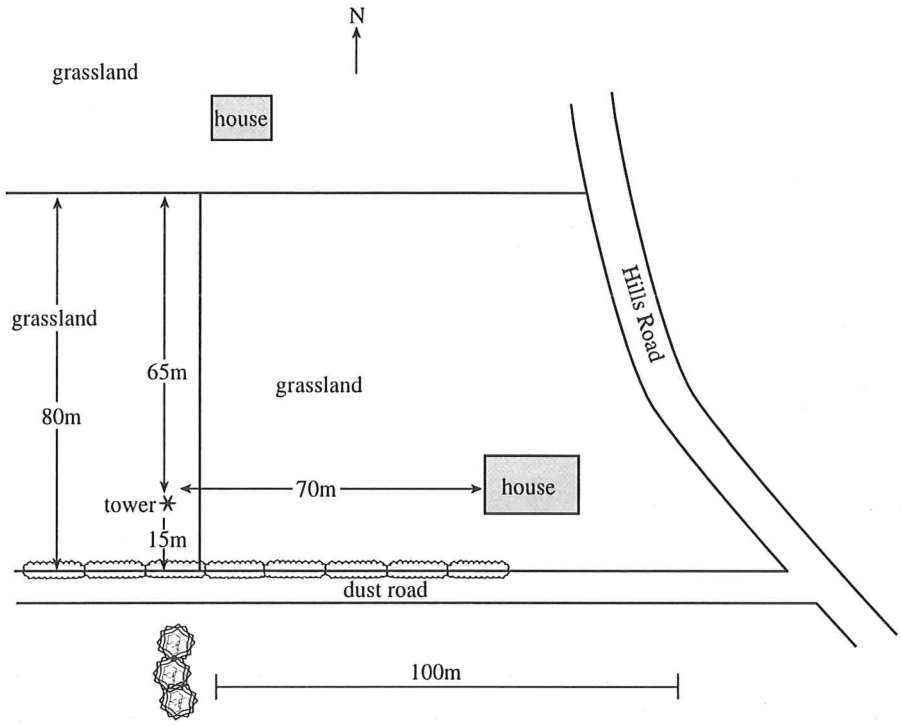

Figure 2.7 Map of the Marshland site.

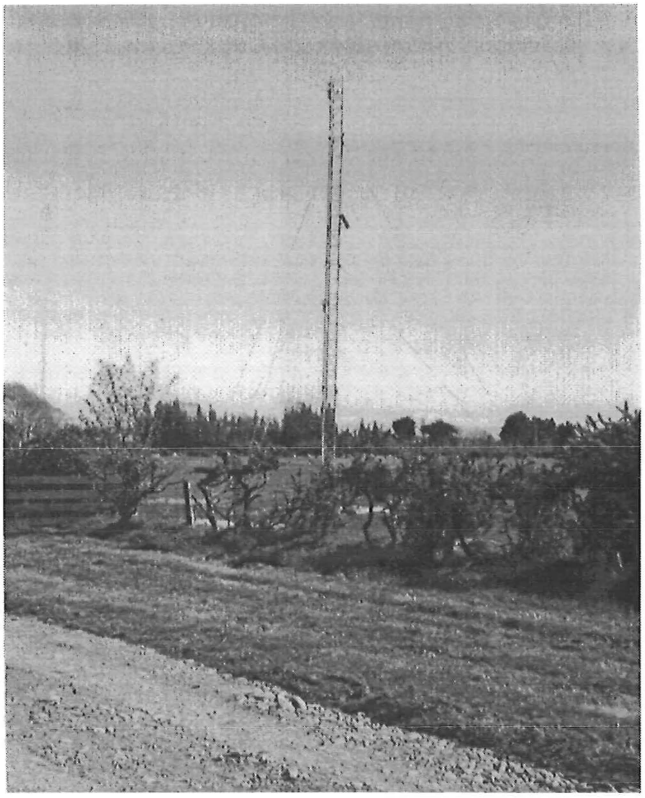

Plate 2.7 Instrumented tower at Marshland looking northwest.

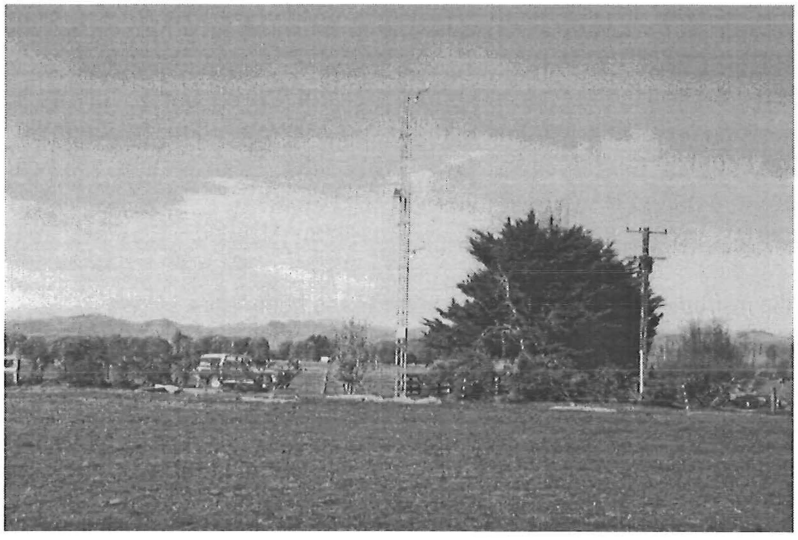

Plate 2.8 Instrumented tower at Marshland looking south.

2.4.6 Blimp sites

The blimp sites were selected in order to be able to observe contrasts in atmospheric boundary layer characteristics due to local effects. Sites were chosen along a south to north line: *Beckenham, Hagley Park, Marshland* and along a west to east line: *West Melton, Hagley Park, Bromley*. Marshland and West Melton were in a rural

environment, the Bromley site was near the oxidation ponds and the estuary, Beckenham was within a residential area and Hagley Park was near the city centre (see Figure 2.3).

Plate 2.9 The tethered balloon being used at the Beckenham site.

2.4.7 Other sites

A brief description of other sites providing additional data is given below:

- *Bromley (CCC) weather station* is situated at an open site, with short vegetation at the surface and large water surfaces nearby.
- *Christchurch Airport weather station (MetService)* is at an open location, although 2 to 3 storey buildings occur nearby.
- *CRC air pollution monitoring stations* are in several areas of Christchurch, having a mixture of buildings, open areas and gardens with bushes and trees. The Beckenham and St. Albans sites are in a residential area, while the Hornby and Opawa monitoring station are in a mixed residential and industrial area.

Table 2.2 Coordinates of the instrumented towers, weather stations and blimp sites.

Location	Latitute (S)	Longitute (E)	Description
Airport	43° 29' 20"	172° 32' 00"	mostly open area
Beckenham	43° 33' 55"	172° 38' 10"	residential
Bromley blimp	43° 32' 10"	172° 42' 15"	mainly open area, close to water
Burnside	43° 30' 30"	172° 34' 20"	residential, open area
Cashmere	43° 34' 45"	172° 38' 25"	mostly open grassland
Cashmere blimp	43° 34' 25"	172° 38' 20"	residential, close to Port Hills
Hagley Park	43° 32' 10"	172° 37' 05"	mainly open area near city centre
Hornby	43° 32' 50"	172° 31' 15"	residential, industry nearby
Marshland	43° 27' 50"	172° 38' 00"	rural, open area
Opawa	43° 33' 20"	172° 40' 00"	residential, industry nearby
St. Albans	43° 31' 00"	172° 38' 30"	residential
University	43° 31' 30"	172° 35' 00"	multi-storey buildings
West Melton	43° 29' 00"	172° 23' 40"	rural, open area

2.5 Instruments

A variety of instruments were employed during the winter of 1995 in the Christchurch area and a detailed description is given below. The different configurations of instruments will be discussed as well as measurement methods, accuracy of the sensors and calibration details.

2.5.1 Towers

A collection of instruments was mounted on the 21 m and 10.5 m towers being used at Burnside, Beckenham, Ensors Garden and Marshland. The towers were constructed from triangular lattice type sections (see Plate 2.3) and each tower had a different combination of instruments. Horizontal 1.5 m long poles were fixed on the towers at various elevations. Anemometers were attached at the end of the poles, wind vanes, temperature and humidity sensors were closer to the tower sections. The net radiometers and the eddy correlation equipment were attached to other cross arms. Table 2.3 shows the heights at which variables were being measured on the four towers, while Table 2.4 shows the types of sensor used. A detailed description of the sensors is given in the following text.

Table 2.3 Details of instrumented towers. T1: 21 m tower at Burnside; T2: 21 m tower at Beckenham; T4: 10.5 m tower at Marshland; T5: 10.5m tower at Ensors Gardens; TT: temperature; RH: relative humidity; ff: wind speed; dd: wind direction; Rn: net radiation; EC: eddy correlation.

Height (m)	T1	T2	T4	T5
20.9	TT RH ff dd Rn	TT RH ff dd Rn		
18.1		EC		
12.1	TT RH ff	TT RH ff		
10.3			TT RH ff dd	TT ff dd
6.1	TT RH	TT RH ff		
5.0			TT RH ff	TT ff
3.1	TT RH	TT		

2.5.2 Campbell 107/207 probe

The Campbell 107/207 (UUT51J1) temperature and 207 (PCRC-11) relative humidity sensors were housed in a radiation screen. According to the manufacturers, the relative humidity sensor has an accuracy typically better than 5% over the 12 to 100% relative humidity range. The temperature sensor is corrected by a 5th order polynomial, giving an accuracy of 0.2 K in the temperature range -10 to +30°C. The 107 probe is a separate sensor used where temperature only was required.

It appeared that several of the 107/207 sensors had incorrect lead lengths. Adding extra lead lengths at the end of the connection end ('pig tail') is not recommended. So, where necessary, the 'pigtail' ends were taken off the original lead lengths and attached to the end of the extra added lead length. The 107 and 207 sensors were then re-calibrated, as is described in Appendix A.

Table 2.4 Types of sensor used at the four towers.

Variable	Sensor type	Manufacturer
Temperature	UUT51J1 thermistor (107 /207)	Fenwal Electronics
Relative humidity	PCRC-11 (207)	Phys-Chem Scientific
Wind speed	A101ML	Vector Instruments
Wind direction	WP200/L	Vector Instruments
Net radiation	Q*7	Radiation and Energy Balance Systems
Eddy correlation	CA27, 127-sensor, KH20	Campbell Scientific

2.5.3 Vector Instruments A101ML anemometer

The A101ML has a threshold of about 0.1 m s^{-1} with a distance constant around 5 m. According to the manufacturer, the instrument is able to survive windspeeds up to 75 m s^{-1}, but during the 1995 field campaign we were not able to verify this. The A101ML is a cup anemometer having 3 cups attached to a vertical axis. One turn of 360° produces n_w pulses, being 13 for the anemometers used at the towers. The accuracy of the A101ML is 1% at 9 m s^{-1}, according to Vector Instruments. The A101ML has a non linear response to wind speed, but this non linearity is almost identical for the individual sensors with respect to the rotation speed. Details of the calibration procedures are given in Appendix A.

2.5.4 Vector Instruments WP200/L wind vane

This sensor was used for wind direction observations. According to the manufacturer, the threshold of the sensor is 0.4 m s^{-1}, the distant constant is 2.3 m with a damping ratio of 0.2. The accuracy is ±2° in a steady wind over 5 m s^{-1}. Calibration was undertaken to obtain a multiplication factor to generate a 360° output, with a 4° gap at the north point.

2.5.5 Radiation and Energy Balance Systems (REBS) Q*7 net radiometer

This sensor has a spectral response from 0.25 to 60 μm, with a time constant of about 30 seconds. The sensor is influenced by wind as well, leading to almost 6% reduction of the positive net radiation values, and up to 1% reduction of the negative values at wind speeds over 7 m s^{-1}. A description of the adjustments for wind effects is given in Appendix A.

2.5.6 Eddy correlation equipment

Introduction. Vertical fluxes in the surface layer (SL) can be measured directly by applying the eddy correlation (EC) technique. Vertical fluxes are proportional to the covariances of the vertical windspeed and the relevant variables (temperature, vapour density, CO_2 concentration, etc), with typical spectra in the SL ranging from $1*10^{-4}$ Hz to over 100 Hz (3 hours to 0.01 s, respectively) (Kaimal et. al., 1972; Stull, 1988). The EC technique therefore requires fast response sensors, and is used for a wide range of applications, including aerodynamics of the SL (Lloyd et. al., 1992), evaporation of vegetated surfaces (Soegaard and Boegh, 1995; Stannard and Rosenberg, 1991; Denhartog et. al., 1994), mass exchange in the SL, including methane fluxes (Edwards et.al., 1994) and CO_2 and O_3 uptake by a forest (Amthor et. al., 1994), studies of global climate change (Ritter et. al., 1993) and research on urban climates (Schmid et. al., 1991; Oikaw and Meng, 1995; Grimmond et. al., 1996). The EC method is particularly useful in an aerodynamically rough environment such as a city, where flux measurements by the profile

method are very difficult, because intense mixing of the air causes relatively small vertical gradients, demanding very accurate measurements.

Although the EC technique is a direct method, which lacks many of the problems faced by the profile method, deviations between observed and actual surface fluxes may well exist. For example, spatial inhomogeneity can result in horizontal advection becoming significant. Schmid and Oke (1990) and Schmid (1994) described a model to estimate the source area contributing to turbulent exchange in the SL, and which provides a tool to estimate the contribution of advection. During the 1995 measurement programme the EC sensors were mounted at 18.1 m high, so that the sensors would be representative of a large source area, within the suburban environment.

Correction procedures are required when heat fluxes are obtained by the EC method, because:

- Atmospheric density variations directly influence the sensible heat flux and to a lesser degree the latent heat flux (Webb *et al.*, 1980). Corrections for air density can be as large as 3% to 8% of the sensible heat flux. A detailed description is given in Appendix A.
- Oxygen has an influence on the absorption of the radiation emitted by the Krypton hygrometer (Tanner and Greene, 1989; Campbell Scientific, 1994). The oxygen correction is significant and can be as large as 20% of the uncorrected latent heat flux. A detailed description is given in Appendix A.
- Of other factors, which are not corrected for during this project include shadowing of the sonic anemometer (not important for 1D sonic anemometers, Massman et. al., 1990), spatial averaging effects on the Krypton hygrometer (Andreas, 1981), and frequency response and spatial separation of the sensors (Moore, 1986).

The data obtained by the EC technique were corrected for air density fluctuations and oxygen influence, and are described in Appendix A, in the section entitled *Derivation of heat fluxes and corrections*.

EC instruments and methods. Eddy correlation equipment was used during several days in August 1995, totalling 180 hours of observations over both day and night. As already mentioned, EC equipment allows a direct measurement of sensible and latent heat fluxes in the surface layer. The EC equipment consisted of the following sensors:

- CA27: a one dimensional sonic anemometer with frequency response of 40 Hz and with a path length of 0.10 m.
- 127-sensor: a 12.7 μm fine wire thermocouple, with a frequency response up to 30 Hz.
- KH20: an ultraviolet krypton hygrometer (Campbell and Tanner, 1985), with a frequency response of 100 Hz.

A horizontal pole of 2 m was used to mount the instruments on the tower at the Beckenham site at a height of 18.1 m. The configuration of the sensors followed the manufacturer's instructions. The thermocouple was not shielded against radiation, which has a negligible effect, according to Campbell Scientific, Inc. The instruments were oriented towards 39° (NE) away from the tower, so that the tower may have disturbed the observations when the wind was between 189° and 249° (south to west south west). The data were recorded by a Campbell 21X datalogger, with a sampling frequency of 10 Hz. Averages of the covariances were collected over 10 minute intervals (6000 samples per average).

Maintenance. The Krypton hygrometer has a window on the source tube which is prone to scaling (deposited water and dust). This scaling attenuates the signal and therefore affects the calibration of the sensor. The window of the hygrometer was cleaned on a daily basis, which should be sufficient to suppress scaling effects. Since the EC equipment is sensitive to liquid water and can be damaged by rain, it was protected when necessary.

2.5.7 Balloon mounted sonde

The sonde is a small instrumented package housed in polystyrene attached to the tethered balloon (see Plate 2.9. The sonde has an antenna for data transmission, two temperature sensors (dry and wet bulb), an anemometer, an electronic compass and a pressure sensor. The wind direction is derived from the compass readings and has to be corrected to true north by adding 23° (magnetic declination). Every 10 seconds the data were transmitted by radio to a receiver at the surface, which was connected to a computer.

The accuracy of the sensors is not known in detail, although simple laboratory calibrations indicated an absolute temperature accuracy of ±1 K, where both sensors are within 0.25 K (both as dry bulb), the anemometer has a threshold of about 0.3 ± 0.1 m s^{-1}, and field data suggested an absolute accuracy of at least within 20%, but it might be better. Laboratory calibrations of the anemometer attached to the blimp were not feasible. The compass has an accuracy within 5°. The barometer had an absolute accuracy ±30 hPa, although this did not restrict the ability to derive the heights of the sonde during a flight. All sensors, except for the barometer appeared to be stable in time, which makes it possible to compare data from different elevations during one flight and also between different flights. The pressure readings however, were not stable: Generally, the pressure just before an ascent appeared to be 0.5 to 1% higher than just after the descent of the blimp, resulting in erroneous heights. A correction procedure to cope with this problem is described in Appendix A. It also appeared that the barometer often showed a series of threshold values at which it changed its output values, creating sudden stepwise pressure changes of 1 to 5 hPa during a steady ascent or descent. This is illustrated in Figure 2.8. The stepwise pressure changes created an increased scatter in the profiles. No correction procedure to reduce this scatter has been developed.

2.5.8 Pilot ballooning

A standard pilot balloon was employed for wind observations at heights from 50 m to more than 2000 m during most of the days when blimp observations were conducted. The balloons were launched between 2 and 3 pm local time and traced from the roof of the Department of Geography building at the University of Canterbury. The single theodolite method was applied (Meteorological Office, 1944; Ryan, 1976). This method requires a known ascent rate which is assumed to be constant, in our situation approximately being 2.0 m s^{-1} (see also Appendix A). The expected ascent rate can be derived from the lift and diameter of the balloon. Deviations between expected and real ascent rate may be caused by:

- incorrect relationship between lift, diameter and ascent rate.
- inaccuracies in values of diameter and lift of the balloon.
- water or ice being deposited on the balloon during its flight.
- vertical winds during the flight
- decreased air density and pressure during the ascent, affecting the balloon's friction and buoyancy.

The errors of the theodolite readings are assumed to be negligible, although incorrect ascent rates will lead to errors in wind profiles. The errors during the 1995 measurements are assumed to be acceptable, especially since the observed profiles did not exceed 3000 m, and the focus of this project is in the near-surface layer. Also major problems can occur during unstable conditions with maximum vertical motion and in complex terrain, neither situations typical of Christchurch on winter days experiencing high air pollution levels.

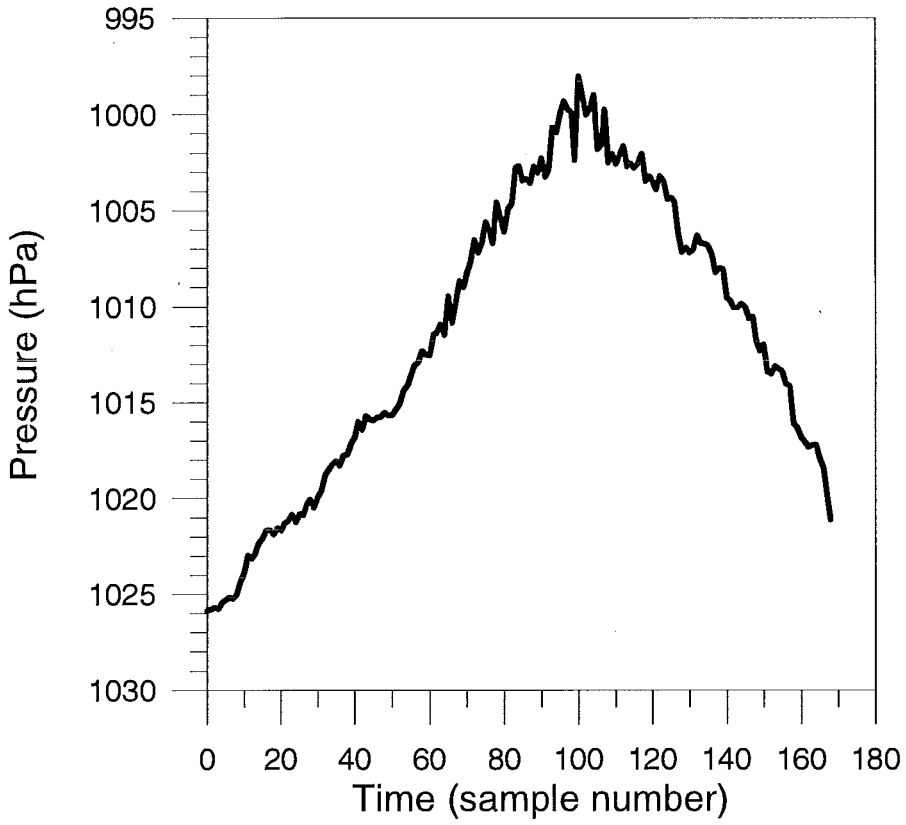

Figure 2.8 Time series of pressure readings obtained from the sonde attached to the blimp on 22 July 1995 at 8 pm. The ascent and descent rates were more or less constant.

2.6 Tools - RAMS: Regional Atmospheric Modeling System

2.6.1 Introduction

RAMS is a flexible, state of the art, prognostic model, able to simulate atmospheric behaviour in three dimensions at scales from the complete Southern Hemisphere to turbulent eddies around individual buildings (Walko et al., 1996). Modelling the atmospheric conditions that control air pollution dispersion in the Christchurch area with its topographic influences, is therefore quite feasible. Several other three dimensional prognostic models exist, such as MM5 (Dudhia, 1993) and MEMO (Moussiopoulos et al.,

1993). RAMS version 3b was chosen for this project, because: **a.** the model contains an extended set of code based on actual physics, **b.** cooperation existed with contacts in NIWA, who were already using RAMS, **c.** the program has flexibility, **d.** it is well documented, and **e.** the model is widely used in the scientific community.

2.6.2 Outline of the model

A summary of RAMS, version 3b, will be given below, but the reader is referred to Pielke et al. (1992) for a general overview, to Tripoli and Cotton (1982) for a detailed description of the model equations and numerical solution schemes and to Walko *et al.* (1996) for a report on model settings and parameterizations. However, certain features of RAMS will be discussed in some detail, since they were important for the simulations undertaken.

The RAMS model is based on the primitive equations (WMO, 1973; Holton, 1979; Pielke, 1984; Bluestein, 1992), that is basically the set of equations expressing the conservation of motion (eqs. 2.1), continuity (eq. 2.2) and thermodynamics (eq. 2.3) without 'sophisticated' simplifications or approximations. For reasons of convenience, the equations are repeated here, based on cartesian local coordinates, where the x-axis points east, the y-axis north and the z-axis is directed positively upwards opposite to the local direction of gravity:

$$\frac{\partial u}{\partial t} = -\vec{v} \bullet \nabla u - \frac{1}{\rho}\frac{\partial p}{\partial x} + fv - ew + \frac{1}{\rho}F_x$$

$$\frac{\partial v}{\partial t} = -\vec{v} \bullet \nabla v - \frac{1}{\rho}\frac{\partial p}{\partial y} - fu + \frac{1}{\rho}F_y \qquad (2.1)$$

$$\frac{\partial w}{\partial t} = -\vec{v} \bullet \nabla w - \frac{1}{\rho}\frac{\partial p}{\partial z} - g + eu + \frac{1}{\rho}F_z$$

$$\frac{\partial \rho}{\partial t} = -\vec{v} \bullet \nabla \rho - \rho \nabla \bullet \vec{v} \qquad (2.2)$$

$$\frac{\partial p}{\partial t} = -\vec{v} \bullet \nabla p - \frac{c_p}{c_v} p \nabla \bullet \vec{v} + \frac{R}{c_v} \rho H \qquad (2.3)$$

with t time, u, v, w the wind speeds in the x, y and z direction, respectively, v the wind velocity, ρ the density of air, $e=2\Omega\cos\varphi$ and $f=2\Omega\sin\varphi$, with Ωthe Earth's rotation and φ the latitude, g is the gravitation acceleration, F is friction, c_p and c_v are the specific heat of air at constant pressure and volume respectively, R is the gas constant of dry air and H is the amount of heat added per unit mass per unit time. In meso-scale meteorology, where small variations become important, it is necessary to consider the turbulent nature of the atmosphere, with the instantaneous value of variable x being the combination of a temporal average $\bar{x}$ and the deviation from the average x':

$$x = \bar{x} + x' \qquad (2.3)$$

It will be obvious, that applying this approach to the full set of equations, parameterizations are necessary for turbulence closure, and a numerical solution will be computationally very demanding. So, several kinds of approximation were invented. Some approximations are length scale dependent such as the hydrostatic approximation, neglecting vertical accelleration, which is only valid when the horizontal scales are not smaller than the vertical scales. During this project the nonhydrostatic mode of RAMS is applied, which is computationally more demanding, but it allows for small horizontal scales. This mode uses the anelastic Boussinesq approximation (Pielke, 1984) which allows deep convection, neglecting the temporal variations of density, except for the buoyancy term $(\rho/\rho')g$. Thunis and Bornstein (1996) give an overview of the different approximations used by a variety of models. The model applies a 1st order turbulence closure scheme, and a few options are available in the model for the formulations. During this project the scheme based on the Smagorinsky (1963) formulation was used for horizontal diffusion and the parameterization according to Mellor and Yamada (1974) was applied for the vertical diffusion.

The model applies an Arakawa C staggered grid for thermodynamic and momentum variables and also staggers variables vertically, with horizontal winds and the Exner pressure function π being defined at half levels, while the vertical wind speed is defined at the layer top. RAMS uses terrain following coordinates, while it is possible to choose cartesian or polar stereographic coordinates. A two way interactive, multiple nested grid scheme is incorporated in RAMS (Clark and Farley, 1984; Walko et al., 1995), which allows focussing on an area of interest, while still being able to resolve larger scale features in an computationally efficient way. The model has constant horizontal grid increments throughout one grid, but the vertical grid increments can be expanded with increasing height. This method creates a higher resolution near the surface, where it is frequently desired.

A damping scheme for vertical gravity waves is applied at the five uppermost levels, in which the amplitudes of the waves are gradually suppressed, so reflection is reduced from the rigid lid at the model top. During all simulations zero-gradient lateral boundaries were used, although the model permits different options. RAMS has a soil model with 11 levels (Tremback and Kessler, 1985) and several different soil types are available. The soil moisture content can be varied by soil layer. It must be noted that the initialization of soil moisture has been recognized as a critical component in the simulation of atmospheric flows (Lyons et al., 1995), since it affects the ratio of the sensible to latent heat fluxes and it changes soil characteristics such as soil heat capacity and soil heat conductivity, which in turn affect the sensible and latent heat fluxes. A vegetation parameterization scheme is available (Avissar and Mahrer, 1988), but it was not used during the project to simplify the simulations.

The surface fluxes are based on similarity theory and calculated by the scheme formulated by Louis (1979). The approximations of the vertical fluxes by the Louis scheme does not require iterations to obtain a solution and is therefore computationally efficient.

RAMS also contains a cloud physics package (Meyers et al., 1992) able to generate cloud formation, precipitation and buoyancy effects due to condensation, but it was not applied during the project, since the complications of cloud physics were not in the scope of the project and the investigated situations had basically clear sky conditions. Two radiation schemes are available, one which neglects the effects of clouds on radiation (Mahrer and Pielke, 1977) The other scheme (Chen and Cotton, 1988) includes effects

such as reflection, absorption and re-emission, and is computationally more demanding. During this project the scheme by Mahrer and Pielke was chosen.

The initialization of the meteorological variables can be achieved by a homogeneous method, using one single vertical profile throughout the model domain, or by Four Dimensional Data Analysis (FDDA), (Fast, 1995), which processes spatially varying atmospheric data and includes a temporal interpolation. During this project the simulations were mostly based on the homogeneous initialization, although the FDDA was made operational and tested. Besides the atmospheric variables, the boundary conditions have to be initialized, such as soil type, soil temperature and soil moisture, land use, sea surface temperature, topography, vegetation type (not applied) and surface roughness length.

2.6.3 Source code

The code of RAMS-3b has been adjusted here and there, but no thorough hunt for 'bugs' deep down in the code has been performed, since the aim of the project was to *apply* a three dimensional prognostic model, not to build one or significantly improve the code. However, the results of the simulations were always checked critically with regard to physical acceptability and the model settings have been kept as simple as possible, because: **a**. it reduces problems associated with interpretation of results; **b**. it avoids the risk of introducing errors by routines performing 'sophisticated' physics, but containing one or more 'bugs'; **c**. the introduction of more realistic (and more complicated) physics is useful only when simple but important initial boundary conditions are accurate. For example, during this project no effects of vegetation were simulated, since the important soil moisture content was not known with any great accuracy. So, the addition of vegetation would not improve the accurary of the sensible and latent heat fluxes. The changes made to the RAMS code are summarized in Table 2.5.

Table 2.5. Changes or additions made to the code of RAMS_3b.

File	Routine(s)	Remarks
ruser.f	toptinit_user	reads topographic data
ruser.f	sfcinitf_user	reads data of sea surface temp., landuse and z_o
ruser.f	varout	generates output variables at specified grid point
rdriv.f	INITLZ + MODEL	calls varout routine
rprint.f	OPTLIB	makes Rn, H, LE, GE available for output
rafld.f	ANALIB	makes Rn, H, LE, GE available for output
ruser.f	force_conc	generates ambient CO concentrations
asgen.f	RAMS_data_prep	activates user input of synoptic data
read_rawi.f	read_rawi	reads input data from radio-sonde soundings
press_read.f	press_read	reads data from pressure grid

3. Examination of surface characteristics and their influence on momentum and heat fluxes in an urban area

3.1 Introduction

As described in Chapter 1, Christchurch has a serious wintertime air pollution problem which is caused by the combination of frequent occurrence of stagnant air associated with a shallow layer of strong temperature inversions and increased emissions due to domestic heating by burning wood and coal. In this chapter, the surface fluxes of momentum and heat, which play an important role in the dispersion of atmospheric pollutants will be investigated in the Chrischurch area. The depth of the mixed layer strongly influences the air pollution concentrations which are experienced at the surface and the surface fluxes play an important role in determining this depth. The theory explaining the trapping of atmospheric pollutants in a stable boundary layer is generally well known (Elsom, 1987; Harrison and Perry, 1986; Lyons and Scott, 1990; Venkatram and Wyngaard, 1988). Oke (1978) described a box-model where air pollution concentrations are inversely proportional to horizontal wind speed and mixing depth. The evolution in time of the mixed layer is closely related to the sensible heat flux (Stull, 1988). Besides diurnal variations, the components of the energy budget may well display spatial variability due to varying surface characteristics (Atwater, 1972; Oke et al. 1991).

The aim of the research discussed in this chapter is to determine the aerodynamic properties related to the momentum flux and the influence of water availability on latent and sensible heat fluxes in the Christchurch area, which can be applied later in modelling studies. Spatial variation of the sensible heat flux may eventually lead to mesoscale circulations (Hjelmfeldt, 1982; Kimura and Takahashi, 1991; Avissar, 1996). Obviously, a high surface roughness generally tends to decrease the wind speed near the surface, so affecting the dispersion of air pollution. However, forced convection, generated by a high surface roughness, affects the mixing depth throug increased turbulence, in particular during the development of the stable nocturnal boundary layer. In a numerical study Byun and Arya (1990) showed an increased mixed layer depth across urban areas due to a combination of urban heat island effects and increased surface roughness, while Uno et al. (1992) reported an elevated nocturnal inversion layer over Sapporo with a near-neutral layer below. In this chapter attention will be given to the urban-rural contrasts in surface fluxes and their relationship to water availability and surface roughness. The findings were only partly included during simulations of the case studies discussed in Chapter 7. Finally, the results as discussed in this chapter could be used more extensively to adjust the boundary conditions of an urban airshed model being developed for the Christchurch area.

Quantifying momentum and heat fluxes can prove difficult in an urban environment, because it is spatially very inhomogeneous and aerodynamically very rough. It is difficult to find locations which are 'representative' and strong mixing of the air results in weak

vertical gradients, making profile methods less accurate. In the following section of this chapter the experimental setup will be discussed, including a brief description of the sites and instruments used. Following that, two methods for evaluating the surface roughness length and displacement height will be described, and finally the energy balance will be presented with several models used to derive the heat fluxes.

3.2 Instruments and data collection

Detailed descriptions of the instruments and sites used can be found in Chapter 2, but for convenience, a brief outline is given here. During winter 1995, observations were obtained from four instrumented towers in the Christchurch area (see Figure 3.1). The 10.5 m tall instrumented towers at Ensors Gardens and Marshland provided wind direction and profiles of wind speed and temperature (both at 5 m and 10.5 m height), while the tower at Marshland also provided humidity profiles. The towers at Beckenham and Burnside High School were 21 m high, providing wind direction and profiles of wind speed, temperature and humidity (at 6, 12 and 21 m) with an additional wind observation at 3 m at the Beckenham site. During 3 weeks in August 1995, eddy correlation equipment was mounted on the Beckenham tower at 18 m height, comprising a one-dimensional sonic anemometer, a fine-wire thermocouple and a Krypton hygrometer, from which the sensible and latent heat fluxes were obtained. Corrections for oxygen (Tanner and Greene, 1989; Campbell Scientific, 1994) and vapour density fluctuations (Webb et al., 1980) were undertaken, as described in Appendix A.

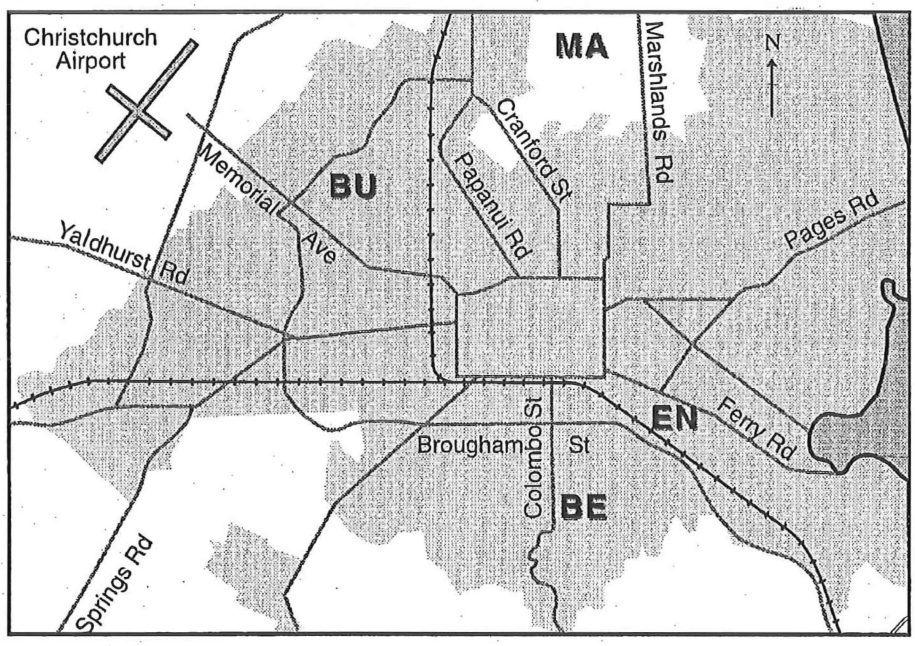

Figure 3.1 Map of the Christchurch area indicating the sites of the instrumented towers. BE=Beckenham; BU=Burnside High School; EN=Ensors Garden; MA=Marshland.

The data presented in this chapter are derived from three data sets: **a.** data set 1, which is the complete dataset, covering the period from the end of June to the beginning of September 1995; **b.** dataset 2, consisting of data from a series of consecutive fine and

relative calm days between 27 July and 1 August 1995 and **c.** dataset 3, composed of mainly fine days during the period from 11 to 28 August 1995 when the eddy correlation equipment was operational. The three hourly readings were assigned to the category 'fine day' when the nocturnal net radiation was less than or equal to -40 W m^{-2}, or it exceeded 100 W m^{-2} at noon or 75 W m^{-2} at 3 pm. The selection of readings shortly after sunrise or sunset at 9 am or 6 pm, respectively, was made on the grounds of preceding conditions (at 6 am or 3 pm, respectively). A reading was in the 'relatively calm' category when the wind speed at 10 m was less than or equal to 5 m s^{-1}.

Data set 1 was used for wind profile analyses, and data set 2 was used to compare the sites of the instrumented towers with respect to temperature, humidity, wind speed and net radiation. Two composite 24 hr time series have been constructed from data sets 2 and 3, using 1 hourly moving average data for both profiles and covariances in order to smooth turbulent fluctuations.

The Marshland site was rural, while the other sites were in residential suburbs. Analysis from aerial photos suggests that within a 2 km radius from the instrumented towers, the fraction of land covered with open green space at Marshland was 80%, 51% at Burnside, 41% at Beckenham and 35% at Ensors Garden.

3.3 Evaluation of the momentum flux by means of the roughness length and displacement height

The momentum flux expresses the quantity of momentum which is transported downwards, predominantly by turbulent processes. The momentum flux is basically caused by surface friction, generating a vertical wind shear. The momentum flux τ is proportional to the density of air ρ and the friction velocity u_* squared:

$$\tau = -\rho\, u_*^2 \tag{3.1}$$

where the friction velocity represents the turbulence of the air

$$u_* = \left[\overline{u'w'}^2 + \overline{v'w'}^2\right]^{1/4} \tag{3.2}$$

with u and v perpendicular horizontal wind speeds, w the vertical wind speed and the prime (') denotes the turbulent deviation from the average values. The strength of advection and the degree of turbulent mixing are important properties when considering dispersion of atmospheric pollutants. Two important parameters, which are directly related to horizontal wind speed and turbulence (or friction velocity), are the roughness length z_o and displacement height d, as given by the well known logarithmic wind profile, based on the Monin-Obukhov similarity theory

$$u(z) = \frac{u_*}{k}\left[\ln\left(\frac{z-d}{z_o}\right) - \Psi_M\left(\frac{z-d}{L}\right) + \Psi_M\left(\frac{z_o}{L}\right)\right] \tag{3.3}$$

with k the Von Karman 'constant' (0.40), Ψ_M the stability correction function and L the Monin-Obukhov length. Both parameters z_o and d are strongly dependent on the type of landuse, e.g. rural covered with grassland, rural covered with crops, urban-residential, urban-commercial, etc. Classifications and empirical relationships between landuse and the parameters roughness length and displacement height have been established, but they show a relatively wide range of possible values for each type of landuse. Therefore, actual observations were undertaken in the Christchurch area, in order to determine local values.

The aerodynamic surface parameters at the rural site in Marshland were obtained using an aerodynamic profile method, while at the suburban site of Beckenham a mass conservation method was used as well. Both methods could not be applied at the Burnside High School site and at the Ensors Gardens, because less then 3 anemometers were operational at these sites, which is a minimum for deriving both the roughness length and displacement height with the profile method. In addition, empirical relationships have been applied to obtain the roughness length and displacement height for all sites.

3.3.1 Aerodynamic method

Fluxes in the surface layer can be obtained by using profiles of wind, temperature and other relevant scalars, such as humidity. Haenel (1993) presented an aerodynamic model based on Monin-Obukhov Similarity Theory (see also Dyer, 1974; Yaglom, 1977; Brutsaert, 1982). The method requires observations at three different elevations as a minimum when the roughness length and displacement height have to be derived, and at two elevations as a minimum when one of these parameters is known beforehand. At the relatively open Marshland site with short vegetation d was fixed at 0.05 m. In this study, a model based on the methods described by Haenel (1993) was developed and tested successfully using data sets provided by Haenel (1993) and Kramm (1989). The model was applied to 1 hourly averaged wind speeds with the 10 m wind speed equal to or exceeding 1.0 m s^{-1}, and it could only be used for data sets from Beckenham and Marshland, as explained above. However, the model was not able to converge its iterations using data obtained in the aerodynamically rough environment of the Beckenham site. Monin-Obukhov similarity theory is valid only in the inertial sublayer, which ranges from a minimum height above the surface to the top of the surface layer. According to Tennekes (1982) the lower limit of the inertial sublayer z_l can be approximated by

$$z_l >> d + 20\, z_o \qquad (3.4)$$

where d is the displacement height and z_o is the roughness length for momentum.

3.3.2 Mass conservation method

A second method was applied to obtain the roughness length and displacement height at the Beckenham site, because the profile method resulted in very inaccurate results. The displacement height d and roughness length for momentum z_o were estimated at the Beckenham site by using the mass conservation method as presented by De Bruin and Moore (1985), which was extended to neutral and unstable conditions.

The mass conservation method is based on the principle that at a height z_n, sufficient above the surface for negligible deviations from the logarithmic wind profile as described by Monin-Obukhov similarity theory, the wind speed u can be calculated by application of equation (3.3), substituting z by z_n. Below height z_n deviations from the Monin-Obukhov similarity theory profile can occur due to vegetation or other objects. However, the

vertically integrated horizontal mass flux, which actually occurs, has to equal the vertically integrated mass flux according to the Monin-Obukhov similarity theory model with the appropriate parameters d and z_o, so that

$$\int_o^{z_n} u(z)dz = \int_{d+z_o}^{z_n} \frac{u_*}{k}\left[\ln\left(\frac{z_n - d}{z_o}\right) - \Psi_M\left(\frac{z_n - d}{L}\right) + \Psi_M\left(\frac{z_o}{L}\right)\right]dz \qquad (3.5)$$

with z the height above the surface. The observed wind speeds at different heights are interpolated by second order polynomials and the wind speed at z=0 is assumed to be zero (u(0)=0).

The mass conservation method, as described above, requires independent data for the friction velocity and the Monin-Obukhov length. Since no three-dimensional sonic anemometer was available, u_* could not be obtained directly. However, according to K-theory (Stull, 1988), the friction velocity can be approximated by

$$u_*^2 = K_M \frac{\partial u}{\partial z} \approx K_M \frac{\Delta u}{\Delta z} \qquad (3.6)$$

and the eddy diffusivity for momentum K_M relates to the eddy diffusivity for heat K_H by:

$$K_M = c_K K_H \qquad (3.7)$$

with $c_K \approx 1.35$. The value of c_K may be dependent on a variety of conditions. Roth and Oke (1995) showed that the efficiency of turbulent transport for heat, vapour and momentum are all different, especially in aerodynamically rough and heterogeneous terrain, where the flux sources may have different locations. The ratios of the efficiencies also appeared to be dependent on atmospheric stability and this may well be true for the ratio K_H / K_E as well. According to K-theory, the sensible heat flux H is proportional to the vertical gradient of temperature:

$$H = -\rho\, c_p\, K_H \frac{\partial \Theta}{\partial z} \approx -\rho\, c_p K_H \frac{\Delta\Theta}{\Delta z} \qquad (3.8)$$

with c_p specific heat of air at constant pressure, and θ the potential temperature. Here, the sensible heat flux data were obtained using the Bowen ratio method. Substituting equations (3.7) and (3.8) into equation (3.6) yields

$$u_*^2 \approx -c_K H \frac{\Delta u}{\Delta\Theta} / \left(\rho\, c_p\right) \qquad (3.9)$$

while the Monin-Obukhov length can simply be obtained from

$$L = -u_*^3 \rho\, c_p \overline{\Theta} / \left(kgH\right) \qquad (3.10)$$

(Stull, 1988) with g the gravitational acceleration.

Finally, using the above mentioned assumptions and relationships, the roughness length z_o and displacement height d can be derived from equations (3.3) and (3.5).

3.3.3 Classification and empirical relations

The actual determination of the roughness length z_o and displacement height d in a given environment can be expensive or impractible. It would be efficient, for example for modeling purposes, to make a classification or to construct empirical relationships between a certain type of land use and the parameters z_o and d. Attempts have previously been undertaken to classify the roughness length and displacement height (see Table 3.1). Empirical relationships have been constructed to relate the roughness length z_o to vegetation or objects on the surface. For a rural environment Szeicz et al. (1969) proposed:

$$z_o = c_1 . h \tag{3.11}$$

with h the height of the vegetation and $0.03 < c_1 < 0.15$, being dependent on the nature of the vegetation. For an urban environment Oke (1978) and Kondo and Yamazawa (1986) used:

$$z_o = \frac{c_2}{S_T} \sum h_i \, s_i \tag{3.12}$$

where S_T is the total area, h_i the height of building i, s_i the surface area of building i and c_2 is an empirical constant (0.25 suggested). As shown in Table 3.1 a wide range of values for roughness length z_o and displacement height d can be derived for each surface type.

Table 3.1 Aerodynamic properties of several surfaces, with $d \approx 0.667$ times canopy height, after Oke (1978), Wieringa (1986) and Stull (1988).

Short description	z_o (m)	d (m)
Water/sea	1.0E-5 - 0.1	-
Open flat terrain, grass, few obstacles	0.01 - 0.03	< 0.07
Low crops	0.01 - 0.10	< 1.00
High crops	0.10 - 0.25	1.50 - 3.00
Parkland, bushes, many obstacles	0.40 - 0.60	0.50 - 5.00
Regular large obstacles, suburb, forest	0.30 - 6.00	< 30.0
City centre	0.80 - 1.10	5.00 - ?

3.4 Derivation of energy fluxes

The nature of energy fluxes at the air-surface interface can be described by using an energy balance approach. In order to simplify matters, the energy balance is defined at a horizontal plane at the top of the urban canopy layer, following the concept of Oke (1978) (see Figure 3.2). In our case, the urban canopy layer is defined at a height of 18 m, being well above most of the objects in the environment and therefore it is considered at the top of the urban canopy layer. The energy balance is given by:

$$R_n + F + A = H + LE + GS \quad (3.13)$$

with R_n the net radiation, F the anthropogenic heat flux, A the advective heat flux and GS the ground storage heat flux. The ground storage heat flux is the energy flow into a volume from the top of the urban canopy layer down to a depth into the soil or buildings and structures where no significant energy flow occurs. Land cover appears to be very important for the individual components of the energy balance through such factors as albedo, emissivity, three dimensional structures trapping radiation, availability of water, thermal admittance and spatial variability generating advection. (Auer 1978; Oke, 1978; Kerschgens and Kraus, 1990; Johnson et al., 1991; Grimmond et al., 1991).

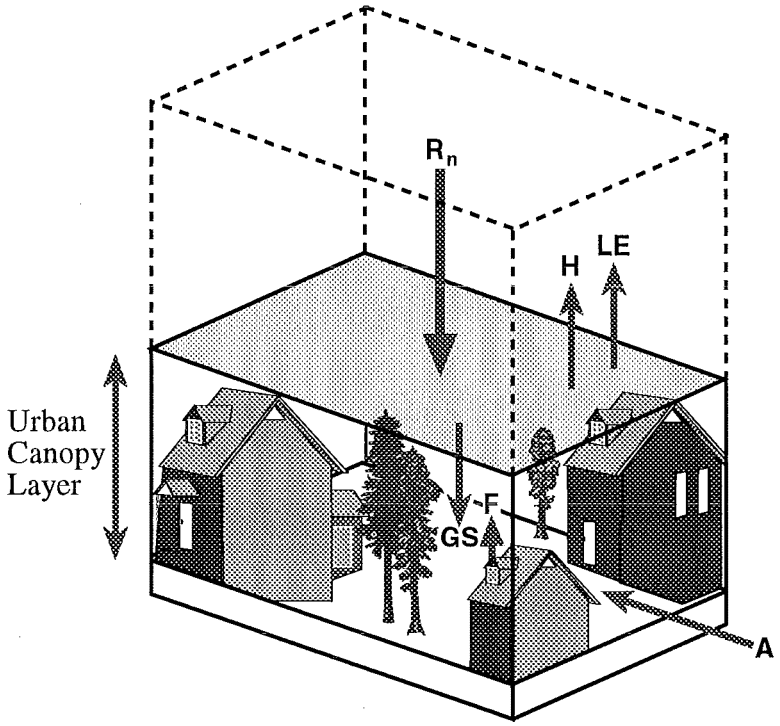

Figure 3.2 Energy fluxes in an urban environment shown in a schematic way. R_n: net radiation; *A*: advection; *F*: anthropogenic heat; *H*: sensible heat; *LE*: latent heat; *GS*: ground storage.

A brief description of each of the heat fluxes is given below:

R_n: the net radiation appears to be spatially conservative in the urban environment, despite the heterogeneity of the surface (White et al., 1978; Arnfield, 1982; Oke et al., 1989; Grimmond et al., 1991). During full daytime, the differences in net radiation between rural and urban sites appears to be small and can be within the error of the estimation technique (Oke, 1988), while during the night the radiative loss at urban sites appears to be larger than at rural sites (Cleugh and Oke, 1986). However, conditions for particular cities may vary due to the influence of albedo, emissivity, surface temperatures, turbidity (smog) and street geometry (Eliasson, 1996; Sakakibara, 1996).

F: the anthropogenic heat flux can be very substantial in inner cities, but reduces in significance in residential suburbs (Oke, 1978). Tapper et al. (1981) estimated an average *F* for Christchurch, New Zealand, around 3.9 W m^{-2}, derived from daily consumption of

fuels and electricity, while updated data (Canterbury Regional Council, 1997) indicate an average around 6.2 W m^{-2}. In this study we neglect F altogether.

A: advection in an urban environment exists at different scales and is dependent on the height of observation. Disregarding advection at the micro-scale, it is generally not significant in cities, except when large contrasts exist in land use (Ching et al., 1983; Steyn, 1985). In this study, no evidence was found of significant advection for hourly averaged intervals. The advective heat flux is therefore neglected here.

H and ***LE***: sensible and latent heat flux, respectively. The sensible and latent heat fluxes H and LE were measured directly at Beckenham by eddy correlation, with

$$H = \rho\, c_p \overline{w'T'} \tag{3.14}$$

$$LE = \rho\, L_v \overline{w'q'} \tag{3.15}$$

where T is the temperature of the air and q is the specific humidity. The Bowen ratio method was also used, where

$$H = \left(\frac{\beta}{1+\beta}\right)(R_n - GS) \tag{3.16}$$

$$LE = \left(\frac{1}{1+\beta}\right)(R_n - GS) \tag{3.17}$$

with β the Bowen ratio ($=(c_p\Delta T)/(L_v\Delta q)$), obtained from the temperature and humidity differences between 6 and 21 m heights, where L_v is the latent heat of vaporisation. The 12 m to 21 m profiles were not used due to reduced differences and limited sensor accuracies. R_n is the net radiation and GS is the ground storage heat flux, which in reality is obtained as either the residual heat flux or as a modelled heat flux, as discussed later.

Neglecting the anthropogenic heat flux and heat advection, the net energy available for sensible and latent heat flux equals net radiation minus the ground storage heat flux. Under ideal conditions with abundant water at the surface the energy used for evaporation yields

$$LE_{eq} = \left(\frac{s}{s+\gamma}\right)(R_n - GS) \tag{3.18}$$

with LE_{eq} the so-called `equilibrium evaporation' (Priestley and Taylor, 1972; De Bruin and Keijman, 1979), s the change of the saturation specific humidity with temperature and γ the psychrometric parameter ($=c_p/L_v$), being slightly temperature dependent. The fraction $s/(s+\gamma)$ is strongly temperature dependent, so that it equals 0.41 at 0° C, 0.54 at 10° C, 0.69 at 20° C and 0.79 at 30° C, respectively. During this analysis, temperatures measured at the 3 m height were used to derive s and γ. Water may not be abundant at the surface, creating a resistance to evaporation and other factors may have an influence on evaporation as well. A simple linear parameterization for daytime latent heat flux was presented by De Bruin and Holtslag (1982) and further described by Holtslag and Van Ulden (1983):

$$LE = b_1\left(\frac{s}{s+\gamma}\right)(R_n - GS) + b_2 \qquad (3.19)$$

where b_1 and b_2 are not only empirical constants, but can be given the physical meaning of water availability and the contribution factor due to horizontal advection and entrainment, respectively. De Bruin and Holtslag (1982) reported $b_1 \approx 1.0$ and $b_2 \approx 20$ W m^{-2} for a well watered grass covered area during fine weather in late spring in The Netherlands. When water stress occurs, b_1 is supposed to decline ($0 < b_1 < 1$). In this study we consider b_2 constant, although Van Ulden and Holtslag (1985) related it to friction velocity u_*. Substituting equation (3.19) into equation (3.13) and neglecting the terms A and F in the energy balance gives a sensible heat flux:

$$H = \left(\frac{s(1-b_1)+\gamma}{s+\gamma}\right)(R_n - GS) - b_2 \qquad (3.20)$$

In an urban environment, evaporation mainly occurs from open green space, and since significant areas in a city are covered with pavement and buildings, the average water availability is reduced. The limited water availability in cities can be an important contributor to the urban heat island phenomenon, although other factors will contribute as well (Oke, 1982; Johnson et al., 1991; Oke et al., 1991). Several authors reported a decreased urban evaporation compared to the rural surroundings (Cleugh and Oke, 1985; Oke, 1988; Kerschgens and Kraus, 1990), but the reverse can happen as well with irrigated gardens and parks in the suburbs, surrounded by a dry rural environment (Myrup et al., 1993; Avissar, 1996). Hjelmfeldt (1982), Byan and Arya (1990) and Avissar (1996) demonstrated, by using numerical models, that mesoscale circulations can be induced by differential heating across the urban - rural interface, partly due to differences in water availability. The water availability is related to, but generally not equal to the Bowen ratio. Combining equation (3.17) with equation (3.19) and neglecting b_2 yields:

$$b_1 = \left(\frac{1}{1+\beta}\right)\Big/\left(\frac{s}{s+\gamma}\right) \qquad (3.21)$$

which shows the relation between b_1 and the Bowen ratio. The average water availability values derived from Oke (1988) for typical summertime energy balances in urban, suburban and rural areas, are 0.50, 0.68 and 0.97 respectively, indicating a relative dry, moderately dry and a humid surface or vegetation having good access to water. The fieldwork on which this chapter is based was undertaken during the winter when the soil of open green space was generally humid, so values of b_1 were expected to be close to unity for rural sites.

GS: ground storage heat flux. In this study, the ground-storage heat flux GS was obtained as a residual flux, and therefore contains also a combination of measurement errors associated with net radiation, sensible and latent heat fluxes, as well as part of the neglected anthropogenic heat flux and advection. The ground storage heat flux can be related linearly to net radiation (Oke, 1978; De Bruin and Holtslag, 1982) as

$$GS = aR_n + b \qquad (3.22)$$

with a and b empirical parameters. However, urban studies indicate a phase shift of the ground storage heat flux, peaking earlier than net radiation. Grimmond et al. (1991)

explained the phase shift by the existence of a shallow mixed layer in the morning hours, causing sensible heat to be more readily transferred into the soil and structures rather than being dispersed through the atmosphere by turbulence. Another explanation may be that in the morning hours the temperatures of the outer layers of the soil and buildings are at a minimum, and they are absorbing heat rather than releasing it to warm the air or causing evaporation. Camuffo and Bernardi (1982) formulated an empirical relationship for GS, showing a phase lag between the ground storage and net radiation

$$GS = a_1 R_n + a_2 \frac{\partial R_n}{\partial t} + a_3 \tag{3.23}$$

with a_1, a_2 and a_3 regression coefficients. Grimmond et al. (1991) related the coefficients a_1 to a_3 to land cover, which can be used in combination with an advection model such as the Source Area Model (Schmid et al., 1991). It appears however, that *GS* is not very sensitive for a variable source area in the urban environment, except when strong contrasts in land cover exist. Another method is follows the approach of the German 'Grundlichkeit' (thoroughness), as applied by Kerschgens and Kraus (1990) who estimated the urban heat storage by using the temperatures of walls outside and inside selected buildings, and taking into account the orientation of buildings and fractions of shaded and sunlit areas. It is obvious, that by following their approach, the estimation of the ground storage heat flux quickly becomes extremely complicated and laborious.

By defining the energy balance at the top of the urban canopy layer, part of the ground storage heat flux is used to heat and moisten the air contained within the urban canopy layer. Defining this the 'air part of the ground storage heat flux' (G_A), it follows that

$$GS = G_A + G_{NA} \tag{3.24}$$

with G_{NA} the non-air part of the ground storage heat flux, which represents the energy used for heating (or cooling) of soil, buildings and other objects in the canopy layer. Introducing f_{air} as the fraction of the urban canopy layer filled with air (≈0.85) at Beckenham with a canopy height of 18 m) and Δz the height of the canopy layer, G_A can be obtained by

$$G_A = f_{air} \rho \, \Delta z \left(c_p \frac{\partial T}{\partial t} + L_v \frac{\partial q}{\partial t} \right) \tag{3.25}$$

A simple calculation shows that on a sunny day in mid winter, with the urban canopy layer at 18 m and 85% of the urban canopy layer filled with air, and an average air temperature increase of 10 K during the interval 10 am to 2 pm local time, the average heat storage flux used to warm the air will be 14 W m^{-2}, being about 15% of the total ground storage heat flux *GS* (see Figure 3.3).

The parameterization of the ground storage heat flux GS according to equation (3.23) could be dependent on the selected height of the urban canopy layer, and therefore on the volume of air that it contains. A way to investigate this dependency, is to split the ground storage heat flux *GS* into the air-part G_A and non-air component G_{NA}. A comparison of the parameterizations of *GS* and G_{NA} according to equation (3.23) will indicate the influence of the air volume.

3.5 Results

So far, in the preceding sections it was suggested that land use and therefore urbanization has significant effects on momentum and heat fluxes. If these effects indeed do exist in the Christchurch area, then local wind speed, temperature and humidity must be influenced as well. The advantage of investigating local wind speed, temperature and humidity is that they can be considered as an integrated expression of the momentum, sensible and latent heat flux, respectively, in time and local space. Using the concept of internal boundary layers (Garrett, 1990), let us consider two approximate areas (e.g. Christchurch and the Canterbury Plains). The area which experiences reduced wind speeds, higher temperatures and lower humidity levels within the internal boundary layer, is expected to have a higher aerodynamic roughness and a dryer surface than the other area.

First, comparisons will be given of wind speed, temperature and humidity at different sites in the Christchurch area. This is followed by analysis of the roughness length z_o and displacement height d, and finally the heat fluxes will be described.

3.5.1 Comparisons of wind speed, temperature and humidity in the Christchurch area

It follows from the theory explained in the former section, that in an urban environment with a relatively high aerodynamic roughness at the surface and reduced areas with green space, the 10 m observations of wind speed, temperature and humidity will show on average lower wind speeds, higher daytime temperatures and lower humidity recordings compared to rural sites nearby. An important assumption made here is that the observation sites are not seriously influenced by local effects such as local advection of momentum or heat, variations in albedo, and topographic effects such as wind funnelling or sheltering.

Tables 3.2 to 3.5 show data from the four instrumented towers in the Christchurch area on fine days during the 1995 winter season. Statistical t-tests are conducted to indicate the significance of deviating values. Table 3.2 shows a diurnal pattern of the average wind speed on fine days, with a pronounced maximum in the afternoon at 3 pm and a minimum at the end of the night at 6 am. The average 24 hr wind speed from data set 2 is slightly more than 2.5 m s^{-1} with 24 hr averaged deviations ranging from -0.25 m s^{-1} at both Beckenham and Burnside up to +0.40 m s^{-1} at Marshland. So, differences of 24 hr averaged 10 m wind speeds are nearly 25% of the average wind speed in the area stretching from Beckenham to Marshland and Burnside to Ensors Garden. The wind speed is below average consistently at both Beckenham and Burnside, reaching their extremes exceeding -0.5 m s^{-1} at 6 pm and 3 pm, respectively. At Ensors Garden the wind speed is nearly continuously above average, but the deviations are not very high. However, at the Marshland site the wind speed recordings are continuesly above average, peaking during the afternoon with deviations exceeding +0.65 m s^{-1}. The differences in wind speed between the four sites during the night reached 0.6 m s^{-1} (25%) and during the afternoon exceeded 1.0 m s^{-1} (30%).

Table 3.3 shows clearly the expected average diurnal pattern of temperature on fine days during the winter, with an average minimum of 4.7° C at 6 am and an average maximum of 9.8° C at 3 pm. The 24 hr averaged temperature from data set 2 is 6.8° C, with deviations ranging from -0.18° C to +0.37° C. Over the 24 hr period, Beckenham and Burnside appear to be the coldest sites and Ensors Garden the warmest. Except for the Ensors

Garden site, which is consistently warmer than average, the other sites show some variability in the sign of the deviations. Nevertheless, it is obvious that most of the time Beckenham and Burnside are colder than average and the Marshland deviations fluctuating around zero.

Table 3.2 10 m wind speeds (m s^{-1}) at the 4 instrumented towers in Christchurch on fine days during the winter 1995 (end of June to beginning of September). Time: local time (hr); fave: average wind speed for all sites; fBe, fBu, fEn, and fMa: wind speeds at Beckenham, Burnside, Ensors Garden and Marshland, respectively. **bold**: wind speed of site is significantly different from all other sites (α=0.05); N: number of cases; AVE: 24 hr average.

Time	fave	(fBe-fave)	(fBu-fave)	(fEn-fave)	(fMa-fave)	N
0	2.34	-0.24	-0.22	+0.10	+0.35	30
3	2.40	-0.02	-0.31	+0.05	+0.28	31
6	2.04	-0.18	-0.17	+0.27	+0.07	32
9	2.31	-0.15	-0.29	+0.07	+0.37	32
12	3.32	-0.44	-0.11	-0.13	**+0.67**	48
15	3.67	-0.23	-0.53	+0.08	**+0.67**	44
18	2.47	**-0.55**	-0.20	+0.19	**+0.57**	43
21	2.55	-0.16	-0.13	+0.09	+0.19	33
AVE	2.64	-0.25	-0.25	+0.12	+0.40	-

Table 3.3 10m temperatures (° C) at the 4 instrumented towers in Christchurch on fine days during the winter 1995. Time: local time (hr); Tave: average temperature for all sites; TBe, TBu, TEn, and TMa: temperatures at Beckenham, Burnside, Ensors Gardens and Marshland, respectively. **bold**: temperature of site is significantly different from all other sites (α=0.05); N: number of cases; AVE: 24 hr average.

Time	Tave	(TBe-Tave)	(TBu-Tave)	(TEn-Tave)	TMa-Tave)	N
0	5.12	-0.18	-0.25	**+0.39**	+0.04	30
3	5.33	+0.02	-0.44	**+0.56**	-0.14	31
6	4.67	-0.39	-0.34	**+0.64**	+0.09	32
9	6.34	+0.08	-0.38	**+0.51**	-0.21	32
12	9.33	**-0.21**	+0.06	+0.11	+0.05	48
15	9.80	-0.14	**+0.32**	0.00	-0.18	44
18	7.36	**-0.26**	-0.07	**+0.27**	+0.06	43
21	6.54	-0.15	-0.37	**+0.48**	+0.04	33
AVE	6.81	-0.15	-0.18	+0.37	-0.03	-

Table 3.4 displays a smooth diurnal pattern of the average specific humidity, quite similar to the temperature wave, with a minimum at 6 am and a maximum at 3 pm. The 24 hr averaged specific humidity was 4.66 g kg^{-1} with deviations ranging from -0.10 g kg^{-1} at Beckenham to +0.12 g kg^{-1} at Marshland. Obviously, the Beckenham site was the driest and the Marshland site the most humid, the differences being most pronounced during the afternoon.

In addition, the energy input was investigated at two different sites. Table 3.5 shows that during daytime the Burnside site received about 10% more net radiation than the Beckenham site, but during the night the differences were negligible.

Table 3.4 10m specific humidities (g kg^{-1}) at 3 instrumented towers in Christchurch on fine days during the winter 1995. Time: local time (hr); qave: average specific humidity for the three sites; qBe, qBu and qMa: specific humidity at Beckenham, Burnside and Marshland, respectively. **bold**: specific humidity of site is significantly different from all other sites (α=0.05); N: number of cases; AVE: 24 hr average.

Time	qave	(qBe-qave)	(qBu-qave)	(qMa-qave)	N
0	4.42	-0.09	+0.02	+0.07	30
3	4.33	-0.01	-0.10	+0.11	31
6	4.18	-0.03	-0.04	**+0.08**	32
9	4.53	+0.02	**-0.10**	+0.08	32
12	5.09	**-0.17**	+ 0.01	**+0.18**	48
15	5.01	**-0.23**	+ 0.04	**+0.19**	44
18	4.93	**-0.15**	+ 0.01	**+0.14**	43
21	4.75	-0.11	-0.01	**+0.11**	33
AVE	4.66	-0.10	-0.02	+0.12	-

Table 3.5 Net radiation (W m^{-2}) at the instrumented towers at Beckenham and Burnside, Christchurch on fine days during the winter 1995. Time: local time (hr); Rave: average net radiation for both sites; RBe, RBu: net radiation at Beckenham and Burnside, respectively. **bold**: net radiation of site is significantly different from the other site (α=0.05); N: number of cases.

Time	Rave	(RBe-Rave)	(RBu-Rave)	N
0	-50.9	-0.3	+0.3	30
3	-47.1	+0.4	-0.4	31
6	-48.9	-0.4	+0.4	32
9	+47.6	**+7.1**	**-7.1**	32
12	+197.0	**+14.7**	**-14.7**	48
15	+117.4	**+8.8**	**-8.8**	44
18	-46.6	-0.2	+0.2	43
21	-46.6	-0.7	+0.7	33
AVE	121.9	+29.4	-29.4	-

3.5.2 Aerodynamic properties

As mentioned before, the roughness length z_o and displacement height d were obtained by using the aerodynamic method, mass conservation method and by applying empirical relations (see Table 3.6). The aerodynamic method was applied on data sets from Beckenham and Marshland, but it failed to produce results for the Beckenham site. However, the mass conservation method could be applied on the Beckenham set, yielding realistic results.

Table 3.6 shows estimations of the roughness length z_o and displacement height d at the four sites in the Christchurch area. According to the aerodynamic method, the Marshland site appeared not to be as aerodynamically smooth as the empirical data suggest, giving z_o=0.29 ± 0.27 (m). However, it must be noted that the displacement height d was fixed at 0.05 m. A re-run using the same data set with d=0.15 m produces z_o=0.27 ± 0.25 (m). Since data were available at only two elevations at the Marshland site, the profile method did not allow solving both z_o and d. However, at Beckenham the mass conservation method

produced results which were quite similar to the values obtained by the empirical method, although the accuracy of the values from the mass conservation method is restricted. The mass conservation method produced a roughness length z_o=0.60 ± 0.18 (m) and a displacement height d=4.50 ± 0.63 (m). At Burnside and Ensors Garden values could only be obtained from the empirical method.

Table 3.6 Roughness length z_0 (m) and displacement height d (m), estimated by: I. empirical relations (eqs. (3.11) and (3.12) or Table 3.1), II. profile method and III. mass conservation method.

Location	I		II		III	
	z_0	d	z_0	d	z_0	d
Beckenham	0.45	4.67	-	-	0.60	4.50
Burnside	0.35	3.50	-	-	-	-
Ensors Garden	0.35	3.50	-	-	-	-
Marshland	0.05	0.05	0.29	0.05	-	-

The mass conservation method appears to be relatively sensitive to changes of K_M, in particular z_o. Expressing the sensitivity of z_o as the change of z_o (Δz_o) relative to z_o divided by the change of K_M (ΔK_M) relative to K_M

$$\frac{\Delta z_o / z_o}{\Delta K_M / K_M} = 1.58 \tag{3.26}$$

and similarly the sensitivity of d as

$$\frac{\Delta d/d}{\Delta K_M / K_M} = -0.64 \tag{3.27}$$

which suggests that a relative small change in K_M leads to a relative larger change in z_o, while d appears not so sensitive. The interpretation of these results is that a relative inaccuracy of K_M, and therefore also a relative inaccuracy of parameter c_k, leads to an even higher relative inaccuracy of z_o, while the relative inaccuracy of d is not as high. Also, a value of K_M which is too high generates a value of z_o which is also too high, and a value of d which is too low, and visa versa. The application of equation (3.4), using the values of z_o and d for the Beckenham and Marshland sites, suggests that the lower limits of the inertial sublayer range from 13.5 m to 16.5 m at the Beckenham site and 1.00 m to 5.85 m at the Marshland site (see Table 3.6). Given the heights of the observations, these results indicate that the aerodynamic method is invalid at Beckenham and at Marshland could be valid, although the height of the inertial sublayer reached almost 6 m, when applying equation (3.4) and using the roughness length and displacement height obtained by the aerodynamic method.

3.5.3 Heat fluxes

The fluxes of the composite time series (data set 3) which are displayed in Figure 3.3 are an average of at least 4 and at most 11 days. It is obvious that the time series does not represent an ideal and smooth pattern. First, the ground storage heat flux will be discussed, followed by the sensible and latent heat fluxes. Finally, the water availability factor will be described.

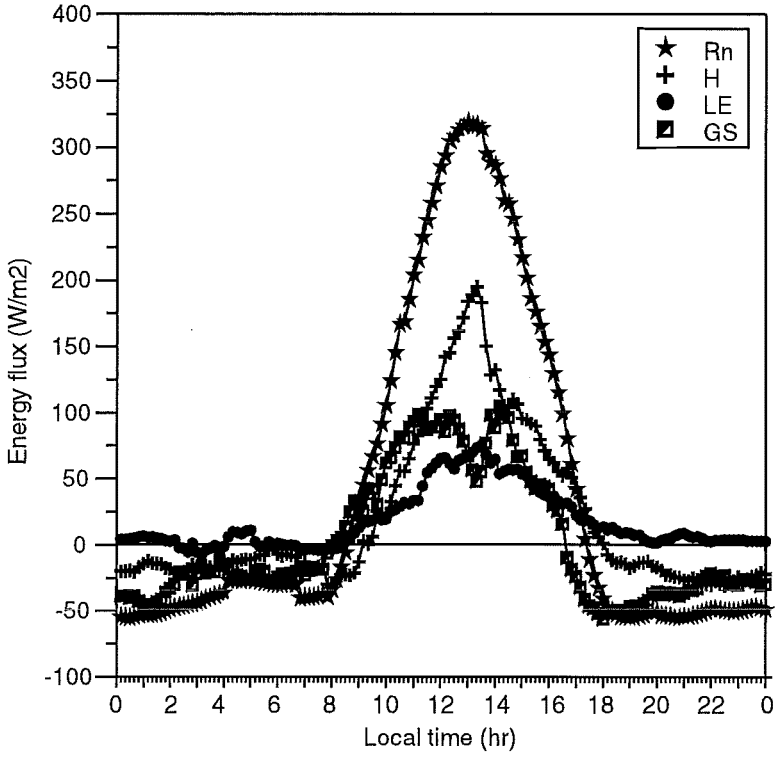

Figure 3.3 Composite time series of energy fluxes at the Beckenham site using data set 3. Sensible and latent heat fluxes are obtained from eddy correlation observations. Time: local time, Rn: net radiation, H: sensible heat, LE: latent heat, GS: residual ground storage.

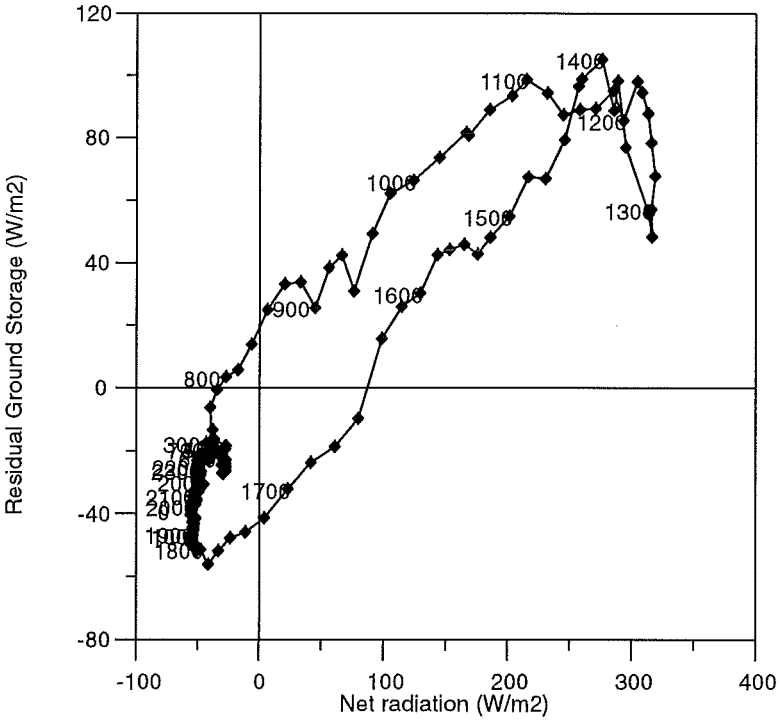

Figure 3.4 Residual ground storage heat flux (W m^{-2}) as a function of net radiation.

Modelling the ground storage heat flux GS. Figure 3.4 shows an important phase shift between net radiation and the residual ground storage heat flux. Multiple regression analysis, relating the ground storage heat flux with net radiation and the change of net radiation over time, using equation (3.23), provides a_1=0.362, a_2=0.224 hr and a_3= -12.1 W m^{-2}. Restricting the regression to daytime data (8-18hr) yields: a_1=0.327, a_2=0.226 hr and a_3= -4.32 W m^{-2}, which is quite similar to the results obtained from the 24 hr data set. These results indicate that about 35% of the net radiation is used for ground storage and the net radiation flux has a time lag of nearly 15 minutes with respect to the ground storage heat flux. In Figure 3.5 the observed residual ground storage heat flux is displayed as a function of the modelled ground storage heat flux found by multiple regression over a 24 hour period. Although significant scatter still exists, the model shows a good linear fit. It must be realized however, that the results represent an average over several days and that further smoothing occurred by using moving average data, averaged over one hour intervals.

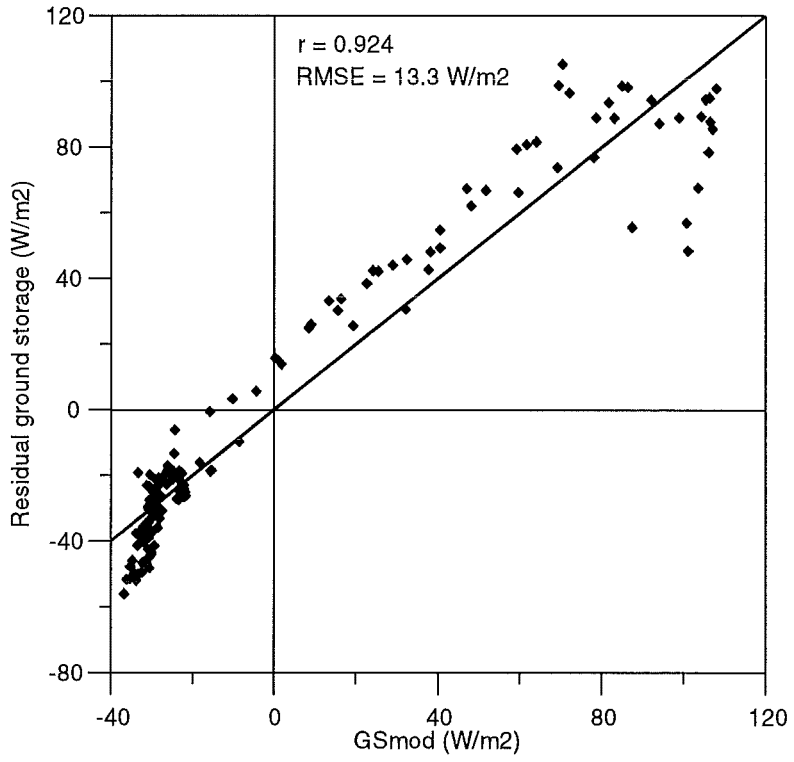

Figure 3.5. Residual ground storage heat flux (W m^{-2}) as a function of modelled ground storage heat flux (GSmod) as given by eq. (3.23).

G_{NA} can be obtained from observations by using the residual ground storage heat flux and by combining equations (3.24) and (3.25). Multiple regression by applying equation (3.23) with GS replaced by G_{NA} yields: a_1=0.360, a_2=0.162 hr and a_3= -11.8 W m^{-2}. Comparing the paramaters a_1 to a_3 obtained by GS with the parameters obtained by G_{NA} suggests that the volume of air in the urban canopy layer has a substantial influence on the parameterization, especially on the phase shift (a_2) and the offset (a_3).

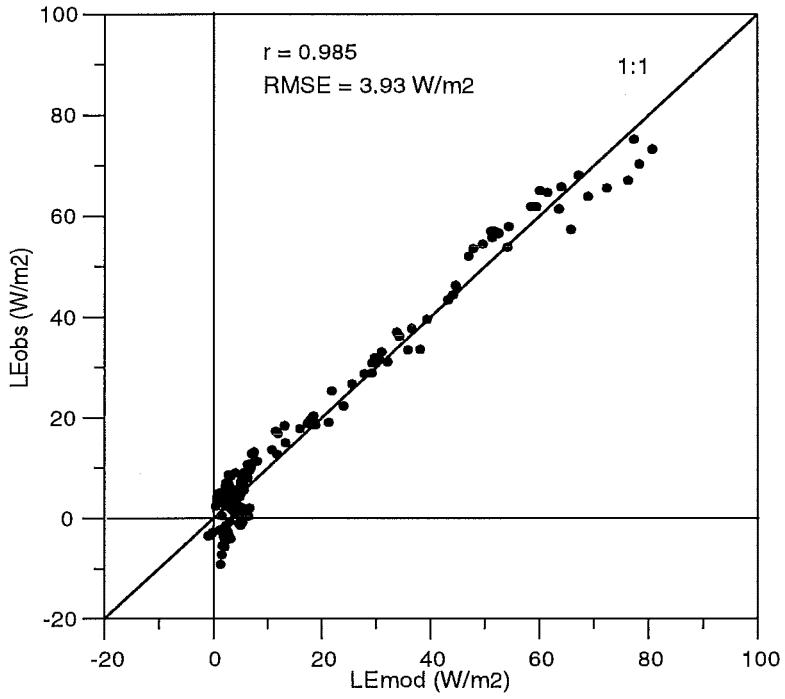

Figure 3.6 Observed latent heat flux by eddy correlation (LEobs) as a function of modelled latent heat flux (LEmod), given by equation (3.19) at Beckenham, using data set 3.

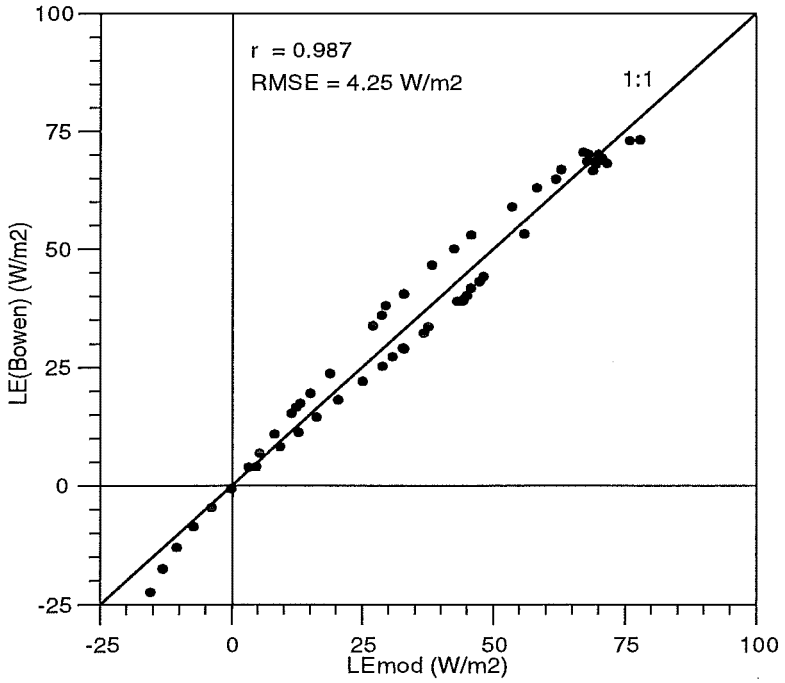

Figure 3.7 Latent heat flux obtained by Bowen ratio method (LEBowen) as a function of modelled sensible heat flux (LEmod), given by equation (3.19) at Burnside, using data set 3.

Sensible and latent heat fluxes. Figures 3.6 and 3.7 show the observed latent heat fluxes, obtained by eddy correlation and the Bowen ratio method, respectively, as a function of the modelled fluxes derived using equation (3.19) at Beckenham and Burnside. The ground storage heat flux GS is calculated here by equation (3.23) at both the Beckenham and Burnside site, using the parameters a_1 to a_3 valid for the combined air and

non-air ground storage heat flux obtained from data set 3 at Beckenham. It is assumed that these parameters did not change too much over time and space. The high correlations are basically due to the nearly constant b_1 during daytime. The modelled heat fluxes obtained from data set 2 are highly correlated as well (not shown here).

A comparison between the heat fluxes obtained by the Bowen ratio method and the eddy correlation method shows that during nighttime the Bowen ratio method did not produce useful data due to near zero vapour gradients. During daytime the Bowen ratio method suggests that on average 3% more energy is used for sensible heat compared to the eddy correlation sensible heat flux data, although individual differences during the afternoon show values ranging up to 15 - 20% (see Figures 3.8 and 3.9).

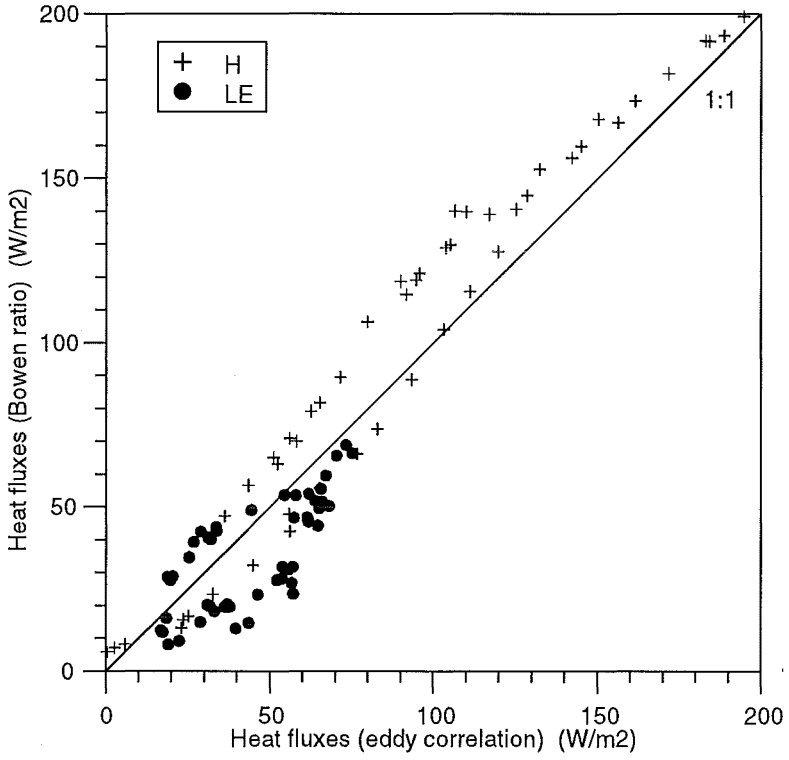

Figure 3.8 Sensible and latent heat fluxes obtained by the Bowen ratio method as a function of sensible and latent heat flux obtained by eddy correlation, respectively, at the Beckenham site, using data set 3.

The sensible and latent heat fluxes of both the eddy correlation and Bowen ratio method are obtained from smoothed data, but nevertheless show some scatter, especially in the latent heat flux. Figure 3.9 shows that during the hours around noon the eddy correlation and Bowen ratio method produced similar results, but serious deviations occurred before and after this interval.

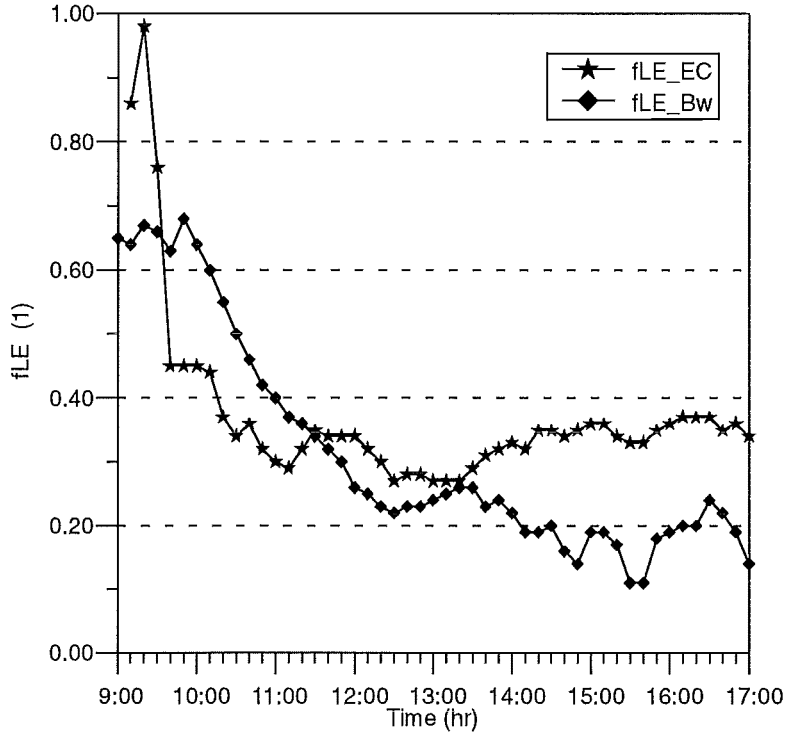

Figure 3.9 Fraction of the energy available for sensible and latent heat, which is used for evaporation, (LE/(H+LE)), at Beckenham, using data set 3; fLE_EC, fLE_Bw: fractions obtained by using eddy correlation data and Bowen ratio data, respectively.

Water availability. The water availability factor b_1 was derived by regression of the latent heat data, using equation (3.19). At the Beckenham site the latent heat flux is obtained by the Bowen ratio and the eddy correlation methods, at the Burnside and Marshland sites by the Bowen ratio method only. At the Marshland site no net radiation was recorded, but the net energy available for sensible and latent heat fluxes is assumed to be similar to the energy available at the Burnside site. However, the net energy available has no influence on the Bowen ratio when derived from temperature and humidity profiles. The ground storage heat flux *GS* is modelled here, using equation (3.23) with values of the parameters a_1 to a_3 which were obtained at the Beckenham site. Using data set 3, the average daytime water availability b_1 equals 0.65 (Bowen ratio) and 0.64 (eddy correlation) for the Beckenham site, 0.75 for Burnside and 0.72 for Marshland, respectively. However, b_1 can also be calculated directly by the application of equation (3.21), and it appeared that during daytime the water availability is not constant, but shows a diurnal cycle. In the morning the b_1 values decline, being almost constant for hours from late morning to the end of the afternoon. Just before sunset, the b_1 values increase again (see Figure 3.10). Afternoon values of water availability (12-15hr) for the Beckenham, Burnside and Marshland sites were 0.42 (0.52 eddy correlation), 0.72 and 0.61 respectively, using data set 3, and 0.46, 0.62 and 0.73, using data set 2.

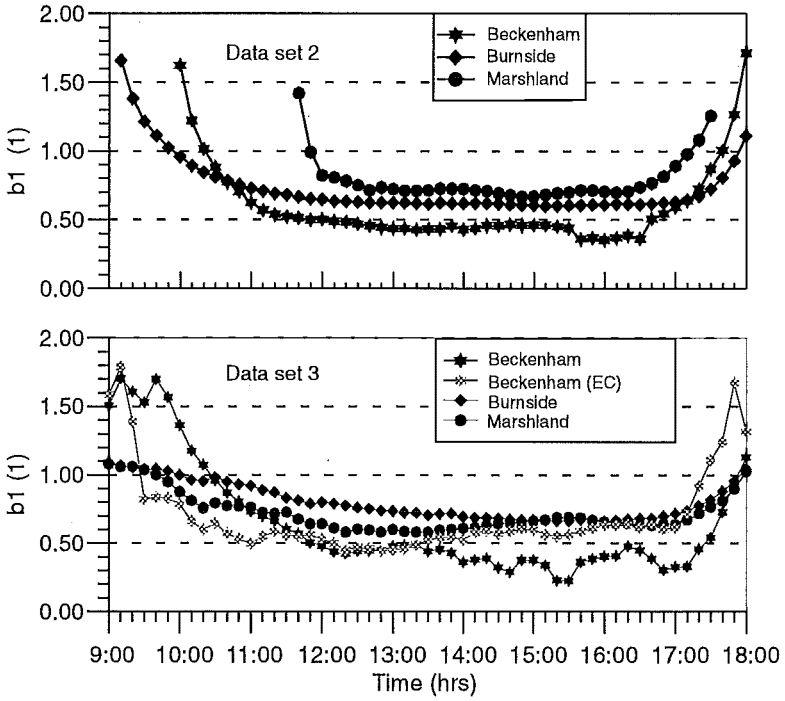

Figure 3.10 Composite daytime time series of water availability factor b_1 obtained from dataset 2 (top) and dataset 3 (bottom), using equation (3.21).

After clear nights, most of the surface will be covered by dew, not only open green space, but also cars, roofs and pavements. During daytime dew has disappeared and evaporation is mainly restricted to open green space areas. At the end of the day, dew is formed again, either by dewfall or by distillation (Rutter, 1975). Distillation is a process occurring mostly during the night when water evaporates from the relative warm soil and condensates on the leaves of vegetation or other objects which are cooled by radiation. The phenomenon that the nocturnal b_1 values are exceeding unity can be explained by the distillation process with vapour transport out of the relatively warm and humid soil. During prolonged intervals the nocturnal Bowen ratio was negative: a sensible heat flux towards the surface, while simultaneously evaporation occurred. Figure 3.11 shows the day to day values of the water availability for different sites. A significant scatter can be observed, with a dependence on rainy and dry intervals.

3.6 Discussion and conclusions

As discussed in the introduction, the objectives of this chapter are to relate surface parameters and surface fluxes to land use characteristics. As expected, the residential areas of suburban Christchurch are aerodynamically rough. Therefore, reduced average wind speeds can be expected, which will decrease the dispersion of atmospheric pollutants. Indeed the average 10 m wind speed at the rural site of Marshland was higher than the at the urban locations. However, a high surface roughness may delay the formation of a stable boundary due to enhanced forced convection and so maintain vertical mixing of pollutants. No observations were available to show the effects of enhanced forced convection in the city (see Chapter 4).

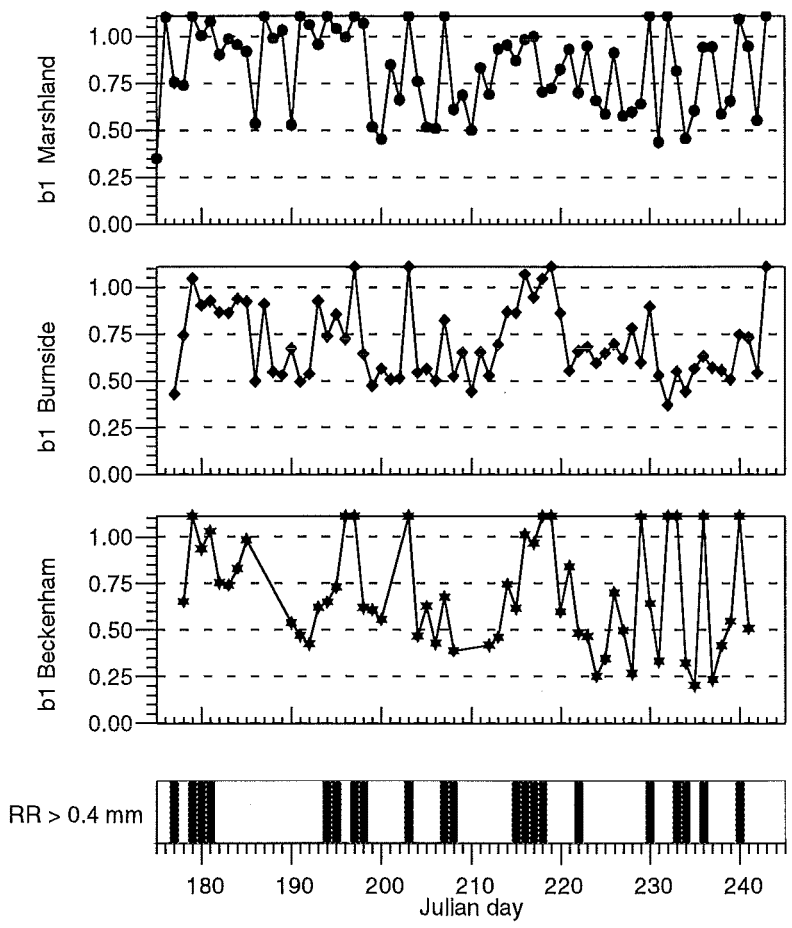

Figure 3.11 Time series of average daytime (1100-1500hr) water availability b_1 during the winter 1995 (dataset 1) in Christchurch at Marshland, Burnside and Beckenham, respectively.

Heat flux observations suggest that during daytime limited open green space in Christchurch reduces the fraction of energy used for evaporation compared to the rural environment. This suggests that especially during the morning hours the boundary layer height over urban Christchurch will grow faster than over the adjacent rural areas, and therefore a faster dilution of air pollution in the urban areas can be expected due to vertical mixing except when fumigation occurs. However, no observations were available to confirm the contrasts between urban and rural boundary layer height development. The 10 m data in the Christchurch area show indeed a lower urban humidity of the air during daytime and nighttime. However, temperatures at 10 m do not suggest a urban heat island effect, which is in contrast with the results published by Tapper (1981; 1990). Various reasons can given for this. Firstly, different sites were used, and particularly the location of the rural site can be very important. Tapper choose a site near Lincoln, about 20 km south southwest of Christchurch, while during this project the observations at Marshland (about 2 km north of the city) represented the rural site. Secondly, Tapper compared paired temperature profiles which were obtained with a time lag. Although a procedure was applied to correct for the time effects on the profiles, it could be inaccurate, and so artificially generate an urban heat island effect. Thirdly, the methods of data collection were different and finally, conditions may vary from year to year. The results of the surface roughness length z_o were incorporated in model settings which were used for the simulations of two case studies (see Chapter 4 and Chapter 7). However, the introduced spatial variations of z_o lacked detail at this stage. The spatial and temporal variations of water availability were not incorporated during the simulations, since it requires a revision

of the current available flux scheme. At a later stage an upgraded flux scheme will be applied.

The results from the application of the mass conservation method using data from the Beckenham tower are not very accurate as wind observations were available at only a limited number of elevations to only 21m height. The resulting z_o and d values show a significant scatter and the method is quite sensitive to the parameterization for K_M, in particular with respect to z_o. The values for roughness length z_o and displacement height d obtained by the empirical and the mass conservation methods suggest a lower limit of the inertial sublayer ranging from 13.5 m to about 16.5 m at Beckenham, so it is no surprise that the aerodynamic method failed to converge, using observations at 6 m, 12 m and 21 m heights. The aerodynamic method generated z_o values with a significant scatter using the Marshland data set. Since the program developed proved to be numerically very accurate when a suitable data set is used, it appears that **a.** the Marshland site was not really suitable for the aerodynamic method with observations at only two elevations, and the lowest level (3 m) being possibly too low or **b.** more manipulation of the data set is required, for example using averaging periods longer than 60 minutes, or selecting subsets on the basis of thermal stability, wind direction and wind speed. Nevertheless, the wind speed observations were able to show that the residential suburbs of Christchurch are aerodynamically rough compared to the rural site at Marshland. This is expressed in the values of z_o and d, as well as in the average observed wind speeds. Generally, the average 10 m wind speed at Marshland is higher than in the suburbs and it is regretted that no data are available for the inner city.

The 24 hr average residual ground storage heat flux at Beckenham during dataset 3 is only 2.6 W m^{-2}, which indicates that on average the energy balance is nearly closed. A substantial proportion of the energy supplied by net radiation in the winter is used for ground storage (a_1=0.36). Grimmond et al. (1996) reported $0.39 < a_1 < 0.59$ for suburbs in American cities during the summer. They found that the ground storage heat flux peaks 0.13 to 0.62 hr earlier than the net radiation flux, which relates well with our phase lag a_2=0.22 hr. The phase lag was 0.16 hr when disregarding the energy used for heating and humidifying the air in the canopy layer. The phase-shift appears to be particularly dependent on the volume of air contained in the ground storage and so it is dependent on the height of observations.

The sensible and latent heat fluxes were derived by the Bowen ratio method, using a modelled ground storage heat flux, which was derived from data set 3 at Beckenham. Any inaccuracies of the parameterization may have affected the absolute values of the sensible and latent fluxes, but not the Bowen ratio and the water availability factor. On average, the daytime sensible and latent heat fluxes obtained by the eddy correlation and Bowen ratio method compared reasonably well, although significant deviations between fluxes from both methods occurred. This may be caused by: **a.** limited accuracy of the Bowen ratio method, due to the quality of the sensors and unequal eddy diffusivities for heat and vapor in an aerodynamically rough and inhomogeneous environment (Roth and Oke, 1995) and **b.** the heat fluxes derived from the observed local 6-21m profiles of temperature and water vapour do not necessarily relate to the observed eddy correlation fluxes at 18 m height due to differences in spatial representation of both fluxes. However, the De Bruin and Holtslag models (equations (3.19) and (3.20), respectively) describing latent heat and sensible heat fluxes gave very good results for both composite data set 2 and data set 3. The accuracy of the heat fluxes obtained by the Bowen ratio method and the models are dependent on the accuracy of the net available energy term (Rn - GS), which can be narrowed down to the parameterization of the ground storage heat flux when this flux is not observed directly or

cannot be derived as a residual. The accuracy of the modelled heat fluxes is also related to the parameters of the models, the water availability b_1 and the advective term b_2,. The Bowen ratio method and the modelled heat fluxes are less suitable for forecasting unsmoothed, short interval heat fluxes, which contain large turbulent fluctuations.

The water availability b_1 showed a clear diurnal pattern, with values equal to or higher than unity during the night and early morning, decreasing during the morning hours, nearly constant during the second part of the morning and the afternoon and finally increasing again at the end of the afternoon and during the evening. Despite the variability of the water availability factor, constant values can be used for daytime modelling. The water availability b_1 at Beckenham frequently fell below 0.50 during fine days in winter 1995, when the soil was generally well watered. The sites at Burnside and Marshland showed generally higher b_1 values. However, the daytime b_1 data at the Marshland site did not reach values close to unity, as would have been expected at a well watered rural environment. So, a positive relationship between the fraction of green space and water availability appears to exist in the Christchurch area during the winter, but the relationship is dependent on time of day and it varies from day to day. Spronken-Smith (1996, pers. comm.) demonstrated a linear response for large American cities during warm and sunny weather conditions, but it can be argued that a non-linear response is also likely due to oasis effects. Too few data are available for the Christchurch situation to establish a statistically significant relationship between green space and water availability. The slightly higher daytime net radiation values at Beckenham cannot compensate for a reduced evaporation due to reduced water availability, compared to the Burnside and Marshland sites. The increased rural evaporation is also reflected in higher absolute humidity data. Apparently, the spatial variation of the water availability factor b_1 is related to land cover, and temporal variation tends to be related to the occurrence of precipitation. So far, it is not clear why the reduced urban evaporation is not related to higher daytime temperatures. Advection or an increased ground storage may be responsible. No independent *GS* models for other sites are available.

4. Qualitative analysis of two cases

4.1 Introduction

As stated before, the main aim of the project is to explain atmospheric behaviour in the Christchurch area and relate this to ambient air pollution conditions. In this chapter a qualitative analysis is given of two 24 hr periods: a case from noon 27 July to noon 28 July 1995 (hereafter C2728) and a case from noon 30 July 1995 to noon 31 July 1995 (hereafter C3031). C2728 and C3031 can be classified as *southwest flow, following the passage of a cold front* and *a high pressure system, generally associated with a weak geostrophic flow,* respectively (after Owens and Tapper, 1977). These particular time intervals are chosen for a detailed case study because:

- High air pollution concentrations were recorded for several hours in Christchurch during both intervals.
- No major changes in the synoptic weather conditions occurred during both intervals.
- Clear sky conditions prevailed, promoting the development of nocturnal drainage flows and very stable boundary layers.
- Intensive data collection was undertaken, including several tethered balloon soundings and a pilot balloon flight on each day.
- Conditions during both cases were different, but also similarities did exist, making comparisons very revealing.
- Although severe air pollution conditions can occur during a variety of atmospheric circumstances, the selected case days can be considered as being representative of 'bad' air pollution days.

Both case studies C2728 and C3031 formed part of a fine spell lasting several days. The data which were collected throughout the winter of 1995 provide sufficient material for other potential case studies, although none contains such a high density of tethered balloon flights as C2728 or C3031. A quantitative analysis of both case days is given in chapter 5, where the 3D prognostic meso-scale model RAMS is applied.

4.2 Materials and methods

The instruments used, sites and data collection are described in detail in Chapter 2. In addition to this, a few items specific to the qualitative analysis are given below. All times are local time unless indicated otherwise. The 10 m wind speed at the University of Canterbury site was estimated by reducing the 30 m observations by 25%, which relates to a logarithmic wind profile model with a surface roughness length of 0.5 m. Two dimensional interpolations have been conducted to produce:

- Maps with temperature and wind distributions in the Christchurch area; a linear kriging technique was used with a radius of 8.66 km.
- Vertical profiles throughout the case study period of wind, temperature and humidity. Linear kriging was used again, but the ratio of the vertical radius, (200m) to the horizontal radius (10 hr) was taken as 20:1, which relates to the ratio of the change of

quantity φ (temperature, wind speed, humidity) per change of height (m) to the change of quantity φ per change of time (hrs) $(\partial\varphi/\partial z) / (\partial\varphi/\partial t)$. The tethered balloon soundings were undertaken at different sites, so that local effects may have influenced the observations, especially at lower altitudes. However, these effects are considered to be of minor importance in the interpretation of the two dimensional (height-time) charts.

4.3 Case 27-28 July 1995 (C2728)

4.3.1 Overview

During the afternoon of the 27th of July 1995 until the morning of the next day the Christchurch area was under the influence of large scale descending air, generated by a west southwesterly flow, giving calm and clear weather conditions. During this interval, local air flow patterns in the Christchurch area were quite significant. The long clear night supported the development of a strong inversion layer near the surface, due to radiative cooling. High air pollution concentrations were associated with the calm conditions which existed during most of the night, because the pollutants were trapped in a relatively shallow layer near the surface and drifted only slowly away. The PM_{10} concentrations at the monitoring sites at Opawa, Beckenham and Hornby exceeded 100 $\mu g\, m^{-3}$ for several hours and at the St. Albans site 200 $\mu g\, m^{-3}$ was exceeded for more than 7 hours.

4.3.2 Weather

At 12 hr local time on 27 July, the mean sea level analysis map shows that a high pressure system was located to the southwest of the South Island and a low pressure centre to the south-southeast, causing southwesterly flow over the region with cyclonic curvature (see Figure 4.1). At the 500 hPa level (at a height of about 5500 m) a strong west southwesterly flow existed over the South Island, having a near zero relative vorticity, with winds around 25 $m\, s^{-1}$. Soundings from Hokitika, Christchurch and Paraparamua show a gradual increase of wind speed with height, with directions generally between southwest and west. Daytime weather in Canterbury was fine and calm with light winds near the surface. The air was dry with daytime mixing ratios near the surface around 3.2 $g\, kg^{-1}$. During the morning of the 27th, cumulus humilis clouds disappeared and the afternoon and night were clear. The 10 m temperatures peaked around 9° C and the minimum values of the following night reached 0° C in the Christchurch area, although local variations were present. The air pressure in Christchurch decreased from 1008.5 hPa at noon on the 27th, to 1000.5 hPa at 6 am in the morning on the 28th and strongly rose afterwards. This pressure tendency can be associated with a shallow inactive cold front passing in the early morning of the 28th. The estimated southwesterly geostrophic wind near the surface increased from 5 ± 2.5 $m\, s^{-1}$ at 6 pm on the 27th to 10 ± 2.5 $m\, s^{-1}$ at 6 am on the 28th due to increased surface pressure gradients. The estimated geostrophic wind relates well with the observations, although the accuracy of the geostrophic winds is insufficient to indicate the existence of a supergeostrophic component in the nocturnal jet. In the morning of the 28th a thin layer of cirrostratus (7 octas) was observed at 8 am local time and a few cumulus humilis clouds (1 octas). During the day of the 28th, more cumulus developed and strato-cumulus formed over the Christchurch area, reaching 5 octas at 4 pm local time.

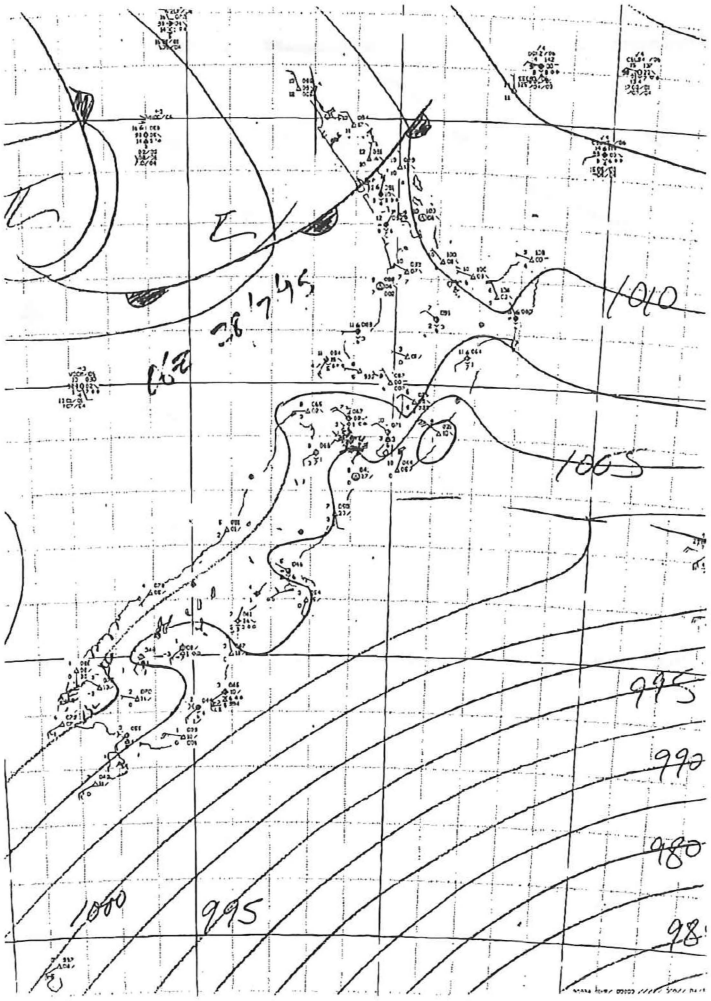

Figure 4.1 Synoptic analysis at 06.00 UTC (18.00 hr local time) on 28 July 1995.

4.3.3 Surface conditions

In the afternoon of 27 July 1995, the weather was fine and calm in the Christchurch area. Solar heating of the surface during daytime resulted in a convective mixed boundary layer, having a depth of at least 500 m. Winds in the area were light and variable (see Figures 4.2a and 4.3), until the onset of a northeasterly breeze between 3.15 pm and 4 pm local time, which was firstly observed at the eastern and northern parts of the area, and finally in the south and west.

The elevated station at Cashmere recorded the start of the northeasterly breeze 30 minutes earlier than the nearby Beckenham station, possibly due to a vertical skewness of the 'northeasterly front'. After passage of the 'northeasterly front', initially the wind speed at the surface stations in the Christchurch area increased slightly, but it did not exceed 2 m s^{-1}, except at the Bromley site. A sudden drop in temperature at the Bromley and St. Albans sites (1.5 K and 0.5 K, respectively) coincided with the passage of the 'northeasterly front', but was not observed at the other stations in the Christchurch area. The concentrations of air pollutants were generally low in the afternoon, which can be seen in Figures 4.4a to 4.4d.

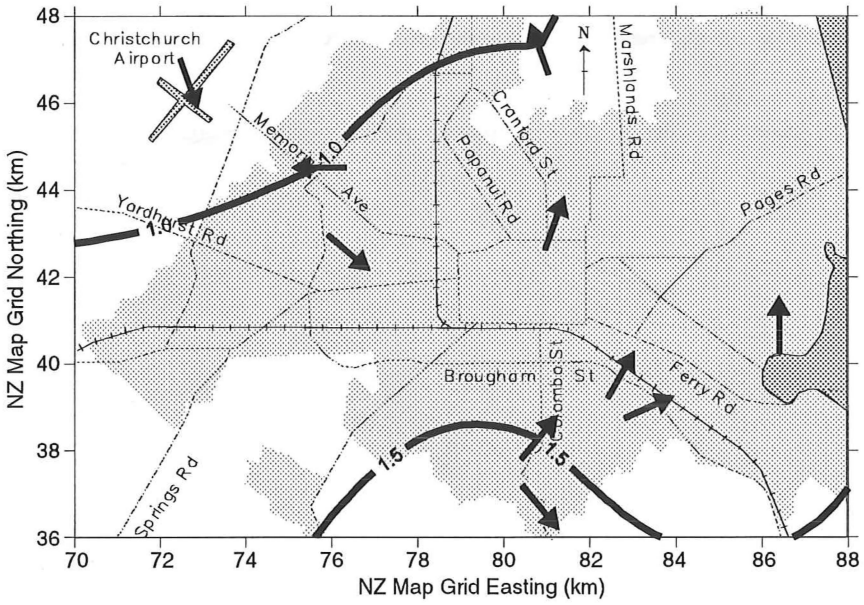

Figure 4.2a Wind distribution on 27 July 1995, 3 pm local time. Arrows indicate wind direction and contour lines show wind speed (m s^{-1}).

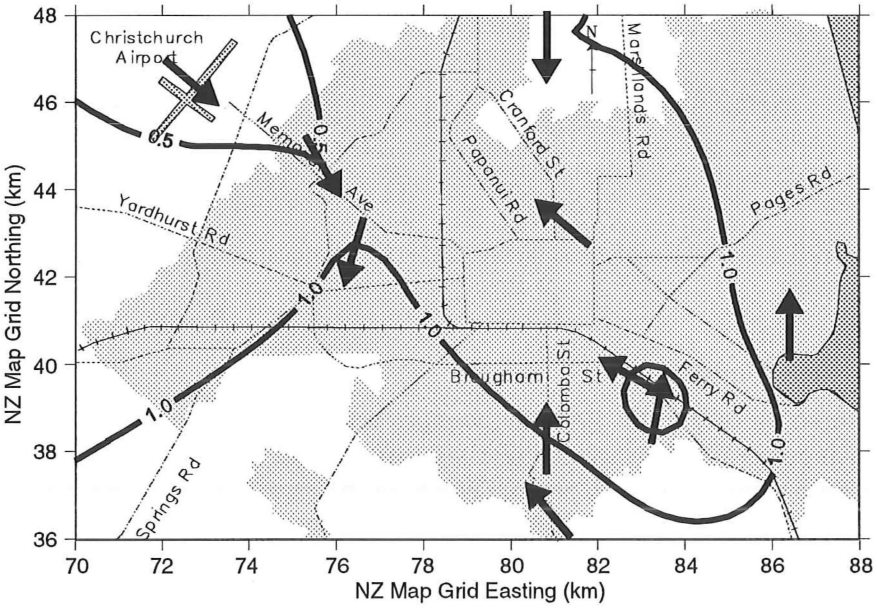

Figure 4.2b Wind distribution on 27 July 1995, 10 pm local time. Arrows indicate wind direction and contour lines show wind speed (m s^{-1}).

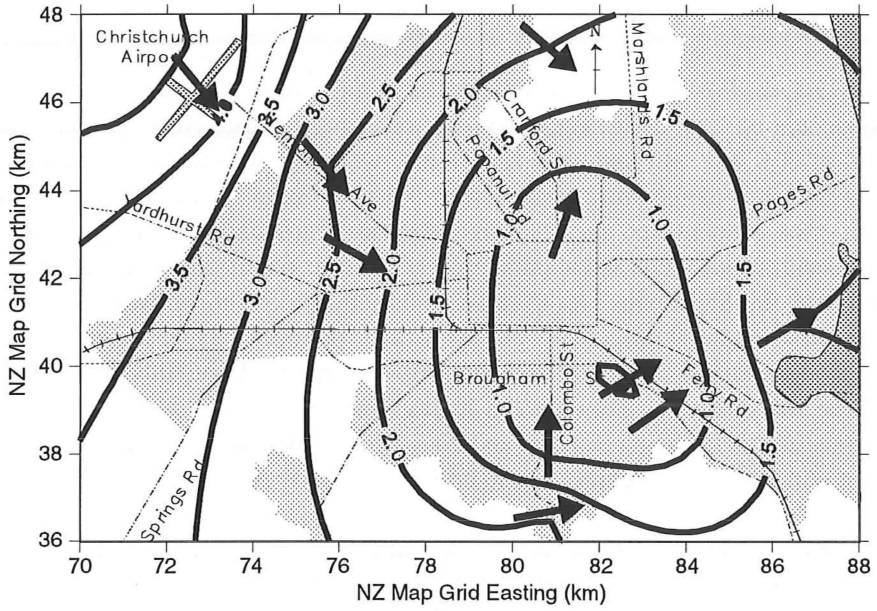

Figure 4.2c Wind distribution on 28 July 1995, 4 am local time. Arrows indicate wind direction and contour lines show wind speed (m s^{-1}).

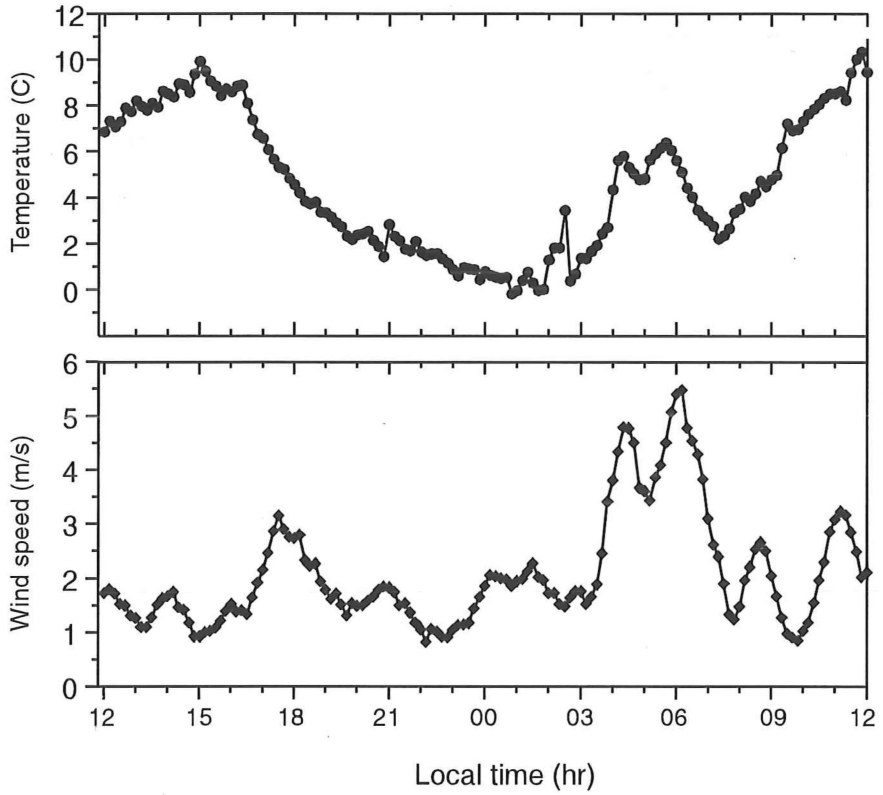

Figure 4.3 Time series of hourly moving average 21m wind speed and 10m temperature at the Burnside tower site on 27-28 July 1995.

At the end of the afternoon, radiative cooling at the surface started, with net radiation values being in the range -60 to -70 W m^{-2} throughout the nocturnal period, stabilising the air near the surface. For example, the differences in air temperature at 21 m elevation and near the surface, (T_{21} - T_{surf}), at the Beckenham tower were respectively -3 K at 3 pm, 0 K at 4.30 pm, +4.5 K at 6 pm and +9.5 K at 8 am, while the difference between the 21 m temperature and 3 m temperature peaked with 5.5 K at 8 am in the morning of 28 July 1995. During the evening, the surface winds decreased gradually in strength and the air pollution concentrations increased significantly at the four monitoring sites in Beckenham, Hornby, Opawa and St. Albans. A dip in air pollution concentrations was recorded at the Beckenham site between 9 pm and 11 pm local time, possibly related to the advection of relatively clean air in the katabatic southerly flow from the Port Hills during this time interval. Note the difference between the highly correlated variations of PM_{10} and CO concentrations at Beckenham, Hornby and St. Albans and the low correlation between PM_{10} and SO_2 in Opawa, apparently due to emissions (see Figures 4.4a to 4.4d).

Throughout a large part of the night, the stations in the south-eastern part of the Christchurch area recorded a southerly component in the wind direction, which is clearly illustrated in the 10 pm plot of the 10 m winds (Figure 4.2b). The 10 m winds at 10 pm appeared to show a katabatic flow from the Canterbury Plains in the northwestern part of the Christchurch area and a drainage flow from the Port Hills in the southern part of the area, converging over the city.

The lowest (10 m) air temperatures during the nocturnal period were recorded at Burnside and Marshland in the northwestern part of the area and at Beckenham and Ensors Gardens in the southern part. The highest temperatures were recorded at the Cashmere station (in the hills) and Bromley (near large water surfaces). The St. Albans site had the highest urban readings. From 3 am to 6 am on 28 July, most surface stations in the Christchurch area showed an increase in wind speed and temperature, associated with a dramatic decline in air pollution concentrations (see Figures 4.2c, 4.3, and 4.4a to 4.4d, respectively). The increased wind speeds were firstly observed in the northwestern parts of the area and at the elevated station at Cashmere, further spreading eastward. The wind directions were predominantly between southwest and northwest. After 7 am in the early morning, the stable and calm conditions were partly restored and the air pollution concentrations increased again.

4.3.4 Waves

During C2728, the time series of wind speed at most stations in the area showed a periodicity which can be related to internal gravity waves (Stull, 1988). The series of the Burnside moving average wind speeds clearly illustrate the waves (see Figure 4.3). Spectral analysis of the wind speed data indicates:

- A combination of long waves with a period in the range 1 to 5 hours dominates the spectrum.
- Local variations existed with respect to the dominant waves, although a significant contribution (of variance in the signal) by waves with a period around 1.2 hours and 2.5 hours was observed at most stations.

The dramatic increase in wind speeds and temperatures in the area between 3 am and 6 am can be put in the context of these gravity waves, which obtained Kelvin-Helmholz characteristics as described by Stull (1988). A Kelvin-Helmholz wave tends to build up its amplitude and finally may break, generating turbulent mixing of air aloft with air at lower

levels. This appears to have occurred in the morning of 28 July 1995, when the air temperatures increased rapidly throughout the area, destroying the ground inversion. At the same time, the wind speed increased and air pollution concentrations decreased significantly. Later in the morning, a moderate northeasterly wind developed, firstly in the eastern parts of the area, as daytime heating destroyed the nocturnal boundary layer.

4.3.5 Vertical structure

Stability. From 3.30 pm on 27 July to 10 am on the 28th, 8 flights were undertaken with the tethered balloon and sonde at different sites in the Christchurch area (see Table 4.1). The profiles show a transition from a convective mixed boundary layer in the afternoon to a stable nocturnal boundary layer with a residual layer aloft during the evening and through to the next morning. During the morning of the 28th, the inversion near the ground was rapidly destroyed.

The soundings at 3.30 pm in Beckenham and 4.30 pm in Hagley Park show a near neutral temperature profile from the surface to over 300 m, indicating good dispersion capacity of the atmosphere over at least this depth. The situation changed at sunset, when an inversion layer was formed near the surface, due to radiative cooling. Apart from local variations, sequential soundings show an increasing stability of the air in the Christchurch area during the nocturnal period. As a numerical illustration, the gradients of the potential temperature over a shallow sub-layer from the surface to an elevation at about 30 m and 40 m increased from 0.050 $K\,m^{-1}$ at 6.45 pm (Marshland) to 0.217 $K\,m^{-1}$ at 7.45 am (Hagley Park) next morning. The depth of the full inversion layer appeared to be variable during the night. The strongest potential temperature gradients occurred near the surface, as clearly illustrated in Figure 4.5a and Table 4.1.

Table 4.1 Height from surface of inversion layers and sublayers (z_i and z_{sub}, respectively), potential temperature differences between top and bottom of these layers ($\Delta\theta$) and potential temperature gradients ($\Delta\theta/z_i$), obtained by tethered balloon soundings. BE=Beckenham; HP=Hagley Park; MA=Marshland; WM=West Melton; '-': not existing; '?': could not be identified.

		Inversion layer			Sub-layer		
Location	Time (hr)	z_i (m)	$\Delta\theta$ (K)	$\Delta\theta/z_i$ (K m^{-1})	z_{sub} (m)	$\Delta\theta$ (K)	$\Delta\theta/z_{sub}$ (K m^{-1})
BE	15.30	?	?	<0.001	-	-	-
HP	16.30	?	?	<0.001	-	-	-
MA	18.45	75	3.2	0.043	40	2.0	0.050
WM	20.30	200	6.0	0.030	40	3.5	0.070
HP	23.00	300	10.7	0.036	50	7.7	0.154
BE	00.45	?	?	?	50	6.0	0.120
HP	07.45	250	9.0	0.036	30	6.5	0.217
BE	09.15	?	?	?	50	3.0	0.060

Wind. At 1.45 pm a pilot balloon was launched from the campus of the University, showing an anti-clockwise turning of the wind from 300° (WNW) near the surface to 245° (WSW) at 1200 m. Above 1200m the wind direction varied little. The wind speed however, steadily increased from 1 m s^{-1} near the surface, to 3 m s^{-1} at 500 m, 11 m s^{-1} at 1200 m, peaking with 20 m s^{-1} at 3000 m. Above 3000 m the wind speed decreased slowly.

During the early afternoon the winds near the surface were generally between west and north in the Christchurch area. A localised 'northeasterly front' passed over the area between 3.15 pm and 4 pm. Vertical soundings showed that the depth of the northeasterly flow appeared to be increasing in time for the next few hours, being 100 m during the Beckenham flight at 3.30 - 4.15 pm, peaking with a depth of more than 300 m during the Hagley Park and Marshland flights at 4.30 pm and 6.45 pm, respectively (see Figure 4.5b).

Soundings undertaken later during the night indicated that the northeasterly flow was lifted from the surface and that the layer had diminished in its depth. The northeasterly flow was observed at the West Melton tethered balloon site, 20 km west of Christchurch at 8.30 pm in a layer between 20m and the inversion at 200m from the surface. Aloft a northwest flow was present, while near the surface a shallow layer with a flow between west and north could be found. The 11 pm sounding at Hagley Park also showed an elevated layer of northeasterly flow between 50 and 180 m, with northwesterly winds below and above this layer. The Beckenham sounding at 0.45 am indicated a shallow layer at the surface with a depth of 25m, having winds between southwest and southeast, while in the layer between 25 and 150m from the surface an easterly to southeasterly flow prevailed. Above 200m northwesterly winds were still present. Interesting to note is that a correlation between wind direction and humidity of the air existed, with northeasterly winds (from the sea) advecting moist air and westerly winds advecting dry air, as shown in Figure 4.5c.

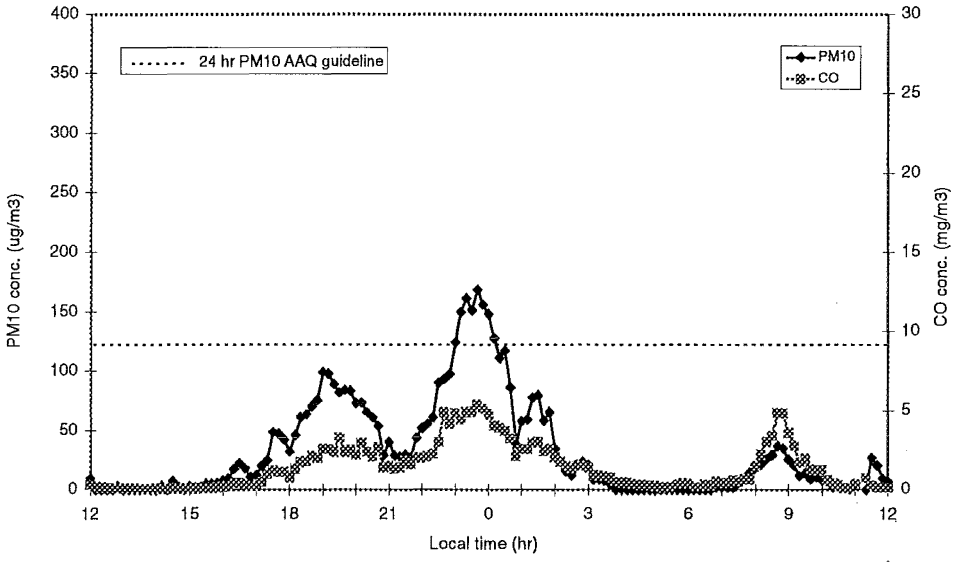

Figure 4.4a Time series of PM_{10} and CO concentrations at Beckenham monitoring site on 27-28 July 1995. AAQ: Ambient Air Quality.

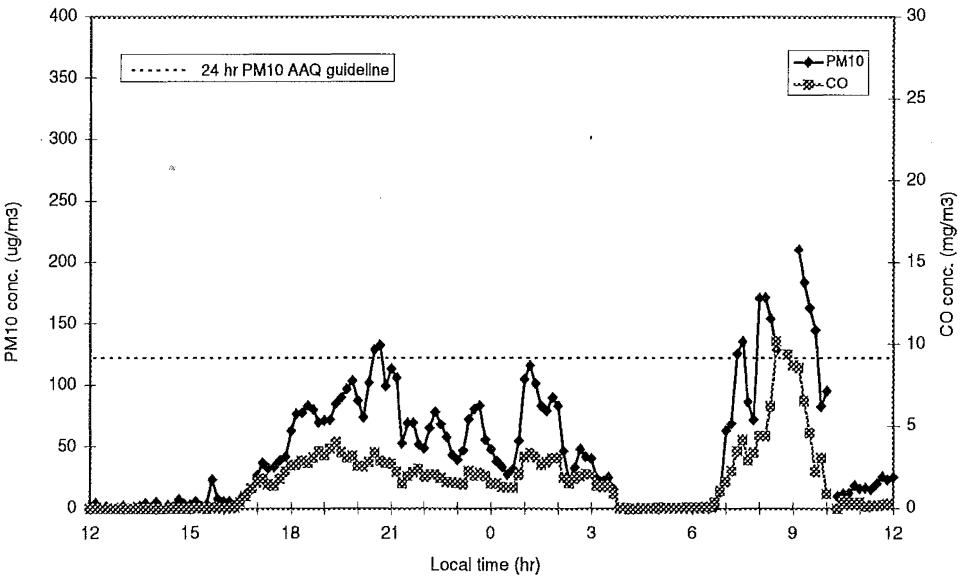

Figure 4.4b Time series of PM_{10} and CO concentrations at Hornby monitoring site on 27-28 July 1995. AAQ: Ambient Air Quality.

During the interval 3 am - 6 am in the early morning of the 28th, the wind speed and temperature near the surface increased dramatically all over the Christchurch area (see Figures 4.2c and 4.3). The winds were mainly between north and west in the northwestern part of the area, and between southwest and west in the southeastern part of the area. No tethered balloon soundings were undertaken during this period, but obviously the strong ground inversion which was formed during the preceding nocturnal time interval was destroyed. At 7 am in the early morning of 28 July the ground inversion was partly restored again, demonstrated by decreasing temperatures near the surface and associated light winds. The 7.45 am sounding at Hagley Park showed a strong ground inversion at 50 m elevation with a southerly wind below and a northwesterly flow above this level.

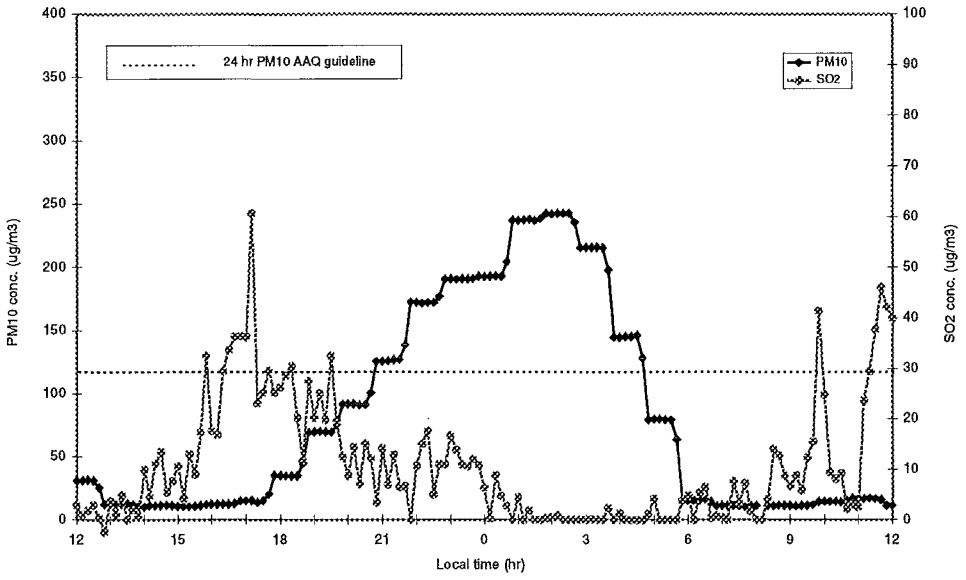

Figure 4.4c Time series of PM_{10} and SO_2 concentrations at Opawa monitoring site on 27-28 July 1995. AAQ: Ambient Air Quality.

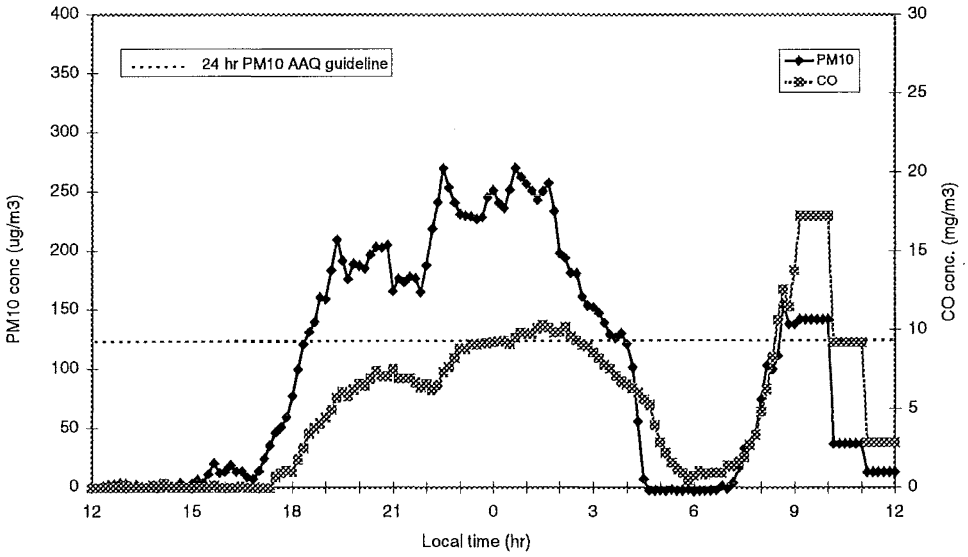

Figure 4.4d Time series of PM_{10} and CO concentrations at St. Albans monitoring site on 27-28 July 1995. AAQ: Ambient Air Quality.

4.3.6 Jet

With the start of the evening a low level jet developed. The 4.30 pm sounding at Hagley Park showed a jet between 60 m and 160 m during its ascent, which had widened and increased in strength in 30 minutes to a layer between 60 to 280 m. During the 6.45 pm sounding at Marshland, the jet was well developed between 80 m and 260 m (see Figure 4.5b). The soundings undertaken later on during the night did not show a layer with a jet, but generally a strong increase of wind speed with height throughout the profile (up to 500 m). The jet may have disappeared altogether or it may have lifted to a higher elevation, partly above the sounding depth. During the tethered balloon soundings in the morning of the 28th, a strong wind shear at 100-200 m was still present.

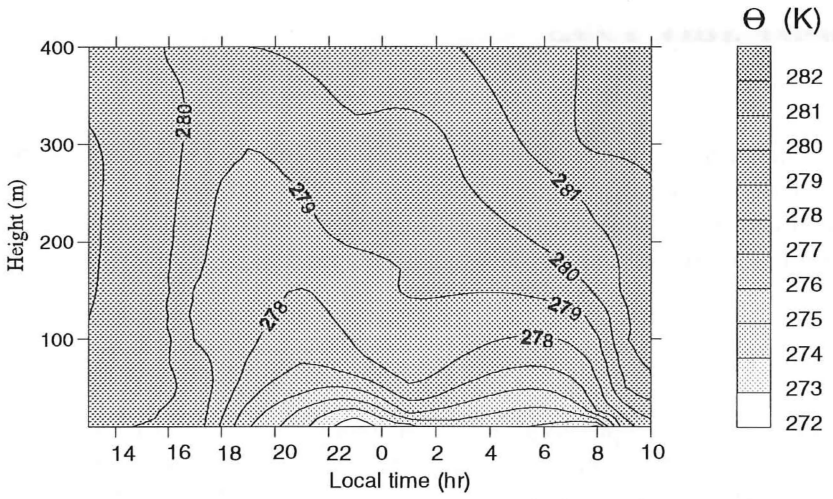

Figure 4.5a Evolution in time of the profile of potential temperature (θ) in the Christchurch area on 27-28 July 1995.

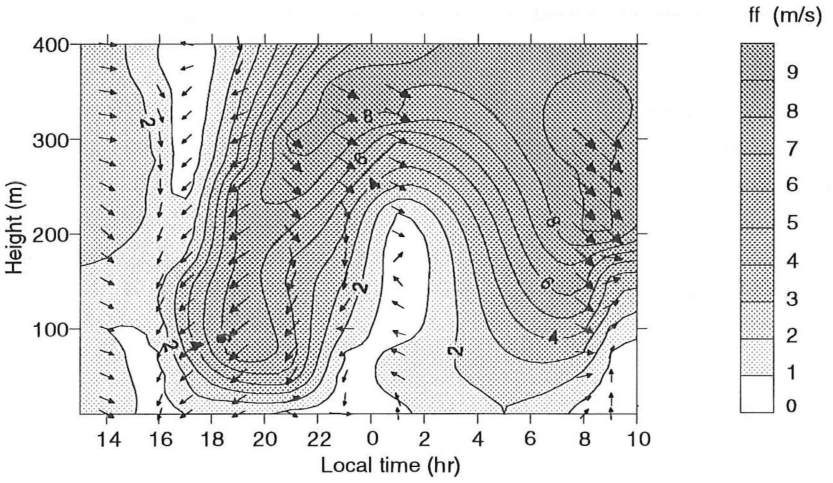

Figure 4.5b Evolution in time of the profile of wind speed (ff) and wind direction in the Christchurch area on 27-28 July 1995.

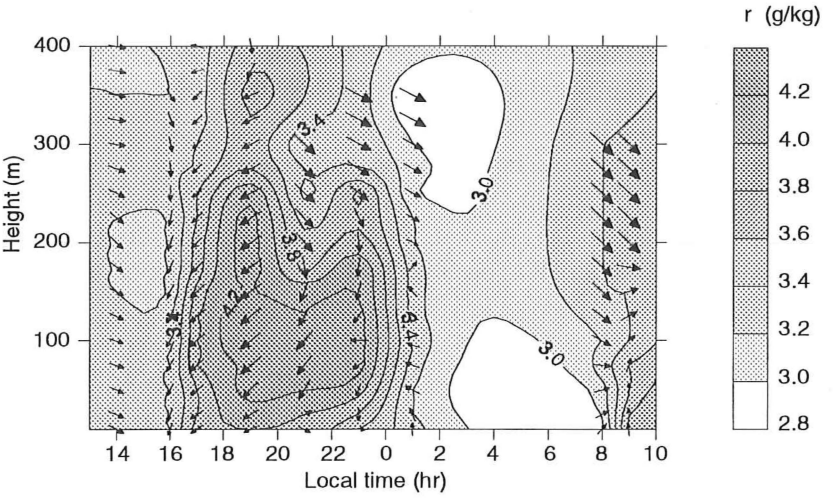

Figure 4.5c Evolution in time of the profile of wind and humidity (r) in the Christchurch area on 27-28 July 1995.

4.4 Case 30-31 July 1995

4.4.1 Overview

The weather during the interval from noon 30 July 1995 to 31 July 1995 (C3031) can be characterised by clear and reasonably calm conditions. Local wind systems were not recorded in the area. Nocturnal cooling generated a strong inversion layer near the surface. High air pollution concentrations were observed at night in Opawa and St. Albans, but not in Hornby.

4.4.2 Weather

On the 30th of July 1995, at 6 pm local time, an anticyclone extended over New Zealand, with its centre (1023 hPa) west southwest of the South Island. At 6 am on the 31st, its centre was located over Otago, with a pressure exceeding 1028 hPa. A south to southwesterly geostrophic flow could be expected in Canterbury, although surface pressure gradients were generally small (see Figure 4.6). At the 500 hPa level (at height of 5500m) a ridge was to be found just west of the South Island, slowly moving eastwards. In the Canterbury region, at noon on the 30th July 1995, the winds were changing with height from 240° (3.5 m s^{-1}) at 850 hPa (at a height of 1500 m), 210° (3 m s^{-1}) at 700 hPa (at a height of 3000 m to 240° (6 m s^{-1}) at the 500 hPa level, respectively. On the 31st, at noon the winds were 200° (3 m s^{-1}) at 850 hPa, 210° (6 m s^{-1}) at 700 hPa and 130° (10 m s^{-1}) at the 500 hPa level, respectively. The weather in Canterbury was calm and clear, although some cirrus had been observed, 1 to 2 octas (1/8 to 2/8), during the 30th. The 10m temperatures in the Christchurch area peaked around 9° C and during the following night the minima ranged from -3.5° C to -1.5° C at non-elevated locations. The relative humidity in the area was around 60% in the afternoon, but at night saturation occurred at low elevations.

4.4.3 Surface conditions

In the afternoon of the 30th light to moderate winds (1.5 to 4.0 m s^{-1}), predominantly between south and west, prevailed near the surface. The maximum temperatures reached 8 to 10° C. The daytime air pollution concentrations were generally low. In the evening significant cooling of the air started near the surface, generating a strong inversion during the night.

Overnight, net radiation observations showed values less than -60 W m^{-2}, but later increased to over -50 W m^{-2}. The 10m wind speed in the Christchurch area decreased to 0.5 to 1.5 m s^{-1}. The air pollution concentrations increased dramatically with PM_{10} concentrations peaking well over 200 μg m^{-3} in St. Albans and Opawa for several hours, while in Beckenham high PM_{10} concentrations were also recorded. As in the previous case study period, the Beckenham monitoring station recorded a dip in air pollution concentrations between 9 pm and 10 pm. For details about air pollution concentrations during C3031, see Figures 4.7a to 4.7d.

In contrast to C2728, no significant nocturnal local wind patterns were observed during C3031. The surface winds remained between south and west in the area throughout the night and following morning. The 10m temperatures however, were not uniform across the area. The lowest temperatures generally occurred at the Beckenham station, followed by Marshland and Burnside. Near the coast and in the central urban areas higher temperatures were observed. The elevated Cashmere station in the Port Hills recorded the highest

temperatures during the nocturnal period, more than 7 K higher than the Beckenham station, only 1 km away.

The lowest 10 m wind speeds in the area were observed between 6 pm and 9 pm (0.5 to 1.5 m s^{-1}), but gradually increased later, reaching 0.5 to 2.5 m s^{-1}, and up to 1.5 to 4.0 m s^{-1} at 8 am near dawn. The air pollution concentrations in the area decreased significantly after midnight, probably due to the combination of increased ventilation and diminished emissions. In early morning, between 8 am and 9 am, a secondary peak of air pollutants was observed, but no high concentrations were recorded. This phenomenon has also been reported by Stokes and Tyson (1981). During the morning, the 10 m temperatures rose quickly, destroying the inversion layer which was formed overnight, with 10 m winds increasing to 2.5 - 5.0 m s^{-1} at noon.

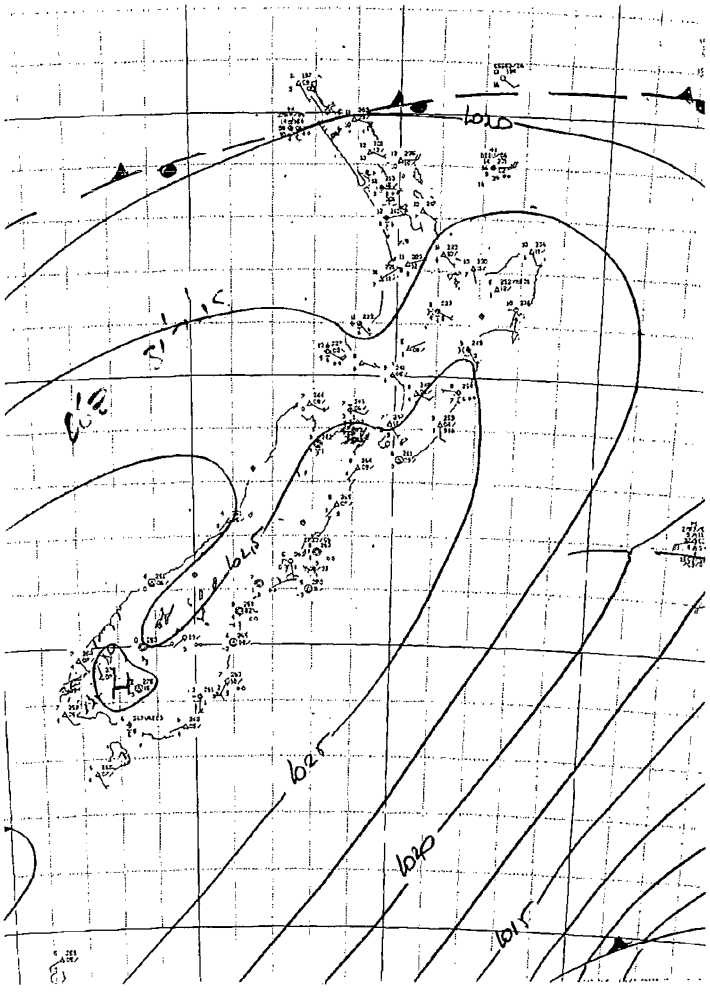

Figure 4.6 Synoptic analysis at 06.00 UTC (18.00 hr local time) on 31 July 1995.

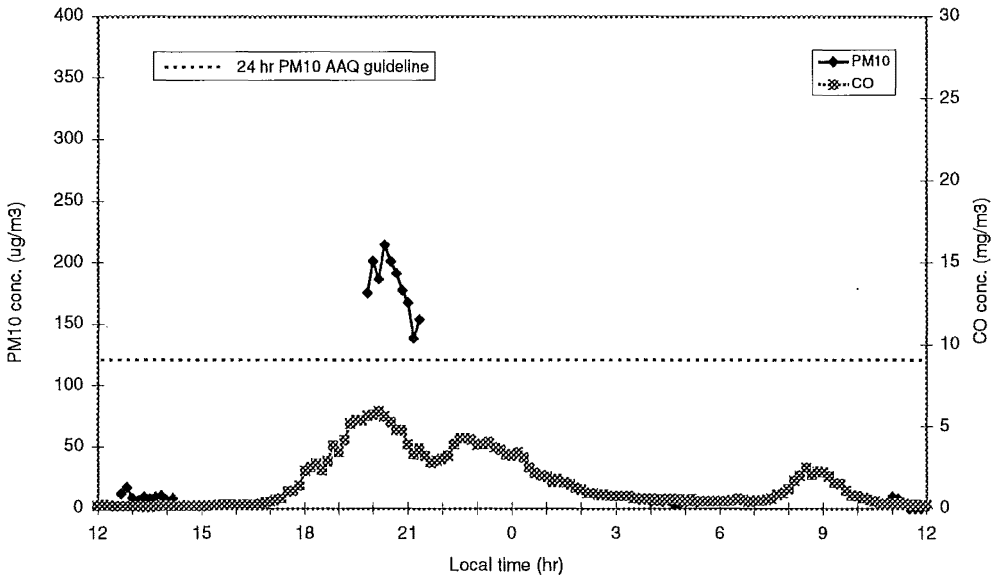

Figure 4.7a Time series of PM_{10} and CO concentrations at Beckenham monitoring site on 30-31 July 1995. AAQ: Ambient Air Quality.

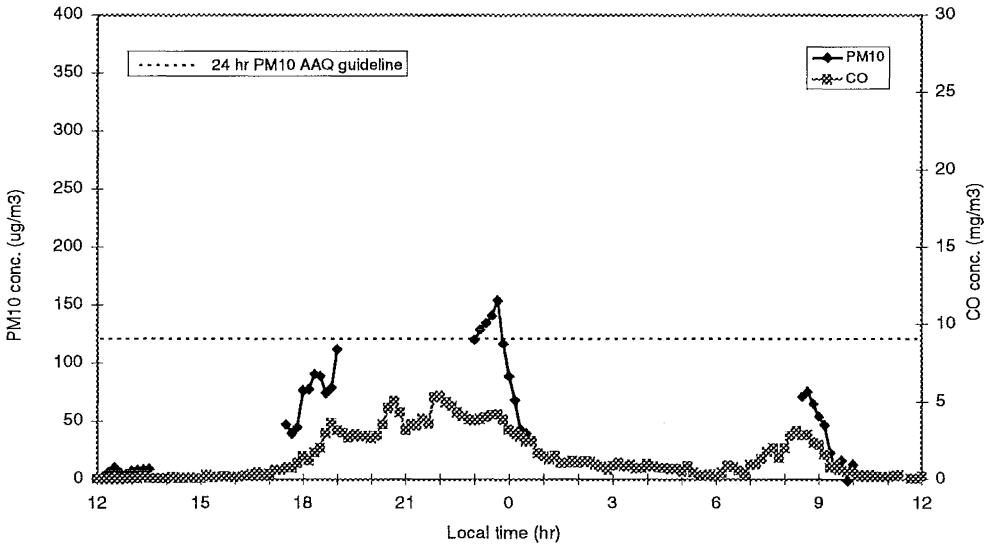

Figure 4.7b Time series of PM_{10} and CO concentrations at Hornby monitoring site on 30-31 July 1995. AAQ: Ambient Air Quality.

4.4.4 Waves

During the nocturnal period of C3031, internal gravity waves were found in the Christchurch area by analysing time series of wind speed, temperature and wind direction. Three classes of wave-periods can be distinguished throughout the area: waves with a period around 0.88, 1.4 and 3.1 hours, respectively, although local variations did exist. Kelvin-Helmholz breaking waves were not observed.

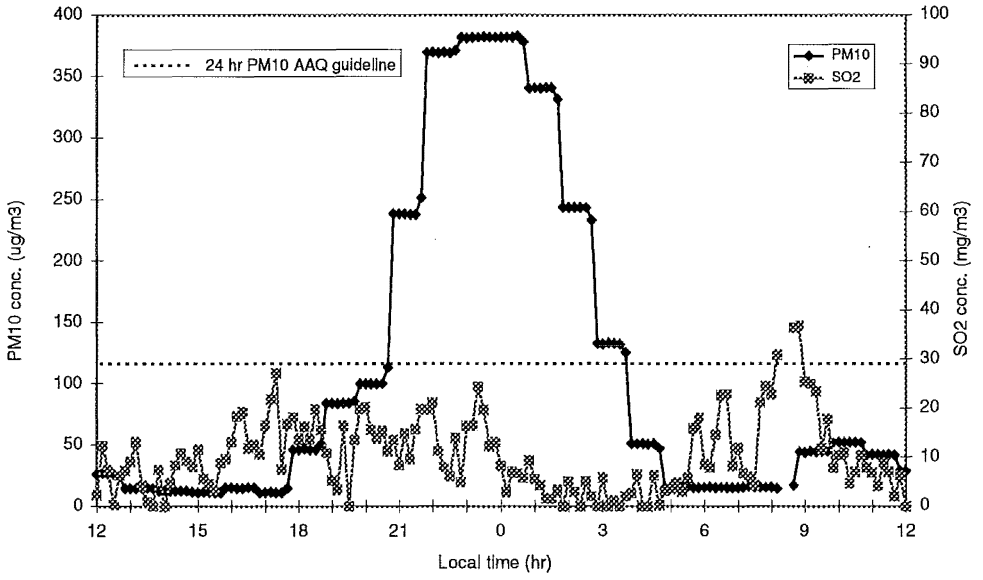

Figure 4.7c Time series of PM_{10} and SO_2 concentrations at Opawa monitoring site on 30-31 July 1995. AAQ: Ambient Air Quality.

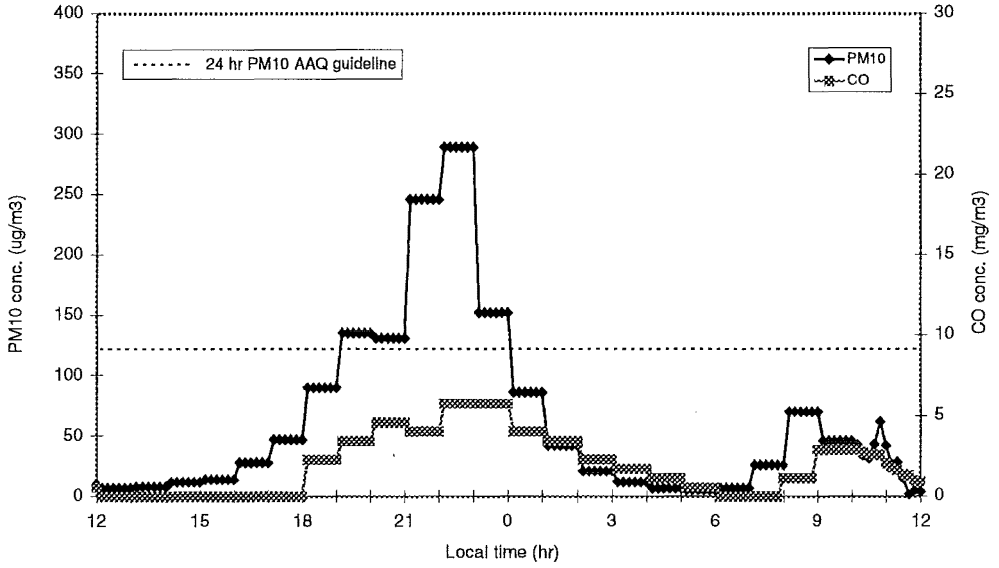

Figure 4.7d Time series of PM_{10} and CO concentrations at St. Albans monitoring site on 30-31 July 1995. AAQ: Ambient Air Quality.

4.4.5 Vertical structure

During C3031, one pilot balloon was launched at 1.15 pm and 10 tethered balloon soundings were undertaken, as indicated in Table 4.2. In the afternoon on 30 July 1995, a well mixed boundary layer existed during the 2.30 pm and 3.45 pm soundings, showing a capping inversion with much drier air aloft at 325 m and 250 m, respectively (see Figure 4.8). The warmer and drier air aloft indicates a different type of air mass, being formed by large scale subsidence or by foehn conditions. During the next sounding at 5.15 pm near West Melton the capping inversion with drier air aloft was found at an elevation of 400 m. The sounding also shows the formation of an inversion layer near the

surface, having a depth of about 30 m. Later soundings undertaken throughout the evening and night did not indicate the existence of the capping inversion with drier air aloft, but a growing depth of the inversion layer near the surface, as well as an increasing gradient in potential temperature (see Figures 4.8 and 4.9a). The highest potential temperature gradients occurred in the layer below 100 m, exceeding 6.5 K per 100 m.

Table 4.2. Time and location of tethered balloon flights during C3031. BE=Beckenham; BR=Bromley; HP=Hagley Park; WM=West Melton

time (hr)	14.30	15.45	17.15	19.15	20.30
location	HP	BE	WM	HP	BE
time (hr)	21.30	23.00	06.15	07.45	09.30
location	HP	WM	HP	BR	WM

The highest absolute humidities occurred at the lower elevations (<100 m) in the afternoon of the 30th, with mixing ratios well above 4.6 g kg^{-1}. Above the capping inversion, which was encountered in the three afternoon soundings, very low humidity values were observed with mixing ratios even below 2.4 g kg^{-1}. This dry air mass aloft was not observed later on. During the nocturnal period, the decrease over time of absolute humidity was most rapid near the surface, and more slow aloft, which agrees well with boundary layer theory (Oke, 1978; Stull, 1988). The evolution of the potential temperature profiles during the night is beautifully illustrated by the successive soundings at Hagley Park (Figure 4.8).

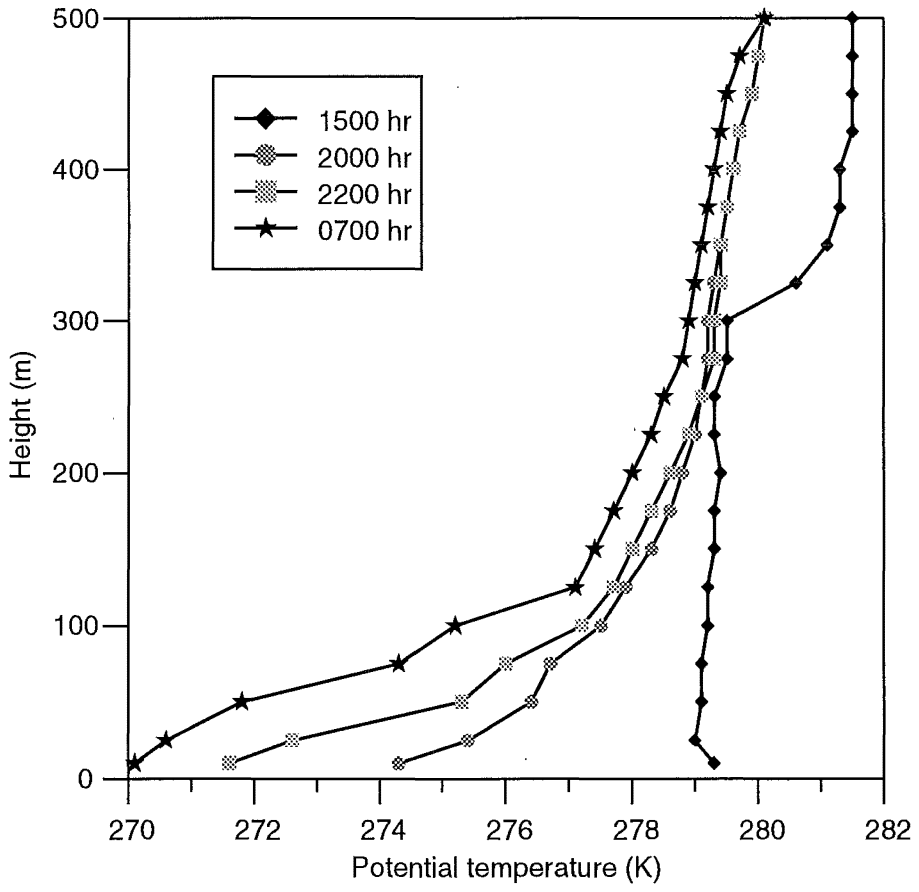

Figure 4.8 Succesive profiles of potential temperature at Hagley Park during C3031.

4.4.6 Winds

Throughout C3031, the wind remained predominantly between south and west, except for a layer between 200 m and 1000 m, where significant variations occurred (see Figure 4.9b). The 1.15 pm sounding showed light winds (<5 m s^{-1}) up to 3000 m. The wind direction from the surface to 400m was between 210° and 240°, between 500 m and 1000 m a layer existed where the winds turned in an anti-clockwise direction from 140° at 500 m to 330° at 750 m and 270° at 1000 m. Above 1000 m the wind direction slowly turned anti-clockwise to 210° at 3000 m, which ties in with the observations at Hokitika and Paraparaumu.

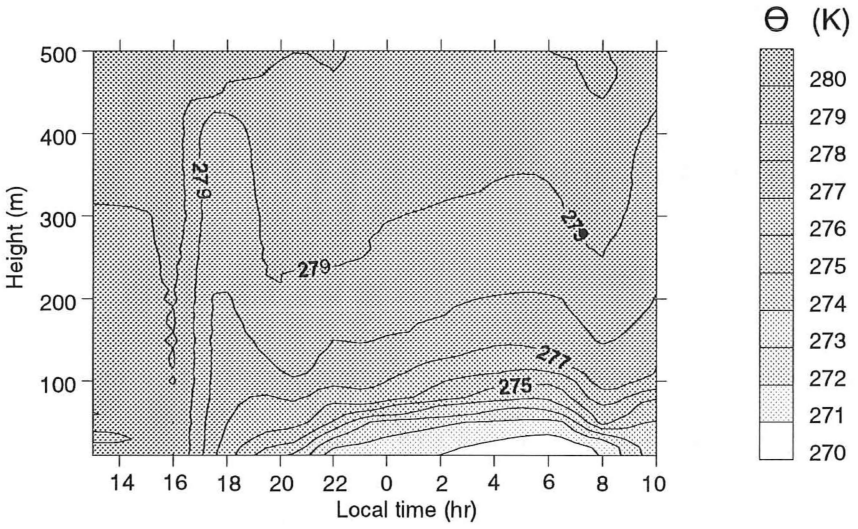

Figure 4.9a Evolution of the potential temperature profile at Hagley Park during the C3031 case.

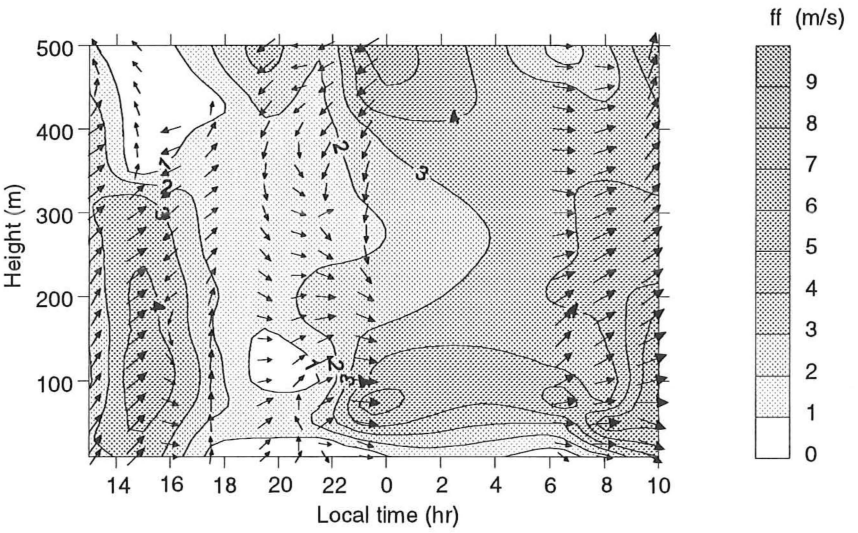

Figure 4.9b Evolution in time of the profile of potential temperature (θ) in the Christchurch area during the C3031 case.

The 2.30 pm sounding showed light to moderate southwesterly winds throughout the mixed layer up to the capping inversion at 325 m. Aloft very light southeasterlies were observed, which were also derived earlier from the pilot balloon readings at 1.15 pm. Later soundings showed no southeasterly winds aloft. However, northeasterlies tended to develop above 350 m in the afternoon in Christchurch, although some delay was observed at the West Melton site. The next morning the northeasterly flow aloft could not be detected at all, but westerlies were present throughout the profile up to 500 m.

A nocturnal low level jet developed relatively late in the evening (after 9 pm) between 50 m and 100 m elevation, with wind speeds exceeding 5 m s^{-1}, as shown by Figure 4.9b. During the night, the jet remained at low levels, just above the layer with the highest potential temperature gradient.

4.5 Discussion and conclusions

The two cases which are analysed share several characteristics. Both cases had light to moderate daytime winds, a well mixed convective boundary layer in the afternoon, low daytime air pollution levels, and persistent clear sky conditions, although some high cloud was present during C3031. Strong nighttime cooling was present, generating a very stable layer of air near the surface, about 100 m thick, and high nocturnal air pollution levels were encountered for several hours in many parts of Christchurch. The contrast between daytime and nighttime air pollution concentrations illustrates that the situation can deteriorate very quickly. A dip in air pollution concentrations at night between 9 pm and 10 pm was observed in both cases, which is likely to be related to the arrival of drainage flow from the Port Hills. A pool of cold air may have formed at the foot of the Port Hills, becoming deeper with time and the drainage flow finally going over the top of this pool. Both cases show the occurrence of a nocturnal low level jet and internal gravity waves. The extent of interaction between the jet and the waves in the Christchurch area needs further investigation. The existence of gravity waves is important with respect to dispersion of air pollutants, especially when breaking Kelvin-Helmholz waves occur, as appeared to have happened during C2728 towards the end of the night. The passage of a weakening cold front in early morning may have played a role as well. Forecasting individual gravity and breaking Kelvin-Helmholz waves will be difficult or even impossible, but their probability may not be.

Besides their common features, both cases also show a few important differences. C2728 had a geostrophic forcing which was stronger than during C3031; local and mesoscale wind systems were clearly present during the C2728 case, but not during C3031. The onset of the low level northeasterly winds in the afternoon of C2728 might be caused by differential heating of air above land and sea, generating solenoids or being part of larger scale, orographic induced, antitriptic airflow. Drainage flows from the Port Hills and the Canterbury Plains were simultaneously observed in C2728 case, converging over the city. Weak drainage air flow components may have been present during C3031, but could not be isolated from the main air flow. The radiative cooling during C3031 was less than during C2728, which also may have contributed to the lack of local, thermally driven circulations. The existence of local wind systems, as shown in C2728, may have important implications for the use of airshed models for predicting pollution dispersion. Gaussian plume models will clearly be unsuitable and generate inaccurate results under these conditions. It is unclear at this stage why the nocturnal jet persisted at low levels

throughout the whole night in the 3031 case, and became elevated or disappeared in C2728. Numerical tools will be required to explain these differences.

Several atmospheric processes occur in the Christchurch area during the winter, including local and mesoscale wind systems, low level jets, gravity waves, and formation of strong inversion layers at the surface. The interaction of these processes affects the dispersion of atmospheric pollutants. So far, a qualitative description and explanation has been given for two cases, but a quantitative, numerical analysis is required to provide further knowledge of the processes and their interactions, specific to the Christchurch area, and create the potential to simulate scenarios under different conditions than existed in C2728 and C3031. The results should then be implemented in airshed models for the Christchurch area.

5. Two dimensional modelling of drainage flows

5.1 Introduction

As shown in Chpater 4, complicated air flow patterns occur in the Christchurch area, due to interaction of several atmospheric processes having different time and space scales. A detailed topographical description of the Christchurch area and surrounding region is given in Chapter 1. A better understanding of the total atmospheric behaviour can be obtained by isolating a few important processes and analysing them in a simplified form. For example, during clear nights drainage flow from both the Port Hills and the Canterbury Plains appears to play an important role in air pollution dispersion over the area. In this research programme, atmospheric modelling studies with increasing complexity have been performed to try and simulate this airflow, starting with two dimensional simulations and then progressing up to full three dimensional runs. Two dimensional single slope simulations for the Port Hills and the Canterbury Plains have been performed, with the aim of studying the timescale, structure and strength of the flows. It will be obvious that the effects of complex terrain and three dimensional interactions are not incorporated here, but they will be discussed in following chapters.

5.2 Background

Pure katabatic winds are generated by the difference in buoyancy between the air near the surface of a slope and the ambient air at the same geopotential height. The air near the surface of a slope may be accelerated not only by buoyancy forces, but also by larger scale advection, local pressure gradients, the Coriolis force and be retarded by friction. In many studies, the effects of advection, pressure gradients and the Coriolis force are neglected. Initially, a relatively shallow layer of air starts moving downslope, gaining momentum, and the thickness of the katabatic layer tends to increase rapidly with distance, due to entrainment. However, the depth of the flow increases more slowly with increasingly longer downhill distances (Horst and Doran, 1986). When the ambient air has a very stable stratification, the entrainment rate is significantly reduced and may even disappear. Under these conditions the katabatic flow tends to be weaker due to reduced negative buoyancy of the katabatic air parcels and more shallow (Gudiksen *et al.*, 1995), and may even become invariant further downslope (Nappo and Rao, 1987). Under the right conditions it is even possible that the katabatic flow shows a pulsating pattern (Mori and Kobayashi, 1996). Mahrt (1982) provided a classification of different types of katabatic flows, based on scale analysis of the momentum equations. These types include nonstationary flow, advective-gravity flow, near-equilibrium flow, shooting flow, combinations flows, combination flows with friction, tranquil flow and non-gravity flows. In the study of two dimensional katabatic flows from the Port Hills and Canterbury Plains, advection and Coriolis forces are neglected, leaving the options open for **a**. nonstationary flows being relatively shallow with a stable stratification of the ambient air; **b**. near-equilibrium flows, when the

gravitational force is balanced by friction, being relatively shallow as well, but with an ambient stratification which is not very stable; and c. tranquil flows, which are deeper and have a stable stratification of the ambient air.

Several models of pure katabatic flows on a constant slope have been developed. For example, Prandtl (1942) and Rao and Snodgrass (1981) presented a one dimensional model, being invariant downslope, while Manins and Sawford (1979) provided a one dimensional hydraulic model which describes the downslope development of the katabatic layer with characteristic scales for wind speed and depth of the layer. Nappo and Rao (1987) developed a time-dependent two dimensional model, showing the dependence of katabatic flow depth, wind speed and entrainment rate on slope angle, downslope distance and ambient stratification. Since cooling of the air near the surface on the slope is the main driving force of pure katabatic winds, any factor seriously influencing this cooling may be expected to be important. The air can cool down by radiation divergence, but this process can be neglected compared to the cooling close to the surface by conduction. Turbulent processes efficiently carry this cooled air further away from the surface. The formulation of turbulent processes, i.e. the order of [turbulent] closure and parameterizations, is important, especially for nocturnal katabatic flow. According to Arrit and Pielke (1986) a turbulent kinetic energy (TKE) based scheme should be implemented in order to allow for proper exchange of TKE across the slope flow. However, such methods are generally numerically more expensive and the results are not necessarily more accurate. Neglecting advection, the katabatic flow is retarded by surface stress, and also by interfacial stress at the top of the layer, which can be significant (Manins and Sawford, 1979). At night, the temperature of the soil at the surface is influenced by the heat capacity of the soil, and the net loss of energy caused by a negative net radiation, partly compensated by heating from air and heat conduction in the soil (Oke, 1978, pp 31-39; Pielke, 1984, pp 380-385; Stull, 1988, pp 283-284). Increased soil moisture content increases generally the soil heat capacity and soil conductivity, and so it restricts the nocturnal cooling of the soil surface. Therefore, enhanced cooling of the soil surface may be expected when the soil is dry. Banta and Gannon (1995) demonstrated the influence of soil characteristics on the development of katabatic flow in a two dimensional numerical study, using RAMS. Enhanced cooling of the air near the surface may be expected with clear skies, a relatively dry soil, and possibly low to intermediate values of the surface roughness. An extremely smooth surface will promote laminar flow and so reduce effective heat exchange, while a very rough surface like a tall crop or a forest may stimulate turbulence initially, but layers of stably stratified air will form in the vegetation, reducing heat exchange with the surface. The interaction of advection and single slope winds tends to be non-linear as discussed by Arrit and Pielke (1986).

5.3 Two dimensional simulations of the Port Hills

For the modelling experiments the Port Hills are assumed to have a constant slope angle of 5.7°, rising from sea level to 400m over a horizontal distance of 4km. The north and south facing slopes are identical, although on the southern side of the slope the domain extends only 4km at sea level, while on the Christchurch side the domain extends for 12 km at sea level. Attention will be focussed on the katabatic flow on the Christchurch side.

5.3.1 Model settings

The two dimensional simulations were run for 6 hours at night, with a horizontal grid increment of 200 m, a vertical grid size of 2 m near the surface, gradually increasing with height to a maximum of 1000 m, and a timestep of 2 seconds. The model was run non-hydrostatically, with first order turbulent closure, dry (no cloud physics), with no Coriolis force, no vegetation and zero gradient flow at the lateral boundaries. Homogeneous initial conditions were used, with no wind (u=v=w=0), a constant vertical potential temperature gradient being 2 K km^{-1} to 2000 m, constant surface roughness length (z_o=0.10 m), with a silt loam soil type, and homogeneous soil profiles for temperature (283 K) and moisture content (60%) to a depth of 0.5 m over the entire domain. A sensitivity analysis was executed by varying soil moisture, vertical potential temperature gradient and vertical grid increment.

5.3.2 Results

As soon as the air started cooling on the Port Hills, the katabatic flow developed along the whole slope. Figures 5.1a and 5.1b show the wind speed and potential temperature of the flow after one hour's simulation. According to both theory and observations, the maximum wind speed and depth of the flow increased further downhill. The flow extended about 2.5 km over the horizontal part of Christchurch at an elevated level. The temperature plot clearly shows the cool air draining from the Port Hills over Christchurch. Figures 5.2a and 5.2b show the situation after 2 hours of simulation, when the katabatic flow had increased in strength and is extended to about 10 km from the foothills. The core of this low level jet is at an elevation around 40 m with wind speeds over 3 m s^{-1}. The winds continued to increase over time, although at a decreasing rate. After 6 hours of simulation (not shown) the structure of the flow had not changed significantly along the slope, but over Christchurch a cold layer of air had formed near the surface with a weak gradient of potential temperature, while above 40 m elevation the potential temperature increased sharply. At this elevation the outflow of the katabatic wind resulted in a low level jet with wind speeds well over 5 m s^{-1}.

5.3.3 Sensitivity analysis

Wind and temperature profiles were investigated after 3 hours simulation on the hills to assess the sensitivity of the model. When the ambient stratification was increased from 2 K km^{-1} to 10 K km^{-1} the maximum wind speed along the slope was reduced to about a third, but the depth of the flow did not change much. Soil moisture content, and therefore the rate of cooling at the surface also had a significant impact on the simulated two dimensional drainage winds along the Port Hills. When the soil moisture content was reduced to 40% a maximum wind speed of 4.4 m s^{-1} was generated at the foothills, while with a soil moisture content of 80% the wind speed reached only 2.5 m s^{-1}. Variations in

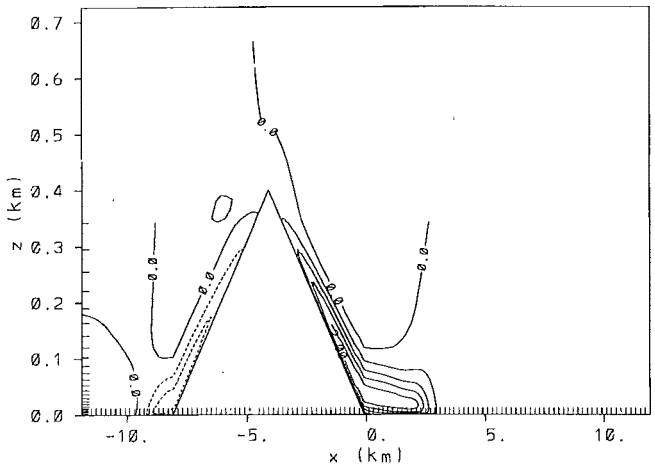

Figure 5.1a Wind speed (m s^{-1}) after one hour simulation.

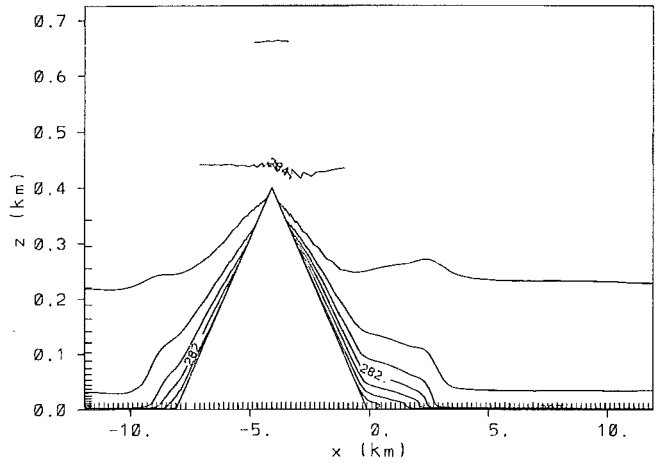

Figure 5.1b Potential temperature (K) after one hour simulation.

vertical grid increment appeared to have a significant effect on the simulated katabatic flow. When the vertical grid increment near the surface was increased from 2 m to 10 m the flow becomes weaker, with the heights of the maximum wind speed at lower elevations, but the overall depth of the flow did not change. Smaller values than 2 m for the vertical grid size produced numerically unstable results with the current settings of the model. Other variables and settings have not been tested for the two dimensional Port Hills simulations.

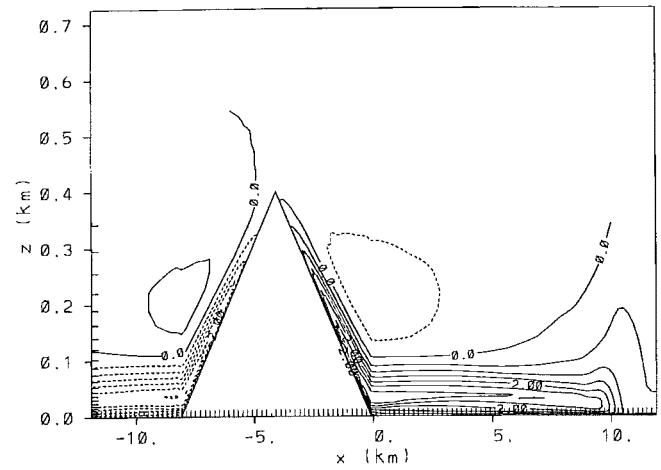

Figure 5.2a Wind speed (m s^{-1}) after two hours simulation.

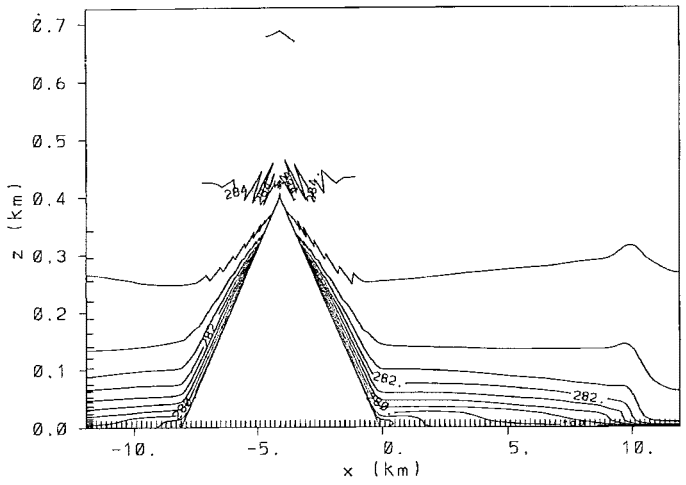

Figure 5.2b Potential temperature (K) after two hours simulation.

5.4 Two dimensional simulation of the Canterbury Plains

The Canterbury Plains can be imagined as an exponential decaying slope oriented in the south east - north west direction, being steepest near the mountain ranges, and being almost horizontal near the coast. The following function approximates the topography from the crest near the Okuku Range to Christchurch:

$$z = a.\exp\{-b.(s-r)\}+c, \qquad 0 \le s \le r \tag{5.1}$$

z is the height of the surface (m), s the horizontal distance from the crest (km) with Christchurch being located between s=50 km and s=60 km, r = 60 km, a=12.5 m, b=0.07324 and c= -12.5 m. The lateral topographical boundary conditions are defined as follows: southeast of Christchurch (s > 60 km) it is assumed that the plains continue for

another 20 km remaining at z=0 m, and northwest of the crest ($s < 0$) the surface height declines 300m over a horizontal distance of 10 km to z=700 m and then it remains at a constant height for another 10 km. Table 5.1 shows heights of the surface and slope angles at different distances from the crest to Christchurch.

Table 5.1 Approximate topography of the two dimensional Canterbury Plains, from the Okuku Ranges at s=0 km to Christchurch at s=60 km. z : height of surface (m); s: horizontal distance from crest (km); α: slope angle (degrees).

s (km)	z (m)	α (deg.)
0	1000	4.3
5	690	2.9
10	474	2.1
20	222	1.0
30	100	0.5
50	14	0.1
60	0	0.0

5.4.1 Model settings

The two dimensional simulations were run for 12 hours at night, with a horizontal grid increment of 1 km, a vertical grid increment of 10 m near the surface, gradually increasing with height, and a timestep of 12 seconds. The remainder of the model settings are similar to those described for the Port Hills two dimensional runs, except that an additional soil type, sandy clay, was used as well. A sensitivity analysis was executed by varying soil moisture, soil type, surface roughness length, vertical potential temperature gradient and vertical grid increment.

5.4.2 Results

As the air near the surface started cooling down, the katabatic flow developed, initially being most pronounced at the steepest part of the slope near the crest. Maximum wind speeds occurred close to the surface between 10 m and 20 m elevation. Later on, the strongest katabatic winds occurred further downhill. Figures 5.3a and 5.3b show profiles of windspeed and potential temperature at different distances downhill after 3 and 6 hours simulation, respectively. It appeared that after 3 hours simulation the strongest katabatic winds occurred 20 km downhill at a height of 50 m above the surface. At Christchurch ($s \geq 50$ km) a shallow temperature inversion had formed, but the katabatic flow was almost negligible. Cross sections are shown in Figures 5.4a and 5.4b which clearly indicates that the katabatic flow had not yet reached the lower, eastern part of the Canterbury Plains after 3 hours, but after about 5 hours the front of the flow reached Christchurch.

The profiles of Figure 5.3b show that after 6 hours simulation a strong low level jet had developed 50 km downslope above a stable layer, peaking with 6 m s^{-1} at 80 m height. This jet can be considered as a lifted outflow of the katabatic winds, which is a common feature over plains near a mountain range (Vergeiner and Dreisetl, 1987). Starting at the crest of the slope, the depth of the katabatic flow increased further downslope, which can be related to entrainment. The height of maximum wind speed increased as well, which can be partly explained by the increased depth of the flow and partly because the slope angle is declining and the flow is gradually lifted above a very stable layer near the surface.

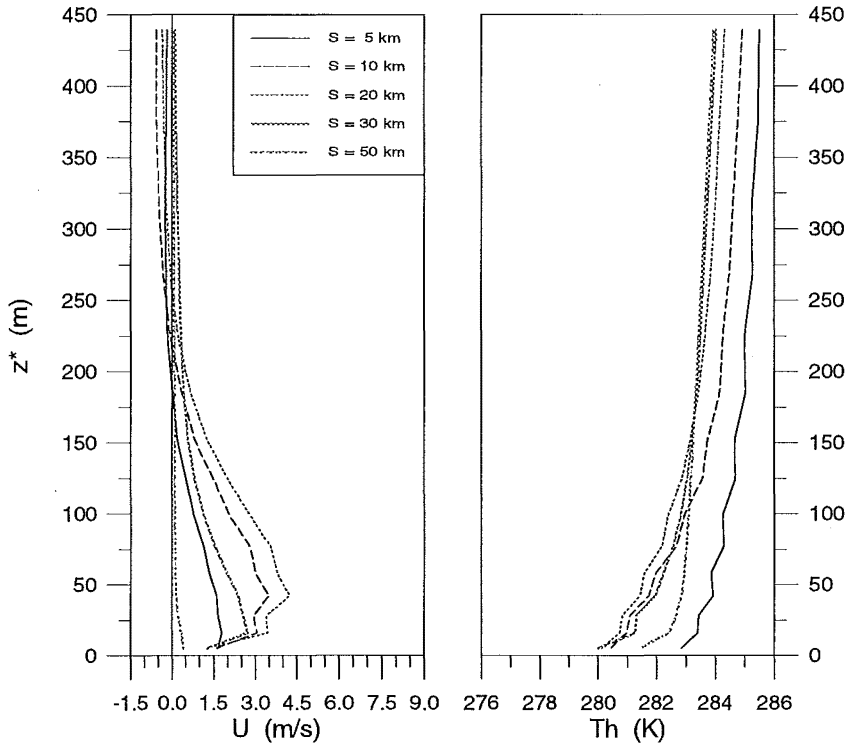

Figure 5.3a Vertical profiles of wind speed (left) and potential temperature (right) at different distances *s* from the crest after 3 hours of simulation. z*: height from surface.

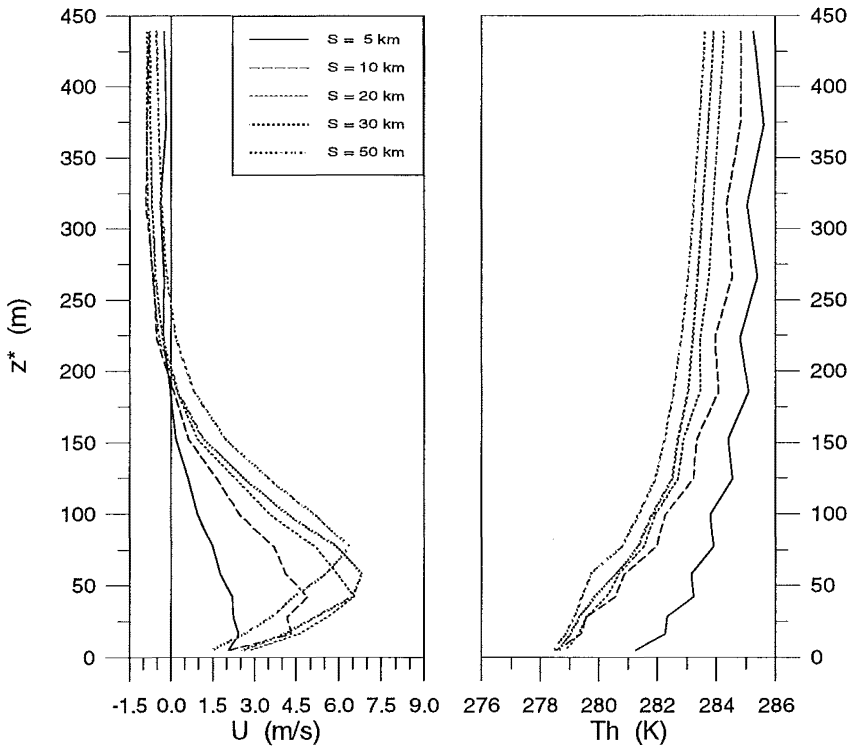

Figure 5.3b Vertical profiles of wind speed (left) and potential temperature (right) at different distances *s* from the crest after 6 hours of simulation. z*: height from surface.

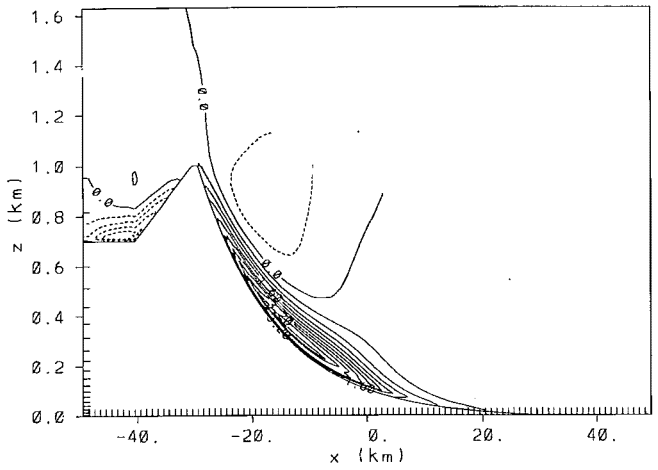

Figure 5.4a East-west cross section over the Canterbury Plains displaying wind speed (m s^{-1}) after 3 hours simulation. s=x+30.

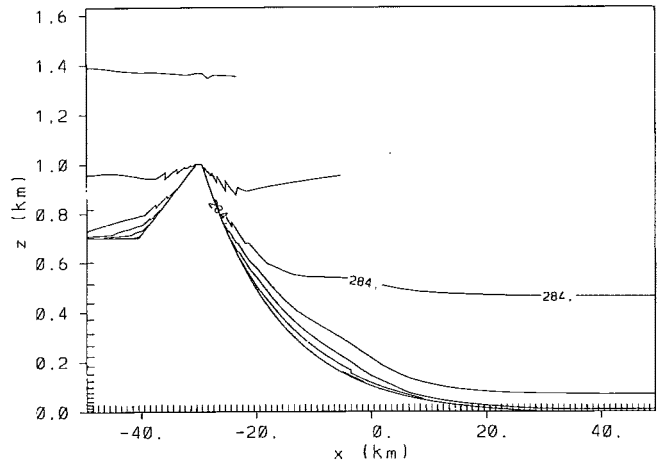

Figure 5.4b East-west cross section over Canterbury Plains displaying potential temperature after 3 hours simulation. s=x+30.

Figure 5.5a clearly shows the katabatic flow over the Canterbury Plains, increasing in speed and getting deeper. The core of the flow and the strong temperature inversion are quite visible over the eastern part of the Canterbury Plains in Figures 5.5a and 5.5b. Simulations showed that the strength of the katabatic flow continued to increase during the night and no steady state was reached, even after 12 hours. However, the increase in wind speed declined with time and was less then 6% per hour after 9 hours simulations along the slope.

5.4.3 Sensitivity analysis

Results of the sensitivity analysis were obtained after 6 hours integration time 50 km downslope (s=50 km). Soil moisture was varied from 40% to 80% for both sandy clay loam and silt loam, producing a dramatic impact on the flow. During the dry soil runs the cooling of the air in the katabatic layer is strongly enhanced and the maximum wind speed is almost double that of the wet soi l runs. The depth of the flow appeared to be slightly

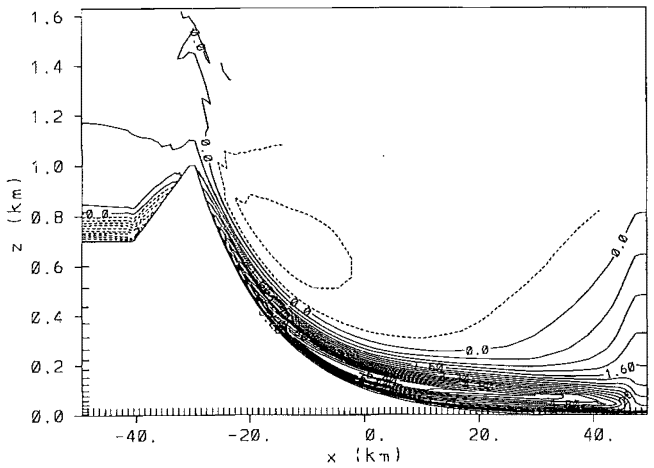

Figure 5.5a East-west cross section over Canterbury Plains displaying wind speed (m s^{-1}) after 6 hours simulation. s=x+30.

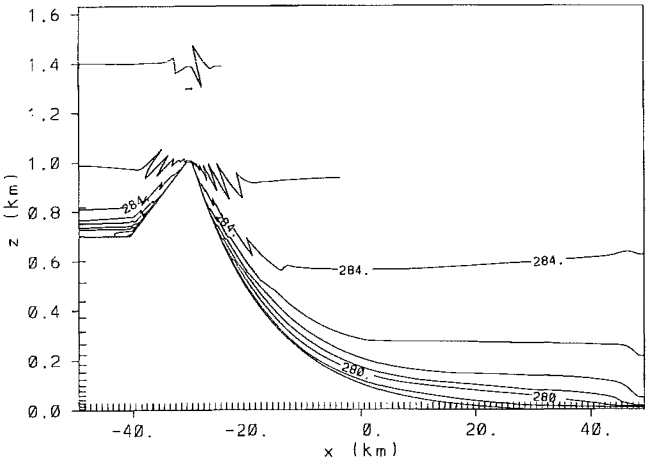

Figure 5.5b East-west cross section over Canterbury Plains displaying potential temperature after 6 hours simulation. s=x+30.

reduced in the dry soil runs. Ambient stratification of the air also had a significant effect on the katabatic flow. Comparing an initially neutral and a very stable case, with a gradient of potential temperature of 0 K km^{-1} and 10 K km^{-1}, respectively, the maximum wind speed in the neutral case was almost twice the speed of the stable case. The flow was very shallow in the stable case with the maximum wind speed at only 16 m height, compared to 77 m for the neutral case. The surface roughness length was varied between 0.05 m and 0.25 m, having no significant effect on the flow, which is in general agreement with the work of Manins and Sawford (1979). The model also appeared not to be very sensitive to the soil types used, silt loam or sandy silt loam. Three values of vertical grid increment were used: 5, 10 and 25 m for the lowest grid near the surface. The 5 m run created a stronger maximum wind speed and tended to produce a slightly deeper flow than the 10 m run, while the 25 m produced a similar maximum wind speed as the 10 m run, but the flow depth was slightly more shallow. So, the vertical grid increment had some effects on the output. Although intuitively the highest resolution would be expected to be the best, this is not necessary so, as the most appropriate value depends on the combination of several parameterizations.

5.5 Discussion and Conclusions

The two dimensional simulations of katabatic flow from the Port Hills and the Canterbury Plains show both that the strongest drainage flows may be expected when the soils are relatively dry and the ambient air has no strong stable stratification, at least up to elevations well over crest height. Interesting situations can occur when, for example, the air at geopotential heights between 0 m and about 500 m is very stable, with a near neutral lapse rate aloft up to about 1500 m or the reverse when air up to 500 m is nearly neutral and aloft very stable. During these circumstances only one of the drainage flows is able to develop quite well, while the other flow remains weak. Both simulations showed that a strong outflow of cold air drainage from both sources can reach Christchurch at an elevated level, but the time scales of the systems were different. Two hours after onset, cold air from the Port Hills may flow over most of the Christchurch area, while it takes more than 5 hours before significant drainage flow from the Canterbury Plains reaches the city. However, the onset of both drainage flows may be different in the real world, since the north facing Port Hills are well irradiated during most of the day under clear conditions, but in the afternoon during the winter, the south-east facing slopes of the Okuru Ranges have a high angle of incidence or are in shadow, and start cooling down rapidly, especially when these mountains are covered with snow. Three dimensional simulations are required to study the interactions of the drainage flows from the Port Hills and the Canterbury Plains, which is discussed in the next chapter.

6. Complex terrain - three dimensional modelling of airflow

6.1 Background

Airflow patterns become much more complicated when full three dimensional topography is introduced. When considering a single valley system, at night cold air descends along the sidewalls of the valley and pools down on the valley floor. A weak counter flow moves from the valley axis upwards for mass conservation. The reduced volume of air in a valley or basin compared to a plain with the same surface area at the top of the volume, the so-called geometric factor, causes an amplification of the diurnal temperature variation pattern in a valley system (Whiteman, 1990; Whiteman et al., 1996). Generally, at night the temperature of the air near the valley floor becomes lower than the air at the same geopotential height on the plains at the valley exit, resulting in a pressure gradient, causing an airflow out of the valley (Defant, 1951; Vergeiner and Dreiseitl, 1987; Whiteman, 1990). During daytime, these processes are reversed. The breakup of the stable and cold layer of air is caused by surface heating and the generation of anabatic winds on surrounding slopes, resulting in descent of the top of the stable layer (Triantafyllou et al., 1995) and advection into the valley. The strength of thermally driven valley winds appears to be proportional to the size of the airshed, according to Doran and Horst (1983) and Gudiksen et al. (1992). The combined katabatic flows may also result in a so called 'micro front' or 'drainage front' associated with a sudden change in wind and temperature when it passes a location at the surface (Orgill, 1981; Mahrt and Larsen, 1982). The reaction time of single slope winds is generally quick, but valley winds (larger systems) are slower. The valley outflow may result in a relatively narrow exit jet, elevated above the stable nocturnal boundary layer over the plains (Bossert and Poulos, 1995). The exit jet sometimes persists over hundreds of kilometers and it can be important for dispersion of atmospheric pollutants (Banta et al., 1995). Whiteman et al. (1996) distinguished well drained, steady state valleys or basins from poorly drained, strongly cooling systems by scaling the overall budgets of heat storage and convergence of heat by advection by the combined convergence of net radiation and the turbulent sensible heat flux of the systems.

A non local pressure gradient, e.g. at the synoptic scale, can be superimposed on the thermally induced pressure gradient in a valley system. Non-geostrophic winds may be generated in the valley due to channeling when the non-local pressure gradient is not perpendicular to the valley axis (Wanner and Filliger, 1989). The wind in a valley system can also be influenced by downward transport of momentum from above the valley by vertical turbulent mixing, sometimes leading to forced channeling, particularly in narrow valleys, and sometimes to countercurrents (Gross and Wippermann, 1987). The relative importance of the above mentioned processes is dependent on the dimensions of the valley-system, the strength of local flows, thermal stratification of air and wind shear (Doran, 1990; Doran and Skyllingstad, 1992; Whiteman and Doran, 1993).

Complex terrain can be considered as a combination of single slopes, sidewalls, valleys and plains, with varying scales and orientations. However, atmospheric behaviour over complex terrain is much more complicated than the sum of individual flow characteristics

associated with each topographic structure, due to multiple interactions, which can occur on different scales. The situation becomes even more complicated when synoptic scale advection occurs. Doran and Skyllingstad (1992) described the situation in the Cascade Mountains, where flow through gaps in the range over 100 km away sometimes had a major influence on local flow; it also appeared that the impact of variations in large scale flow patterns may be amplified or dampened locally due to topographic effects.

Sometimes perturbations of smooth well defined drainage flows do occur (Nappo et al., 1991; Gudiksen et al., 1992; Parker and Raman, 1993), as described in Chapter 3 for case C2728. The forcing of these perturbations is not always obvious and can possibly be linked to such terrain induced disturbances as vortex shedding, streamline deformation and gravity waves, interacting drainage flows, breaking Kelvin-Helmholz waves or larger scale phenomena. According to Nappo (1991) and the observations of the C2728 case, during the sporadic breakdowns of stability in the nocturnal boundary layer, significant portions of momentum, heat and atmospheric pollutants are exchanged between the surface layer and the air aloft. Since these perturbations are generally not incorporated in numerical models, short-term forecasts of nocturnal fluxes may be highly inaccurate.

Considering the above mentioned characteristics of atmospheric behaviour in complex terrain, it appears extremely difficult to make accurate predictions in this environment. Realizing that at least 4 grid points (in one direction) are required to resolve a 1 dimensional wave (Pielke, 1984), modelling in complex terrain requires grids with a high resolution to resolve the dominant topographic features. Such smaller scale structures as little side valleys, ridges and gorges, are necessarily smoothed out. Chaos theory suggests that a chaotic regime, pre-eminently the atmosphere, is highly sensitive to initial conditions (Lorenz, 1963; Gleick, 1987). So, especially in complex terrain error growth in predictive models is expected to be high. Surprisingly, the contrary appears to happen (Paegle et al., 1990). They suggest that the strong forcing by the lower boundary conditions, such as topography, makes the flow more predictable than over flat terrain. Nevertheless, although error growth in complex terrain seems to be restricted, local deviations can still be significant due to unresolved topographic features. For example, the nocturnal exit jet from the Hoon Hay valley system at Christchurch, having a horizontal extent of only a few kilometers, cannot be generated by a three dimensional model when the smallest grid increment is 1000 m, but it does occur when the grid increment is reduced to 250 m (see section 6.3) McQueen et al. (1995) also showed that the accuracy of meso-scale simulations with complex terrain was highly sensitive to resolved topography and vertical grid-size.

As mentioned before, the main topographic features in the Christchurch area are Banks Peninsula with the Port Hills at the southern fringe of the city, the modestly sloping Canterbury Plains and the southwest - north-east stretching Southern Alps, with the Okuku Range north of Christchurch. An extra complicating factor is the existence of the sea east of the Canterbury Plains, possibly enhancing the daily cycle of the anabatic and katabatic flows. A shallow onshore airflow can develop in Canterbury due to the combination of an orographically induced lee trough and a sea breeze system (Sturman and Tyson, 1981; McKendry et al., 1986). During clear nights several drainage fronts from the surrounding hills and mountain structures may develop and interactions may occur between the drainage systems themselves and the prevailing winds. Simulations have been undertaken to study **a**. the interaction of the drainage flows from both the Port Hills and Canterbury Plains, **b**. the sensitivity to advection and **c**. the influence of increased resolution on air flow patterns by using a grid increment of only 250 m, instead of 1000 m in the finest grid (see 6.2.2).

6.2 Model settings

Two series of simulations were undertaken, labelled after the number of nested grids being used: N4* and N3*, with the '*' a code number, related to a specific set of model settings. The final symbol of this code contains a character such as 'N', 'W', 'S' or 'E', indicating simulations with synoptic scale advection, or 'X' (no advection).

6.2.1 N4* runs

The N4* runs represent full three dimensional simulations of the atmosphere over the Port Hills and Canterbury Plains during mid-winter. Since the spatial scales of the Port Hills and Canterbury Plains are quite different, requiring different model resolutions, model grid nesting was undertaken. Four nested grids were used with grid increment ranging from 1 km to 100 km, as described in Table 6.1 and illustrated in Figure 6.1.

Table 6.1 Dimensions of nested grids and their grid increments used by the N4* runs.

grid	size	grid increment(km)
1	41 x 49	100
2	46 x 46	25
3	42 x 42	5
4	32 x 32	1

Topographic data were derived from appropriate topographic maps, missing grid points were interpolated by the quadratic inverse distance method. Finally, smoothing was done, twice for grids 1 and 2 and once for grids 3 and 4, using a 80% silhouette technique. The smoothing was necessary to avoid too spiky topography which can generate numerical instabilities and the silhouette technique maintains effective mean barrier heights (Walko et al., 1995). Despite lost topographic detail, the major features are still preserved (see Figures 6.2a to 6.3b).

The vertical grid increment of the two coarsest grids is 100 m at the lowest grid level, gradually increasing with increasing grid level. However, the vertical grid increment of the two finest grids was only 25 m at lowest grid level, gradually approximating the vertical grid increment of the coarsest grids with increasing height. The model was run for 27 hours, starting at 3 pm local time. The timestep was 120 s for the coarsest grid, but only 10 s for the finest grid. Again, the model is run dry without cloud physics and only one soil type was used, (silt loam) soil moisture of 60%, without vegetation. The model started with a soil and sea temperature of 283 K. Five different situations were tested: no advection at all (N405X run), constant advection (5 m s^{-1}) at 1000 hPa level, increasing to 10 m s^{-1} at 800 hPa and above from either north, east, south or west (N405N, N405E, N405S and N405W runs, respectively). The constant advection throughout the largest grid is a simplification of airflow at the synoptic scale. The more complicated airflow patterns at the synoptic scale can be represented by inhomogeneous initialization, using Four Dimensional Data Assimilation (FDDA), as described earlier.

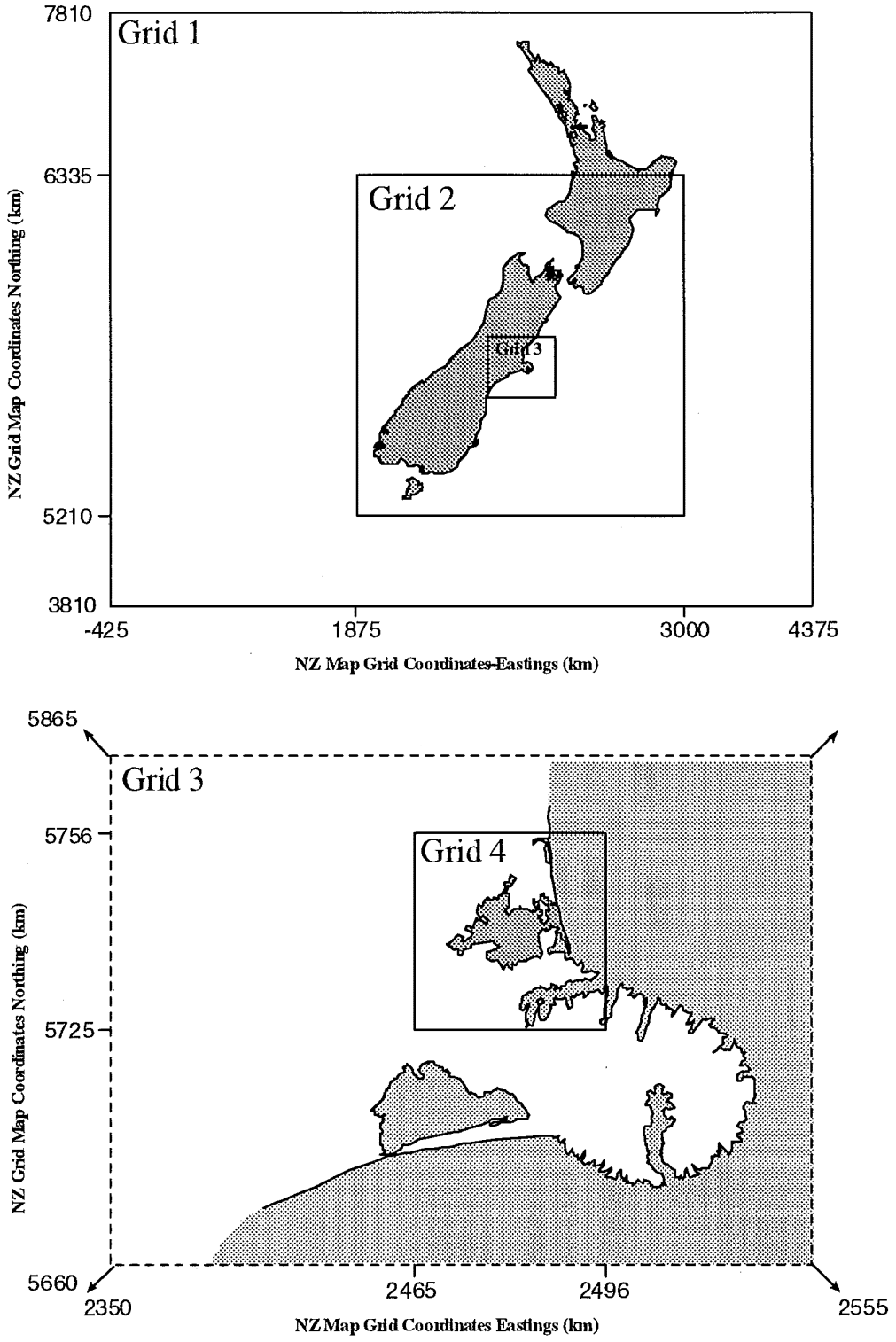

Figure 6.1 Plan view of the nested grids used by N4* runs.

6.2.2 High resolution run N303X

The N303X run was undertaken by using three nested grids with horizontal grid increments of respectively 5000, 1000 and 250 m. The two coarsests grids were similar to grid 3 and grid 4 of the N4* simulations. The topography in the domain of the finest grid was obtained from an appropriate topographic map and is smoothed once, using a 80% silhouette technique. This grid obviously contained more topographic detail than the grid with a 1000 m grid increment. Little valleys in the Port Hills, such as the Cashmere and Hoon Hay valleys are now reasonably well represented (see Figures 6.4a to 6.4e). The vertical grid increment in grid 2 and 3 was 12 m near the surface, gradually increasing with height. All other model settings were similar to the N405 settings, with no enforced advection. The N303X settings did not include a variation of surface characteristics, such as roughness length, soil moisture or urban versus rural.

6.3 Results

6.3.1 No advection run

The simulation without advection, N405X, will be discussed first. First, at sub-synoptic scale, the development of apparent sea breezes can be seen during both afternoons, even in midwinter. In the evening, the winds from the sea were replaced by land breezes, which persisted throughout a large part of the morning. Drainage flow from the Port Hills appeared as late as 7 pm, but at that time the drainage flow from the Alps and the Canterbury Plains had not yet developed. However, one hour later a south-easterly drainage flow from the Port Hills and a north-westerly drainage flow over the Canterbury Plains were both present, converging at low levels in the vicinity of Christchurch, stretching from about Hornby to Redwood (see Figures 6.2a and 6.2b). At 9 pm, the flow from the Canterbury Plains tended to dominate and had partly suppressed the drainage flow from the Port Hills. At midnight an elevated west-southwest jet flowed over Christchurch at about 200 m geopotential height with a maximum wind speed exceeding 8 m s^{-1}. During the night the jet increased slightly in strength and its core rose to a geopotential height of about 300 m. Figure 6.3a shows an east-west cross section of grid 3 at midnight, passing through Christchurch, with the u-component of the drainage flow from the Alps, which became elevated over the Canterbury Plains. A weak reverse flow aloft had developed. A north-south cross-section at midnight over Christchurch shows a northerly component in the drainage flow from the Okuku Range, which undercuts the flow aloft, which has a southerly component (see Figure 6.3b). Along the northern slopes of the Port Hills a shallow layer with a separate drainage flow can still be distinguished. A pool of cold and stable air is formed near the surface during the night in the Christchurch area, increasing in depth. At 6 am a strong inversion was formed at a height of 250 m, with a weakly stable layer underneath. In the morning hours the air near the surface warmed slowly and the low level jet persisted until 11 am. In the afternoon, anabatic winds had started in the mountains. As late as 4 pm a sea breeze developed along the Canterbury coast and the front moved westward over the Canterbury Plains.

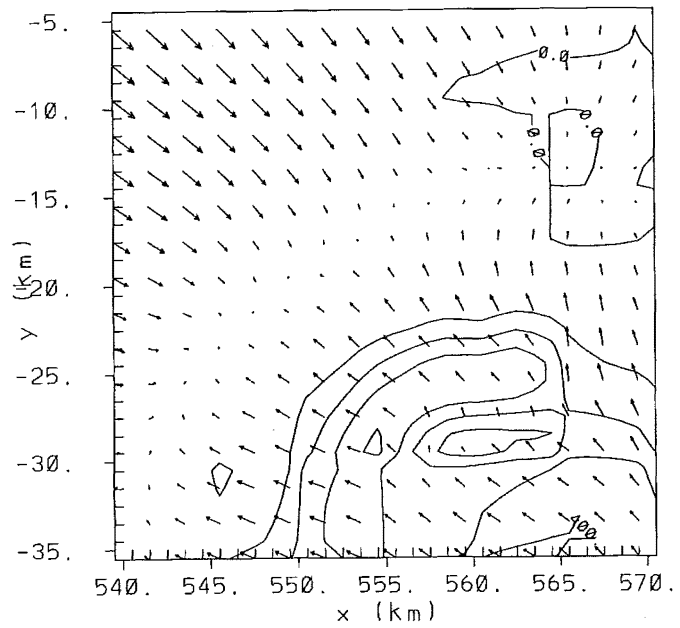

Figure 6.2a Vector plot in grid 4 generated by N405X at 12m after 5 hours simulation at 8 UTC (8 pm local time). Contour lines display geopotential height (m) and maximum wind speed shown is 2.2 m s^{-1}.

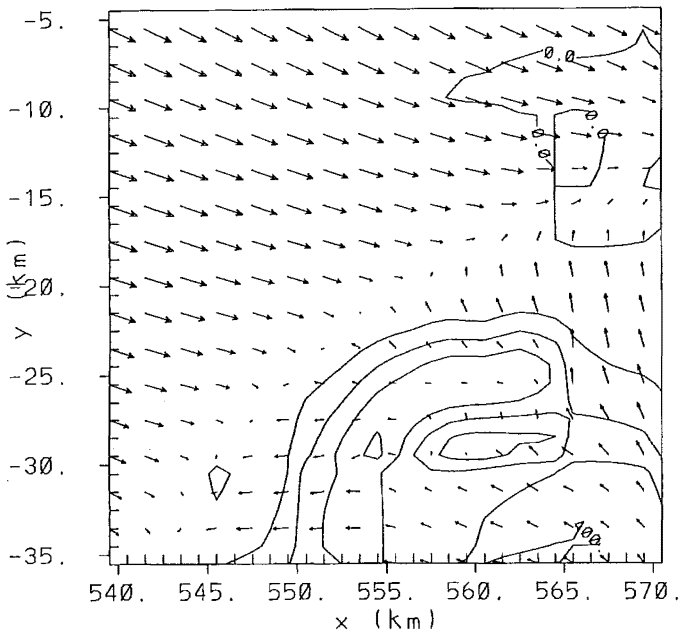

Figure 6.2b Vector plot in grid 4 generated by N405X at 12m after 6 hours simulation at 9 UTC (9 pm local time). Contour lines display geopotential height (m) and maximum wind speed shown is 2.7 m s^{-1}.

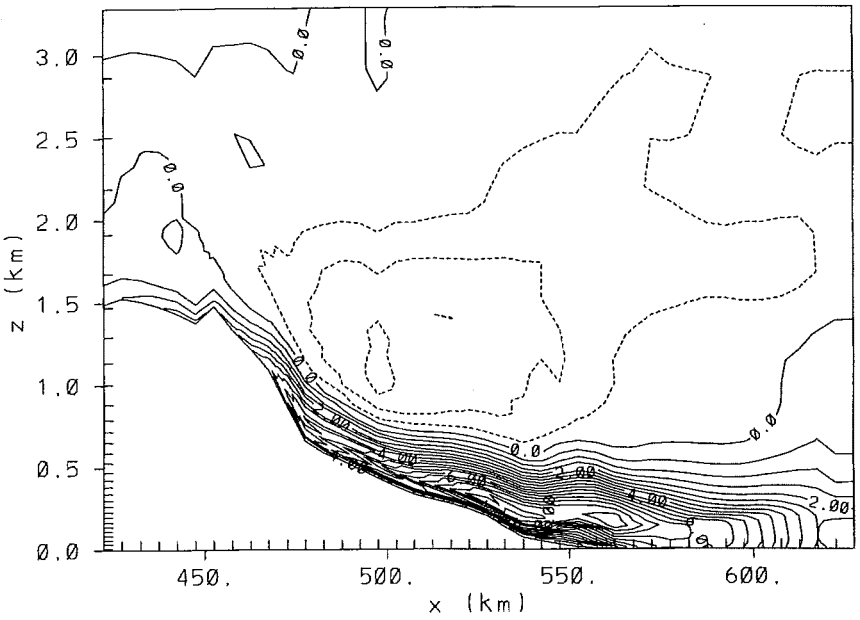

Figure 6.3a East-west cross section in grid 3 generated by N405X after 9 hours of simulation at 12 UTC (midnight local time)showing contours of the x-component of wind velocity (u) (m s^{-1}) with Christchurch between x=565 and x=585.

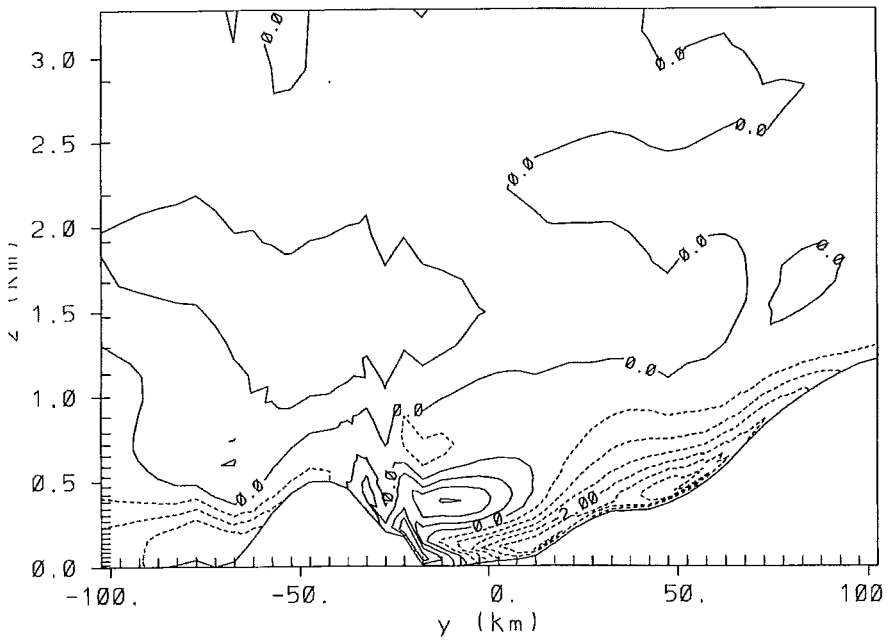

Figure 6.3b North-south cross section in grid 3 generated by N405X after 9 hours of simulation at 12 UTC (midnight local time) showing contours of the y-component of wind velocity (v) (m s^{-1}) with Christchurch between y= -20 and y=0.

6.3.2 Advection runs

During the afternoons the near surface air flow patterns of the four runs with advection from respectively west, north, east and south, were all very different, although all runs showed low level convergence over the South Island. However, due to decoupling of low

level air flow from that aloft during stable stratification, the structure of the nighttime drainage flows was very similar in all four advection cases in general, although variations are apparent when examined in detail.

In the afternoons the air at lower levels is not decoupled from air aloft, which implies that advection had a strong influence. Advected air is influenced by topography, forcing the air to flow partly around the South Island. The daytime airflow pattern can be considered as a combination of sea breeze, anabatic flow, lee trough and advection effects. The winds near the surface of the N405W run showed a divergence of air near the West Coast, a strong west to northwest air flow through Cook Strait, and winds curving around the sourthern end of the South Island. However, along the east coast of Canterbury only a very weak westerly breeze existed, which at the end of the afternoon developed into a north easterly sea breeze; a west northwest wind continued over the Alps. The N405N simulation showed a strong north-northwest flow through Cook Strait, a north-easter along the east coast of Canterbury with an easterly sea breeze developing over the Canterbury Plains. A north-west flow existed over the Alps and the western part of the Canterbury Plains. The N405E run displayed a south-easterly flow in Cook Strait and over the Alps, while a south south-easterly flow existed along the Canterbury Coast. The N405S simulation showed a southerly flow through Cook Strait, over the Alps and the Canterbury Plains, while along the Canterbury east coast a south westerly developed.

It is interesting and encouraging to see that at the sub-synoptic scale these simulations showed a good similarity to observed air flow patterns around the South Island during similar advective conditions.

6.3.3 Nocturnal flows

During the night the winds above 750 m from the surface were strongly influenced by advection. However, the simulated clear nights generated strong near surface cooling which induced drainage flows in all cases. The low level nocturnal flows of the advection cases were similar to the non-advection simulation (N405X), except for: minor variations in wind direction and differences in wind speed. The simulations with southerly (N405S) and easterly advection (N405E) generated stronger low level flow, while in the westerly and northerly advection cases (W- and N- case, respectively), the wind speed was generally similar to the non-advection case (N405X). See Figures B.1a to B.1d in Appendix B. Vertical east-west cross sections at the latitude of the Christchurch area reveal in the easterly advection case (N405E) a stronger drainage flow from the Alps than in the N405 run. During the N405S simulation the drainage flow was deeper and even stronger than during the N405E run. However, the N405N showed a strong westerly flow over the higher parts of the mountains, but a weak separate drainage flow and even an area with a countercurrent can be distinguished. The N405W run also produced a strong flow over the higher part of the Southern Alps and no separate drainage flow at lower levels was generated on the eastern side of the main divide. The east-west cross sections of the advection cases are displayed in Figures B.2a to B.2d in Appendix B. Figures B.3a to B.3d show vertical north-south cross sections at the longitude of the Christchurch area. They indicate that the N405W run was very similar to the no-advection simulation, while in the N405N run stronger katabatics were created from both the Port Hills and the Okuku Range. Both flows became elevated at an early (spatial) stage, due to a deep pool of cold air over the Christchurch area, with generally very weak winds close to the surface. The N405E run showed a well developed drainage flow from the Port Hills, but a negligible south-component in the drainage flow from the Okuku Range. A strong nocturnal south westerly jet was present over the Christchurch area at geopotential heights between 300 m and 600 m. During the N405S run no separate drainage flow could be distinguished from

the advected air over the Port Hills. However, despite the strong southerly advection, a very shallow drainage flow with a north-component developed over the Okuku Range. A strong elevated south-westerly jet could also be found in the Christchurch area.

6.3.4 High resolution run

The N303X showed that during the afternoon, anabatic winds developed on the slopes of the Port Hills, especially in the west to north facing valleys, which disappeared around 5 pm. At 6 pm, katabatic flows developed, creating a drainage front, approximately 3 to 6 km away from the Port Hills at an elevation of 30 m, and moving away from the hills (see Figure 6.4b). The spatial variability of the drainage flow is apparent, with a stronger flow out of the valleys and weaker flows in areas extending from the ridges. Variations in wind direction within distances of 1000 m can be observed clearly. At 9 pm the drainage front had moved more than 10 km away from the Port Hills, but the frontline was less pronounced than at 6 pm. The ridge at Kennedy's Bush (labeled B in Figure 6.4c) caused a well defined area with reduced drainage flow on the plains. At 10.30 pm the drainage flow form the Port Hills had generally weakened, but the drainage flows from the valleys at Cashmere, Bowenvale and especially Heathcote were still well pronounced. Between the Bowenvale and Heathcote valleys (over suburbs of Opawa and Woolston) an area with very calm conditions was generated. Note as well, a large area with very calm conditions in the south western part of grid 3 (Halswell). At the same time a westerly flow from the Canterbury Plains was developing and approaching the city. From midnight onwards, the westerly drainage flow from the Canterbury Plains dominated over most of Christchurch, although drainage flow from the Port Hills still existed close to the hills, especially at lower levels. The valleys in the Port Hills provided some sheltering from the flow over the plains (see Figures 6.4d and 6.4e).

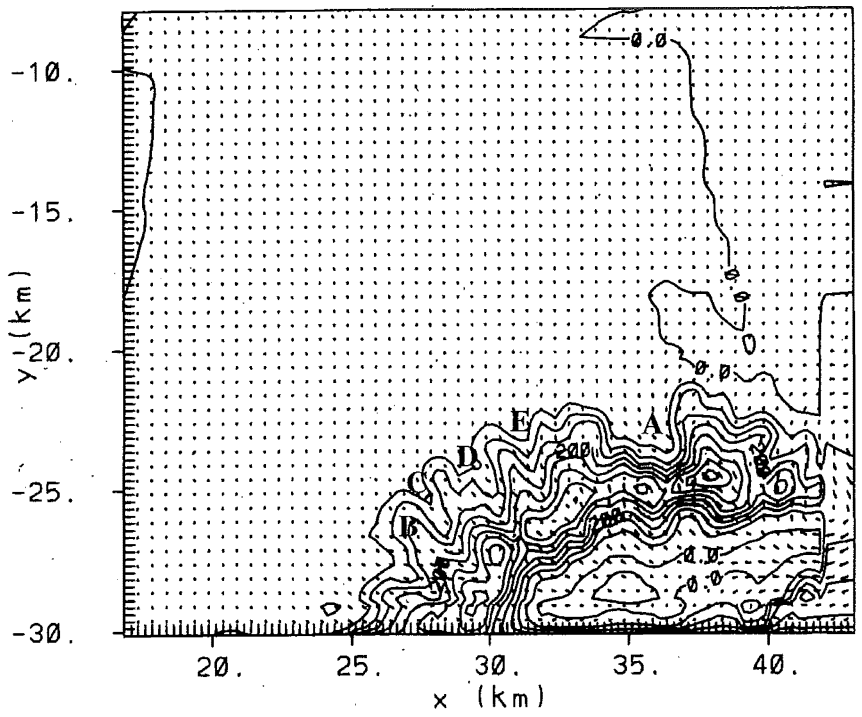

Figure 6.4a Vector plot in grid 3 generated by N303X at z=30m after 1 hour simulation at 4 UTC (4 pm local time). Contour lines display geopotential height (m) and maximum wind speed shown is 1.0 m s^{-1}. **A**: Heathcote valley; **B**: Kennedy's Bush; **C**: Hoon Hay valley; **D**: Cashmere valley; **E**: Bowenvale valley.

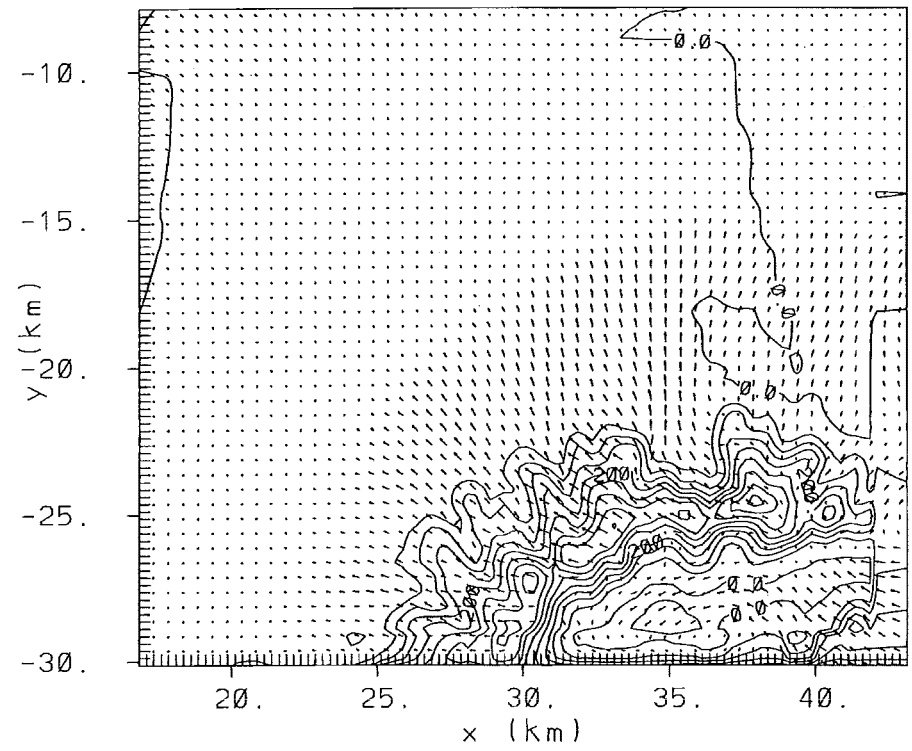

Figure 6.4b Vector plot in grid 3 generated by N303X at z=30m after 3 hours simulation at 6 UTC (6 pm local time). Contour lines display geopotential height (m) and maximum wind speed shown is 4.3 m s^{-1}.

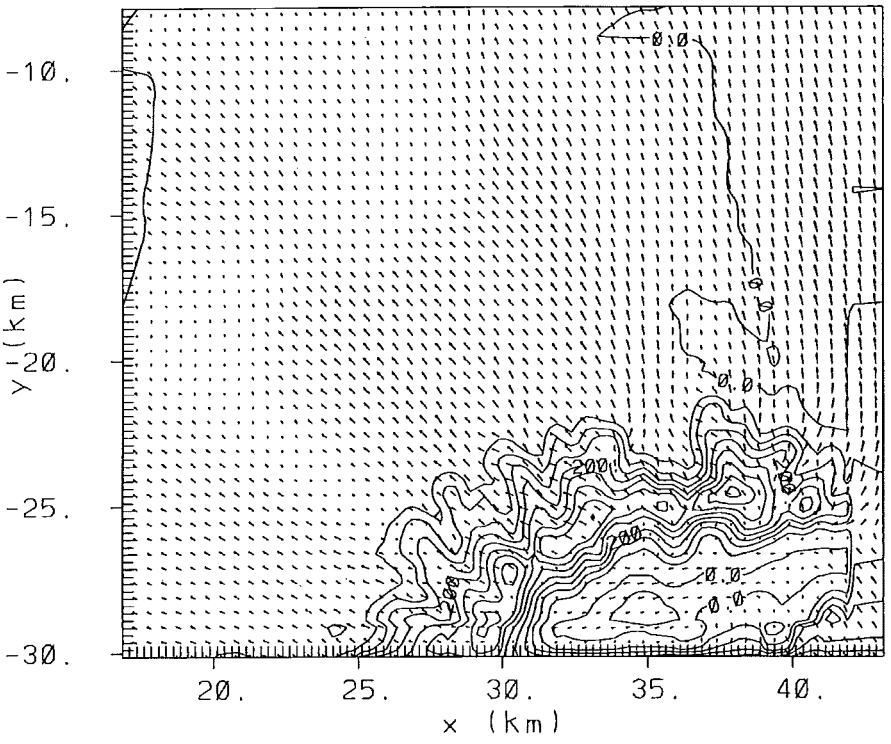

Figure 6.4c Vector plot in grid 3 generated by N303X at z=30m after 6 hours simulation at 9 UTC (9 pm local time). Contour lines display geopotential height (m) and maximum wind speed shown is 5.8 m s^{-1}.

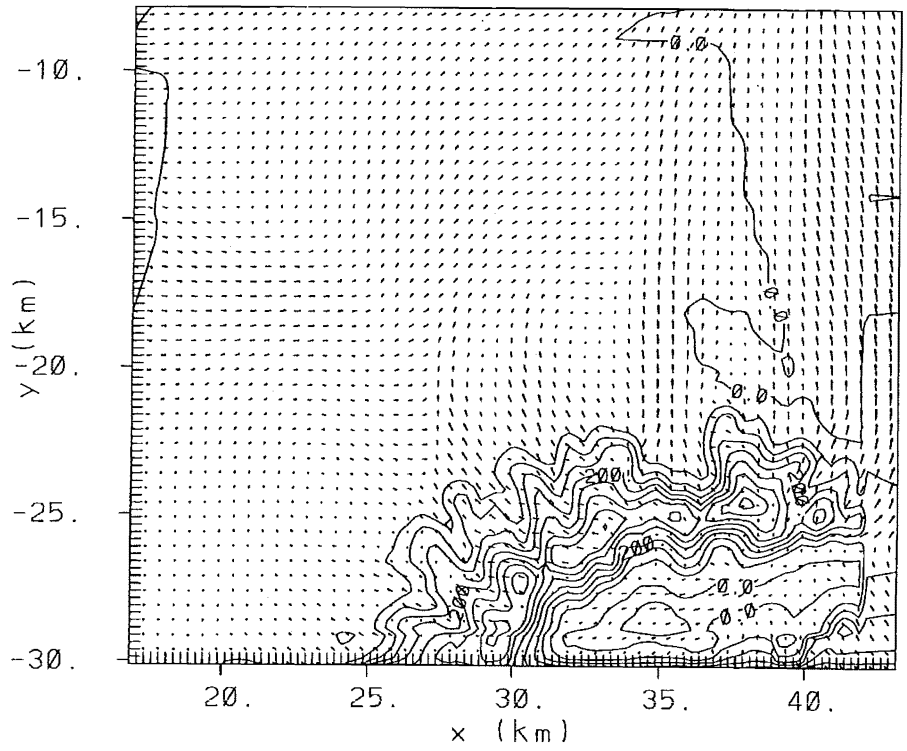

Figure 6.4d Vector plot in grid 3 generated by N303X at z=30m after 7.5 hours simulation at 10.30 UTC (10.30 pm local time). Contour lines display geopotential height (m) and maximum wind speed shown is 5.9 m s^{-1}.

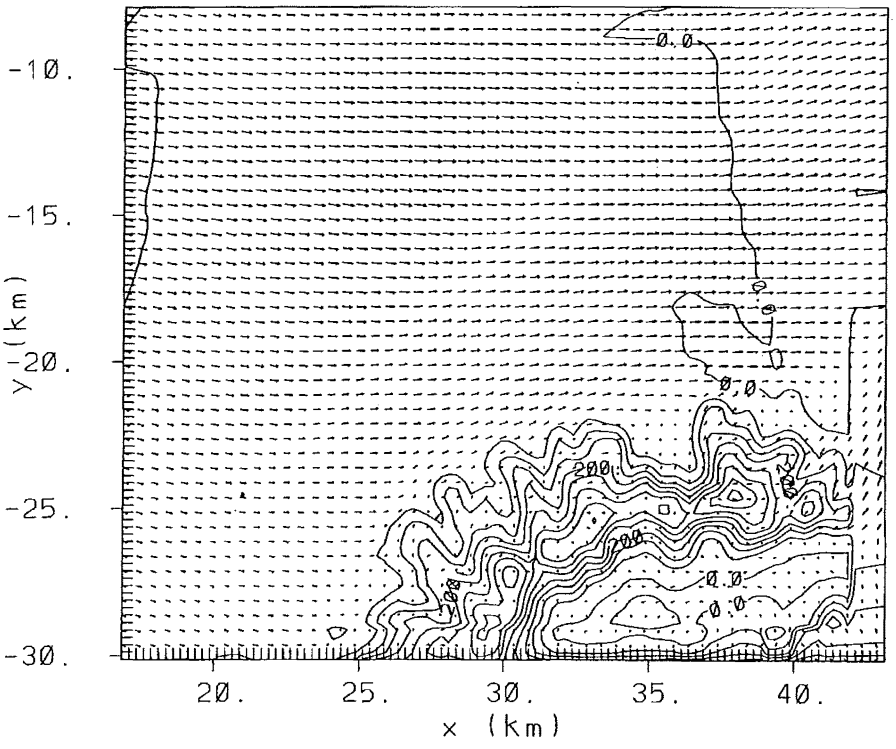

Figure 6.4e Vector plot in grid 3 generated by N303X at z=30m after 9 hours simulation at 12 UTC (midnight local time). Contour lines display geopotential height (m) and maximum wind speed shown is 6.5 m s^{-1}.

6.5 Discussion and conclusions

The N405 simulations have demonstrated that even in mid-winter daytime convergence over the South Island could develop, due to thermal activity. Apparently, the reduced daytime heating of the air near the surface in the winter season is sufficient to generate anabatic flows and possibly even sea breezes. It can be argued however, that the relatively low soil moisture content of 60%, which favours a high amplitude in the diurnal surface layer temperature wave, is too low during the winter season for a silt type soil. However, preliminary two dimensional studies over bare silt loam soil with soil moisture content ranging from 40% to 100% showed that the observed diurnal cycle of air temperature at 10 m elevation above the surface correlated best with simulations having a soil moisture content near 60%. It must be said, that the surface layer scheme based on the combined models for soil (Tremback and Kessler, 1985), vegetation - not used here (Dickinson et al., 1986) and surface fluxes (Louis, 1979) is efficient computationally, but simplified and could be improved. It will be obvious that the occurrence of daytime convergence over land is also dependent on the difference between the advected air mass and sea surface temperatures, cloud cover and the character of the larger scale advection.

The daytime advection cases showed that both direction and speed of low level air flow is strongly influenced by topography. The simulations generated airflow structures which show good resemblance with observed patterns during similar advective conditions. However, it must be realized that the homogeneous advection cases are a serious simplification of the actual synoptic conditions, which can be approximated by inhomogeneous simulations, using FDDA.

The strong radiative cooling at the surface in the N405 simulations favoured the development of relatively cold and stable layers. In these circumstances, the vertical exchange of momentum, and sensible and latent heat to or from higher levels of the atmosphere are strongly reduced due to the suppressed vertical component of turbulence. So, the layer near the surface is more or less 'decoupled' from the layer aloft. The occurrence of drainage flows in the advection cases, which were very similar to the drainage flows of the non-advective case, suggest the existence of 'decoupling'. Apparently, forced convection (Stull, 1988, pp. 118, 158) generated by the advection was generally too weak to disrupt the formation of the cold stable layers near the surface. Nevertheless, the larger scale advection had some influence on the low level air flows, as demonstrated by the variations in nocturnal flow patterns of the different cases. The easterly advection generated a more shallow drainage flow with similar maximum wind speeds at lower elevations compared to the non advection simulation east of the Southern Alps. A similar pattern could not be observed with the southerly advection and the drainage flow from the Okuku Range. In this case the northerly component of the drainage flow was suppressed. Generally, the wind speeds of the drainage flows and low level jets during the advection cases were higher than during the non-advection case. The N303X run, having a horizontal grid increment of only 250 m in the finest grid, was computationally very demanding, taking over three weeks to complete a 27 hr simulation on a SUN Sparc Station 10 (model 512 BSX). Interesting features were revealed, which were not generated by the simulations with a lower resolution. Variations in wind speed and direction on the scale of individual suburbs in Christchurch were shown, which can have implications for the dispersion of atmospheric pollutants. Although the N303X run did not allow for variations in surface characteristics, the simulation with homogeneous surface conditions showed the dramatic

impact of the increased resolution by topographic effects on air flow patterns over Christchurch. Therefore, when future dispersion studies concerned with small scale variations are undertaken in the Christchurch area, model resolution have to be seriously considered. This is particularly important when a single point source is investigated, especially near the Port Hills. It will be obvious that dispersion models such as Gaussian plume models, which are not three dimensionally prognostic, will be prone to be inaccurate in the Christchurch area.

7. Application to air pollution dispersion

7.1 Introduction

The computer power currently available enables simulation of atmospheric behaviour on a small scale, showing details which cannot be generated by larger scale models. A variety of meso-scale models has been and will be developed, while existing models are continuously improved and upgraded. Several of these models, like RAMS version 3b, contain detailed formulations of the physical processes involved, and therefore they make realistic simulations. The models have a wide range of potential applications, for example in:

- Agriculture and forestry: pest control, epidemiology, warnings (frost, other adverse phenomena), fire control.
- Planning: analysis of local climate and potential extremes in an area, indicating suitable locations for housing, wind turbines, industry, etc.
- Special events: America's Cup wind forecasts; Olympic Games; regional forecasts for hot air balloon trips and gliders; film industry.
- Military: detailed forecasts for surveillance, an attack by commandos, air drops, etc.
- Air pollution dispersion: the extent of dispersion in an area; emergency response; air quality models linked with the atmospheric output of meso-scale models (this item will be discussed in more detail).

7.2 Dispersion of air pollution

Meso-scale models are able to generate three dimensional prognostic meteorological fields. When the model is applied with a particular resolution and other settings, and the ratio of computer time to real time is well below 1.0, the model can be used for emergency response systems, as discussed by Fast et al. (1995) and Lyons et al. (1995a). Increasing the resolution will also require more computer time, so at a certain stage the limit will be reached when computer time equals or even surpasses simulated time, disabling emergency response applications. A solution to this problem can be found by **a.** not resolving at such a small scale (e.g. less then 250m), **b.** making the code more efficient, **c.** using more powerful computers and **d.** using another, faster type of model. Often these faster models contain simplified physics, which can cause unrealistic phenomena to evolve. A large group of these simplified models also use diagnostic meteorological fields, so they cannot properly anticipate changes in meteorological conditions during an event. When time is not critical, the prognostic three dimensional meso-scale models can be used to analyse historic or potential events in certain areas with a very high resolution, being most useful in areas with complex terrain or variable land use. Lyons et al. (1995a) demonstrated the benefits of applying a three dimensional prognostic dispersion model (RAMS combined with a Langrangian particle dispersion module in a coastal environment, where fumigation, relatively strong vertical motions and re-circulations occurred due to sea breezes, creating

complex dispersion patterns). They showed that conventional, non three dimensional prognostic models would fail to generate these dispersion patterns.

Despite the high potential of three dimensional prognostic models, two important factors often hamper good results of air quality models linked with these meteorological models: **a.** use of local observations, which are not necessarily representative of the area involved, and **b.** emissions inventories of limited accuracy. A few examples of air pollution studies will now be discussed.

7.2.1 Athens

Athens has a very serious photochemical air pollution problem, caused by high emissions and an unfavourable topography (Moussiopoulos et al., 1995), combined with frequently occurring calm, stagnant and clear conditions. Sea breezes and re-circulations are common phenomena in this area. Pilinis et al. (1993) used RAMS in combination with CALGRID, an Eulerian air quality model, to simulate NOx and ozone concentrations in the greater Athens area. However, their results provided only an indication, and they suggested that errors were caused by a poor emissions inventory and possibly by the limited resolution, although the horizontal grid increment was 2 km and near the surface the vertical grid increment only 5 m. Kunz and Moussiopoulos (1995) used MEMO, a three dimensional prognostic, non-hydrostatic model, with 1st order turbulence closure and a grid increment of 2 km in the finest grid, to simulate air flow patterns in the Athens region, giving satisfactory results for two case days. Moussiopoulos et al. (1995) linked MARS, an air quality model with MEMO and applied an improved emissions inventory, resulting in realistic patterns of atmospheric pollutants. Lagouvardous et al. (1996) demonstrated that simulated dispersion of air pollution in the Athens region is highly sensitive to the way the model is initialized. They used RAMS in combination with HYPACT, a hybrid Lagrangian and Eulerian dispersion model. It appeared that vertical soundings with a high resolution were important for reliable results in the morning hours, while synoptic and regional scale observations had to be incorporated for good results in the afternoon. Grossi et al. (1996) compared a diagnostic objective analysis procedure with RAMS, MEMO and TVM, a three dimensional prognostic model based on the hydrostatic approximation with a 1.5 order turbulence closure, linked with CIT, a three dimensional photochemical air quality model, simulating air pollution dispersion in the Athens area during the same case day. The diagnostic objective analysis method was as good as the observations permitted: it was not able to generate small scale flow patterns and drainage flow in areas without observations. The three prognostic models had a similar horizontal resolution (2 km grid increment) in the finest grid and produced generally similar flow patterns, although significant differences occurred, particularly at night. According to the authors, the differences could be related to vertical resolution, hydrostatic versus non-hydrostatic and numerical diffusion schemes, but the important schemes for surface fluxes were not mentioned explicitly. The simulated air pollution concentrations within the city were very similar, but outside the city significant differences were generated, which is not surprising, since within an area source differences in air flow patterns do not affect the predicted air pollution concentrations much, but outside the main source they become important. In another study, Moussiopoulos *et al.* (1997) used MEMO contemporary with the photochemicial dispersion models MARS and MUSE to simulate the impact of a new airport near Athens on the air quality in the region. The deterioration of the air quality would remain within acceptable limits, according to their studies.

7.2.2 Los Angeles

Los Angeles has a well known reputation for its poor air quality, caused by high emissions from traffic and industry over an extended area, in combination with climatic conditions, a coastal location, and a regional topography favouring stagnant air masses, low level inversions and recirculations. Many papers and reports have been published, describing the meteorological conditions, emissions, observed air pollution, and haze development. An extensive effort has also been put into modelling the dispersion and photochemistry of atmospheric pollutants. A few recent publications are mentioned here. Ulrickson and Mass (1990a and 1990b) used a predecessor of RAMS, CSUMM, to simulate dispersion of pollutants in the Los Angeles Basin. Their model used the hydrostatic approximation and a smallest grid increment of 5 km. They reported a reasonable daytime simulation of meso-scale circulations, but during the night the results were less succesful. Poulos and Pielke (1994) applied RAMS in combination with a Lagrangian particle disperion model (LPDM) to study the long range transport of air pollution from the Los Angeles Basin. Their investigation focussed on the possibility of transport into the Grand Canyon National Park, which could result in the deterioration of visibility in the Park. They used three nested grids, with the finest grid having a grid increment of 8 km. According to their simulations, the Grand Canyon National Park was hardly affected by pollutants from the Los Angeles Basin. Lu and Turco (1996) used SMOG, an hydrostatic, three dimensional prognostic model, integrated with an air quality module. They also concluded that atmospheric pollutants are easily confined to the Los Angeles Basin, which is surrounded by high mountains. However, their simulations showed that during the afternoon atmospheric pollutants may escape from the basin by anabatic flow, injecting air into the free atmosphere and by advection through a few mountain passes. In the Los Angeles area itself, their modelling system was able to predict actually observed stable layers aloft containing pollutants, generated by recirculations and entrainment. These layers can play an important role in the build up of very high concentrations during multiple day events.

7.2.3 Mexico City

Mexico City has an extremely serious air pollution problem with ozone concentrations exceeding the Mexican air quality standards most days of the year, with peak concentrations much higher than those observed in Los Angeles. The city is surrounded on three sites by high mountains forming an effective barrier. The air pollution problem is most pronounced during the winter when strong inversions can develop and clear sky conditions prevail. The city experiences generally a morning peak with primary pollutants and a second peak in the afternoon with secondary pollutants like ozone (Jauregui, 1988; Bossert, 1997). Williams et al. (1995) applied HOTMAC, a three dimensional prognostic, higher order turbulence closure model with the hydrostatic approximation, combined with RAPTAD, a Monte Carlo dispersion and transport model, to simulate air flow patterns and dispersion of air pollution in the Mexico City region. Their coarsest model grid covered an area of only 150 x 120 km^2, not including such features as the coastal plains and the Gulf of Mexico. The finest grid spacing was 2km. The model was initilized homogeneously, and some nudging of wind data aloft was allowed during the simulation. The model was able to generate the major wind structures reasonably well, but failed to resolve convergence over the city and predicted nocturnal low level temperatures over the city which are too high. Improvements were expected with the introduction of an upgraded radiation scheme and the addition of an extra coarse grid covering a larger area. Bossert (1997) used RAMS in an FDDA mode, combined with HYPACT, to simulate a three day event in the Mexico City region. His coarsest grid covered an area of more than 600 x 800 km^2, containing the coasts of the Pacific Ocean and the Gulf of Mexico. The vertical grid increment near the

surface was 100 m and the finest grid had a horizontal increment of 4 km. Generally the simulations provided good results, although significant differences from observations also occurred, which can partly be related to inaccuracies in initialization and the relatively coarse resolution. The model was able to simulate complicated air flow patterns at the meso-scale which were largely influenced by the dramatic topography in combination with synoptic interaction and air mass differences over land and the Gulf of Mexico. Both the above mentioned papers do not include simulations with an attached air quality module, containing chemistry, so the simulated ozone concentrations could be improved.

7.2.4 Other environments

Several other environments have been investigated by three dimensional prognostic models. Lyons et al. (1995b) reported a study of dispersion of ozone over Lake Michigan, using RAMS. Silvan Perego (1996) developed the integrated model BERPHOMOD, containing an air quality module, to investigate the air pollution in highly complex terrain in Switzerland and obtained promising results. McKendry (1994) and Steyn (personel communication) used RAMS to explain dispersion of pollutants in the Vancouver region. Hedley and Singleton (1997a and 1997b) discussed the satisfactory performance of the non-hydrostatic model MC2, combined with the photochemical model CALGRID, simulating ozone events in the Vancouver Region. Poulos and Bossert (1995) applied RAMS, combined with LPDM in complex terrain in eastern Colorado to simulate dispersion from two canyons. Mueller et al. (1996) studied ozone transport in the southern Appalachian mountains, using different settings of RAMS. They concluded that FDDA strongly improved their results and the simulations enabled them to make certain deductions about sources of ozone. The interaction between atmospheric pollutants and the complicated patterns of sea breezes in the Auckland area was investigated by McKendry and Revell (1991) and McKendry (1989; 1992), using different generations of RAMS.

7.2.5 Christchurch

Christchurch has an air pollution problem during the winter, which is described in more detail in Chapters 1 and 4. Christchurch, with its coastal location and pronounced topography, may share several characteristics of the air pollution dispersion processes with the examples given. However, the typical shape and orientation of the topography, the prevailing synoptic conditions and emissions, create a rather unique situation in Christchurch. Simulations of dispersion have been undertaken, using RAMS and the Eulerian mode for a passive tracer, carbon monoxide. The Eulerian mode can be justified, because CO can be considered as an area source. The estimated emission data were provided by NIWA, Christchurch, and contain a specification per suburb and for four different time intervals per day. The emissions for the Christchurch area are shown in Figures B.4a to B.4d in Appendix B. However, the most important pollutant in Christchurch, PM_{10} was not included in this study, since this pollutant can not be treated as a passive tracer due to complicated depositional characteristics, which are outside the scope of this project. Results of the CO dispersion study will be discussed in the following sections.

7.3 Model validations

Two case study days, 27-28 July 1995 and 30-31 July 1995 (hereafter C2728 and C3031, respectively), were chosen for validation of the RAMS simulations. Validated data include wind and temperature at 10 m above the surface, at Beckenham, Bromley, Burnside and Marshland, CO data at Beckenham, Hornby and St. Albans, and profile data of wind and temperature up to 500 m elevation from Hagley Park, Marshland and West Melton (see Figure 7.1). The observations are compared with predicted model data from the nearest grid point. In the text local time is used which is UTC plus 12 hours.

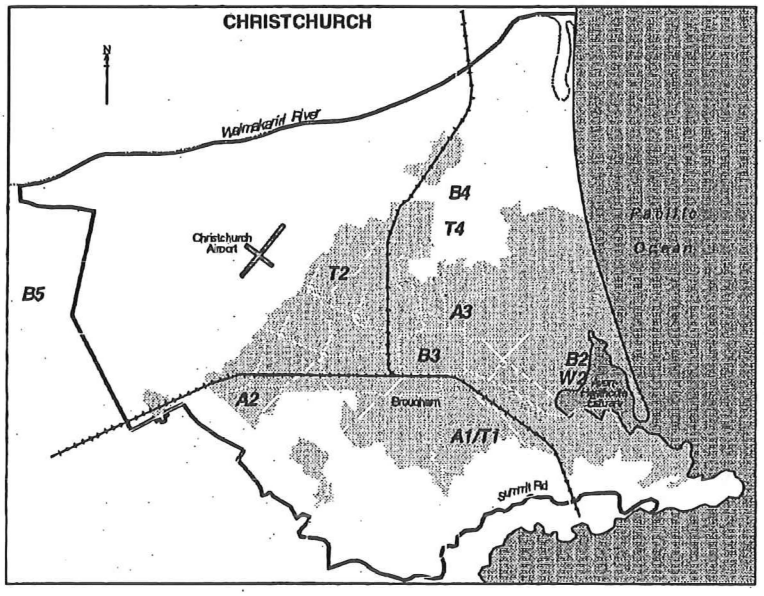

Figure 7.1 The Christchurch area with locations used for validations. A1/T1: Beckenham; B2/W2: Bromley; T2: Burnside High; B3: Hagley Park; A2: Hornby; B4/T4: Marshland; A3: St. Albans; B5: West Melton.

7.3.1 Statistical methods

Qualitative analysis was undertaken by means of graphical presentation of time series and profiles. Quantitative analysis follows the methods described by Steyn and McKendry (1988). The methods were applied to surface data only. The circular nature of wind direction data is taken into consideration when calculating bias and the root mean square error. For convenience, the methods used for analysing the time series are summarized below.

The bias of the predicted data is expressed by the mean error, ME:

$$ME = \frac{1}{N} \sum_{i=i\min}^{i\max} (P_i - O_i) \tag{7.1}$$

where P_i is the predicted value at sample time i and O_i the observed value at the same sample time, *imin* the minimum and *imax* the maximum value of i, and N is the total number of samples analysed (N = *imax-imin*+1). The Root Mean Square Error (*RMSE*) is defined as:

$$RMSE = \left[\frac{1}{N} \sum_{i=i\min}^{i\max} (P_i - O_i)^2 \right]^{1/2} \tag{7.2}$$

A method to distinguish systematic deviations of the predictions from deviations caused by scatter can be expressed by the Root Mean Square Systematic Deviation (*RMSSD*):

$$RMSSD = \left[\frac{1}{N} \sum_{i=i\min}^{i\max} (Q_i - O_i)^2 \right]^{1/2} \tag{7.3}$$

and the Root Mean Square Unsystematic Deviation (*RMSUD*):

$$RMSUD = \left[\frac{1}{N} \sum_{i=i\min}^{i\max} (Q_i - P_i)^2 \right]^{1/2} \tag{7.4}$$

where Q_i is a linear function of the observations:

$$Q_i = a + b * O_i \tag{7.5}$$

with a and b parameters obtained from linear regression of P and O. Finally, the index of agreement (D) is defined as:

$$D = 1 - \frac{\sum_{i=i\min}^{i\max} (P_i - O_i)^2}{\sum_{i=i\min}^{i\max} \left(|P_i - \overline{O}| + |O_i - \overline{O}| \right)^2} \tag{7.6}$$

ranging from 0 (no agreement) to 1 (perfect agreement).

The above described methods do not allow effects caused by a time lapse between observed and predicted signal to be distinguished. This could be done by replacing P_i with P_{i-lt}, where lt is the sample time lag. Methods using a time lag are not applied in this study.

7.3.2 Box model definition

The quality of the emissions inventory can be estimated when observed ambient concentrations of pollutants are compared with output from different types of models, using the estimated emissions. Therefore, together with the simulated dispersion using RAMS, a simple box or cylinder model was constructed. For the sake of completeness, a brief description of this model is given here. A certain area - in this case Christchurch - is covered by a box with dimensions l x l x h, l being the horizontal length and h the height of the box. It is assumed that the atmospheric pollutants are homogeneously mixed throughout the volume of the box and no diffusion of pollutants through its sides occurs. Ventilation by advection is homogeneous and the box has one side always perpendicular to the wind. When using a cylindrical concept, this requirement is obsolete, with l being the diameter of the circle times $\pi/4$. The net pollutant flux R (kg m^{-2} s^{-1}) is given by:

$$R = I + E - D - O \tag{7.7}$$

with I the influx of pollutants by advection, E the emissions flux, D the deposition flux and O the outflow flux by advection. Assuming advection of clean air (I=0) and neglecting the deposition (D=0), at time t the ambient pollutant concentration C_t in the box (kg m^{-3}) becomes:

$$C_t = C_{t-1} + \Delta t * \left(\frac{E_{t-1}}{h_t} - \frac{O_{t-1}}{l} \right) \tag{7.8}$$

using the finite differences technique, with Δt the time lapse between (t-1) and t. The outflow flux O is proportional to average windspeed $\overline{U}$ and pollutant concentration. An implicit method which is numerically stable gives:

$$O_{t-1} = \overline{U}_{t-1} * C_t \tag{7.9}$$

Taking into account that during morning hours with an increasing mixing depth, clean air will be entrained into the volume, a dilution factor h_{t-1}/h_t is introduced. Combining equations (7.8) and (7.9) and applying the dilution factor yields:

$$C_t = \left(C_{t-1} * \min(1, \frac{h_{t-1}}{h_t}) + \Delta t * \frac{E_{t-1}}{h_t} \right) \Big/ \left(1 + \Delta t * \frac{\overline{U}_{t-1}}{l} \right) \tag{7.10}$$

with the value of the function min($a1$,$a2$) equal to the argument having the lowest value. The dimensions of the box covering the Christchurch area are set at: l=13.5 km and h is 500 m from 10 am to 4 pm, declining to 30 m at 6 pm until 7.30 am the next morning, when it starts increasing to 500 m at 10 am. The settings of the applied box model resemble realistic values for clear sky, midwinter conditions and are not 'tuned' to fit the observations! The average emissions are derived from the most recent emissions inventory (Christchurch Regional Council, 1997), being respectively 12.5 μg m^{-2} s^{-1} from 6 to 10 am, 17.3 μg m^{-2} s^{-1} from 10 am until 4 pm, 20.1 μg m^{-2} s^{-1} from 4 to 10 pm and 2.6 μg m^{-2} s^{-1} from 10 pm until 6 am the next morning. The average wind speed $\overline{U}_t$ is derived from 10 m observations or simulations by RAMS at four locations more or less around the boundaries of the city: Beckenham, Bromley, Marshland and Burnside. The chosen time-step Δt is 30 minutes.

7.3.3 RAMS model settings

The RAMS grid configuration was similar to the N405-setup, using four nested grids with a horizontal grid increment of 100, 25, 5, 1 km, respectively. The model was initialized homogeneously, using one sounding which was a composition of the soundings at Invercargill, Hokitiki, Paraparaumu and the pilot balloon data at Christchurch. The model started at 00 UTC (noon local time), not using a spinup time. Initial profiles for both case days are given in Figure B.5 in Appendix B. Case C3031 will be discussed first, since synoptic forcing was weak on this occasion, so that atmospheric conditions could be represented reasonably well by a single sounding. During case C2728 however, synoptic forcing was stronger, so the homogeneous initialisation did not resemble the larger scale features so well, increasing the need for FDDA.

The following runs were undertaken:

- S1: all settings as the N405 runs (see Chapter 6).

- S2: as S1, except soil moisture set at 0.75 and sea surface temperature at 284.5 K.
- S3: as S2, but AKMIN, a parameter determining the minimum horizontal diffusivity is changed from 1.0 for all grids to 1.0, 0.5, 0.25, 0.1 respectively from coarsest to finest grid.
- S4: as S3, but the roughness length z_o is changed from homogeneous 0.10 m over land to 1.0 m in Christchurch and mountaineous terrain, and 0.5 m elsewhere.
- S5: as S4, but with different sounding for initialisation.

The changes introduced in S3 reduced diffusivity which appeared too large according to the results obtained from S1 and S2. S1, S2, S3 and S4 were run to simulate C3031, while S5 simulated C2728. The settings of S1 quickly appeared to be physically unrealistic with soil moisture at only 0.60 and sea surface temperature at 283 K, resulting in a sea breeze in the afternoon and drainage flows at night, which were much too strong. The changes in the settings of runs S1 to S4 were attempts to improve the model, since it became obvious that certain settings were physically inaccurate.

7.4 Case C3031

The South Island was covered by an anticyclone, giving generally calm and clear conditions. A detailed description can be found at Chapter 4. Several simulations of the case by RAMS have been undertaken, using settings S2, S3 and S4.

7.4.1 Surface Data

During the afternoon of 30 July 1995, light winds from west to southwest were observed in the Christchurch area. During the period from noon to 3 pm local time the simulated wind speeds were generally too low, possibly due to a lack of spin up time, but the simulated wind directions agreed quite well with the observations (see Figures 7.2a to 7.2d). The simulated 10 m temperatures in the afternoon agreed very well with the observations (see Figures 7.3a and 7.3b). Around 5 pm local time a seabreeze was observed briefly at Bromley, but it failed to penetrate much fuller inland. Only S2 successfully predicted this pattern to occur, although both S3 and S4 predicted a northeasterly flow over sea and near the shore (see Figure 7.4), which lasted until 7 pm. The first part of the evening (6 - 9 pm) showed an increased southerly component at both Burnside and Marshland locations. No observations at Beckenham were available until later at night. At the Bromley site the northeasterly winds changed back again to the southwesterly direction. The simulated winds (S2, S3, S4) showed a pronounced southern component at both Beckenham and Bromley, but only S4 generated a short interval with southerly wind for the Marshland site. All simulations failed to create a southerly wind for Burnside and generated westerlies instead. The S4 simulation predicted that the katabatic flows from the Port Hills would start to develop around 6 pm. At 7 pm an area with south to southwest winds was generated over the eastern part of Christchurch, extending about 10 km northwards, while the remainder of the city was covered by winds mainly from west to northwest. According to the S4 simulation, this pattern became more pronounced during the evening and lasted throughout the night. S4 generated a discontinuity around 9 pm at Beckenham, Bromley and Marshland, characterised by a sharp drop in temperature, increased wind speed and at Beckenham and Bromley a change in wind direction from south to west. The observations did not follow the S4-simulated pattern, but an increase in wind speed at Bromley occurred and at Marshland the wind direction changed from south to west and remained westerly during the rest of the night. From midnight on, the observed

wind speeds increased slightly at all sites, which was also simulated by S2, S3 and S4. However, althought the simulated *tendencies* of wind speed agreed reasonably well with the observations, significant differences in *absolute values* occurred. Except for Bromley, S2 and S3 generated much too strong nocturnal wind speeds, although S4 simulated wind

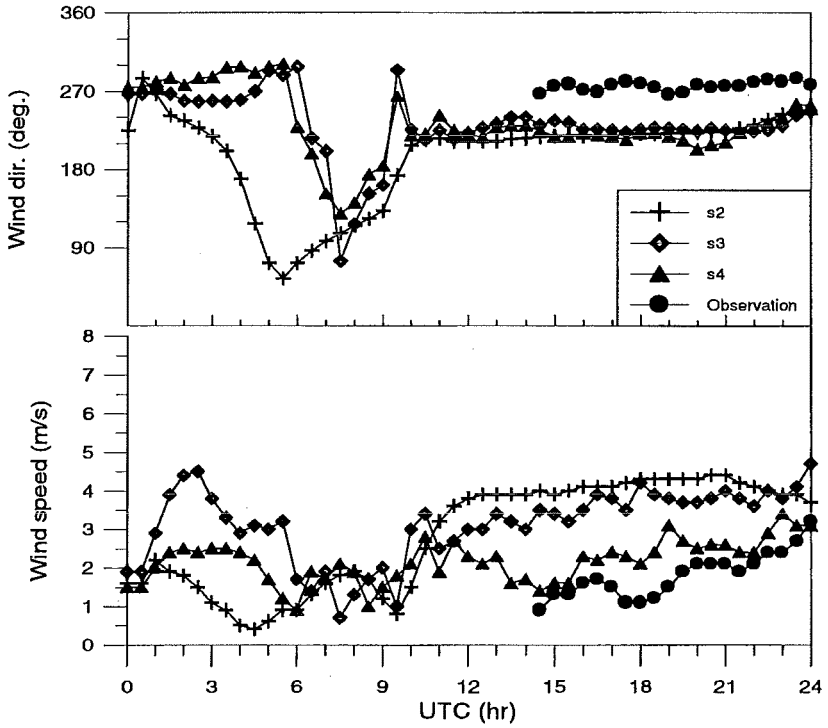

Figure 7.2a Time series of the 10 m wind direction and wind speed at Beckenham during C3031.

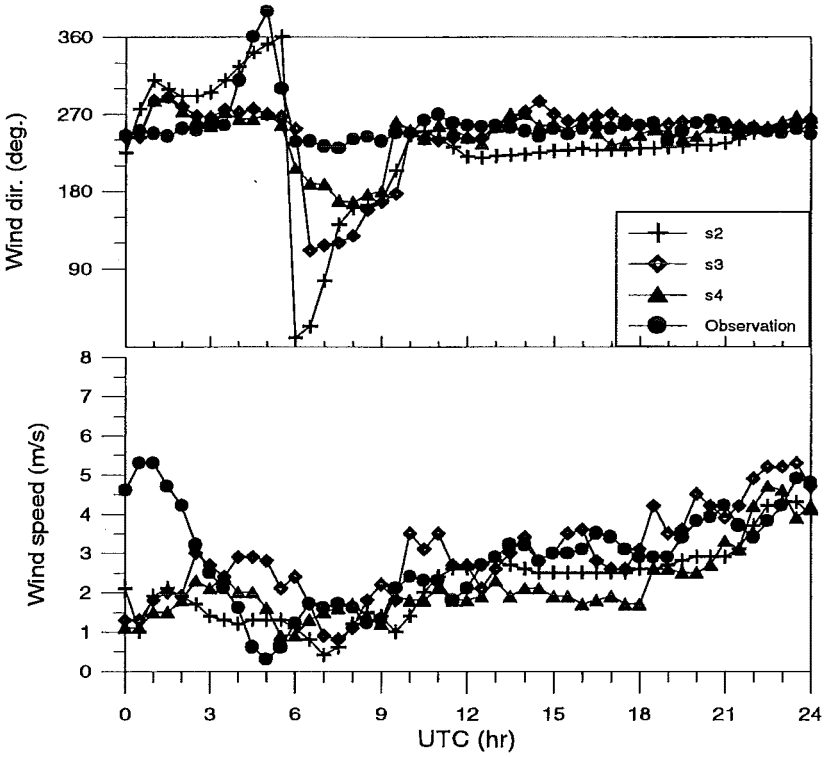

Figure 7.2b Time series of the 10 m wind direction and wind speed at Bromley during C3031.

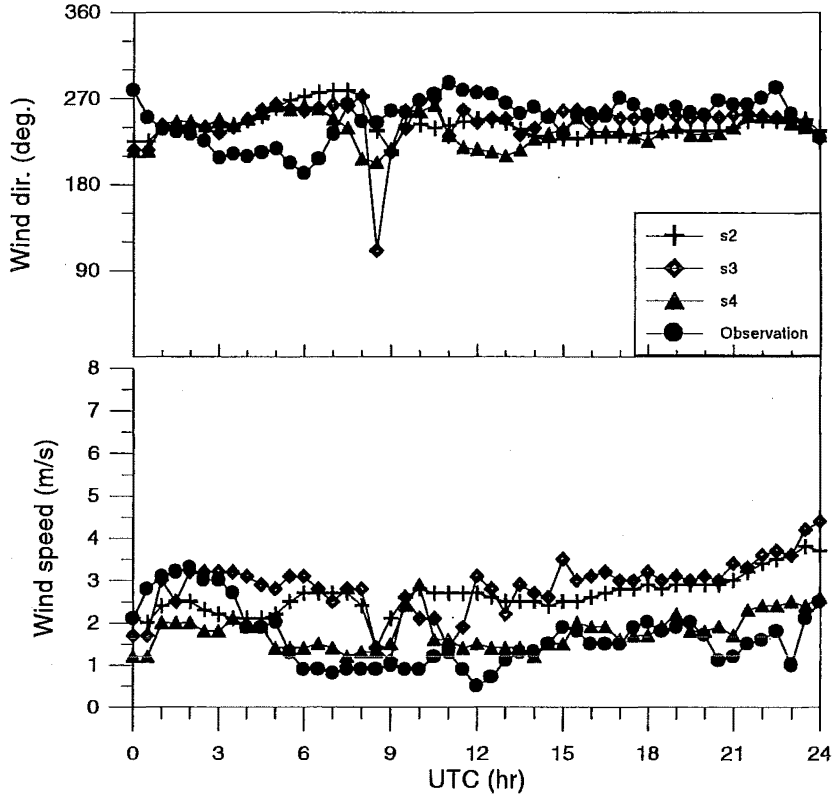

Figure 7.2c Time series of the 10 m wind direction and wind speed at Burnside during C3031.

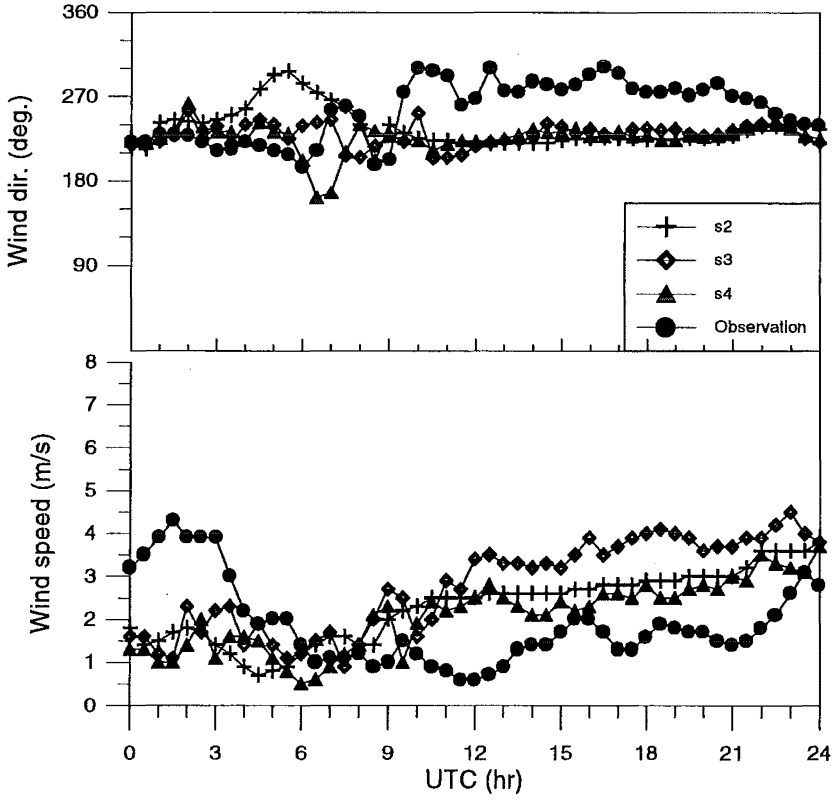

Figure 7.2d Time series of the 10 m wind direction and wind speed at Marshland during C3031.

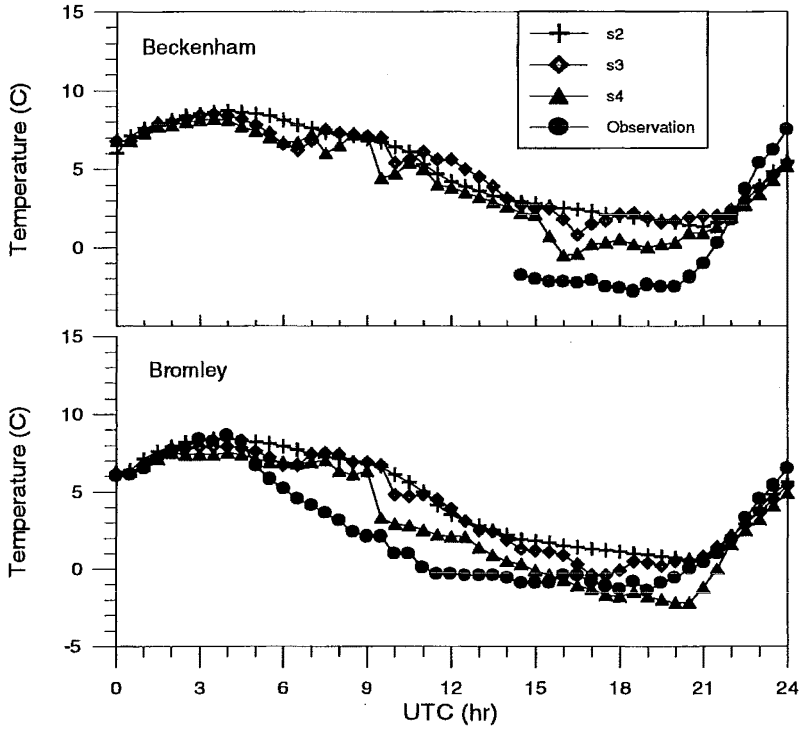

Figure 7.3a Time series of 10 m temperatures at Beckenham (top) and Bromley (bottom) during case C3031.

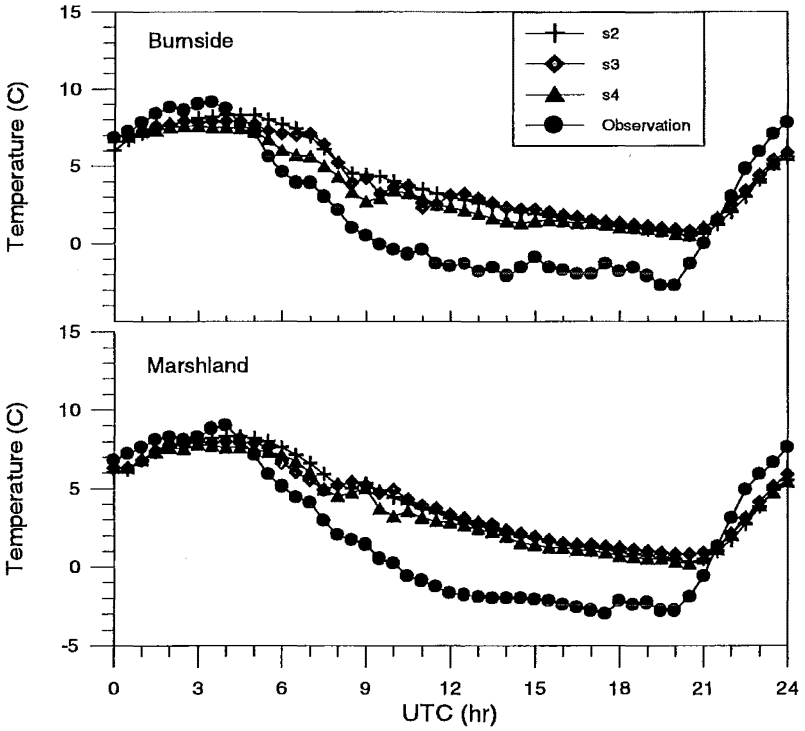

Figure 7.3b Time series of 10 m temperatures at Burnside (top) and Marshland (bottom) during case C3031.

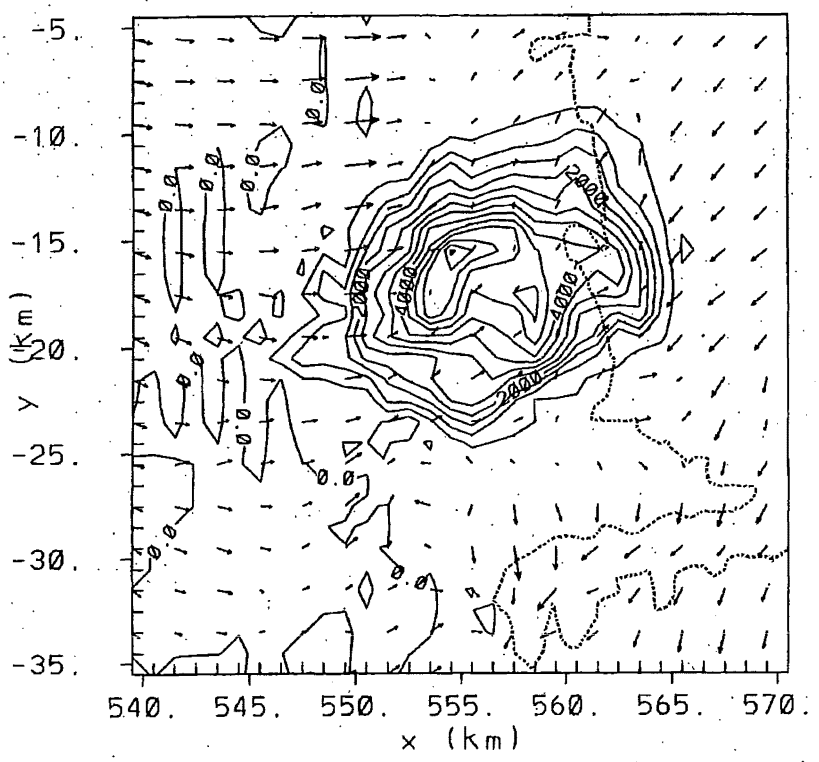

Figure 7.4 Vector plot in grid 4 (see Figure 6.1) showing the wind field and contours of CO concentrations ($\mu g\ m^{-3}$) over Christchurch at a height of 12 m simulated by run S4 at 6 pm local time on 30 July 1995. Maximum plotted wind speed is 3.5 m s^{-1}.

speeds, agreed better with the observations, but were still generally too strong. The observed 10 m temperatures during the night at all sites were lower than simulated. However, at Bromley, due to a lack of further cooling after midnight, related to the stronger wind speeds at that site, the simulated temperatures were similar to the observed values after 3 am. During the morning hours all the observed 10 m temperatures rose faster than the simulated temperatures (see Figures 7.3a and 7.3b), possibly due to a more shallow and stable boundary layer, entraining warmer air from aloft than simulated, or due to the existence of higher sensible heat fluxes than simulated.

7.4.2 Profiles

The vertical profile data from Hagley Park showed that at 3 pm local time the simulated winds matched the observations up to 500 m reasonably well, except for the S2-generated wind speeds, which were too low up to 300 m (Figures 7.5a to 7.5d). At 8 pm all wind predictions created by S2, S3 and S4 from 300 m to 500 m elevation were reasonably accurate. However, S3 and S4 generated a weak low level jet at 100 m elevelation, which was not observed, but the S4 wind directions agreed quite well with the observations. The S2 wind speed profile resembled the observations well, but the S2 wind directions below 300 m showed differences over 90°. Around 10 pm S2, S3 and especially S4 generated too strong low level jets, but above 300 m the simulated wind speeds agreed well with the observations. Between 50 and 200 m the simulated wind directions agreed very well with the observations, but above 200 m the observed wind direction changed from west at 200 m to northwest at 300 m to northeast at 500 m, while the simulated winds remaind westerly. At the end of the night, at 6 am, the simulated and observed wind speeds showed a strong increase from 10 m to 100 m elevation, although the observed winds were weaker than simulated.

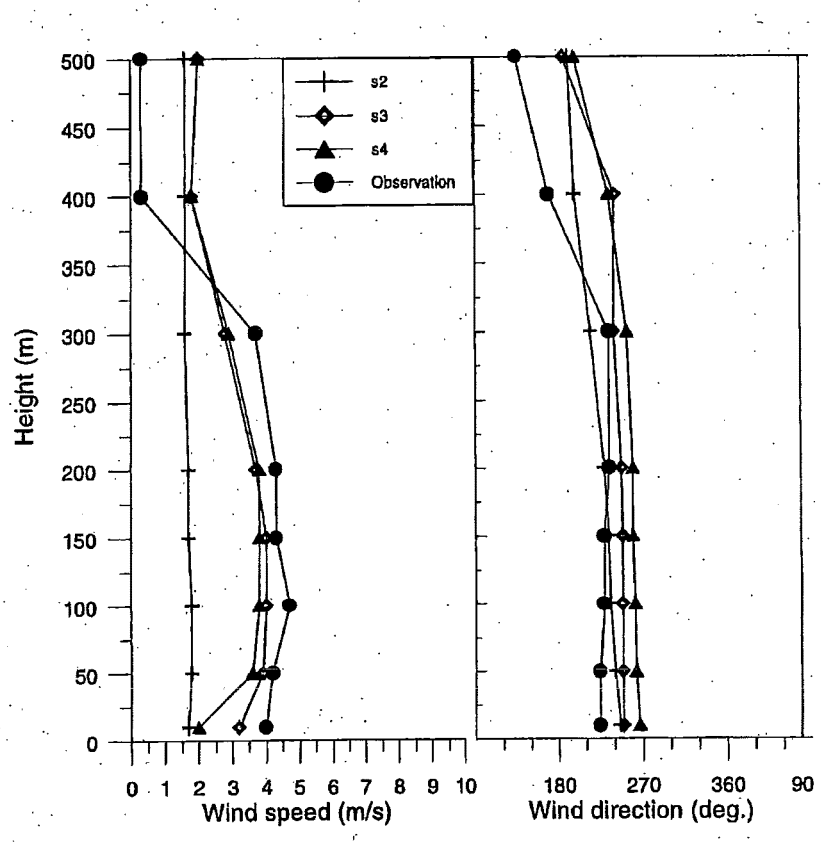

Figure 7.5a Wind profiles at Hagley Park, 3 pm local time on 30 July 1995.

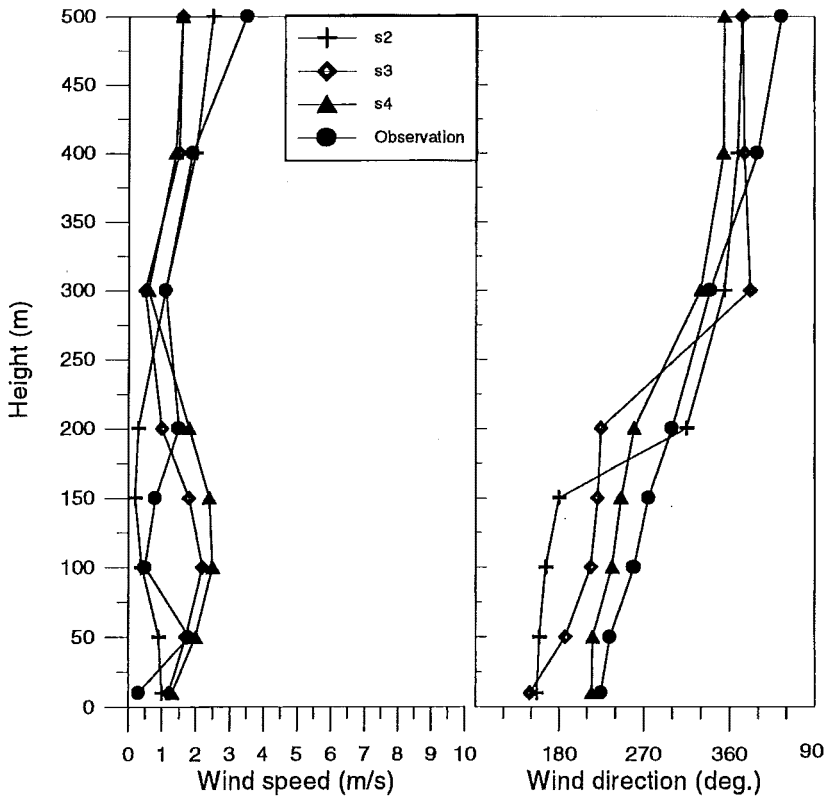

Figure 7.5b Wind profiles at Hagley Park, 8 pm local time on 30 July 1995.

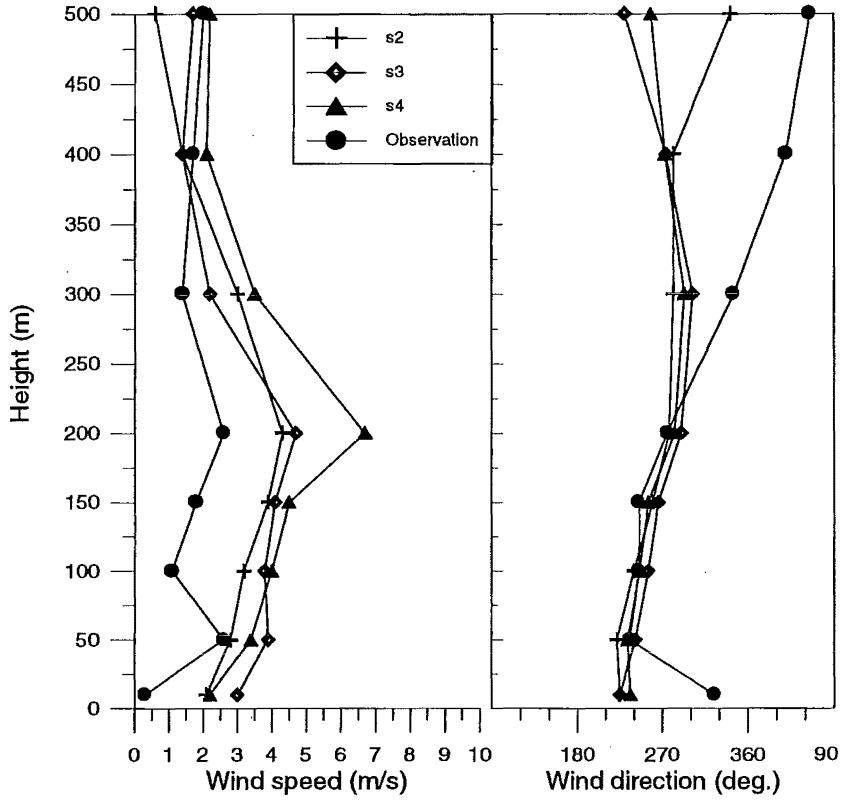

Figure 7.5c Wind profiles at Hagley Park, 10 pm local time on 30 July 1995.

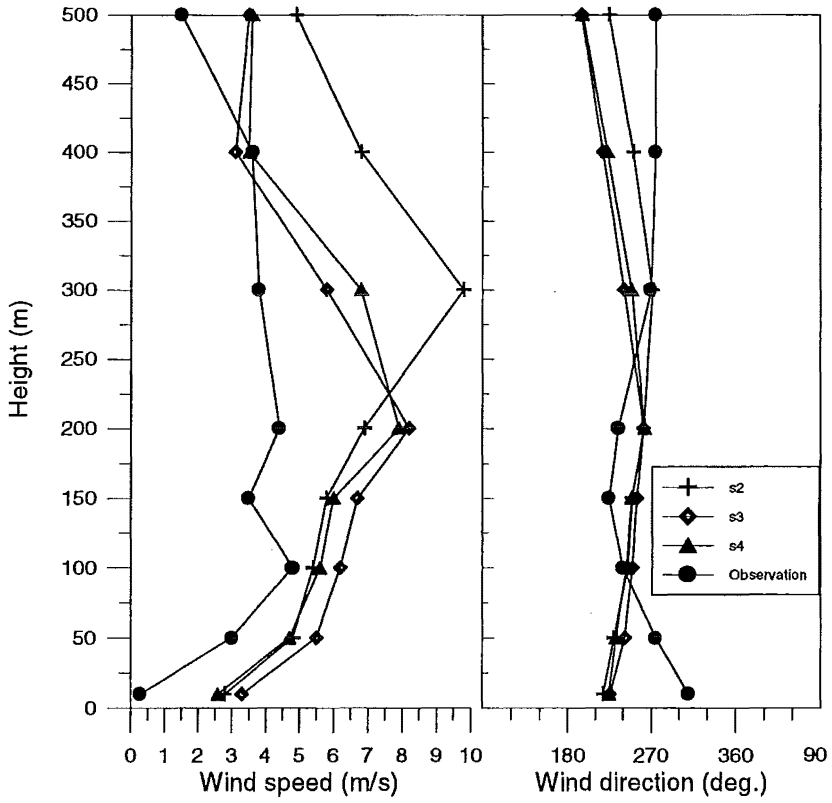

Figure 7.5d Wind profiles at Hagley Park, 6 am local time on 31 July 1995.

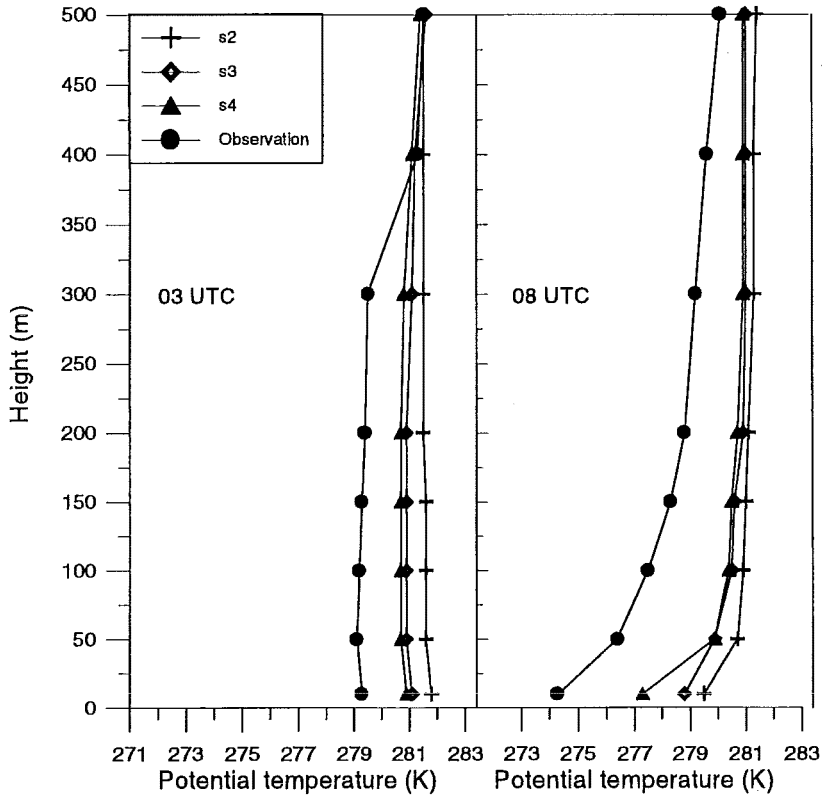

Figure 7.6a Temperature profiles at Hagley Park, 3 and 8 pm local time, respectively on 30 July 1995.

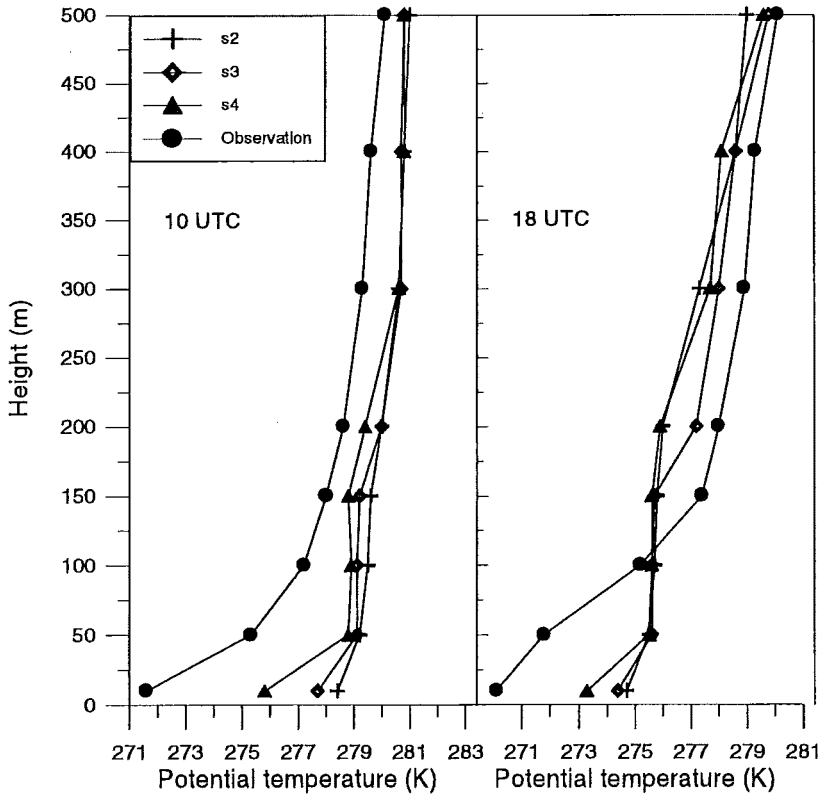

Figure 7.6b Temperature profiles at Hagley Park, 10 pm and 6 am local time on 30 and 31 July 1995, respectively.

Above 100 m the simulated wind speeds continued to increase, which was not observed. The simulated low level jets peaked around 200 m for S3 and S4, while S2 showed an even higher wind maximum at 300 m. The simulated wind directions agreed reasonably well with the observations.

The observed and simulated temperature profiles at 3 pm, Hagley Park, were basically neutral between 50 to 300 m elevation (see Figures 7.6a and 7.6b). Up to 50 m from the surface the profiles were slighly superadiabatic, while the observed profile showed an inversion between 300 m and 400 m, which was not simulated by either S2, S3 or S4. Below the actual inversion the simulated profiles were too warm. At 8 pm the observed boundary layer had stabilised, being most stable at the lower elevations. This was also represented by the simulations, especially S4, although the observed profile was still cooler than simulated. At 10 pm the cooling of the boundary layer had continued, stabilising the boundary layer even further, particularly at lower elevations. The observed potential temperature gradient was 0.10 $K\,m^{-1}$ between 10 and 50 m, while S4 generated a gradient of only 0.05 $K\,m^{-1}$. S2 and S3 produced even weaker gradients. Curiously enough, the simulations S2, S3 and S4 created a near neutral layer between 50 m and 200 m, which was clearly not observed. Above 200 m elevation, the gradients of simulated temperature agreed reasonably well with the observations, though the simulated profiles were still too warm. At the end of the night, at 6 am 31 July 1995, a strongly stable layer was observed up to 150 m, with an average potential temperature gradient of 0.05 $K\,m^{-1}$, while the simulated profiles had generated an average gradient which was less than 0.02 $K\,m^{-1}$. Above 150 m elevation the simulated profiles agreed reasonably well with the observations, although the simulated profiles were now *colder* than observed.

7.4.3 Ambient CO concentrations

The observed CO concentrations over the same period at Beckenham, Hornby and St. Albans showed an increase during the evening and a decline after midnight, followed by a secondary peak during the morning rush-hour (see Figure 7.7). The CO concentrations predicted by S2, S3 and S4 were too low at Beckenham and Hornby and the temporal pattern at all sites did not agree with the observations: the predicted peaks occurred between 6 and 9 pm with a sharp decline afterwards, while the observed peaks were later and the decline was more gradually. At St. Albans the predicted peak in the morning was about 2 hours too early and at Beckenham and Hornby the predicted peak was almost insignificant. Generally, the S4 simulated CO concentrations agreed best with the observations. The CO concentrations generated by S4 show low values during the afternoon in the Christchurch area, which increase sharply in the evening (see Figure 7.7). According to the S4 simulations, strong horizontal gradients of CO concentrations developed at the foothills of the Port Hills and at the western and eastern boundaries of the city around 7 pm. The strong CO gradient was maintained over the southeastern part of Christchurch during the rest of the evening, where clean air from the Port Hills drained down and met the polluted air from the city. In the northeastern part of Christchurch the CO polluted air was predicted to be transported eastwards over the sea. During the rest of the night the simulated CO concentrations were low, due to increased drainage flows and low values of estimated emissions. In the morning, the simulated CO concentrations increased again, and strong horizontal gradients were predicted near the Port Hills and in the northwestern part of the city, where a convergence line was generated, caused by the southwest flow over the city and the west-northwest flow from the Canterbury Plains.

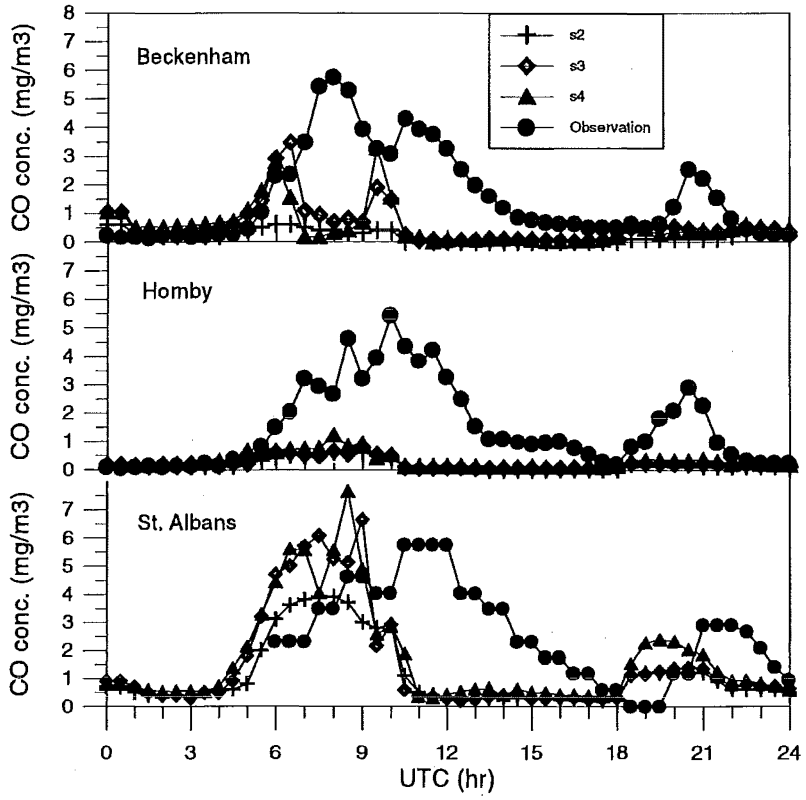

Figure 7.7 Time series of simulated and observed ambient CO concentrations during C3031.

7.4.4 Box model results

The box model was run using observed average wind speed and average speed simulated by RAMS (see Figure 7.8). The predicted ambient CO concentrations by the box model are surprisingly good, except for the peak during the morning rush-hour, which is predicted about 2 hours too early, and the predicted ambient CO concentrations were about 25% too low. In general the box model predicted not only the variations in time of ambient CO concentrations quite well, but also the magnitude of the ambient concentrations. The results of the box model appeared not to be very sensitive to the applied wind speeds, either from observations or modelled by RAMS.

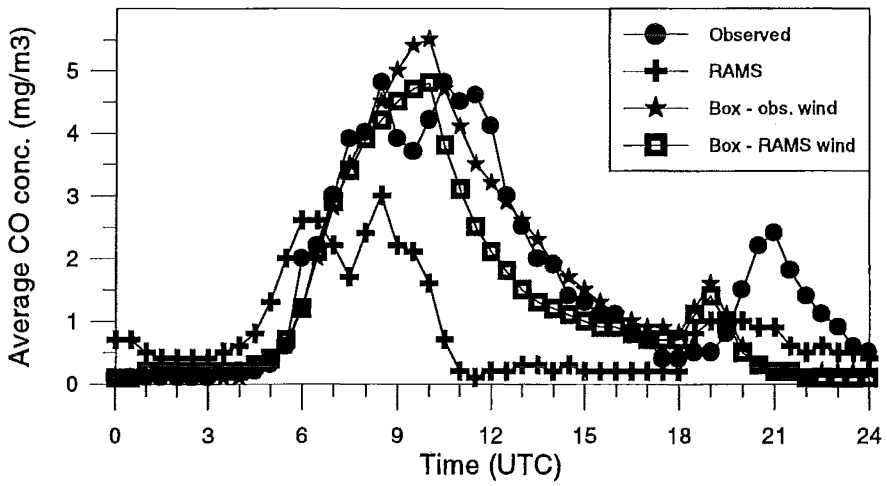

Figure 7.8 Time series of observed and simulated spatially averaged ambient CO concentrations over Christchurch during C3031.

7.4.5 Quantitative analysis

Analysis of the dataset over the 24 hour period from noon 30 July 1995 to noon the next day shows that generally S2 and S3 scored quite similarly for wind speed and temperature, and S4 scored slightly better. However, the error scores of the data produced by S2, S3 and S4 do not differ very much for wind direction and ambient CO concentrations. Table 7.1 displays the results only for S4 at Bromley, Burnside and Marshland. The wind speed data produced an index of agreement, which is moderate at the Bromley and Burnside sites, but rather poor at Marshland. The regression parameters indicate a poor direct relation between predicted and observed wind speed for all sites. The data for temperature show high indices of agreement at all sites. The results for Burnside and Marshland are quite similar, having an average bias around 1.5 K and a predicted temperature amplitude which is less than 60% of the observed. At Bromley the S4 temperature predictions were quite reasonable, having a bias close to 0.5 K and an amplitude close to the observed. The CO data reveal that the simulations seriously underestimated the ambient CO concentrations and that a relatively poor direct relation exists between observations and predicted, as reflected by the low values of parameter *b* and index *D*.

Table 7.1 Validation of S4 data over a 24 hour period using half hourly samples, starting at noon 30 July 1995. **U**: windspeed (m s^{-1}); **dd**: wind direction (deg.); **T**: temperature (K); **CO**: ambient CO concentration (mg m^{-3}). ***ME***: mean error; ***RMSE***: root mean square error; ***RMSSD***: root mean square systematic deviation; ***RMSUD***: root mean square unsystematic deviation; ***D***: index of agreement; ***a*** and ***b***: regression coefficients of predictions to observations (***a***: intercept; ***b***: slope).

VAR.	SITE	ME	RMSE	RMSSD	RMSUD	D	a	b
U	Bromley	-0.74	1.37	1.11	0.80	0.64	1.22	0.32
	Burnside	0.13	0.74	0.63	0.40	0.50	1.54	0.14
	Marshland	0.20	1.40	1.16	0.78	0.26	2.42	-0.18
dd	Bromley	-12	32	-	-	-	-	-
	Burnside	-12	35	-	-	-	-	-
	Marshland	-29	45	-	-	-	-	-
T	Bromley	0.50	1.67	0.54	1.56	0.94	0.67	0.93
	Burnside	1.47	2.44	2.30	0.81	0.87	2.43	0.57
	Marshland	1.75	2.77	2.56	1.06	0.85	2.65	0.56
CO	Beckenham	-1.00	1.96	1.85	0.65	0.45	0.54	0.02
	Hornby	-1.16	1.80	1.79	0.25	0.48	0.23	0.06
	St. Albans	-0.55	2.17	1.36	1.68	0.55	1.11	0.25

The analysis of the nocturnal subsets for wind speed and temperature are displayed in Figures 7.9 and 7.10. The simulated wind speeds were too high in Burnside and Marshland, particularly those predicted by S2 and S3. The RMSE of S4 was the lowest as well at these sites, but at Bromley however, S4 appeared to be scoring slightly worse than S2 and S3. At Bromley, S2 and S4 underestimated the nocturnal wind speed. Figure 7.10 displays the improved temperature predictions of S4, compared to S2 and S3 at all sites, although the differences were minor at Burnside and Marshlands. The scores of wind direction and ambient CO concentrations generated by S2, S3 and S4 were generally similar, and no improved performance by S4 could be distinguished. The data sets were broken down into six hourly periods and the results are displayed in Figures 7.11 to 7.14 for the S4 runs only. During the afternoon wind speeds were severely underestimated by S4 at Bromley and Marshland, and to some extent at Burnside. However, during the night and following morning S4 overestimated the wind speed at Burnside and Marshland, but underestimated it at Bromley. The wind direction data show a similar pattern at Burnside and Marshland, with a positive bias in the afternoon and a negative bias during the

following 18 hours, peaking during the late night period. Again, at Burnside the predictions appeared better than at the other sites. The temperatures during the afternoon were predicted very well by S4 at Bromley, Burnside and Marshland. However, a serious bias existed during the evening period at all sites, which was even worse during the night, except for Bromley.

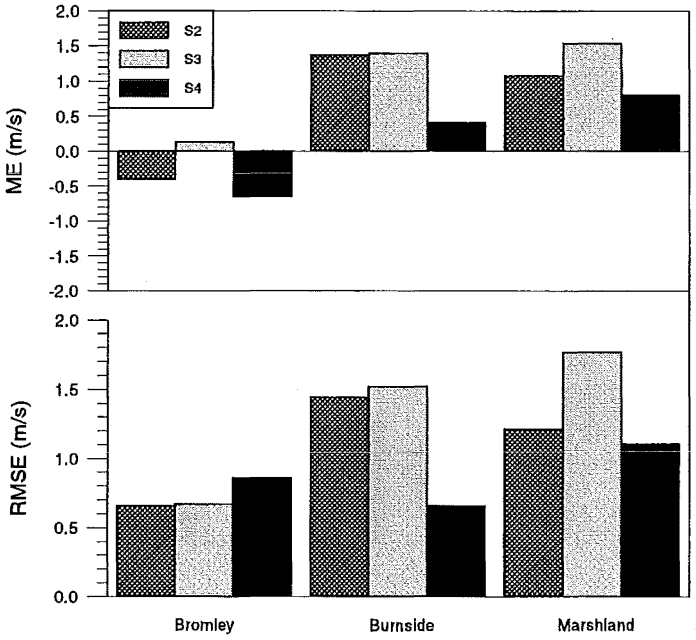

Figure 7.9 Mean Error and Root Mean Square Error of nocturnal wind speeds (06 – 18 UTC) during C3031.

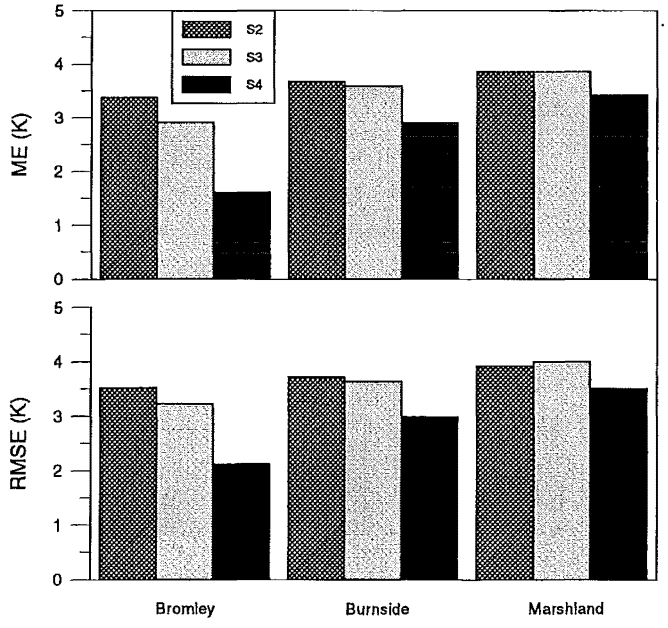

Figure 7.10 Mean Error and Root Mean Square Error of nocturnal temperatures (06 – 18 UTC) during C3031.

The CO data show a similar pattern at Beckenham, Hornby and St. Albans, with most serious absolute deviations in the evening, when the highest concentrations were also recorded. Note however, the peaking of the bias in St. Albans occurred at night and not during the evening.

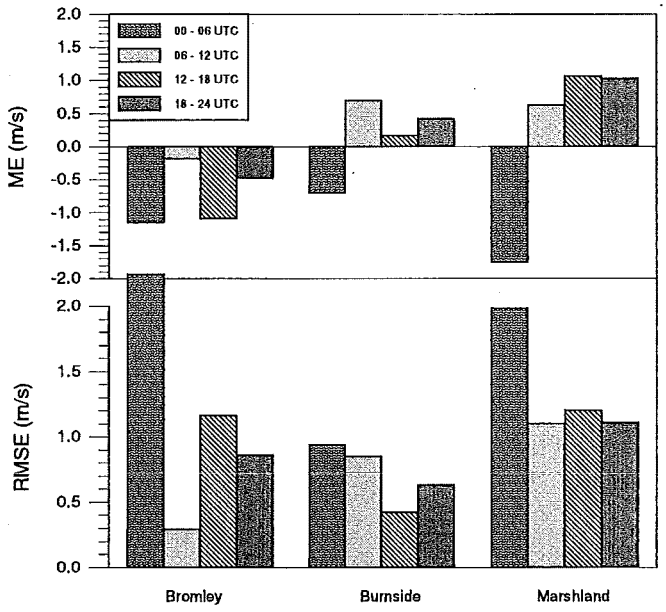

Figure 7.11 Mean Error and Root Mean Square Error of wind speed data generated by S4 during C3031.

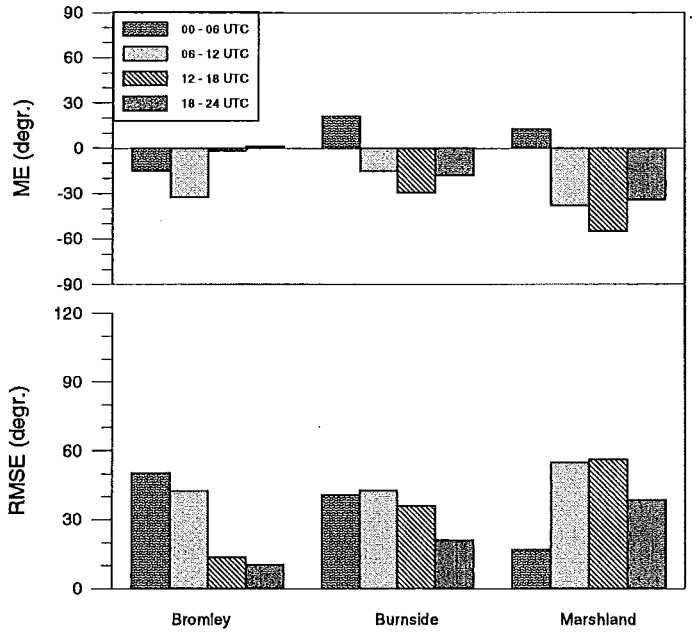

Figure 7.12 Mean Error and Root Mean Square Error of wind direction data generated by S4 during C3031.

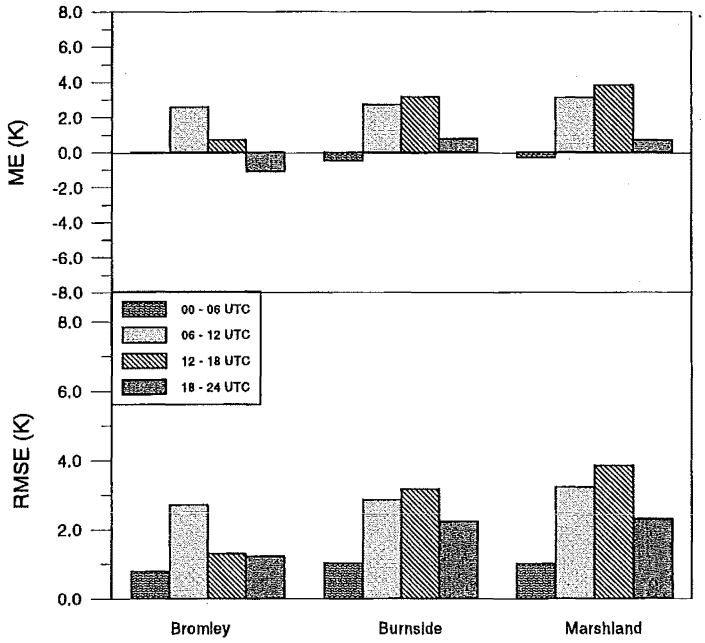

Figure 7.13 Mean Error and Root Mean Square Error of temperature data generated by S4 during C3031.

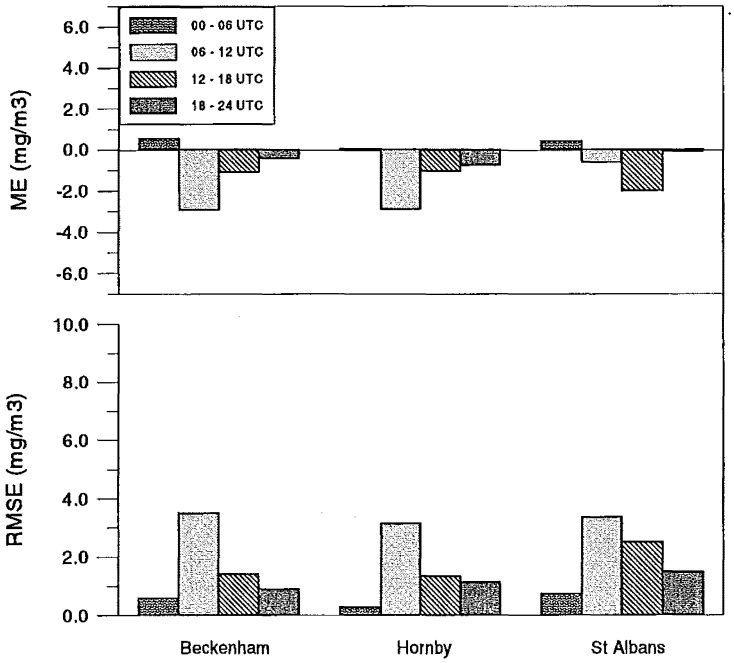

Figure 7.14 Mean Error and Root Mean Square Error of ambient CO concentration data generated by S4 during C3031.

7.5 Case C2728

On 27 July 1995 an anticyclone was located to the southwest of the South Island and a cyclone to the south-southeast, causing a south westerly flow over the island, which was significantly stronger than during the C3031 case. Clear sky conditions continued throughout the C2728 case. A detailed description of the case can be found at Chapter 4. The C2728 case was simulated by S5, with settings similar to S4, except for a different sounding for initialization, as described in relation to the C3031 case. Again, a homogeneous initialisation was undertaken, using one vertical sounding (see Figure B.5 in Appendix B).

7.5.1 Surface data

Generally, the simulated 10 m data agreed reasonably well with the observations, but the vertical profiles showed significant discrepancies. At the beginning of the afternoon, winds were light to moderate from westerly directions all over Christchurch, as simulated by S5. Around 3 pm, a northeasterly wind developed, combined with an increase in wind speed, first being observed at Bromley and Marshland, and later at Beckenham and Burnside. Although S5 predicted a change in wind direction from southwest to southeast at most locations in the area between 3 and 6 pm, it failed to generate the sudden onset of a northeasterly, as S4 did for the C3031 case. Nevertheless, the predicted wind speeds at the validation locations agreed very well with the observations (see Figures 7.15a to 7.15d), although the predicted temperatures agreed quite well with the observations during the afternoon only (Figures 7.16a and 7.16b). During the beginning of the evening (6 - 9 pm) the observed and simulated wind speeds decreased, while the observed wind direction turned gradually clockwise at all sites, except Burnside, which remained between north and east. The simulated wind directions were within 90° from the observations, except in Marshland, where a southerly flow was predicted and a northwest wind was observed. The 9 pm S5 vector plot (Figure 7.17) shows a convergence line running from southwest to northeast over the northwestern part of Christchurch, where the southerly flow over the city met the northwest winds from the Canterbury Plains. According to the S5 run, the flow from the Canterbury Plains started to dominate over most of the Christchurch area north of the Port Hills later during the night. The observed sharp increase in wind speed around 3 am at Bromley, Burnside and Marshland was not simulated. In the morning after 9 am the observed wind directions turned to the northeast again, but the winds generated by S5 were west to southwest. The simulated 10 m temperatures in the afternoon at Beckenham, Bromley, Burnside and Marshland agreed very well with the observed values (Figures 7.16a and 7.16b). However, during the evening and most of the night the observed 10 m temperatures became cooler than simulated, except for Bromley, where simulated temperatures were close to the observed until 2 am. At 2 am at the Bromley site and around 3 am at Beckenham, Burnside and Marshland, the observed temperatures rose significantly, while the simulated temperatures continued to decrease until sunrise. This phenomenon is described in more detail in Chapter 4. S5 was not able to reproduce this feature, causing the simulated 10 m temperatures to be too cold.

7.5.2 Profiles

Around 5 pm on the 27th of July 1995 a vertical profile was taken at Hagley Park up to 400 m elevation (see Figure 7.18a). The wind speeds simulated by S5 agreed very well with the observations up to 200 m, but did not show the decline in strength aloft as observed. The observed wind directions had changed from southwesterly to northeasterly

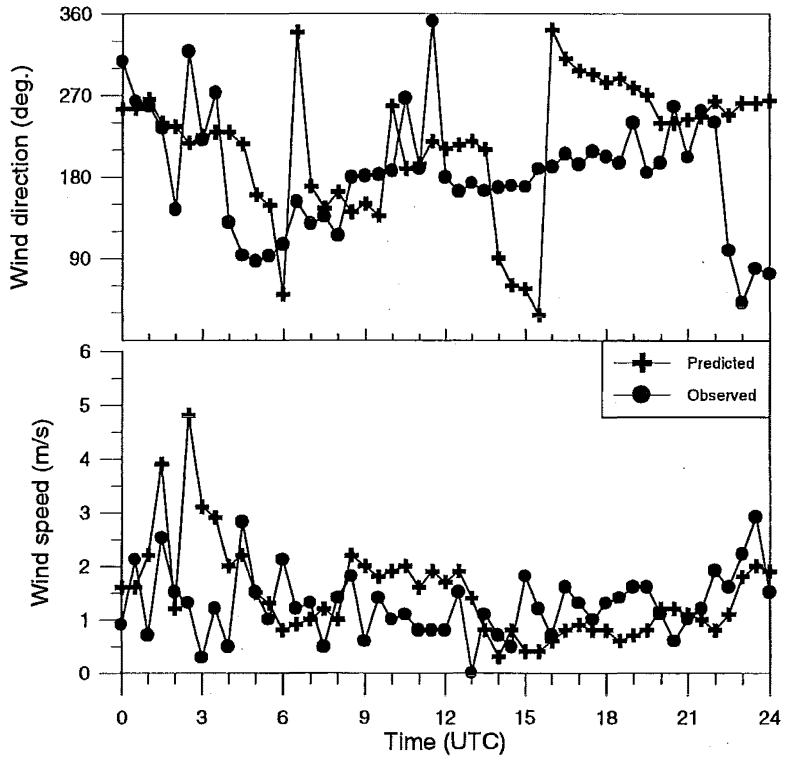

Figure 7.15a Time series of the 10 m wind direction and wind speed at Beckenham during C2728.

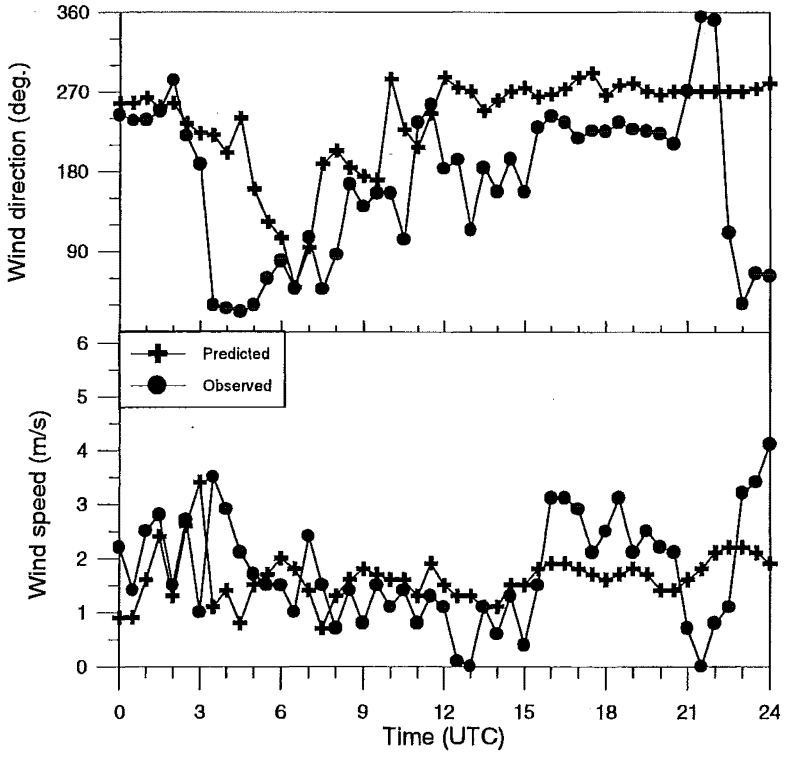

Figure 7.15b Time series of the 10 m wind direction and wind speed at Bromley during C2728.

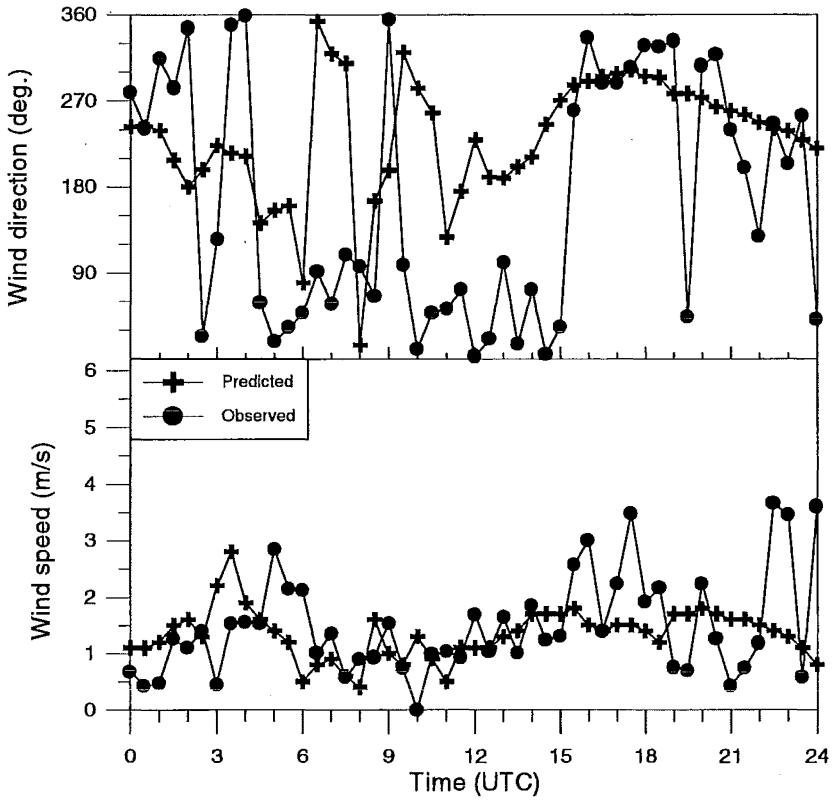

Figure 7.15c Time series of the 10 m wind direction and wind speed at Burnside during C2728.

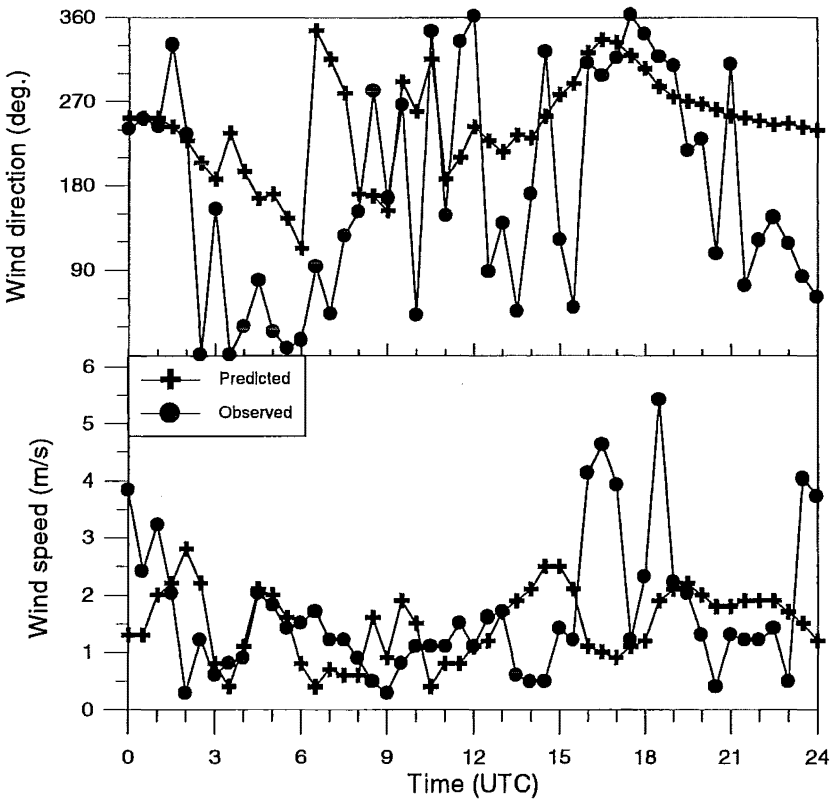

Figure 7.15d Time-series of the 10 m wind direction and wind speed at Marshland during C2728.

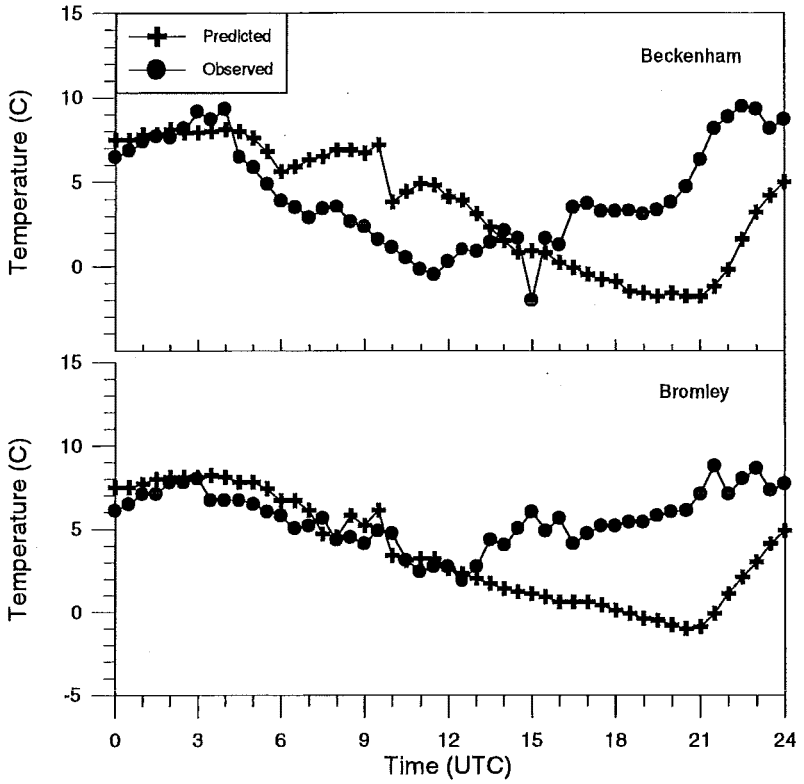

Figure 7.16a Time-series of the 10 m temperatures at Beckenham (top) and Bromley (bottom) during C2728.

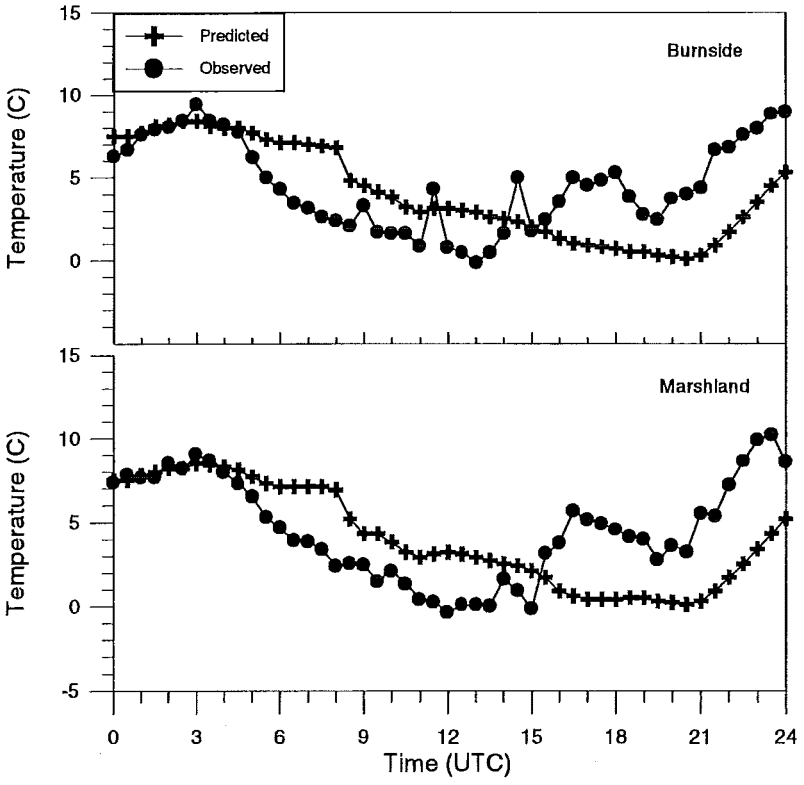

Figure 7.16b Time-series of the 10 m temperatures at Burnside (top) and Marshland (bottom) during C2728.

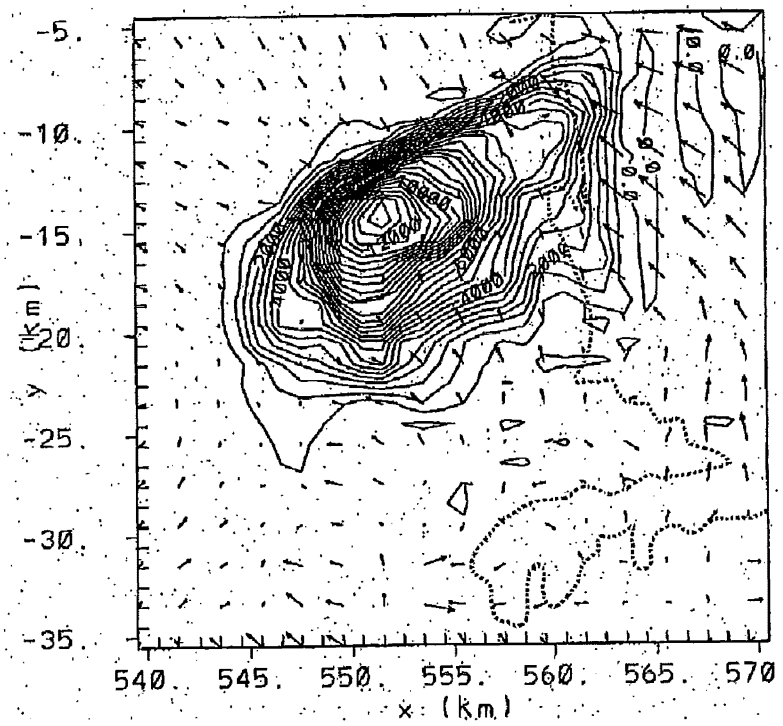

Figure 7.17 Vector plot in grid 4 showing the wind field and contours of CO concentrations ($\mu g\ m^{-3}$) at a height of 12 m simulated by run S5 at 9 pm local time on 27 July 1995. Maximum plotted wind speed is 4.5 $m\ s^{-1}$.

during early afternoon, from the surface up to at least 400 m, but S5 continued to generate a southwesterly flow. At 7 pm a low level jet was observed between 100 m and 200 m elevation near the Marshland site, but S5 failed to generate this jet (see Figure 7.18b). However, at 400 m the predicted and observed wind speeds were quite similar. The wind direction up to 200 m was predicted reasonably well by S5, but aloft major deviations from the observations occurred, where the observations showed the northeasterlies to continue up to higher elevations, while the S5 winds were southerly. Later that evening a sounding was taken near West Melton at 8.30 pm (see Figure 7.18c). The observations showed a well distinguished low level jet between 50 and 150 m from the surface, although S5 completely failed to generate any low level jet. However, the predicted wind directions agreed to a certain extent with the observations. At 11 pm a sounding was undertaken at Hagley Park again (see Figure 7.18d), showing a windspeed profile which was simulated very well by S5 up to 200 m, but aloft the observed strong low level jet was completely absent in the S5 data. Next morning at 8 am, the vertical profile at Hagley Park showed a strong incease in wind speed from calm near the surface up to 8 $m\ s^{-1}$ at 150 m, and to more than 10 $m\ s^{-1}$ at 300 m elevation (see Figure 7.18e). Up to an height of 100 m, S5 predicted wind speeds which were too strong, but followed the observations to some degree. However, the strong jet aloft was not simulated. The observed wind direction changed from south-southwest near the surface to northwest at 100 m and aloft, but S5 generated wind between south and west throughout the profile.

At 4.30 pm on the 27th of July 1995 in Hagley Park the observed and simulated temperature profiles both show a mixed layer to at least 400 m elevation, but the simulated profile was about 2 K too warm (see Figures 7.19a to 7.19c). At 7 pm the profile at Marshland had stabilised, particularly in the lower 50 m. The simulated profile was less

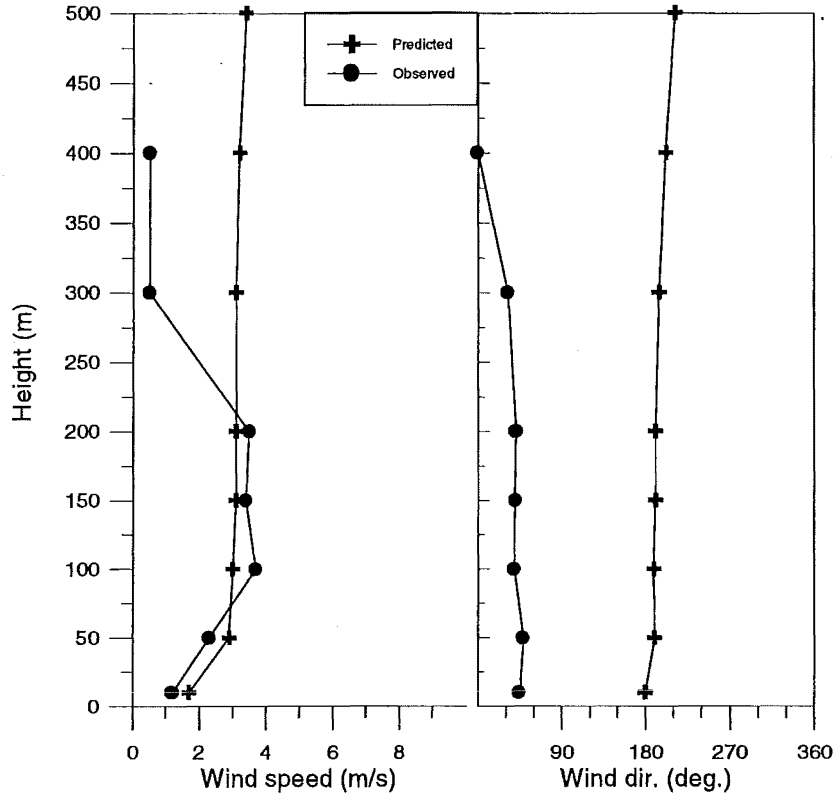

Figure 7.18a Wind profiles at Hagley Park, 04.30 pm local time on 27 July 1995.

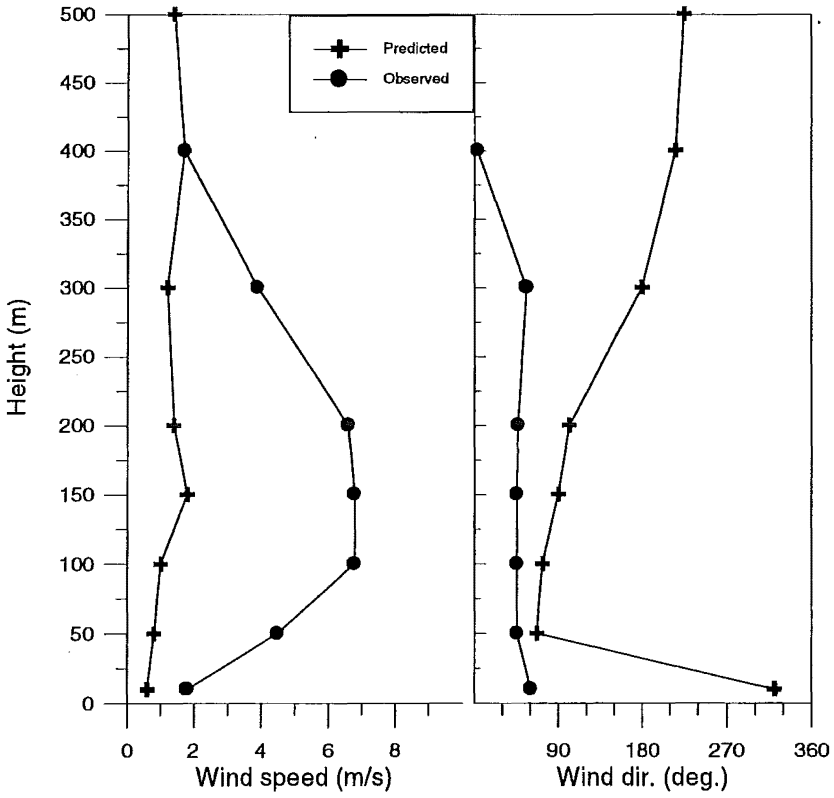

Figure 7.18b Wind profiles at Marshland, 7 pm local time on 27 July 1995.

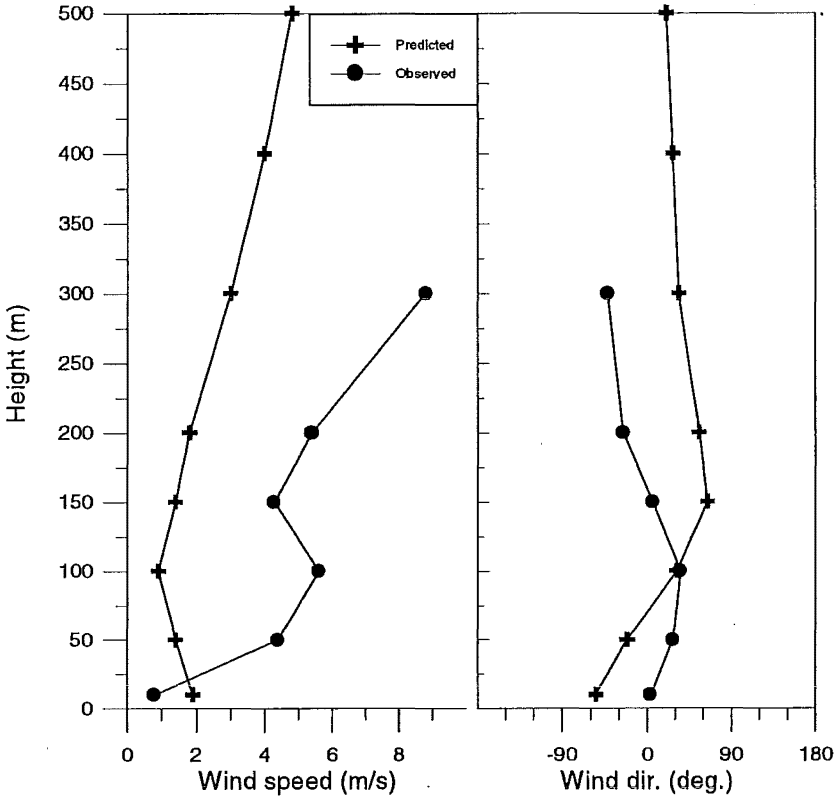

Figure 7.18c Wind profiles at West Melton, 8.30 pm local time on 27 July 1995.

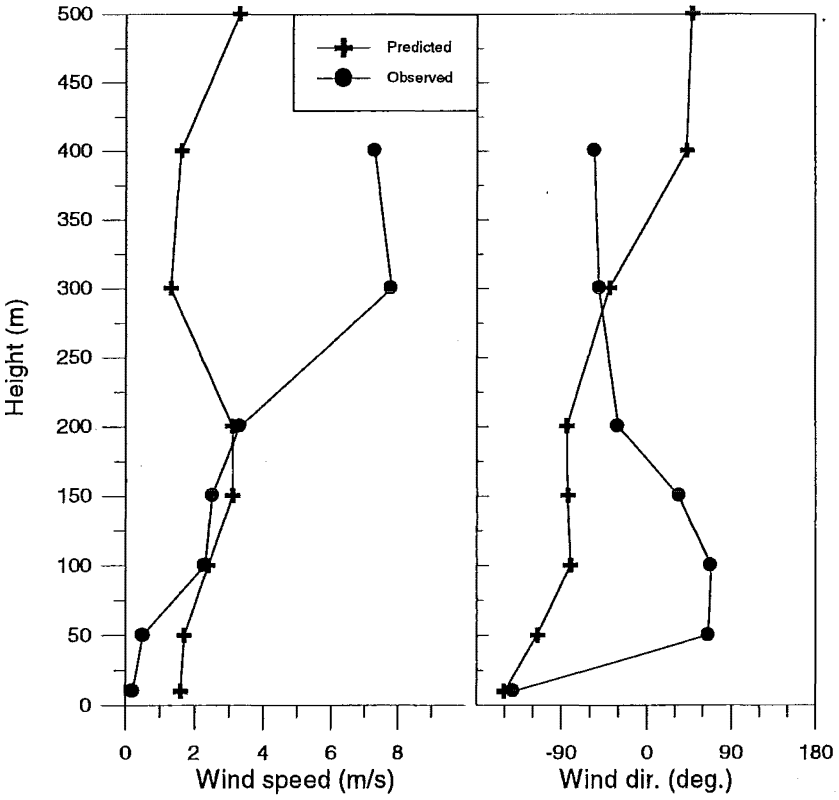

Figure 7.18d Wind profiles at Hagley Park, 11 pm local time on 27 July 1995.

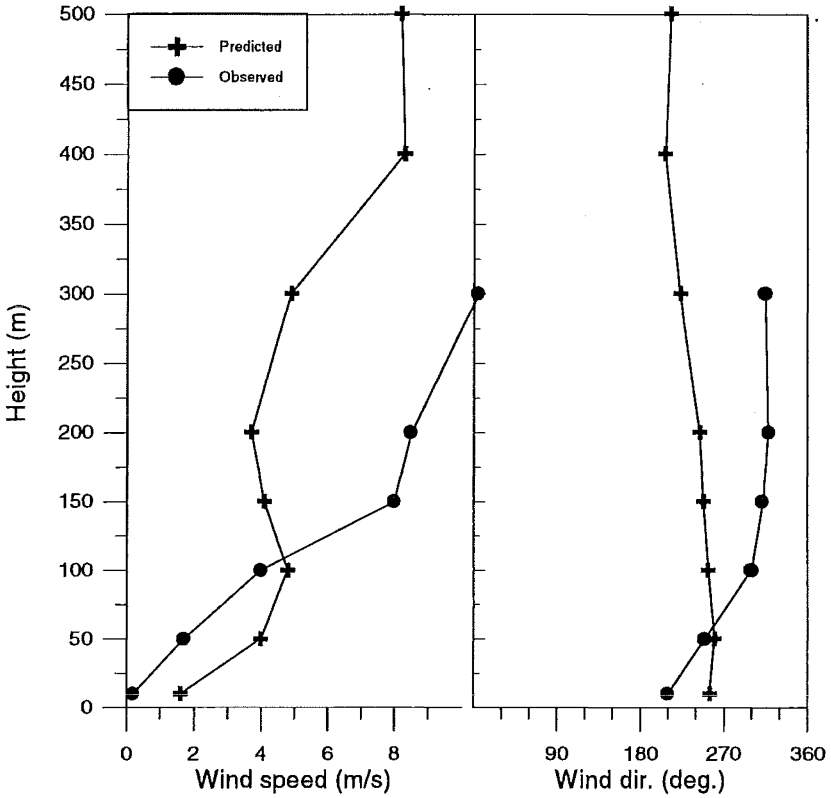

Figure 7.18e Wind profiles at Hagley Park, 8 am local time on 28 July 1995.

stable than observed and on average about 3 K too warm. At 8.30 pm near West Melton, the boundary layer had stabilised further, with an average observed potential temperature gradient of 0.055 K m^{-1} and a simulated gradient being 0.033 K m^{-1} in the layer from 10 m to 50 m. The simulated profile was on average about 3 K too warm. At 11 pm the sounding at Hagley Park showed a very stable layer at lower elevations, being 0.095 K m^{-1} from 10 m to 50 m, while S5 generated a gradient of only 0.015 K m^{-1}. However, at 100 m elevation and aloft, the simulated temperature profile agreed very well with the observations. The profile in the morning at 8 am in Hagley Park showed a very stable layer up to 50 m from the surface, with an potential temperature gradient being 0.113 K m^{-1} in the layer 10 m to 50 m, while S5 had generated only 0.025 K m^{-1}. Above 50 m elevation the vertical gradients of potential temperature of both the observations and simulations agreed reasonably well, although the simulated profile was about 4 K too cold.

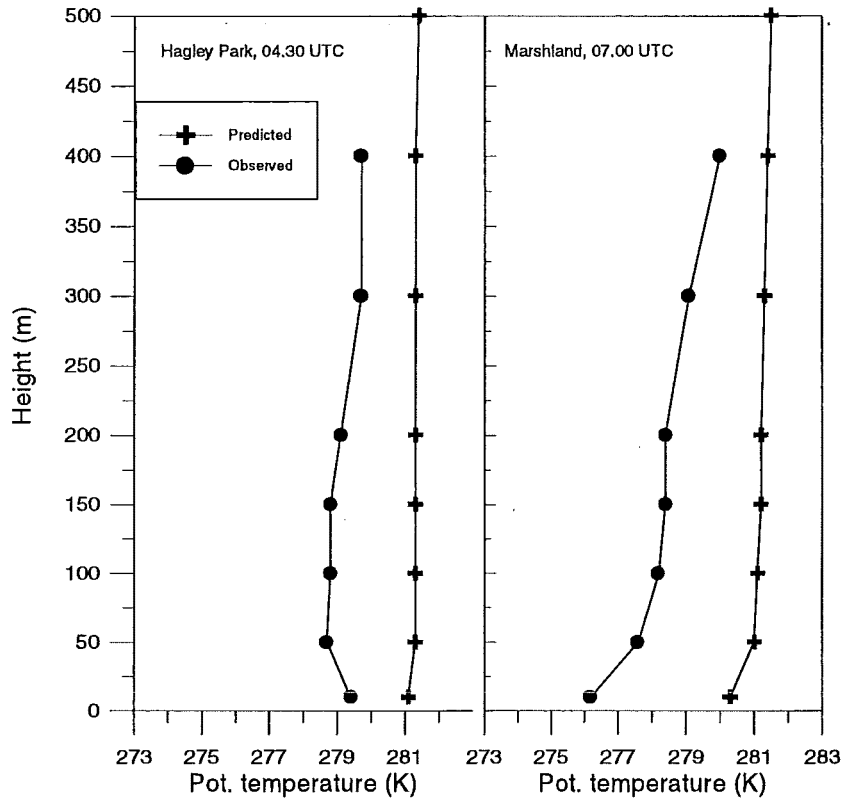

Figure 7.19a Temperature profiles at Hagley Park at 4.30 pm and at Marshland at 7 pm local time, respectively, on 27 July 1995.

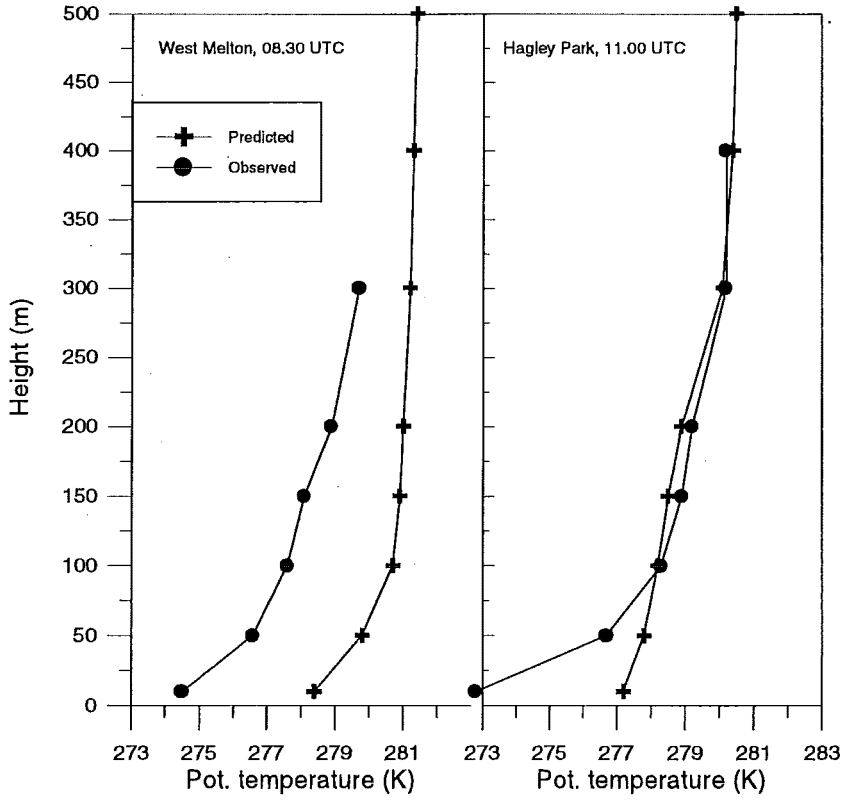

Figure 7.19b Temperature profiles at West Melton at 8.30 pm and at Hagley Park at 11 pm local time, respectively, on 27 July 1995.

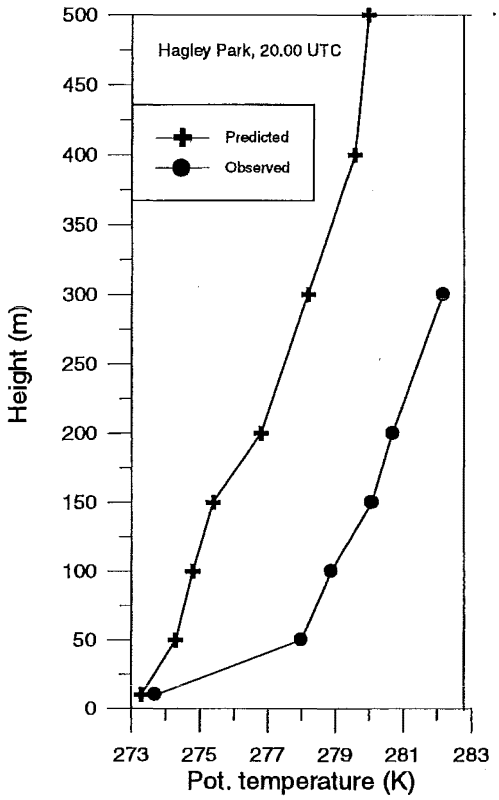

Figure 7.19c Temperature profiles at Hagley Park at 8 am local time on 28 July 1995.

7.5.3 Ambient CO concentrations

The time series of the CO concentrations at Beckenham, Hornby and St. Albans show that the magnitudes of the concentrations simulated by S5 agreed reasonably well with the observations (see Figure 7.20). However, the simulated temporal patterns deviate significantly at times from the observed patterns. During the evening, the observed CO concentrations rose at Beckenham, peaking between 7 and 8 pm, declining afterwards with a local minimum around 9 pm, followed by a second, even higher maximum, at around midnight with a slow decline afterwards. The simulated CO concentrations followed this pattern very well, although the second peak was simulated earlier, around 10 pm, followed by a sharp decline in the CO concentrations. During the morning, the rush-period peak occurred around 9 am, but S5 generated a double peak: one at 7 am and the other at 10 am. In Hornby, the simulated CO concentrations followed the observations reasonably well until midnight when the observed CO concentrations stayed around the same level for several hours, while the simulated CO concentrations declined to near zero values. The observed rush-hour morning peak occurred between 7 and 10 am, peaking with 10 mg m^{-3} around 8.30 am, while S5 created a very weak increase, having its maximum just after 6 am. In St. Albans the CO concentrations increased gradually from 5 pm until 1.30 am, declining to a minimum between 5 am and 8.30 am and rising sharply hereafter, peaking at 9 am. The predicted concentrations agreed reasonably well during the afternoon and evening until 9 pm. The model generated a sharp peak around 10 pm and a dramatic decline hereafter, which was not observed. The simulated peak in the morning was too early and too small.

7.5.4 Box model results

The box model was also applied for C2728, using observed and modelled average wind speeds (see Figure 7.21). Again, the simple box model approach created good results during the evening and night, but failed during the morning rush period, which showed a very high observed peak, not simulated by the box model. The box model appeared to be not very sensitive to the wind speeds applied, either from observations or simulated by RAMS.

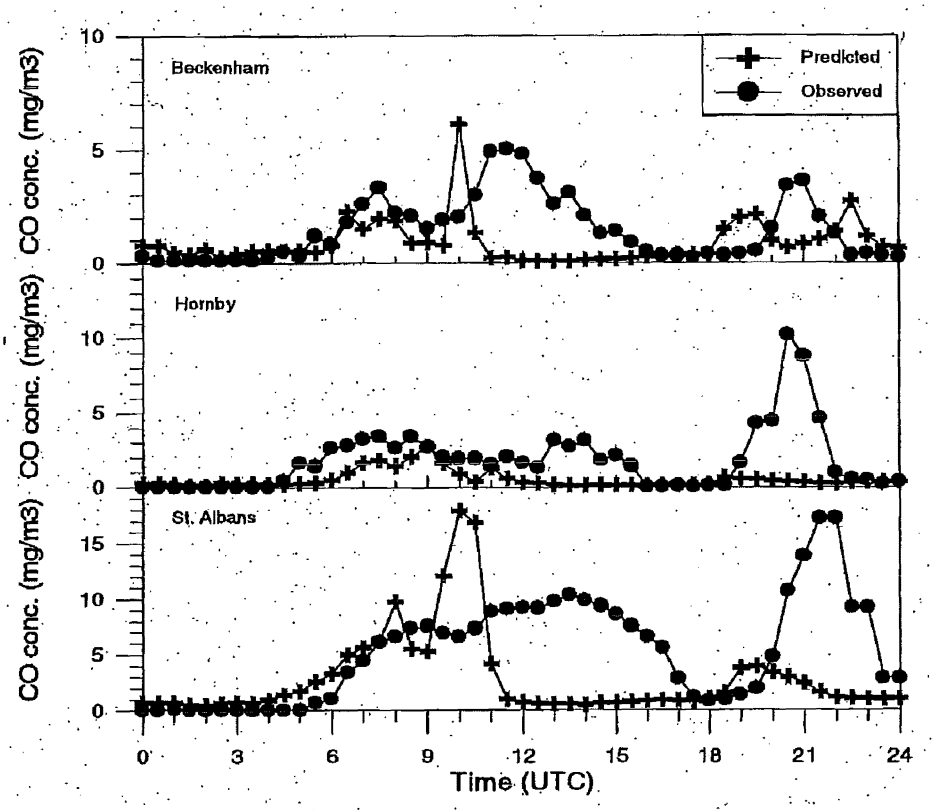

Figure 7.20 Time series of simulated and observed ambient CO concentrations during C2728.

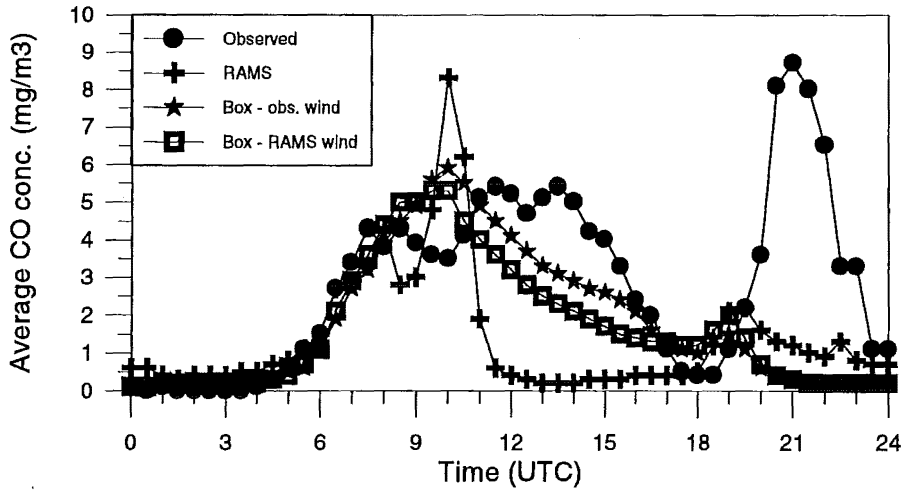

Figure 7.21 Time series of observed and simulated spatially averaged ambient CO concentrations over Christchurch during C2728.

7.5.5 Quantitative analysis

Analysis of the 24 hour period from noon 27 July 1995 to noon the following day shows that the model S5 bias for wind speed was low at Beckenham, Bromley, Burnside and Marshland. However, a rather poor direct relationship between observed and predicted wind speed existed, which is expressed by the low values of the index of agreement *D* and slope *b* (see Table 7.2).

Table 7.2 Validation of S5 data over a 24 hour period using half hourly samples, starting at noon 27 July 1995. **U**: windspeed (m s^{-1}); **dd**: wind direction (deg.); **T**: temperature (K); **CO**: ambient CO concentration (mg m^{-3}). ***ME***: mean error; ***RMSE***: root mean square error; ***RMSSD***: root mean square systematic deviation; ***RMSUD***: root mean square unsystematic deviation; ***D***: index of agreement; ***a*** and ***b***: regression coefficients of predictions to observations (***a***: intercept; ***b***: slope).

Var.	Site	ME	RMSE	RMSSD	RMSUD	D	a	b
U	Beckenham	0.20	1.02	0.55	0.86	0.43	1.28	0.15
	Bromley	-0.12	1.03	0.92	0.46	0.41	1.50	0.08
	Burnside	-0.14	0.98	0.87	0.44	0.34	1.30	0.03
	Marshland	-0.20	1.41	1.27	0.61	0.29	1.56	-0.04
dd	Beckenham	2	87	-	-	-	-	-
	Bromley	31	87	-	-	-	-	-
	Burnside	-16	104	-	-	-	-	-
	Marshland	17	102	-	-	-	-	-
T	Beckenham	-0.64	4.08	2.27	3.39	0.55	2.41	0.30
	Bromley	-1.94	3.67	2.11	3.00	0.44	0.92	0.49
	Burnside	-0.47	2.93	1.46	2.54	0.67	1.89	0.48
	Marshland	-0.46	3.21	1.82	2.64	0.65	2.21	0.42
CO	Beckenham	-0.56	1.82	1.52	0.99	0.40	0.89	-0.01
	Hornby	-1.28	2.39	2.32	0.56	0.45	0.37	0.07
	St. Albans	-2.46	6.18	4.87	3.82	0.48	2.34	0.09

S5 generated serious deviations of predicted wind direction from observations. The temperatures predicted by S5 were on average too low, the diurnal amplitudes being less than 50% of the observed temperature signal. The index of agreement values were moderate, but the deviations of predicted from observed data were rather high, reflected by RMSE, RMSSD and RMSUD. The CO data show a virtual non-existent direct response between observations and predicted values. On average the predicted ambient CO concentrations were underestimated. Sequential 6 hourly data analysis shows that the bias of wind speed at all sites was within ±0.5 m s^{-1} at all sites, except for Beckenham during the afternoon (see Figures 7.22 to 7.25).

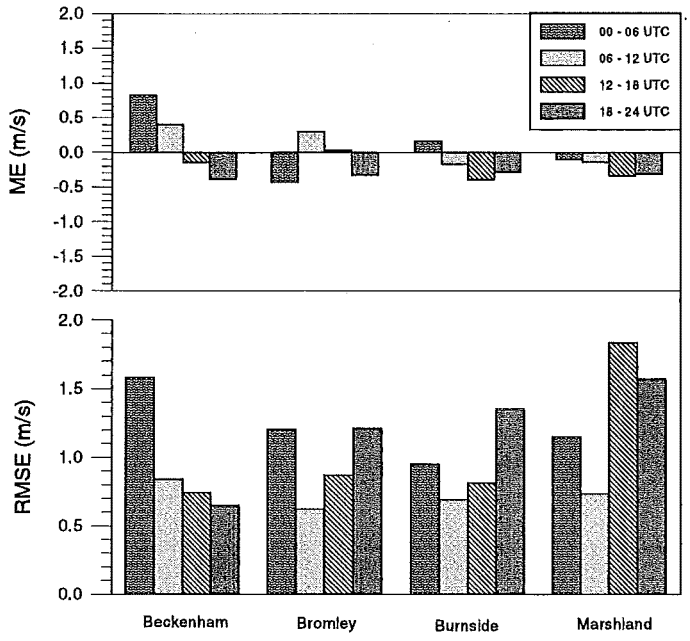

Figure 7.22 Mean Error and Root Mean Square Error of wind speed data generated by S5 during C2728.

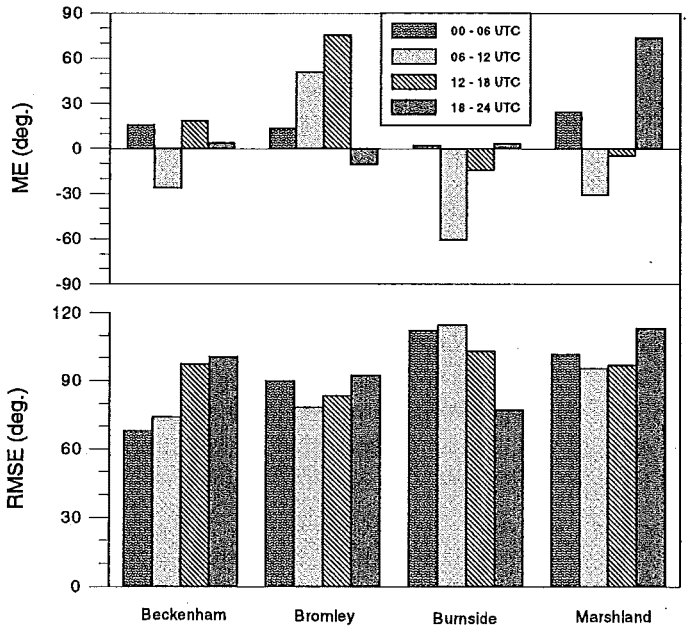

Figure 7.23 Mean Error and Root Mean Square Error of wind direction data generated by S5 during C2728.

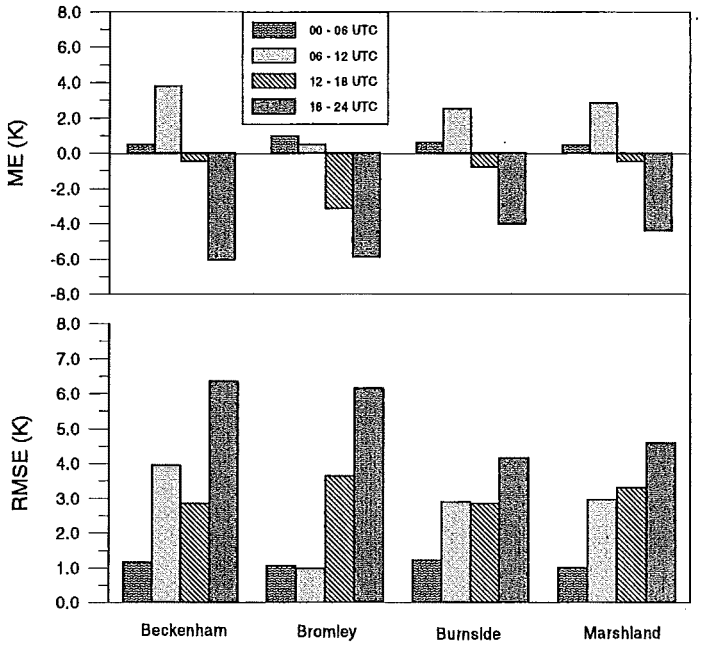

Figure 7.24 Mean Error and Root Mean Square Error of temperature data generated by S5 during C2728.

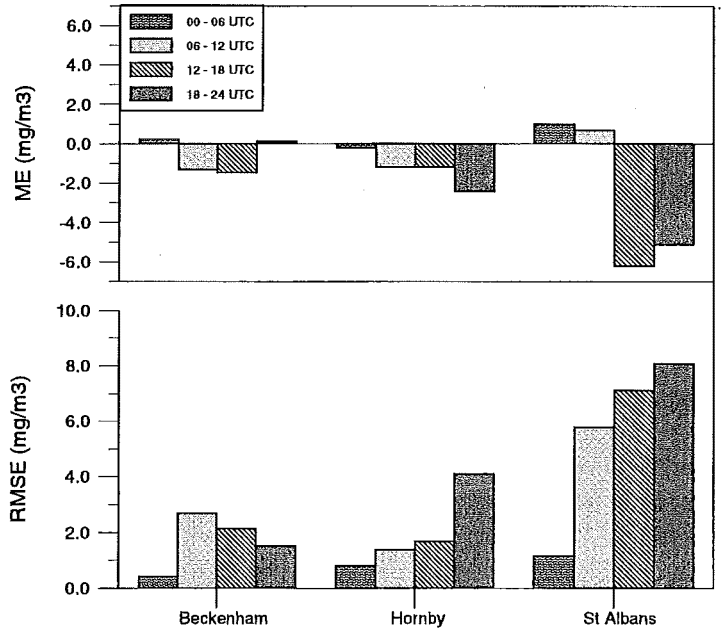

Figure 7.25 Mean Error and Root Mean Square Error of ambient CO concentration data generated by S5 during C2728.

The deviations of the predicted wind speed values from the observations declined in the evening at all sites, but increased again later at Bromley, Burnside and Marshland and slowly continued to decline at Beckenham. A limited positive bias in wind direction existed at all sites during the afternoon interval, being replaced by a moderate negative bias for the evening period at all sites, except Bromley where the bias was nearly +50°. During the following period the predicted wind direction decreased less or increased more than observed at all sites, resulting in increased bias values. At Bromley the bias exceeded 70°. The bias of the morning interval was near zero for all sites, except Marshland, which

exceeded 60°. Despite the variations in bias during the 24 hour period, the RMSE remained constantly high, exceeding 60° at all sites. The bias of temperatures showed a similar pattern at all sites. A limited overestimation was generated by S5 during the afternoon, which increased during the evening, except for Bromley. A limited underestimation of temperature occurred during the night, except for Bromley, where the bias exceeded -3 K, followed by a serious negative bias during the morning interval. The RMSE data indicated reasonable afternoon predictions, moderate to poor evening and night simulations, and rather poor morning predictions. The ambient CO concentrations show the highest absolute values of ME and RMSE at St. Albans, where the highest concentrations were also observed. Analysis of concentrations scaled by observed values has not been undertaken. The absolute bias was limited during the afternoon and evening at Beckenham, Hornby and St. Albans, but the values increased dramatically at St Albans during the night and morning interval.

7.6 Discussion and Conclusions

The validation runs S2 - S5 were similar to the N405 simulations, except for a few model settings, the strength, direction and shear of the advection and the initial thermal stratification of the atmosphere (see Figure B.5 in Appendix B). Not surprisingly, the flow patterns generated by S2 - S5 resembled the patterns of the N405 runs, particularly during the night and morning when decoupling occurred. Both sets of simulations showed that during the evening anabatic winds were replaced by katabatics. Christchurch was affected firstly by a drainage flow from the Port Hills, but later the westerly drainage flow from the Canterbury Plains dominated. Strong nocturnal low level jets (100 - 500 m elevation) were simulated over the city and disappeared later in the morning.

The validations at the Bromley site showed in general a different pattern than identified at the other locations, which may be explained by its position close to large water surfaces and being very exposed. During the C2728 case, the deviations of wind direction at all sites were relatively high, which may be related to the low wind speeds, favouring high variability of wind direction.

At noon on the 27th July 1995, the thermal stratification was weak throughout a deep layer, a condition which favours the development of deep and strong drainage flows under clear sky conditions at night as demonstrated by the two dimensional studies. Soundings in the evening showed that the air stabilized only in the lower 100 m. The development of elevated strong winds during the night were indeed observed over Christchurch during the C2728 case. During the beginning of the evening the development of a low level jet was observed in the Christchurch area, which was not related to an elevated drainage flow, since it was from the north-easterly direction and too early. It was more likely to be caused by an inertial oscillation or the remnant of the seabreeze or lee trough induced onshore flow. However, the West Melton sounding at 8.30 pm showed that the low level jet peaked around 100 m elevation, but above this jet the wind was between west and north, with a further increase again in speed. Later during the night, the northeasterly jet disappeared and the more elevated northwesterly jet increased in strength. The northwesterly jet was likely to originate from the Southern Alps drainage flow, although advection could have contributed as well. The limited vertical extent of the observations did not allow these ideas to be tested further. The vertical east-west cross sections of the S5 runs (not shown) indicated the development of a drainage flow combined with strong advection. Validation

showed that the simulated jet over Christchurch was too late and at elevations which were too high. Interestingly, the westerly advection run N405W also demonstrated a suppressed and more elevated low level jet over the Christchurch area, compared to the non-advection run. On 30 July 1995, the atmosphere had considerably stabilized due to warming at higher elevations and the strength of advection was significantly decreased compared to case C2728. The observed nocturnal jet was clearly weaker than during the C2728 case, but overestimated by the S2, S3 and S4 model runs.

The changed settings between model runs S2 to S4 have generally resulted in an improved performance, although S4 (and S5) failed to generate a very stable and shallow layer near the surface during the night. The improvements of S4 were most noticeable for wind speed by reducing the overestimation. However, the predicted wind speeds near the surface might become too low, if the model is adjusted so that it is able to generate the observed strong nocturnal inversions, despite the fact that the introduced roughness lengths in S4 and S5 can be physically justified. During nighttime the model runs S2 to S5 demonstrated insufficient cooling of the air layer below 100 m, while at higher elevations the cooling was too strong, indicating excessive vertical heat exchange. The simulated nocturnal heat loss by radiation appeared to be accurate, since differences of simulated and observed net radiation at Beckenham and Burnside were very small during the night (not shown). However, during daytime the model underestimated the net radiation by 15 %. No observations of sensible, latent and ground storage heat fluxes were available for either events, but if the ratios of these fluxes to net radiation were similar to the ratios derived from heat flux observations in August at the Beckenham site (see Chapter 3) then the cooling of the boundary layer (by sensible heat flux) was simulated reasonably accurately. The inaccurate simulation of the nocturnal vertical temperature gradient could be blamed on the vertical grid increment (25 m at lowest level) and the turbulence closure used (1st order). However, increased vertical resolution is computationally expensive and higher order turbulence closure schemes are not available as a standard option in RAMS-3b.

The spatial wind patterns simulated by S4 and S5 matched reasonably well with the observations, although some serious deviations occurred. This may be partly caused by a lack of spin up time and by the homogeneous initialisation, particularly during case C2728 when synoptic forcing was relatively strong. The deviations may also be caused by limited horizontal resolution. The N303 run (see Chapter 6) demonstrated the importance of increased resolution in the Christchurch area, when the horizontal grid increment was changed from 1000 m to 250 m.

The predictions of ambient CO concentrations were generally more accurate near the centre of Christchurch (St. Albans) than at its perifery (Beckenham, Hornby), which can be explained by the lower horizontal gradients of concentrations in the city centre, resulting in a lower sensitivity to inaccurate advection. The fact that local observations were compared to model predictions which were spatially averaged per grid cell, may have contributed to the inaccuracy. Generally, the simulations of CO dispersion by RAMS were not very successful, but surprisingly good results were obtained by the box model. During both case days the RAMS simulations showed a sharp decline in ambient CO concentrations during the second part of the evening, which was not observed and also not simulated by the box model. Too strong advection at lower elevations generated by RAMS can be excluded as the major contributor of the simulated decline of ambient CO during the evenings, since the box model, when using the RAMS winds, generated almost similar results as when using observed winds. Explanation of the RAMS dispersion results must be found in either: **a.** application of the Eulerian mode, which generates a too strong

horizontal dilution, particularly when the source area is small compared to the size of the grid cells; **b.** too strong vertical exchange of CO in a similar way to the vertical heat exchange; **c.** inaccurate emissions data, although results from the box model suggest otherwise. The temporal patterns indicate that the relative contributions of the estimated emissions during the evening and night were accurate during the case study days C2728 and C3031. However, the box model might have produced good results by using incorrect parameterizations in combination with inaccurate emissions. The morning rush hour was clearly not well represented in the emissions inventory, as all the model simulations generated a peak in the morning, which was about 2 hours too early, and its relative contribution was too low.

It is well known, that accurate emission inventories are extremely hard to obtain, especially when domestic emissions are major contributors. Despite the fact that the Christchurch emissions inventory contains much detail with a spatial resolution down to a few square kilometers, and four different emission regimes per day, it still lacks variations due to the day of the week or even month. Even when these numbers are available and on average accurate, the day to day and the hourly variations might also be significant. One may wonder if instead of an emissions inventory based on questionaires, should it not be supplemented by actual observations of emissions, which can be used to create an emissions model? Such a model could use such information as outdoor temperature, wind, cloudiness, month, day of the week, but possibly also the age of houses, type of suburb, and possibly social factors? Due to the initial success of the box model approach, it would be interesting to analyse a series of days and compare observed CO concentrations with values simulated by the box model and RAMS with adjusted settings and dispersion by the Lagrangian mode, in order to compare both models during different conditions and estimate the actual variability of the emissions and so the value of the current estimated emissions. Despite the limited inital success of the CO dispersion by RAMS in the Eulerian mode with the S4 and S5 runs, RAMS still proves to be useful by being able to forecast a wind field which produced good results in the box dispersion model and being able to generate local variations in pollutant concentrations, e.g. the 'evening dip' at Beckenham. The S4 and S5 dispersion studies have shown that a three dimensional prognostic model for dispersion in Christchurch is very promising, especially when using : **a.** FDDA (Four Dimensional Data Analysis), **b.** Lagrangian dispersion mode, **c.** an improved vertical diffusion scheme, and **d.** enhanced horizontal resolution. Finally, it must be made clear, that reliable air pollution forecasts can be obtained only when *instantaneous* emissions are accurate **and** the simulated dispersion of the pollutants is realistic.

8. Conclusions

8.1 Objectives recalled

The aim of this project is to provide knowledge about the meteorological conditions in the Christchurch area, which are important for dispersion of atmospheric pollutants. Since the dispersion of air pollution is strongly dependent on factors at a small scale affecting the surface layer, such as momentum and energy exchanges, but also on features at a larger scale, such as drainage flows and synoptic advection, it was decided to take a wide approach in this project. Therefore, research covered the following wide ranging topics:

- analysis of surface roughness in the Christchurch area, which affects horizontal wind speed and so the dispersion of air pollution.
- analysis of heat fluxes in the Christchurch area, which are responsible for variations in thermal stability and mixing depths of the boundary layer.
- develoment and structure of drainage flows from the Port Hills and the Canterbury Plains.
- interaction of synoptic advection with drainage flows.
- modelling of atmospheric dispersion.

The objectives of this Ph.D. project were formulated in Chapter 1, section 1.6. All the objectives have been met, providing the basis for further research which should explore selected aspects of the air pollution dispersion problem in more detail. In the next section, the final conclusions are given and placed in perspective with regard to the original aims of this project. Finally, recommendations for further research are discussed.

8.2 Summary of major findings

The results of this project reflect the complexity of the Christchurch environment, and indicate the significant amount of effort required to quantify dispersion of atmospheric pollutants in an accurate way. As expected, the suburbs of Christchurch are aerodynamically rough. The values of the roughness length z_o and the displacement height d, which were derived from observations, agree reasonably well with values obtained by empirical methods. However, the aerodynamical properties of commercial and industrial areas of Christchurch could be obtained by empirical methods only. Analysis of heat fluxes suggest that substantially reduced water is available for evaporation during fine daytime intervals in the winter at urban sites, while a less pronounced reduction of water availability could be observed on the northwestern fringe of Christchurch and at a rural site. A relationship between the water availability factor and rainfall events was demonstrated. The distribution of energy available for evaporation and heating of the air has important effects on the vertical dilution of air pollution, although no observations were available to demonstrate spatial variations.

Two case studies were conducted, representing different synoptic conditions, typically associated with high air pollution events. Both studies indicate that drainage flow from the Port Hills affects air pollution concentrations on the southern fringe of the city, while the northwestern areas are more influenced by drainage flow from the Canterbury Plains. Strong low level jets occurred over Christchurch during these case studies, while the wind speeds near the surface were low. The case studies indicate the existence of gravity waves and the possibility of breaking Kelvin Helmholz waves was evident, with dramatic effects on the ambient air pollution concentrations.

The three dimensional prognostic model RAMS version 3b, was used for simulations of airflow in the Christchurch area. All simulations had clear sky conditions and lacked cloud physics. Sensitivity analysis of drainge flows showed that soil moisture content and ambient thermal stratification of the air have a significant effect on the strength and depth of drainage flows. Simulations showed that under conditions with no large scale advection, drainage flow from the Port Hills covers Christchurch within two hours after sunset, but that drainage flow from the Canterbury Plains reaches the city several hours later. Large scale advection had the most pronounced impact on airflow patterns near the surface during daytime, while its role is reduced at night due to decoupling. Decreasing the horizontal grid size increment by a factor of four to only 250 m, allowed the incorporation of more topographic details, and dramatic spatial variations in airflow patterns in the Christchurch area were simulated at the expense of considerable computer time.

Simulations of the two case studies produced airflow patterns which agreed reasonably well with observations. However, simulated vertical profiles indicated that excessive vertical exchange of heat and momentum was generated during the night, resulting in a weaker thermal stratification near the surface than observed. Improved performance could be created by changing the parameterization of turbulence, by using smaller vertical grid increments, and by the introduction of a scheme for higher order closure of turbulence.

Simulations of ambient CO were conducted for both case studies, using the Eulerian disperion mode. The predictions of CO concentrations were generally more accurate near the centre of Christchurch than at the perifery. Strong horizontal gradients in CO concentrations were generated at times on the western and eastern fringes of Christchurch due to low level convergence of airflow. The results were only in reasonable agreement with observations during the end of the afternoon and the first part of the evening, while a later strong decline in CO concentrations was simulated, but not observed. Analysis suggests that the premature decline of ambient CO concentrations can be linked to excessive vertical diffusion, and that it was not caused by deviations in estimated emissions. However, it appears that actual emissions of CO during morning rush hour are not well presented in the 1997 emissions inventory work.

8.3 Suggestions for further research

As stated before, the downstream objective of this project is to contribute to improved air quality management through improved understanding of the role of the atmosphere. A powerful tool could be the application of a three dimensional prognostic atmospheric model, which is established to run operationally. The model could be used in two different modes. Firstly, it could be used for detailed analysis of air pollution dispersion to represent historic events or potential situations, e.g. when emissions are changed and it could assist procedures for Resource Consent Applications. Since this mode is applied to non-real time events, a high resolution can be used, which provides more detail at the expense of high computational demands. Secondly, it could be used in the forecasting mode, using a lower resolution, but running faster. This mode could be applied to forecast air pollution events and the results could be used to issue warnings or even enforce restrictions on emissions.

The results in Chapter 7 demonstrate that RAMS version 3b, simulated the general atmospheric patterns reasonably well, with the settings used in this project. However, serious deviations from observations also occurred, which need to be reduced when the model is applied as a management tool for dispersion studies. One way to improve the performance of the model is by 'tuning' (manipulating) settings and boundary conditions, until the performance is satisfactory during given case studies. A disadvantage of this approach is the increased empirical nature of the model, being more loosely based on actual physical relationships. If this approach was taken, the model is likely to lose its flexibility to be transferred to other areas and it may not perform well outside the range of atmospheric conditions of the given case studies. However, the above mentioned approach could be an relatively easy method to obtain satisfactory results in a defined area within a defined range of conditions.

Another approach is to gradually reduce all the simplifications introduced in this modelling project, by incorporating Four Dimensional Data Analysis (FDDA), which allows non-homogeneous initialisations, by applying the surface flux scheme with vegetation and by introducing cloud physics. The above mentioned procedures are available as a standard option in RAMS, version 3b. Dispersion can be simulated by applying the Lagrangian or hybrid mode, and models are available which use RAMS output files. Obviously, the performance of the model should be further improved by the introduction of detailed information about initial atmospheric conditions, spatial variations of soil moisture content and land use. However, except for land use data, detailed data collection could be very laborious, and not a realistic option for operational model runs on a routine basis.

In addition, new physical relationships can be introduced into the model, which can be expected to happen with new upgrades of RAMS. Additional research can contribute to this, including the addition of new schemes for turbulent closure. It appears that fluxes in the boundary layer are sensitive to the formulation of closure (Alapaty, 1997). Other useful additions could be the formulation of a more sophisticated surface layer flux scheme, the inclusion of different types of land use (urban residential, industrial, commercial) and the possibility to define subgrid heterogeneity, which can have dramatic impacts on bulk values of momentum and heat fluxes (Mahrt, 1996).

Finally, this project has illustrated a variety of processes occurring in the Christchurch area. Due to the wide ranging approach taken in this thesis, some topics could be

investigated only superficially. Suggestions for further research include firstly, a more extensive investigation of surface fluxes in the urban environment of Christchurch, especially the city centre and industrial areas. The use of three dimensional eddy correlation equipment for evaluation of surface fluxes would be helpful, since profile methods proved to be rather inaccurate. Comparing results from different seasons could be very interesting. Secondly, the addition of several detailed case studies, would provide a better picture of the nature of airflow patterns, which develops under during various atmospheric situations. Such a work should include profiles from tethered balloons to altitudes greater than 1000 m, the application of acoustic sounders and possibly a lidar, could be included, in addition to aircraft measurements. Thirdly, research on atmospheric waves in the Christchurch area would make a separate topic, with a particular focus on their role in dispersion of air pollution. The 1995 dataset contains frequent occurrencies of persistent atmospheric waves. Due to limited atmospheric data from upper levels, no further analysis was undertaken during the project. Fourthly, as mentioned before, topics not included in this project, but related to the air pollution problem of Christchurch, are the development of an extensive statistical or empirical model of ambient air pollutants and the creation of an accurate emissions model.

References

Chapter 1.

Bellasio, R.,1997. Modelling traffic air pollution in road tunnels. *Atmospheric Environment*, **31**: 1539-1551.

Benarie, M.M., 1980. *Urban air pollution modelling.* MacMillan, London, 1980.

Bose, N.K. and P. Liang, 1996. *Neural network fundamentals with graphs, algorithms and applications.* New York. McGraw-Hill.

Bouma, W.J., G.I. Pearman and M.R. Manning, 1996. *Greenhouse: coping with climate change.* Collingwood, Vic., CSIRO Publisher

Brady, T.J. and D.R. Pullen, 1985. *Survey of fuel, energy and air pollution in the Christchurch metropolitan area.* Department of Health, Christchurch.

Briggs, G.A., 1975. *Plume rise predictions. Lectures on air pollution and environmental impact analysis.* Workshop Proceedings, Boston, Massachusetts, Sep. 29 - Oct. 3, pp. 59-111, American Meteor. Soc., Boston, Massachusetts.

Broennimann, S. and U. Neu, 1997. Weekend - weekday differences of near-surface ozone concentrations in Switzerland for different meteorological conditions. *Atmospheric Environment*, **31**: 1127-1135.

Canterbury Regional Council, 1993. *Let's clear the air. Issues and options for air quality management in Canterbury and background information.* Canterbury Regional Council, Christchurch.

Canterbury Regional Council, 1997. *Christchurch inventory of home heating and motor vehicle emissions.* Technical Report. Environmental Management Group. Prepared by NIWA, May 1997, Report No. R97/5.

Christchurch Regional Planning Authority, 1966. *Air Pollution.* New Zealand Department of Scientific and Industrial Research, Information Series No 55, Christchurch.

Carruther, D., D. Thomson, R.E. Britter and J.C.R. Hunt, 1992. Description of the United Kingdom atmospheric dispersion modeling system (ADM). In: *Proc. CEC Workshop on objectives for next generation of practical short-range atmospheric dispersion models.* Riso National Laboratory, Denmark.

Collier, C.G. and P.J. Hardaker, 1995. Weather, air quality and health. *Meteorology Applied*, **2**: 313-322.

Curtiss, P.S. and A. Rabl, 1996. Impacts of air pollution: general relationships and site dependence. *Atmospheric Environment*, **30**: 3331-3342.

Elsom, D.M., 1992. *Atmospheric pollution: a global problem.* Blackwell Publisher, Oxford, U.K.

Elsom, D.M., 1996. *Smog Alert. Managing urban air quality.* Earthscan Publications Ltd, London.

Fast, J.D., 1995. Mesoscale modeling and four-dimensional data assimilation in areas of highly complex terrain. *Journal of Applied Meteorology*, **34**: 2762-2782.

Feshback, M. and A. Friendly, 1992. *Ecocide in the USSR.* Aurum.

Fujita, E.M., B.E. Croes, C.L. Bennett, D.R. Lawson, F.W. Lurmann and H.H. Main, 1992. Comparison of emission inventory and ambient concentration ratios of CO, NMOG and NOx in California's South Coast Air Basin. *Journal of Air and Waste Management Association.*, **42**: 264-276.

Garratt, J.R., 1992. *The atmospheric boundary layer.* Cambridge University Press, UK, 316pp.

Golay, M.W., 1982. Numerical modeling of buoyant plumes in a turbulent, stratified atmosphere. *Atmospheric Environment*, **27A**: 2147-2160.

Gong, W.M. and H.R. Cho, 1993. A numerical scheme for the integration of the gas-phase chemical rate equations in 3 dimensional atmospheric models. *Atmospheric Environment*, **27A**: 2147-2160.

Goodin, W.R., C.J. McRae and J.H. Seinfeld, 1980. An objective analysis technique for constructing three-dimensional urban-scale wind field. *Journal of Applied Meteorology*, **21**: 1441-1454.

Griffin, R.D., 1994. *Principles of air quality management.* Lewis Publishers, London.

Hagan, M.T., H.B. Demuth and M. Beale, 1996. *Neural network design.* Boston, PWS Publisher

Hales, J.M. D.C. Powel and T.D. Fox, 1977. *STRAM. An air pollution model incorporating non-linear chemistry, variable trajectories, and plume segment diffusion.* U.S. EPA Document 450/3-77-012, Research Triangle Park, North Carolina.

Hanna, S.R., G.A. Briggs and R.P. Hosker, 1982. *Handbook on atmospheric diffusion.* Techn. Information Center, U.S. Dept. of Energy. DOE/TIC - 11223, 102pp.

Hanna, S.R. and J.C. Chang, 1993. Hybrid plume dispersion model (HPDM) improvements and testing at 3 field sites. *Atmospheric Environment*, **27A**: 1491-1508.

Hanna, S.R., J.V. Ramsdell and H.E. Cramer, 1987. Urban Gaussian diffusion parameters. In: *Modeling the urban boundary layer.* Amer. Meteorol. Soc., Boston, pp 337-379.

Harrison, R.M. 1990. *Pollution: causes, effects and control.* Cambridge: Royal Soc. of Chemistry.

Kennedy, A.M., N.N. Peet, J.C. Marlow and K.J. Brown, 1974. *Survey of fuel, energy and air pollution in the Christchurch urban area.* Department of Chemical Engineering, University of Canterbury, Christchurch, New Zealand, 71pp.

Kristensen, L., N.O. Jensen and E.L. Peterson, 1982. Lateral dispersion of pollutants in a very stable atmosphere. The effect of meandering. *Atmospheric Environment*, **15**: 837-844.

Lefohn, A.S., D.S. Shadwick, U. Fiester and V.A. Mohnen, 1992. Surface-level ozone: climate change and evidence for trends. JAPCA - *Journal of Air and Waste Management Association*, **42**: 136-144.

Luhar, A.K., and R.E. Britter, 1989. A random walk model for dispersion in inhomogeneous turbulence in a convective boundary layer. *Atmospheric Environment*, **23**: 1911-1924.

Lyons, W.A., R.A. Pielke, C.J. Tremback and R.L. Walko, 1995. Modeling impacts of mesoscale vertical motions upon coastal zone air pollution dispersion. *Atmospheric Environment*, **29**: 283-301.

Lyons, T.J. and W.D. Scott, 1990. *Principles of air pollution meteorology*. Boca Raton, Florida: CRC Press.

Matzoros, A. and D. van Vliet, 1992. A model of air pollution from road traffic, based on the characteristics of interrupted flow and junction control: part I - model description. *Transportation Research*, **26A**: 315-330.

McKendry, I.G., A.P. Sturman and I.F. Owens, 1986. A study of interacting multi-scale wind systems, Canterbury Plains, New Zealand. *Meteorology and Atmospheric Physics*, **35**: 242-252.

McKendry, I.G., A.P. Sturman and I.F. Owens, 1988. Numerical simulation of local thermal effects on the wind field of the Canterbury Plains, New Zealand. *New Zealand Journal of Geology and Geophysics*, **31**: 511-524.

Moody, T., 1983. Air pollution in Canterbury: into the '80s or back to the '30s? In: *Canterbury at the Crossroads: issues for the eighties*. Eds. Bedford, R.D. and A.P. Sturman.

Moran, M.D. and R.A. Pielke, 1996. Evaluation of a meso scale atmospheric dispersion modeling system with observations from the 1980 Great Plains mesoscale trace field experiment. 2. Dispersion simulations. *Journal of Applied Meteorology*, **35**: 308-329.

Nieuwstadt, F.T.M. and H. van Dop, 1982. *Atmospheric turbulence and air pollution modelling*. Reidel, Dordrecht.

Nieuwstadt, F.T.M. and J.P. de Valk, 1987. A large-eddy simulation of buoyant and non-buoyant plume dispersion in the atmospheric boundary layer. *Atmospheric Environment*, **21**: 2573-2587.

Oke, T.R., 1978. *Boundary Layer Climates*. Halsted Press, New York, 372pp.

Oleson, H.R., 1988. *Users guide for OML-Point. An air pollution model for point sources*. MST LUFT-A 125, National Agency of Environmental Protection, Roskilde, Denmark.

Owens, I.F. and N.J. Tapper, 1977. The influence of meteorological factors on air pollution occurrence in Christchurch. *Proc. 9th N.Z. Geography Conference, Dunedin, New Zealand, pp. 33-35.*

Paterson, R.M., 1981. *Air pollution survey*. Christchurch, Department of Health.

Pielke, R.A., W.R. Cotton, R.L. Walko, C.J. Tremback, W.A. Lyons, L.D. Grasso, M.E. Nocholls, M.D. Moran, D.A. Wesley, T.J. Lee and J.H. Copeland, 1992. A comprehensive meteorological modeling system - RAMS. *Meteorology and Atmospheric Physics.*, **49**: 69-91.

Pilinis, C., P. Kassomenos and G. Kallos, 1993. Modelling of photochemical pollution in Athens, Greece. Application of the RAMS-CALGRID modeling system. *Atmospheric Environment*, **27B**: 353-370.

Roberts, J.J., E.S. Croke and A.S. Kennedy, 1970. An urban atmospheric dispersion model. *Proc. Symposium on multple-source urban diffuse models.* Air pollution control office publ. AP-86, pp. 6.1-6.72.

Ryan, A.P., 1980. *Northwest drifts and night cooling in winter in Christchurch.* N.Z. Met. Service, Techn. Note 243, Wellington, New Zealand.

Sasaki, Y. and J.M. Lewis, 1970. Numerical variational objective analysis of the boundary layer in conjunction with squall line formation. *Journal of the Meteorological Society of Japan*, **48**: 381-393.

Sashegyi, K.D. and R.V. Madala, 1994. Initial conditions and boundary conditions. In: *Mesoscale modeling of the atmosphere.* Pielke, R.A. and R.P. Pierce (eds). Meteorol. Mon. 25(47). American. Meteorological. Society., Boston.

Saylor, R.D. and R.I. Fernandes, 1993. On the parellelization of a comprehensive regional-scale air-quality model. *Atmospheric Environment*, **27A**: 625-631.

Shahgedanova, M. and T.P. Burt, 1994. New data on air pollution in the former Soviet Union. *Global Environmental Change*, **4**: 201-207.

Scheffe, R.D. and R.E. Morris, 1993. A review of the development and application of the urban airshed model. *Atmospheric Environment*, **27B**: 23-29.

Schwela, D.H., 1995. Public health implications of urban air pollution in developing countries. In: *Proc. of the 10th World Clean Air Congress, Espoo, Finland, May-June 1995, Vol 3*, Finnish Air Pollution Prevention Society, Helsinki.

Simmonds, I. and K. Keay, 1997. Weekly cycle of meteorological variations in Melbourne and the role of pollution and anthropogenic heat released. *Atmospheric Environment*, **31**: 1589-1603.

Smith, F.B., 1968. Conditioned particle motion in a homogeneous turbulent field. *Atmospheric Environment*, **2**: 491-508.

Sparrow, C.J., 1968. A survey of the New Zealand air pollution literature and a bibliography. *Public Health*, **83**: 25-33.

Stauffer, D.R. and N.L. Seaman, 1990. Use of four-dimensional data assimilation in a limited-area mesoscale model. Part I: experiments with synoptic scale data. *Monthly Weather Review*, **118**: 1250-1277.

Stern, A.C., A. Boubel, D.B. Turner and D.L. Fox, 1984. *Fundamentals of air pollution.* Academic Press, 492pp.

Stokes, M.J. and P.D. Tyson, 1981. Modelling average winter smoke pollution over the Christchurch urban area. *Weather and Climate*, **1**: 4-13.

Stull, R., 1988. *An introduction to boundary layer meteorology.* Kluwer Academic Publisher, Dordrecht.

Sturman, A.P. and P.D. Tyson, 1981. Sea breezes along the Canterbury coast in the vicinity of Christchurch, New Zealand. *Journal of Climatology*, **1**: 203-219.

Sturman, A.P., 1982. Statistical analysis of spatial patterns of smoke concentrations in Christchurch. *New Zealand Geographer*, **38**: 9-18.

Sturman, A.P., 1985. An examination of the role of local wind systems in the concentration and dispersion of smoke pollution in Christchurch, New Zealand. *New Zealand Geographer*, **41**: 67-76.

Surridge, A.D., 1980. Examples of wind shear and temperature inversion surfaces over Christchurch. *New Zealand Journal of Science*, **23**: 283-288.

The Economist, 1996. Take a deep breath. *The Economist*, **Sept. 17th**: 91-93.

The Press, 1997a. UN chief warns expectations low for Earth Summit. In: *The Press*, **21 June 1997**.

The Press, 1997b. Summit warns of catastrophe. In: *The Press*, **25 June 1997**.

Turner, D.B., 1994. *Workbook of atmospheric dispersion estimates. An introduction to dispersion modeling.* Lewis Publisher, London.

Uliasz, M., 1993. The atmospheric mesoscale dispersion modeling system. *Journal of Applied Meteorology*, **32**: 139-149.

Van Dop, H., F.T.M. Nieuwstadt and J.C.R. Hunt, 1985. Random walk models for particle displacement in inhomogeneous unsteady turbulent flows. *Physics of Fluids*, **28**: 1639-1653.

Venkatram, A. and J.C. Wyngaard, 1988. *Lectures on air pollution modeling*. A. Venkatram and J.C. Wyngaard, ed. Americ. Meteorol. Soc. (Proc.), Boston.

Wagner, H.M., 1990. *Photochemical smog in Europe: an overview*. Air Hygiene Report 2, WHO Collaborating Centre for Air Quality management and air pollution control, Langen, Germany.

Weil, J.C., 1992. *Updating the ISC model through EARMIC*. 85th Annual meeting of Air and Waste Management Assoc., Kansas City, MO.

Wilson, J.D., G.W. Thurtell and G.E. Kidd, 1981a. Numerical simulation of particle trajectories in inhomogeneous turbulence - I. Systems with constant turbulent velocity scale. *Boundary-Layer Meteorology*, **21**: 295-313.

Wilson, J.D., G.W. Thurtell and G.E. Kidd, 1981b. Numerical simulation of particle trajectories in inhomogeneous turbulence - II. Systems with variable turbulent velocity scale. *Boundary-Layer Meteorology*, **21**: 423-441.

World Health Organisation, 1992. Urban air pollution in megacities of the world. Blackwell Publisher, Oxford, UK.

World Meteorological Organisation, 1972. Dispersion and forecasting of air pollution. WMO Techn. Note 121, Geneva, 116pp.

Wyman, R.L., 1991. *Global climate change and life on earth*. New York, Rontledge, Chapman and Hall.

Yamartino, R.J., J.S. Scire, G.R. Carmichael and Y.S. Chang, 1992. The CALGRID mesoscale photochemical grid model - I. Model formulation. *Atmospheric Environment*, **26A**: 1493-1512.

Zanetti, P., 1990. *Air pollution modelling. Theories, computational method, and available software*. Computational Mechanics Publisher, New York.

Zlatev, Z., J. Christensen and O. How, 1992. An Eulerian air pollution model for Europe with non linear chemistry. *Journal of Atmospheric Chemistry*, **15**: 1-37.

Chapter 2.

Avissar,R. and Y. Mahrer, 1988. Mapping frost-sensitive areas with a three-dimensional local scale model, I. Physical and numerical aspects. *Journal of Applied Meteorology*, **27**: 400-413.

Bluestein, H.B., 1992. *Synoptic - dynamic meteorology in midlatitudes. Volume I. Principles of kinematics and dynamics*. Oxford University Press,Oxford, 431pp.

Chen, S., and W.R. Cotton, 1988. The sensitivity of a simulated extratropical mesoscale convective system to longwave radiation and ice-phase microphysics. Journal Atmospheric Science, **45**: 3897-3910.

Clarke, T.L. and R.D. Farley, 1984. Severe downslope windstorm calculations in two and three spatial dimensions using anelastic interactive grid nesting. A possible mechanism for gustiness. *Journal of the Atmospheric Sciences*, **41**: 329-350.

Dudhia, J., 1993. A nonhydrostatic version of the Penn State-NCAR mesoscale model: validation tests and simulation of an Atlantic cyclone and cold front. *Monthly Weather Review*, **121**: 1493-1513.

Fast, J.D., 1995. Mesoscale modeling and four dimensional data assimilation in areas of highly complex terrain. *Journal of Applied Meteorology*, **34**: 2762-2782.

Holton, J.R., 1979. *An introduction to dynamic meteorology*. Academic Press, New York, 319pp.

Louis, J.F., 1979. A parametric model of vertical eddy fluxes in the atmosphere. *Boundary-Layer Meteorology*, **17**: 187-202.

Lyons, W.A., C.J. Tremback and R.A. Pielke, 1995. Applications of the Regional Atmospheric Modeling System (RAMS) to provide input to photochemical grid models for the Lake Michigan Ozone Study (LMOS). *Journal of Applied Meteorology*, **34**: 1762-1786.

Mahrer, Y. and R.A. Pielke, 1977. A numerical study of the airflow over irregular terrain. *Beitrage zur Physik der Atmosphaere*, **50**: 98-113.

Meyers, M.P., P.J. DeMott, and W.R. Cotton, 1992. New primary ice nucleation parameterizations in an explicit cloud model. *Journal of Applied Meteorology*, **31**: 708-721.

Moussipoulos, N., T. Flassak, P. Sahm and D. Berlowitz, 1993. Simulation of the wind field in Athens with the nonhydrostatic mesoscale model MEMO. *Environtal Software*, **8**: 29-42.

Pielke, R.A., 1984. *Mesoscale meteorology*. Academic Press, Orlando, Florida.

Pielke, R.A., W.R. Cotton, R.L. Walko, C.J. Tremback, W.A. Lyons, L.D. Grasso, M.E. Nicholls, M.D. Moran, D.A. Wesley, T.J. Lee and J.H. Copeland, 1992. A comprehensive meteoroligical modeling system - RAMS. *Meteorology and Atmospheric Physics*, **49**: 69-91.

Thunis, P. and R. Bornstein, 1996. Hierachy of mesoscale flow assumptions and equations. *Journal of the Atmospheric Sciences*, **53**: 380-397.

Tremback, C.J. and R. Kessler, 1985. A surface temperature and moisture parameterization for use in mesoscale numerical models. In: *Preprints, 7th Conference on numerical weather predictions, 17-20 June 1985*, Montreal, Canada, American Meteorological Society, 355-358..

Tripoli, G.J. and W.R. Cotton, 1982. The Colorado State University three-dimensional cloud/mesoscale model - 1982, Part I: General theoretical framework and sensitivity experiments. *Journal of Rech. Atmosphere.*, **16**: 185-219.

Walko, R.L., C.J. Tremback and R.A. Pielke and W.R. Cotton, 1995. An interactive nesting algorithm for stretched grids and variable nesting ratios. *Journal of Applied Meteorology*, **34**: 994-999.

Walko, R.L., C.J. Tremback and R.F.A. Hertenstein, 1996. *RAMS. The Regional Atmospheric Modeling System, Version 3b, User's Guide.* *Aster Division Mission Research Corporation, P.O. Box 466, Fort Collins, CO 80522, 117 pp.

Chapter 3.

Arnfield, A.J., 1982. An approach to the estimation of the surface radiative properties and radiation budgets of cities. *Physical Geography*, **3**:97-122.

Atwater, M.A., 1972. Thermal effects of urbanisation and industrialization in the boundary layer. *Boundary-Layer Meteorology*, **3**:229-245.

Auer, A.H.,1978. Correlation of land use and cover with meteorological anomalies. *Journal of Applied Meteorology*, **17**: 636-643

Avissar, R., 1996. Potential effects of vegetation on the urban thermal environment. *Atmospheric Environment*, **30**: 437-448.

Brutsaert, W.A., 1982. *Evaporation into the atmosphere.* Reidel Publisher, Dordrecht, 299pp.

Byun, D.W. and S.P.S. Arya, 1990. A two-dimensional mesoscale numerical model of an urban mixed layer - I. Model formulation, surface energy budget, and mixed layer dynamics. *Atmospheric Environment*, **24A**: 829-844.

Campbell Scientific Inc., 1994. *Eddy correlation system operations, manual.* Revision: 8/94.

Camuffo, D. and A. Bernardi, 1982. An observational study of heat fluxes and their relationship with net radiation. *Boundary-Layer Meteorology*, **23**: 359-368.

Canterbury Regional Council, 1997. *Christchurch inventory of home heating and motor vehicle emissions.* Technical Report. Environmental Management Group. Prepared by NIWA, May 1997, Report No. R97/5.

Ching, J.K.S., J.F. Clarke and J.M. Godowitch, 1983. Modulation of heat flux by different scales of advection in an urban environment. *Boundary-Layer Meteorology*, **25**: 171-191.

Cleugh, H.A. and T.R. Oke, 1986. Suburban-rural energy balance comparisons in summer for Vancouver B.C. *Boundary-Layer Meteorology*, **36**: 351- 369.

De Bruin, H.A.R. and J.Q. Keijman, 1979. The Priestley- Taylor evaporation model applied to a large shallow lake in the Netherlands. *Journal of Applied Meteorology*, **18**: 898-903.

De Bruin, H.A.R. and A.A.M. Holtslag, 1982. A simple parameterization of the surface fluxes of sensible and latent heat during daytime compared with the Penman-Monteith concept. *Journal of Applied Meteorology*, **21**: 1610-1621.

De Bruin, H.A.R. and C.J. Moore, 1985. Zero plane displacement and roughness length for tall vegetation, derived from a simple mass conservation hypothesis. *Boundary-Layer Meteorology*, **31**: 39-49.

Dyer, A.J., 1974. A review of flux-profile relationships. *Boundary-Layer Meteorology*, **7**: 363-372.

Eliasson, I., 1996. Urban nocturnal temperatures, street geometry and land use. *Atmospheric Environment*, **30**: 379-392.

Elsom, D.M., 1987. *Atmospheric pollution - causes, effects and control policies.* Blackwell Publisher, Oxford, 256pp.

Garratt, J.R., 1990. The internal boundary layer - a review. *Boundary-Layer Meteorology*, **50**: 171-203.

Grimmond, C.S.B., H.A. Cleugh and T.R. Oke, 1991. An objective urban heat storage model and its comparison with other schemes. *Atmospheric Environment*, **25B**: 311-326.

Grimmond, C.S.B., T.R. Oke, R. Spronken-Smith, E. Jauregui, C. Souch, T. Newton, T.S. King, J. Voogt, and M. Hubble, 1996. Heat storage in urban areas. *Preprint: 12th Conference on biometeorology and aeriobiology, 76th American Meteorological Society Annual Meeting, Atlanta GA, 28January - 2 February 1996.*

Harrison, R.M. and R. Perry, 1986. *Handbook of air pollution analysis*. Chapman & Hall, London, 656pp.

Haenel, H.D. 1993. Surface-layer profile evaluation using a generalization of Robinson's method for the determination of d and z_o. *Boundary-Layer Meteorology*, **65**: 55-67.

Hjelmfeldt, M.R., 1982. Numerical simulation of the effects of St Louis on mesoscale boundary-layer airflow and vertical air motion: simulation of urban vs. non urban effects. *Journal of the Atmospheric Sciences*, **21**: 1233-1257.

Holtslag, A.A.M. and A.P. van Ulden, 1983. A simple scheme for daytime estimates of the surface fluxes from routine weather data. *Journal of Climate and Applied Meteorology*, **22**:517-529.

Johnson, G.T., T.R. Oke, T.J. Lyons, D.G. Steyn and I.D. Watson, 1991. Simulation of surface urban heat islands under ideal conditions at night. 1. Theory and tests against field data. *Boundary-Layer Meteorology*, **56**: 275-294.

Kerschgens, M.J. and H. Kraus, 1990. On the energetics of the urban canopy layer. *Atmospheric Environment*, **24B**: 321-328.

Kondo, J. and H. Yamazawa, 1986. Aerodynamic roughness over an inhomogeneous ground surface. *Boundary-Layer Meteorology*, **35**: 331-348.

Kramm, G. 1989. The estimation of the surface-layer parameters from wind velocity, temperature and humidity profiles by least- squares methods. *Boundary-Layer Meteorology*, **48**: 315-327.

Lyons, T.J. and W.D. Scott, 1990. *Principles of air pollution meteorology*. Boca Raton, Fla: CRC Press.

Myrup, L.O., C.E. McGinnan, and R.G. Flocchini, 1993. An analysis of microclimatic variation in a suburban environment. *Atmospheric Environment*, **27B**: 129-156.

Oke, T.R., 1978. *Boundary layer climates*, Halsted Press, New York. 372 pp.

Oke, T.R., 1982. The energetic basis of the urban heat island. *Quarterly Journal of the Royal Meteorological Society*, **108**: 1-24.

Oke, T.R., 1988. The urban energy balance. *Progress in Physical Geography*, **12**: 471-508.

Oke, T.R, H.A. Cleugh, C.S.B. Grimmond, H.P. Schmid and M. Roth, 1989. Evaluation of spatially-averaged fluxes of heat, mass and momentum in the urban boundary layer. *Weather and Climate*, **9**:14-21.

Oke, T.R., G.T. Johnson, D.G. Steyn and I.D. Watson, 1991. Simulation of surface urban heat islands under ideal conditions at night. 2. diagnosis of causation. *Boundary-Layer Meteorology*, **56**: 339-358.

Priestley, C.H.B. and R.J. Taylor, 1972. On the assessment of surface heat flux and evaporation using large scale parameters. *Monthly Weather Review*, **106**: 81-92.

Roth, M. and T.R. Oke, 1995. Relative efficiences of turbulent transfer of heat, mass, and momentum over a patchy urban surface. *Journal of the Atmospheric Sciences,* **52**: 1863-1874.

Rutter, A.J., 1975. The hydrological cycle in vegetation, pp 123. In: *Vegetation and the atmosphere, I,* ed. J.L. Monteith. Academic Press, Inc., New York.

Sakakibara, Y., 1996. A numerical study of the effect of urban geometry upon the surface energy budget. *Atmospheric Environment,* **30**: 487- 496.

Schmid, H.P., H.A. Cleugh, C.S.B. Grimmond and T.R. Oke, 1991. Spatial variability of energy fluxes in suburban terrain. *Boundary-Layer Meteorology,* **54**: 249-276.

Steyn, D.G., 1985. An objective method to achieve closure over determined surface energy budgets. *Boundary-Layer Meteorology,* 33:303-310.

Stull, R.B., 1988. *An introduction to boundary layer meteorology.* Kluwer Academic Publisher, Dordrecht.

Szeicz, G., G. Enrodi and S. Tajchman, 1969. Aerodynamic and surface factors in evaporation. *Water Resources Research,* **5**: 380-394.

Tanner, B.D. and J.P. Greene, 1989. *Measurement of sensible heat and water vapor fluxes using eddy correlation methods.* Final Report, Campbell Scientific Contract No. DAA09-87-D0038 to U.S. Army Dugway Proving Grounds. Salt Lake City, UT: Campbell Scientific, 17pp.

Tapper, N.J., P.D. Tyson, I.F. Owens and W.J. Hastie, 1981. Modeling the winter urban heat island over Christchurch, New Zealand. *Journal of Applied Meteorology,* **20**:365-376.

Tapper, N.J., 1990. Urban influences on boundary layer temperature and humidity: results from Christchurch, New Zealand. *Atmospheric Environment,* **24**: 19-27.

Tennekes, H., 1982. Similarity relations, scaling laws and spectral dynamics. In: *Atmospheric turbulence and air pollution modelling,* Nieuwstadt and Van Dop, D. Reidel Publisher Co., Dordrecht, Holland, pp 37-64.

Van Ulden, A.P. and A.A.M. Holtslag, 1985. Estimation of atmospheric boundary layer parameters for diffusion applications. *Journal of Climate and Applied Meteorology,* **24**:1196-1207.

Venkatram, A. and J.C. Wyngaard, 1988. *Lectures on air pollution modeling.* A. Venkatram and J.C. Wyngaard, ed. Boston: American Meteor. Soc. (proceedings).

Webb E.K., G.I. Pearmann and R. Leuning, 1980. Correction of flux measurements for density effects due to heat and water vapor transfer. *Quarterly Journal of the Royal Meteorological Society,* **106**: 85- 100.

White, J.M., F.D. Eaton and A.H. Auer, 1978. The net radiation budget of the St Louis metropolitan area. *Journal of Applied Meteorology,* **17**: 593- 599.

Wieringa, J., 1986. Roughness-dependent geographical interpolation of surface wind speed averages. *Quarterly Journal of the Royal Meteorological Society,* **112**: 867- 889.

Yaglom, A.M., 1977. Comments on wind and temperature flux profile relationships. *Boundary-Layer Meteorology,* **11**: 89-102.

Chapter 4.

Oke, T.R., 1978. *Boundary-Layer Climates*. Halsted Press, New York. 372pp.

Owens, I.F. and N.J. Tapper, 1977. The influence of meteorological factors on air pollution occurrence in Christchurch. *Proc. 9th N.Z. Geography Conference, Dunedin, New Zealand, pp. 33-35.*

Stokes, M.J. and P.D. Tyson, 1981. Modelling average winter smoke pollution over the Christchurch urban area. *Weather and Climate*, **1**: 4-13.

Stull, R., 1988. *An introduction to boundary layer meteorology*. Kluwer Academic Publisher, Dordrecht.

Chapter 5.

Arrit, R.W. and R.A. Pielke, 1986. Interactions of nocturnal slope flows with ambient wind. *Boundary-Layer Meteorology*, **37**: 183-195.

Banta, R.M. and P.T. Gannon, 1995. Influence of soil moisture on simulations of katabatic flow. *Theoretical and Applied Climate*, **52**: 85-94.

Gudiksen, P.H., J.M Leone, C.W. King, D. Ruffieux and W.D. Neff, 1992. Measurements and modelling of the effects of ambient meteorology on nocturnal drainage flows. *Journal of Applied Meteorolgy*, **31**: 1023-1032.

Horst, T.W. and J.C. Doran, 1986. Nocturnal drainage flow on simple slopes. *Boundary Layer Meteorology*, **34**: 263-286.

Mahrt, L., 1982. Momentum balance of gravity flows. *Journal of the Atmospheric Sciences*, **39**: 2701-2711.

Manins, P.C. and B.L. Sawford, 1979. A model for katabatic winds. *Journal of the Atmospheric Sciences*, **36**: 619-630.

Mori, M., and T. Kobayashi, 1996. Dynamic interaction between observed nocturnal drainage winds. *Journal of the Meteorological Society of Japan*, **74**: 247-258.

Nappo, C.J. and K.S. Rao, 1987. A model study of pure katabatic flows. *Tellus*, **39A**: 61-71.

Oke, T.R., 1978. *Boundary layer climates*. Halsted Press, New York. 372 pp.

Pielke, R. A., 1984. *Mesoscale meteorological modeling*. Orlando, Florida: Academic Press.

Prandtl, L., 1942. *Fuerhrer durch die Stroemungslehre*. Vieweg Sohn, Brunschweig, 373-375. Translated: Essentials of fluid dynamics. Hafner Publishing Co., New York, 1952.

Rao, K.S and H.F. Snodgrass, 1981. A nonstationary nocturnal drainage flow model. *Boundary-Layer Meteorology*, **20**: 309-320.

Stull, R., 1988. *An introduction to boundary layer meteorology*. Kluwer Academic Publisher, Dordrecht.

Vergeiner, I. and E. Dreiseitl, 1987. Valley winds and slope winds - Observations and elementary thoughts. *Meteorology and Atmospheric Physics*, **36**: 264-286.

Chapter 6.

Banta, R.M., L.D. Olivier, W.D. Neff and D. Ruffieux, 1995. Influence of canyon-induced flows on flow and dispersion over adjacent plains. *Theoretical and Applied Climatology*, **52**: 27-42.

Bossert, J.E. and G.S. Poulos, 1995. A numerical investigation of mechanisms affecting drainage flows in highly complex terrain. *Theoretical and Applied Climatology*, **52**: 119-134.

Canterbury Regional Council, 1997. *Christchurch inventory of home heating and motor vehicle emissions.* Technical Report. Environmental Management Group. Prepared by NIWA, May 1997, Report No. R97/5.

Defant, F., 1951. *Local Winds. Compendium of meteorology*. T.J. Malone, (ed.), American Meteorological Society., pp 655-672.

Dickinson, R.E.,A. Henderson-Sellers, P.J. Kennedy, and M.F. Wilson, 1986. *Biosphere-Atmosphere Transfer Scheme (BATS) for the NCAR Community Climate Model.* NCAR Tech. Note NCAR/TN-275 +STR, National Center for Atmospheric Research, Boulder, CO, 69 pp.

Doran, J.C. and T.W. Horst, 1983. Observations and models of simple nocturnal slope flows. *Journal of the Atmospheric Sciences*, **40**: 708-717.

Doran, J.C., 1991. The effects of ambient winds on valley drainage flows. *Boundary-Layer Meteorology*, **55**: 177-189.

Doran, J.C. and E.D. Skyllingstad, 1992. Multiple-scale terrain forcing of local wind fields. *Monthly Weather Review*, **120**: 817-825.

Gleick, J., 1987. *Chaos: making a new science.* New York, USA, Viking.

Gross, G. and F. Wippermann, 1987. Channeling and countercurrent in the upper Rhine valley: numerical simulations. *Journal of Climate and Applied Meteorology*, **26**: 1293-1304.

Gudiksen, P.H., J.M Leone, C.W. King, D. Ruffieux and W.D. Neff, 1992. Measurements and modelling of the effects of ambient meteorology on nocturnal drainage flows. *Journal of Applied Meteorolgy*, **31**: 1023-1032.

Lorenz, E.N., 1963. The predictability of hydrodynamic flow. *Trans. N.Y. Acad. Sci., series II*, **25**: 409-432.

Louis, J.F., 1979. A parametric model of vertical eddy fluxes in the atmosphere. *Boundary-Layer Meteorology*, **17**: 187-202.

McQueen, J.T., R.R. Draxler and G.D. Rolph, 1995. Influence of grid size and terrain resolution on wind field predictions from an operational mesoscale model. *Journal of Applied Meteorology*, **34**: 2166-2181.

Nappo, C.J., 1991. Sporadic breakdowns of stability in the PBL over simple and complex terrain. *Boundary-Layer Meteorology*, **54**: 69-87.

Paegle, J., R.A. Pielke, G.A. Dalu, W. Miller, J.R. Garratt, T. Vukicevic, G. Berri and M. Nicolini, 1990. Predictability of flows over complex terrain. In: Blumen, W. (ed.). Atmospheric processes over complex terrain. American Meteorological Society, *Meteorological Monographs*, **23**(45), pp. 285-299.

Parker, M.J. and S. Raman, 1993. A case study of the nocturnal boundary layer over a complex terrain. *Boundary Layer Meteorology*, **66**: 303-324.

Pielke, R. A., 1984. *Mesoscale meteorological modeling*. Orlando, Florida: Academic Press.

Stull, R., 1988. *An introduction to boundary layer meteorology*. Kluwer Academic Publisher, Dordrecht.

Tremback, C.J. and R. Kessler, 1985. *A surface temperature and moisture parameterization for use in mesoscale numerical models*. Preprints, 7th Conference on Numerical Weather Prediction, 17-20 June 1985, Montreal, Canada, AMS.

Triantafyllou, A.G., C.G. Helmis, D.N. Asimakopoulos, and A.T. Soilemes, 1995. Boundary layer evolution over a large and broad mountain basin. *Theoretical and Applied Climatology*, **52**: 19-25.

Vergeiner, I. and E. Dreiseitl, 1987. Valley winds and slope winds - Observations and elementary thoughts. *Meteorology and Atmospheric Physics*, **36**: 264-286.

Walko, R.L., C.J. Tremback and R.F.A. Hertenstein, 1995. *RAMS The Regional Atmospheric Modeling System. Version 3b User's Guide.* ASTER Division Mission Research Corporation. P.O. Box 466, Fort Collins, CO 80522.

Wanner, H. and P. Filliger, 1989. Orographic influence on urban climate. *Weather and Climate*, **9**: 22-28.

Whiteman, C.D., 1990. Observations of thermally developed wind systems in mountaneous terrain. In: Blumen, W. (ed.), Atmospheric processes over complex terrain. *American Meteorological Society, Meteorology Monograph*, **23**(45).

Whiteman, C.D. and J.C. Doran, 1993. The relationship between overlying synoptic scale flows and winds within a valley. *Journal of Applied Meteorology*, **32**: 1669-1681.

Whiteman, C.D., T.B. McKee and D.C. Doran, 1996. Boundary layer evolution within a canyonland basin. Part I: Mass, heat, and moisture budgets from observations. *Journal of Applied Meteorology*, **35**: 2145-2161.

Chapter 7.

Bossert, J.E., 1997. An investigation of flow regimes affecting the Mexico City region. *Journal of Applied Meteorology*, **36**: 119-140.

Canterbury Regrional Council, 1997. *Christchurch inventory of home heating and motor vehicle emissions.* Technical Report. Environmental Management Group. Prepared by NIWA, May 1997, Report No. R97/5.

Fast, J.D., B.L. Osteen and R.P. Addis, 1995. Advanced atmospheric modeling for emergency response. *Journal of Applied Meteorology*, **34**: 626-649.

Grossi, P., J.M. Giovannoni, and A.G. Russell, 1996. Intercomparison of meteorological models applied to the Athens area and the effect on photochemical pollutant predictions. *Journal of Applied Meteorology*, **35**: 993-1008.

Hedley, M. and D.L. Singleton, 1997. Evaluation of an air quality simulation of the Lower Fraser Valley – I. Meteorology. *Atmospheric Environment*, **31**: 1605-1615.

Hedley, M. and D.L. Singleton, 1997. Evaluation of an air quality simulation of the Lower Fraser Valley – II. Photochemistry. *Atmospheric Environment*, **31**: 1617-1630.

Jauregui, E., 1988. Local wind and air pollution interaction in the Mexico basin. *Atmosphera*, **1**: 131-140.

Kunz, R. and N. Moussiopoulos, 1995. Simulation of the wind field in Athens using refined boundary conditions. *Atmospheric Environment*, **29**: 3575-3591

Lagouvardos, K., V. Kotroni and G. Kallos, 1996. Exploring the effects of different types of model initialisation: simulation of a severe air-pollution episode in Athens, Greece. *Meteorology Applied*, **3**: 147-155.

Lu, R. and R.P. Turco, 1996. Ozone distributions over the Los Angeles basin - three dimensional simulations with the SMOG model. *Atmospheric Environment*, **30**: 4155-4176.

Lyons, W.A., R.A. Pielke, C.J. Tremback, R.L. Walko, D.A. Moon, and C.S. Keen, 1995a. Modeling impacts of mesoscale vertical motions upon coastal zone air pollution dispersion. *Atmospheric Environment*, **29**: 283-301.

Lyons, W.A., C.J. Tremback and R.A. Pielke, 1995b. Applications of the Regional Atmospheric Modeling System (RAMS) to provide input to photochemical grid models for the Lake Michigan Ozone Study (LMOS). *Journal of Applied Meteorology*, **34**: 1762-1786.

McKendry, I.G., 1989. Numerical simulation of sea breezes over the Auckland region, New Zealand - air quality implications. *Boundary-Layer Meteorology*, **49**: 7-22.

McKendry, I.G. and C.G. Revell, 1991. Mesoscale eddy development over South Auckland - a case study. *Weather and Forecasting*, **7**: 134-142.

McKendry, I.G., 1992. Numerical simulation of seabreeze interactions over the Auckland region, New Zealand. *New Zealand Journal of Geology and Geophysics*, **35**: 9-20.

McKendry, I.G., 1994. Synoptic circulation at Vancouver, British Colombia. *Journal of Applied Meteorology*, **33**: 627-641.

Moussiopoulos, N., P. Sahm and C. Kessler, 1995. Numerical simulation of photochemical smog formation in Athens, Greece - a case study. *Atmospheric Environment*, **29**: 3619-3632.

Moussiopoulos, N., P. Sahm, K. Karatzas, S. Papalexiou, and A. Karagiannidis, 1997. Assessing the impact of the new Athens airport to urban air quality with contemporary air pollution models. *Atmospheric Environment*, **31**: 1497-1511.

Mueller, S.F., A. Song, W.B. Norris, S. Gupta, and R.T. McNider, 1996. Modeling pollutant transport during high-ozone episodes in the southern Appalachian mountains. *Journal of Applied Meteorology*, **35**: 2105-2120.

Perego, S., 1996. *Numerical simulation of local ozone reduction scenarios*. Meteotest, Bern, Switzerland, 18 pp.

Pielke, R. A., 1984. *Mesoscale meteorological modeling*. Orlando, Florida: Academic Press.

Pilinis, C., P. Kassomenos and G. Kallos, 1993. Modeling of photochemical pollution in Athens, Greece. Application of the RAMS-CALGRID modeling system. *Atmospheric Environment*, **27B**: 353-370.

Poulos, G.S. and J.E. Bossert, 1995. An observational and prognostic numerical investigation of complex terrain dispersion. *Journal of Applied Meteorology*, **34**: 650-669.

Poulos, G.S. and R.A. Pielke, 1994. A numerical analysis of Los Angeles Basin pollution transport to the Grand Canyon under stably stratified, southwest flow conditions. *Atmospheric Environment*, **28**: 3329-3357.

Steyn, D.G. and I. McKendry, 1988. Quantitative and qualitative evaluation of a three-dimensional mesoscale numerical model simulation of a sea breeze in complex terrain. *Monthly Weather Review*, **116**: 1914-1926.

Ulrickson, B.L. and C.F. Mass, 1990a. Numerical investigation of mesoscale circulations over the Los Angeles Basin. Part I: a verification study. *Monthly Weather Review*, **118**: 2138-2161.

Ulrickson, B.L. and C.F. Mass, 1990b. Numerical investigation of mesoscale circulations over the Los Angeles Basin. Part II: synoptic influences and pollution transport. *Monthly Weather Review*, 118: 2162-2184

Williams, M.D., M.J. Brown, X. Cruz, G. Sosa and G. Streit, 1995. Development and testing of meteorology and air dispersion models for Mexico City. *Atmospheric Environment*, **29**: 2929-2960.

Chapter 8.

Alapaty, K., J.E. Pleim, S. Raman, D.S. Niyogi and D.W. Byun, 1997. Simulation of atmospheric boundary layer processes using local- and nonlocal-closure schemes. *Journal of Applied Meteorology*, **36**: 214-233.

Mahrt, L., 1996. The bulk aerodynamic formulation over heterogeneous surfaces. *Boundary-Layer Meteorology*, **78**: 87-119.

Appendix A.

Campbell Scientific Inc., 1994. *Eddy correlation system operators manual.* Revision: 8/94.

Meteorological Office 1944. *The measurement of upper winds by means of pilot balloons.* Third ed., London, printed and published by His Majesty's Stationary Office.

McIntosh D.H. and A.S. Thom, 1978. *Essentials of meteorology.* Wykeham Publications Ltd., London, 239pp.

Stull, R., 1988. *An introduction to boundary layer meteorology.* Kluwer Academic Publisher, Dordrecht.

Tanner, B.D. and J.P. Greene, 1989. *Measurement of sensible heat and water vapor fluxes using eddy correlation methods.* Final report, Campbell Scientific contract No. DAA09-87-D-0038 to U.S. Army Dugway Proving Grounds. Salt Lake City, UT: Campbell Scientific, 17pp.

Appendix A

A.1 Calibrations of the Campbell 107 and 207 sensors

The delivered temperature and relative humidity sensors were calibrated, but a re-calibration was conducted after extra lead lengths were added. The calibration temperature range was 0 to 20°C. Since no adjustable climate chamber was available, absolute calibrations were not possible, except for 0°C in melting ice.

The four sensors of the Beckenham tower were calibrated by:

- comparing the data at Beckenham during periods when vertical gradients were likely to be weak: periods were selected when 10 minute averaged 21 m winds exceeded 5 m s^{-1} and the absolute value of net radiation was less than 25 W m^{-2}. The selected data form the *windy / cloudy* data set. The temperature range of the windy/cloudy data set was 3 to 16°C.
- the four Beckenham sensors were positioned outside of the 2nd floor of the Geography building in a shaded area, the shields thermally isolated from a concrete platform. Data were collected during a 24 hour period. This forms the *veranda* data set. The calibration temperature range was 9 to 15°C.
- the sensors without radiation screens have been put in a thermally isolated box in melting ice. This is the *ice* data set.

Linear regression showed that systematic differences in temperature of the four sensors were not temperature dependent over the range 0 to 16°C. The absolute slopes of temperature differences between the sensors as a function of temperature were less than 0.01 (K K^{-1}). These results were most clearly evident in the combined ice-veranda data set, having less scatter than in the windy/cloudy data set (RMSE < 0.15 and > 0.50, respectively). It is therefore concluded that calibration by an offset only is sufficient for the temperature range 0 to 16°C.

All the other temperature sensors from the instrumented towers at Burnside, Ensors Garden and Marshland were calibrated in ice only. Using an offset only, calibrated temperatures of sensor *i* can be given by:

$$T_{i,real} = T_{i,meas} + O_i \qquad \text{(A.1)}$$

where $T_{i,real}$ is the calibrated, $T_{i,meas}$ the measured temperature and O_i the offset value. Table A.1 gives an overview of the offset values. It is obvious from Table A.1 that adding extra lead lengths increased the offset values, even when the 'pigtail' ends were transferred. The calibrations showed that differences in relative humidities were typically within 2% over a range 40 to 95%.

Table A.1 Offset values of the temperature sensors used at the instrumented towers during the 1995 winter measurements. *: extra lead length added.

Tower location	Sensor height (m)	Offset (K)	Remarks
Burnside	21	-0.84	*
	12	-1.68	*
	6	0.01	
	3	0.00	
Beckenham	21	-0.93	*
	12	-1.73	*
	6	0.17	
	3	-0.05	
Ensors	10	-0.38	*
	5	-0.03	
Marshland	10	-0.40	*
	5	0.12	

A.2 Calibration of the Vector Instruments A101ML anemometers

The anemometers were calibrated before delivery and they were partly re-calibrated in the wind tunnel at the School of Engineering at the University of Canterbury. Both calibrations appeared to produce similar results.

Calibration details. Since all the individual A101ML sensors have the same non linearity factor with respect to their rotation speed, a linear individual calibration factor for each sensor and a universal (non linear) correction factor are sufficient to provide wind speeds from the measured pulse output. The manufacturer provided a table of the universal correction factor, being defined as unity at 425 rpm (revolutions per minute) when the wind speed is about 9 m s^{-1}. The correction ranges from 0 to 10% at windspeeds from 1.0 m s^{-1} to over 32.0 m s^{-1}. However, at windspeeds below 1.0 m s^{-1} the correction can be up to 500%, due to the relative importance of rotational friction of the anemometer, although the absolute correction (in m s^{-1}) at these wind speeds is small. The A101ML shows a non linear response to windspeed, which is given by:

$$V = a_{ane} \frac{\Omega_{ane}}{60} \frac{1}{F_{cor}} \qquad \text{(A.2)}$$

where V is the wind speed (m s^{-1}), a_{ane} the individual calibration factor of an anemometer (m revolution^{-1}), Ω_{ane} the rotation speed (revolution per minute) and F_{cor} the correction factor (1), which is a function of the rotation speed only. The error of the correction factor is within 0.1%, according to Vector Instruments. Equation (A.2) does not provide a threshold wind speed for the individual anemometers, nor were they obtained by calibrations in the wind tunnel more accurately than ±0.10 m s^{-1}. In practical terms, the threshold has been set at 0 m s^{-1}, the axis rotation friction being considered implicit in the correction factor F_{cor}. Since pulse frequencies are measured, it would be convenient to replace Ω_{ane}. Using

$$\frac{f}{n_w} = \frac{\Omega_{ane}}{60} \tag{A.3}$$

with the f the pulse frequency (s^{-1})and n_w the number of pulses per axis rotation (revolution^{-1}), equation (A.2) becomes:

$$V = a_{ane} \frac{f}{n_w} \frac{1}{F_{cor}} \tag{A.4}$$

The calibration data are provided by Vector Instruments as

$$R = \frac{60}{a_{ane}} \tag{A.5}$$

with R in rounds per minute per m s^{-1}. The calibration factors of the anemometers which were used at the instrumented towers and the mobile stations, are given in Table A.2. All the anemometers were calibrated before the measurement programme, but two instruments were re-calibrated afterwards as well to check the reliability of the calibration factors. It appeared that the calibration factors of the anemometers were hardly affected by time, with all the anemometers having a calibration factor close to 10 pulses per 1 m s^{-1} wind speed.

Table A.2 Calibration factor a_{ane}/n_w for the A101ML anemometers being used in 1995. Cups: serial number of rotor; Anemometer: serial number of anemometer; re-calib.: re-calibrated *after* measurements.

Cups	Anemometer	a_{ane}/n_w	n_w	Location	Height (m)
SH1	4240	0.1001	13	Burnside	20.9
SH1	4240	0.1004	13	re-calib.	-
SH0	4239	0.1001	13	Burnside	12.1
SG5	4234	0.1009	13	Burnside	6.1
SG7	4236	0.1008	13	Beckenham	20.9
SG9	4238	0.1003	13	Beckenham	12.1
SG3	4232	0.1010	13	Beckenham	6.1
SG6	4235	0.1008	13	Ensors	10.3
SG8	4237	0.1006	13	Marshland	10.3
SG8	4237	0.1009	13	re-calib.	-
SG4	4233	0.1008	13	Marshland	5.0
63E	3398	0.1024	10	Mob1	2.5
9X9	2107	0.1024	10	Mob2	2.5

A.3 REBS Q*7.1 net radiometer correction for wind effects

The manufacturer provides an empirical correction formula for wind effects:

$$Rn_{cor} = C_{cor}\, Rn_{meas} \tag{A.6}$$

with Rn_{cor} and Rn_{meas} the corrected and measured net radiation (W m^{-2}) respectively, and C_{cor} the correction factor, which is described by:

$$C_{cor} = 1 + 0.059(1 - 2.8^{-u}) + \frac{0.0096u}{0.216 + u^3} \tag{A.7}$$

for positive net radiation and

$$C_{cor} = 0.99 + 0.021(1 - 1.45^{-u}) + \frac{2^{-7u}}{100} \tag{A.8}$$

for negative net radiation values, with u the wind speed (m s^{-1}).

The accuracy of the net radiometers is not provided by the manufacturer. The sensors were calibrated before the 1995 field campaign. The sensors are supposed to remain stable for long periods, requiring only annual checks. At 8 and 9 April three REBS Q*7.1 net radiometers were mounted alongside each other near the Horotane Valley in Christchurch. During this period the net radiation varied from -35 to 150 W m^{-2}. On average the three sensors differed only 0.2 W m^{-2}, with maximum differences being less than 1.2 Wm^{-2} over 15 minute intervals.

Calibration details. The net radiation Rn_{meas} of the Q*7.1 instruments was obtained by using the multipliers of 9.42 W m^{-2} mV^{-1} for positive net radiation and 11.89 W m^{-2} mV^{-1} for negative radiation at Burnside, and 9.44 and 12.01 W m^{-2} mV^{-1} at Beckenham, respectively.

A.4 Derivation of heat fluxes and corrections

A.4.1 Introduction

Vertical transport of energy by means of sensible and latent heat fluxes can be directly measured by recording the covariances of vertical wind speed with temperature and humidity (Stull, 1988):

$$H = \rho\, c_p \overline{w' T'} \tag{A.9}$$

and

$$LE = \rho\, L_v \overline{w' q'} \tag{A.10}$$

where H and LE are the sensible and latent heat fluxes, respectively, ρ is the air density, c_p the heat capacity of air at constant pressure, w is the vertical windspeed, T the air temperature, L_v the latent heat of vaporation, q the specific humidy of the air, ' denotes the temporal perturbation and the overbar the time average. A similar approach can also be followed for (vertical) fluxes of momentum and trace gases.

The heat fluxes obtained by the EC method, using equations (A.9) and (A.10) respectively, have to be corrected for air density fluctuations and atmospheric oxygen. A derivation of the applied correction procedures is given below.

A.4.2 Correction procedures

Correction for air density. During the measurements the density of air and the heat capacity of air were taken as constant (ρ_o = 1.2 kg m^{-3}; $c_{p,o}$ = 1004.67 J kg^{-1} K^{-1}), so that the uncorrected sensible heat flux H_o yields:

$$H_o = \rho_o\, c_{p,o} \overline{w' T'} \tag{A.11}$$

The density of moist air can be rewritten as:

$$\rho = \rho_a + \rho_v \tag{A.12}$$

where ρ_a and ρ_v are the densities of dry air and water vapour, respectively. Using the gas law (McIntosh and Thom, 1978; Stull, 1988):

$$\rho_a = \frac{(P - e)}{R_a T} \tag{A.13}$$

and

$$\rho_a = \frac{e}{R_v T} \tag{A.14}$$

where P is the air pressure, e the vapour pressure, R_a and R_v the gas constants for dry air and water vapour (287.04 J kg^{-1} K^{-1}, 461.5 J kg^{-1} K^{-1}) respectively, and T the air temperature (K). The vapour pressure can be derived from relative humidity (RH) values:

$$e = RH.e_s \tag{A.15}$$

with e_s the saturated vapour pressure, which can be approximated by (Stull, 1988):

$$e_s = 6.112\exp(17.67(T - 273.16) / (T - 29.66)) \tag{A.16}$$

with T the absolute air temperature (K) and e_s in hPa. The actual heat capacity at constant pressure is slightly dependent on the water vapour content of the air (Stull, 1988):

$$c_p = c_{p,d}(1 + 0.84q) \tag{A.17}$$

with $c_{p,d}$ the heat capacity at constant pressure for dry air (=1004.7 J kg^{-1} K^{-1}) and the specific humidity (kg kg^{-1}), given by:

$$q = \frac{\varepsilon e}{P - (1-\varepsilon)e} \approx \varepsilon\frac{e}{P} \tag{A.18}$$

with $\varepsilon = 0.622$, being the ratio of molecular weight of water and dry air (18/29). However, the variation in the heat capacity of air at constant pressure is typically less than 0.1% and is therefore neglected.

So, substituting equations (A.12), (A.13) and (A.14) into equation (A.11), the corrected sensible heat flux H_{cor} yields:

$$H_{cor} = H_o\frac{\rho}{\rho_o} = H_o\left(\frac{P-e}{R_aT} + \frac{e}{R_vT}\right)\frac{1}{\rho_o} \tag{A.19}$$

It is easily shown, that the correction procedure proposed by equation (A.19) can be as large as 3 to 8% within a temperature range from 0 to 20°C.

Correction for oxygen. The latent heat flux obtained by the EC method has to be corrected for atmospheric oxygen, but also for changes of the latent heat of vaporation L_v. Initially, during the observations the latent heat of vaporation was taken as constant ($L_{v,o}$ = 2.47*10^6 J kg^{-1}). However, a temperature dependency exists, which can be approximated by (Stull, 1988):

$$L_v \gg (2.501 - 0.00237(T - 273.16)).10^6 \tag{A.20}$$

with T the temperature (K). In the temperature range 0 to 20°C the latent heat of vaporation L_v varies about 2%. During the operation period of the eddy correlation period no significant frosts occurred and so the latent heat of sublimation did not need to be introduced. Using the specific humidity q (kg water vapour per kg humid air)

$$q = \frac{\rho_v}{\rho} \tag{A.21}$$

and substituting into equation (A.10), the uncorrected latent heat flux LE_o can be given by:

$$LE_o = L_{v,o}\overline{w'\rho_v'} \tag{A.22}$$

The KH20 hygrometer emits a major wave at 123.58 nm, which is absorbed by both water vapour and atmospheric oxygen. Neglecting the minor wave at 116.49 nm, the signal voltage V_h of the hygrometer can be given by (Campbell Manual, 1994):

$$V_h = V_o \exp(-xk_w\rho_v).\exp(-xk_{O2}\rho_{O2}) \tag{A.23}$$

where V_o is the signal with no absorption, x the path length of the hygrometer (0.01431 m), k_w the absorption coefficient for water vapour ($15.2*10^3$ m^2 kg^{-1}), being the value valid for a low vapour density range, k_{O2} the absorption coefficient for atmospheric oxygen ($0.85*10^3$ m^2 kg^{-1}, Tanner and Greene, 1989; Spronken-Smith, personnel communication, 1995) and ρ_v is the density of atmospheric oxygen. Solving equation (A.23) for ρ_v yields:

$$\rho_v = -\frac{\ln(V_h)}{xk_w} + \frac{\ln(V_o)}{xk_w} - \frac{k_{O2}}{k_w}.\overline{w'\rho_{O2}'} \tag{A.24}$$

The covariance between the vertical windspeed deviations and vapour density fluctuations can be derived from equation (A.24):

$$\overline{w'\rho_v'} = -\frac{\overline{w'\ln(V_h)'}}{xk_w} - \frac{k_{O2}}{k_w}\overline{w'\rho_{O2}'} \tag{A.25}$$

The density of atmospheric oxygen can be found by using the ideal gas law:

$$\rho_{O2} = \frac{C_{O2}PM_{O2}}{RT} \tag{A.26}$$

with C_{O2} the concentration of atmospheric oxygen (≈20.95%), M_{O2} the molecular weight of O_2 (32.0 kg kmol^{-1}) and R the universal gas constant ($8.314*10^3$ J kmol^{-1} K^{-1}). Fluctuations of oxygen density due to pressure and temperature fluctuations can be found by differentiating equation (A.26):

$$\rho_{O2}' = \left(\frac{C_{O2}M_{O2}}{RT}\right)P' - \left(\frac{C_{O2}M_{O2}}{RT^2}\right)T' \tag{A.27}$$

Since pressure fluctuations are small during flux averaging periods the first term to the right of the equal sign can be neglected. Substituting equations (A.22) and (A.27) into equation (A.25) yields:

$$LE_o = L_{v,o}\left(-\frac{\overline{w'\ln(V_h)'}}{xk_w} + \frac{k_{O2}}{k_w}\frac{C_{O2}M_{O2}P}{RT} * \overline{w'T'}\right) \tag{A.28}$$

The datalogger provided the averaged covariance of $w'V_h'$, not the averaged covariance $w'\ln(V_h)'$. However, using Taylor's expansion, f(x)=f(a)+f'(a).(x - a) + h.o.t., with f( ) = ln( ), x - a=V_h and a is the average V_h, the following approximation can be derived:

$$\overline{w'\ln(V_h)'} = \frac{1}{\overline{V_h}}\overline{w'V_h'} \tag{A.29}$$

Substituting equations (A.20), (A.22), and (A.29) into equation (A.28) provides the latent heat flux, LE_{cor}, corrected for L_v variations and atmospheric oxygen:

$$LE_{cor} = L_v\left(-\frac{\overline{w'V_h'}}{\overline{V_h}xk_w} + \frac{k_{O2}}{k_w}\frac{C_{O2}M_{O2}P}{RT^2} * \overline{w'T}\right) \tag{A.30}$$

A.4.3 Calibration details

The sensors were calibrated at delivery:

- Sonic anemometer CA27: 1V per m s^{-1}.
- Thermocouple: 0.25V K^{-1}
- Krypton hygrometer: x=0.01431 m
  k_w = -14.2 m^3 kg^{-1} m^{-1}, with vapour range 1.74 to 19.20 g m^{-3} ,
  k_w = -15.2 m^3 kg^{-1} m^{-1}, with vapour range 1.74 to 9.11 g m^{-3} ,
  k_w = -13.8 m^3 kg^{-1} m^{-1}, with vapour range 8.05 to 19.20 g m^{-3}

According to equation (A.30), LE is directly proportional to $1/k_w$, which can show a slow drift due to ambient water vapour concentrations.

A.5 A correction procedure for blimp flight pressure deviation

During the majority of blimp flights the pressure sensor of the sonde showed a 'hysteresis effect': a reluctance to change pressure values. It has been observed that the pressure after a descent was generally lower than just before the ascent of the same flight. When profiles from raw input data are plotted, a distorted picture results, because features of the boundary layer at the displayed heights (derived from pressure data) from ascent and descent do not relate properly to each other. A simple method to correct this distortion has been applied: the data from the descent are 'stretched' out from the lowest pressure level to the pressure level at the surface, as measured at the start of the ascent.

Let us define P_{min} the minimum pressure observed during the flight, P_a and P_d the pressure during the ascent and descent, respectively, while $P_a(0)$ and $P_d(0)$ are the pressures at the surface (z=0) at the start and end of a flight, respectively. The corrected pressure during the descent $P_{d,cor}$ obtained by means of 'stretching' is given by:

$$P_{d,cor} = P_{min} + (P_d - P_{min})\frac{P_a(0) - P_{min}}{P_d(0) - P_{min}} \tag{A.31}$$

resulting in:

$$P_{d,cor}(z) = P_a(z) \qquad \text{(A.32)}$$

The height z (m) of the sonde is derived by:

$$z = R\overline{T}/g.\ln(P_a(0)/P(z)) \qquad \text{(A.33)}$$

R = 287 J kg^{-1} K^{-1}, g the gravitation force, $\overline{T}$ the temperature over the whole layer, neglecting variations with height and P(z) the pressure, the (uncorrected) ascent pressure or the corrected descent pressure, P_a or $P_{d,cor}$, respectively.

The 'stretching' method is based on the following assumptions:

- Hysteresis effect occurs only during the descent, so P_{min} is correct
- $P_a(0)$ and P_a are correct
- Hysteresis effect behaves in a progressive linear manner.

At this stage we are unsure to what extent these assumptions are met. In order to quantify the success of the 'stretching' method, a statistical method has been applied. The scatter of points along a moving average profile has been calculated for temperature, dew point, wind speed and wind direction. A reduction in scatter is expected when the boundary layer features observed during the ascent and descent match at comparable heights. The analysis shows that scatter on average was reduced by the 'stretching' method.

A.6 Pilot ballooning

The nearly constant ascent rate of a pilot balloon, being inflated with hydrogen gas or helium, can be described by empirical equations. An empirical equation is given by Meteorological Office (1944), converted to SI units:

$$w_{pilot} = 265\frac{\sqrt{L_{pilot} - A}}{\sqrt[3]{L_{pilot} + B_{pilot}}} \qquad \text{(A.34)}$$

where w_{pilot} is the ascent rate (m s^{-1}), L_{pilot} the lift of the inflated pilot balloon (kg), A is the weight of possible attachments and B is the weight of the balloon itself. During our project we used standard 0.020 kg balloons. Another relationship can be derived where size and aerodynamic drag of the balloon ($\rho.C_d.\pi.d^2/4$) are taken into account:

$$w_{pilot} = \sqrt{\frac{8g(L_{pilot} - B_{pilot} - A)}{\rho\, C_d \pi\, d_{pilot}^2}} \qquad \text{(A.35)}$$

where g is the gravitational force, ρ the density of the ambient air, $C_{d,pilot}$ the drag coefficient of the pilot balloon ($\approx$0.65) and d_{pilot} the diameter of the inflated pilot balloon.

Appendix B

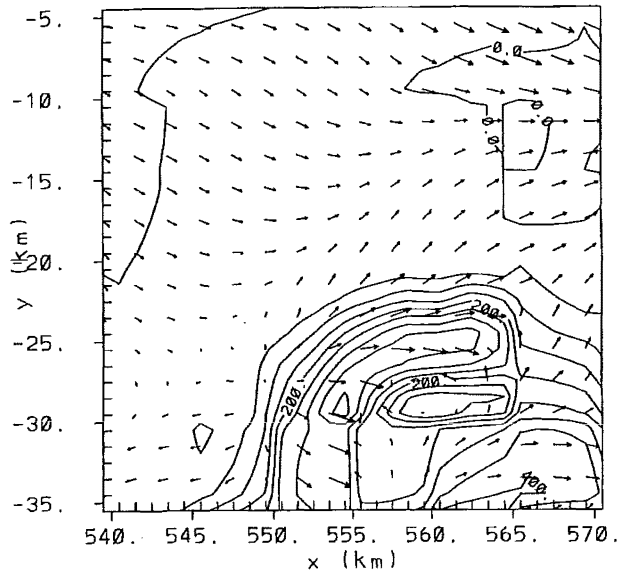

Figure B.1a Vector plot in grid 4 generated by N405W at 12m after 6 hours simulation at 9 UTC. Contour lines display geopotential height (m) and maximum wind speed shown is 5.5 m s^{-1} (See Chapter 6 for details).

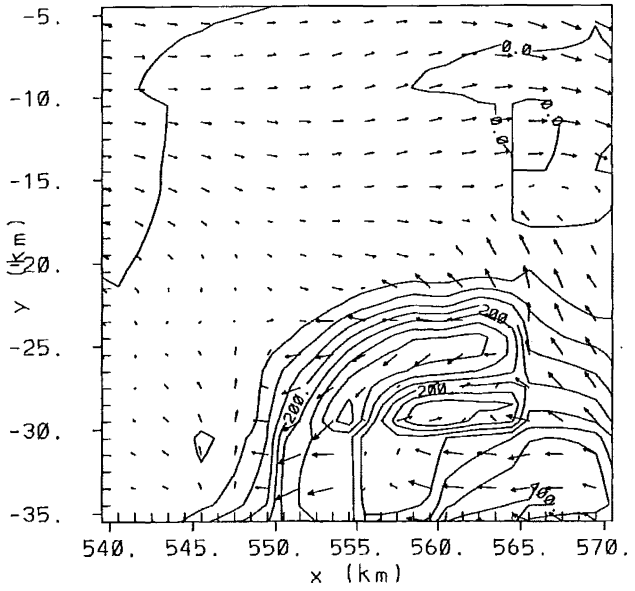

Figure B.1b Vector plot in grid 4 generated by N405N at 12m after 6 hours simulation at 9 UTC. Contour lines display geopotential height (m) and maximum wind speed shown is 4.4 m s^{-1}. (See Chapter 6 for details).

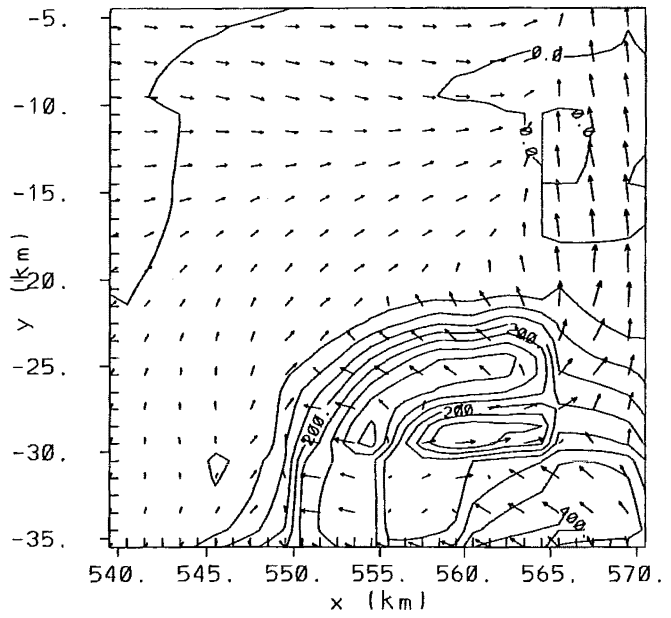

Figure B.1c Vector plot in grid 4 generated by N405E at 12m after 6 hours simulation at 9 UTC. Contour lines display geopotential height (m) and maximum wind speed shown is 5.8 m s^{-1}. (See Chapter 6 for details).

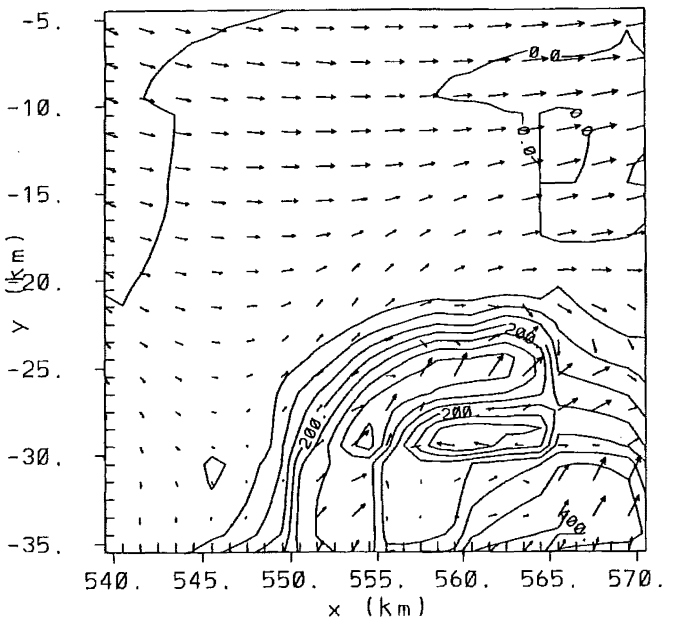

Figure B.1d Vector plot in grid 4 generated by N405S at 12m after 6 hours simulation at 9 UTC. Contour lines display geopotential height (m) and maximum wind speed shown is 4.4 m s^{-1}. (See Chapter 6 for details).

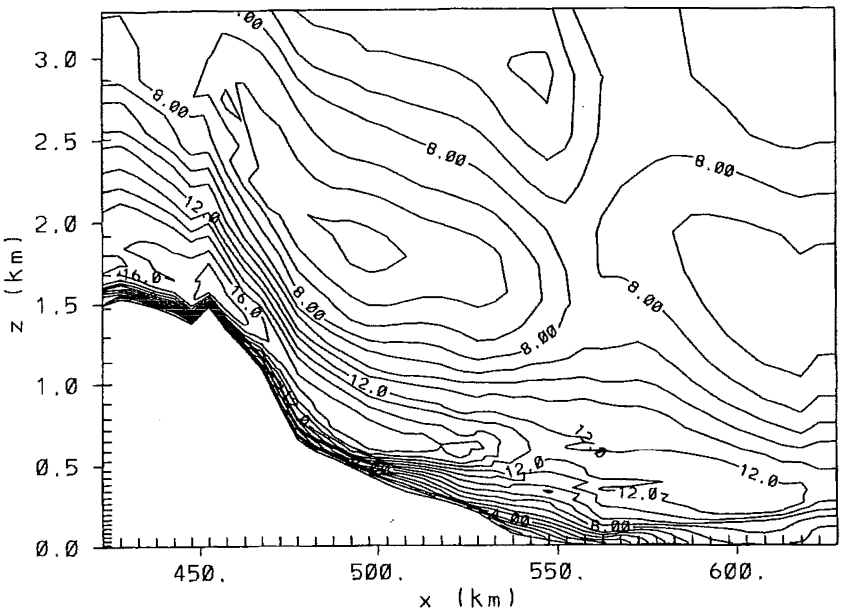

Figure B.2a East-west cross section in grid 3 generated by N405W after 9 hours of simulation at 12 UTC (midnight local time) showing contours of the x-component of wind velocity (u) (m s^{-1}) with Christchurch between x=565 and x=585 (see Chapter 6 for details).

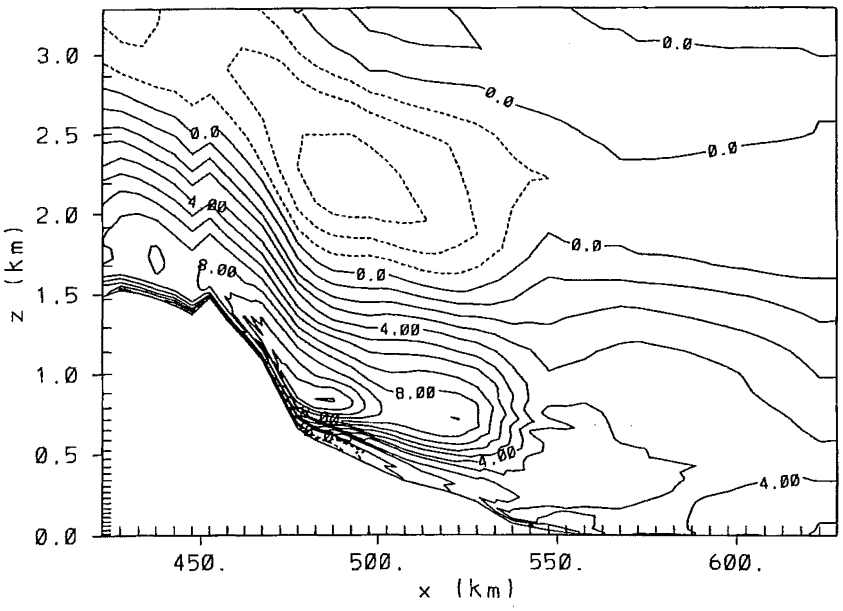

Figure B.2b East-west cross section in grid 3 generated by N405N after 9 hours of simulation at 12 UTC (midnight local time) showing contours of the x-component of wind velocity (u) (m s^{-1}) with Christchurch between x=565 and x=585 (see Chapter 6 for details).

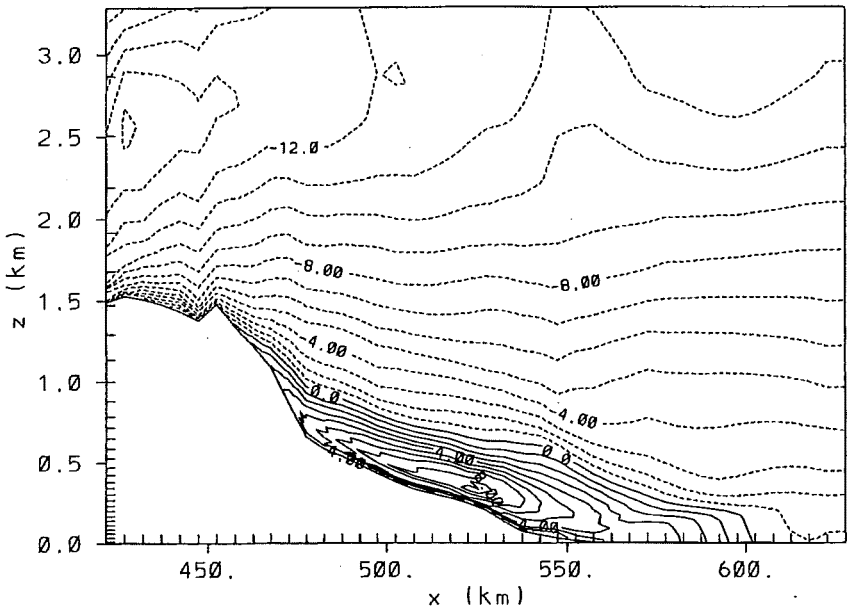

Figure B.2c East-west cross section in grid 3 generated by N405E after 9 hours of simulation at 12 UTC (midnight local time) showing contours of the x-component of wind velocity (u) (m s^{-1}) with Christchurch between x=565 and x=585 (see Chapter 6 for details).

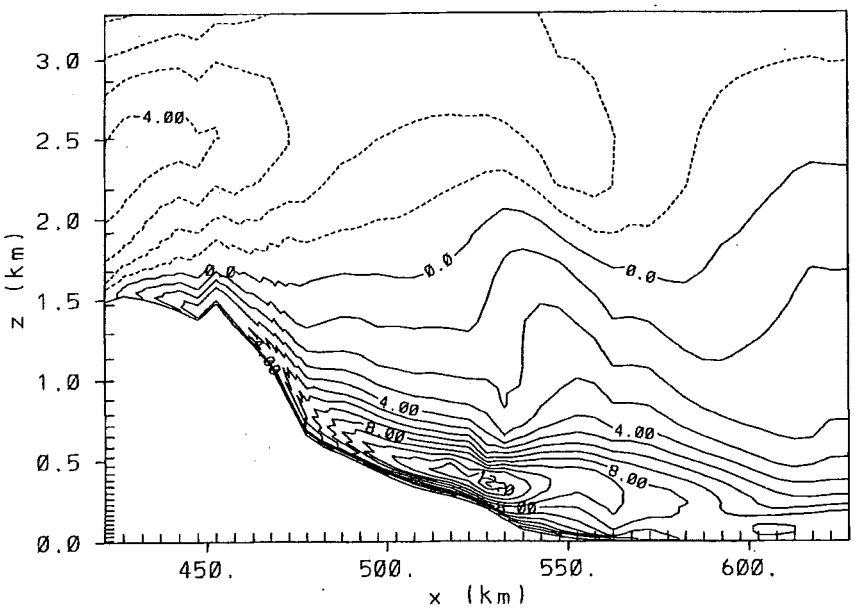

Figure B.2d East-west cross section in grid 3 generated by N405S after 9 hours of simulation at 12 UTC (midnight local time) showing contours of the x-component of wind velocity (u) (m s^{-1}) with Christchurch between x=565 and x=585 (see Chapter 6 for details).

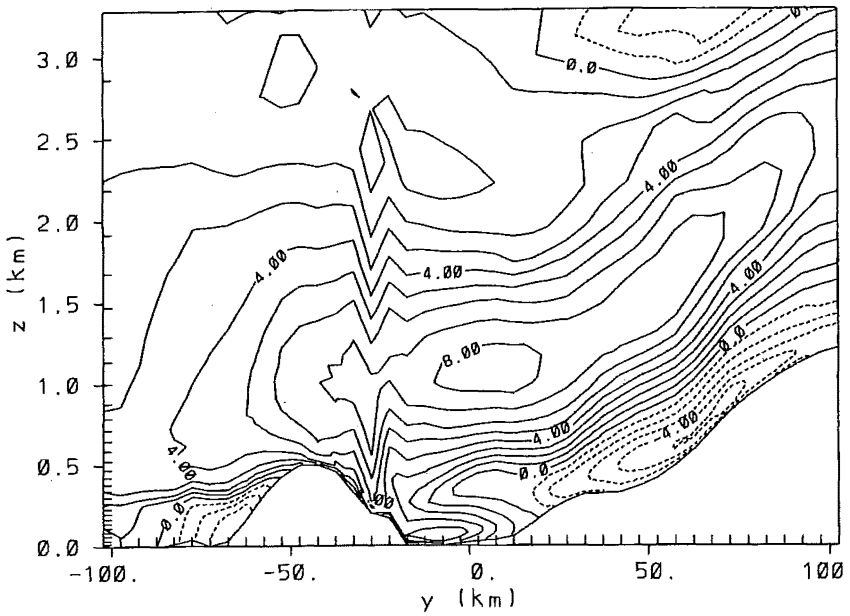

Figure B.3a North-south cross section in grid 3 generated by N405W after 9 hours of simulation at 12 UTC (midnight local time) showing contours of the y-component of wind velocity (v) (m s^{-1}) with Christchurch between y= -20 and y=0 (see Chapter 6 for details).

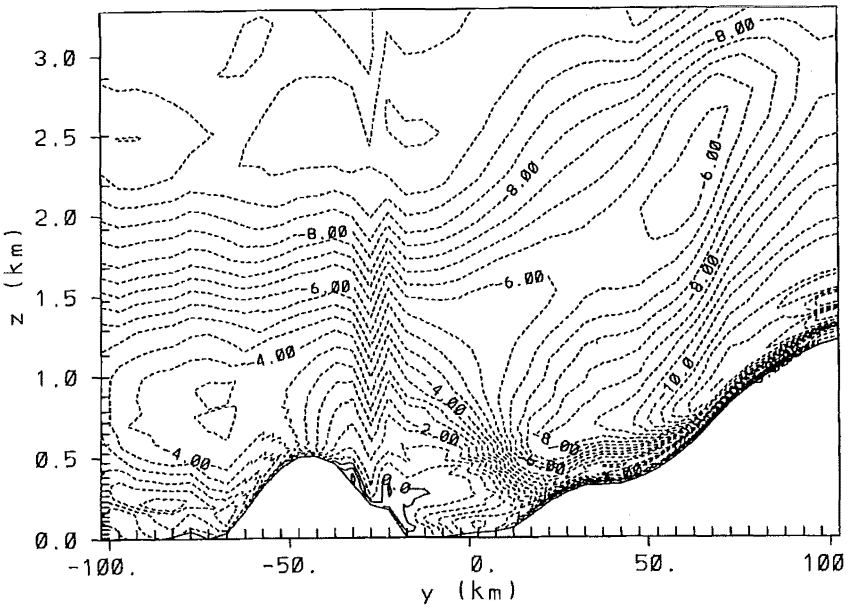

Figure B.3b North-south cross section in grid 3 generated by N405N after 9 hours of simulation at 12 UTC (midnight local time) showing contours of the y-component of wind velocity (v) (m s^{-1}) with Christchurch between y= -20 and y=0 (see Chapter 6 for details).

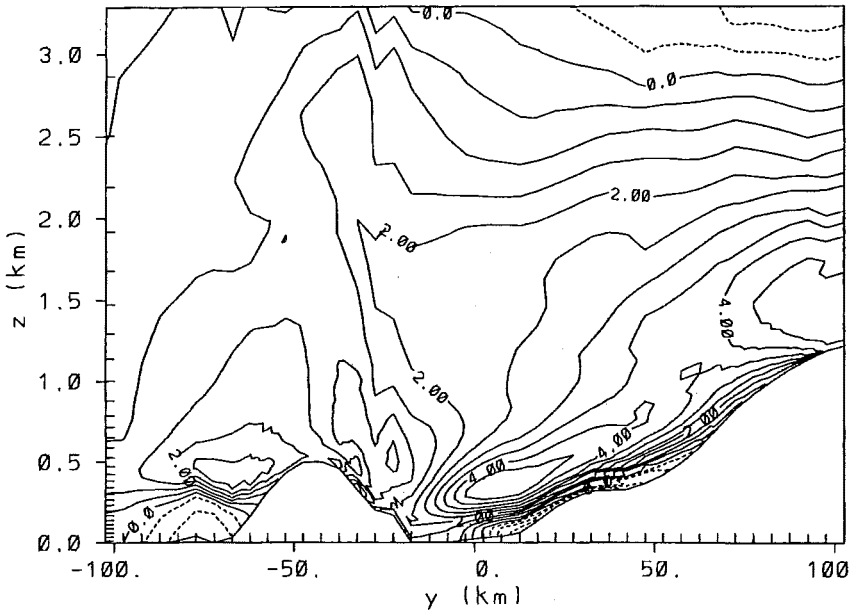

Figure B.3c North-south cross section in grid 3 generated by N405E after 9 hours of simulation at 12 UTC (midnight local time) showing contours of the y-component of wind velocity (v) (m s^{-1}) with Christchurch between y= -20 and y=0 (see Chapter 6 for details).

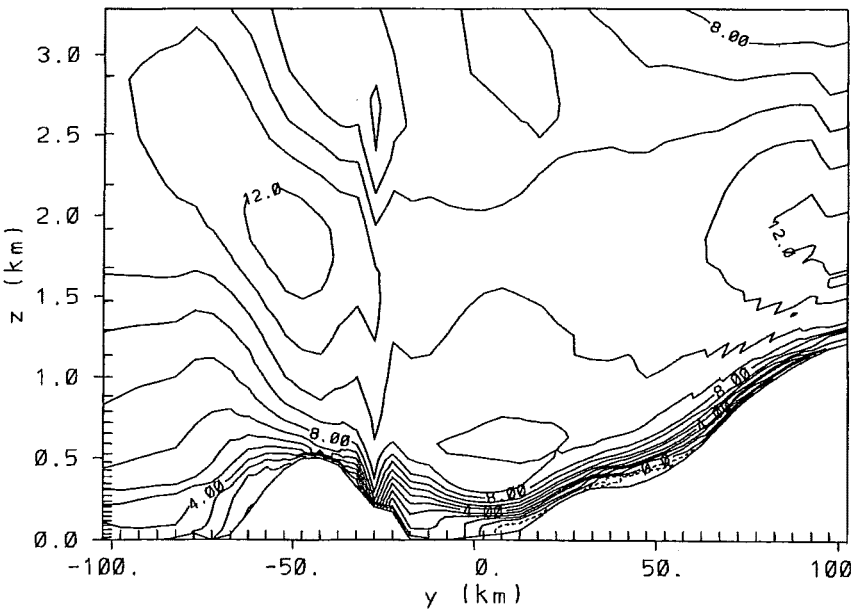

Figure B.3d North-south cross section in grid 3 generated by N405S after 9 hours of simulation at 12 UTC (midnight local time) showing contours of the y-component of wind velocity (v) (m s^{-1}) with Christchurch between y= -20 and y=0 (see Chapter 6 for details).

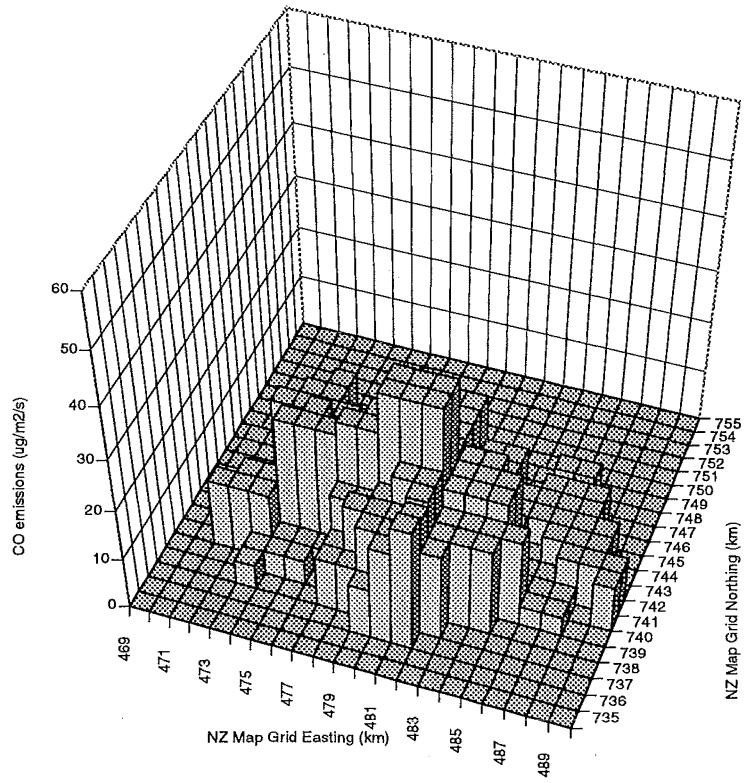

Figure B.4a Average estimated CO emissions in Christchurch from 6 am to 10 am local time, according to emissions inventory by Canterbury Regional Council (1997).

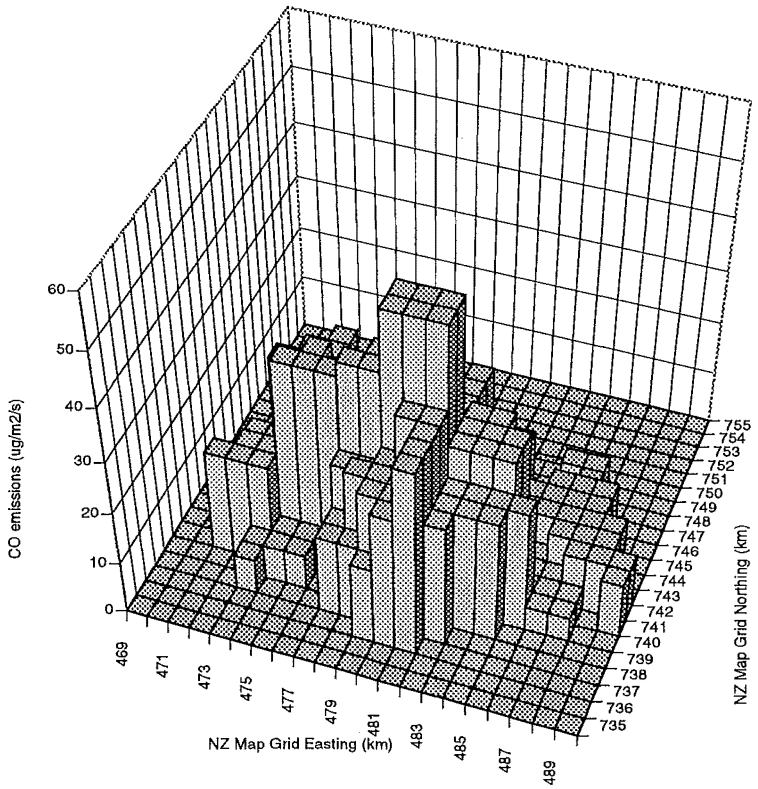

Figure B.4b Average estimated CO emissions in Christchurch from 10 am to 4 pm local time, according to emissions inventory by Canterbury Regional Council (1997).

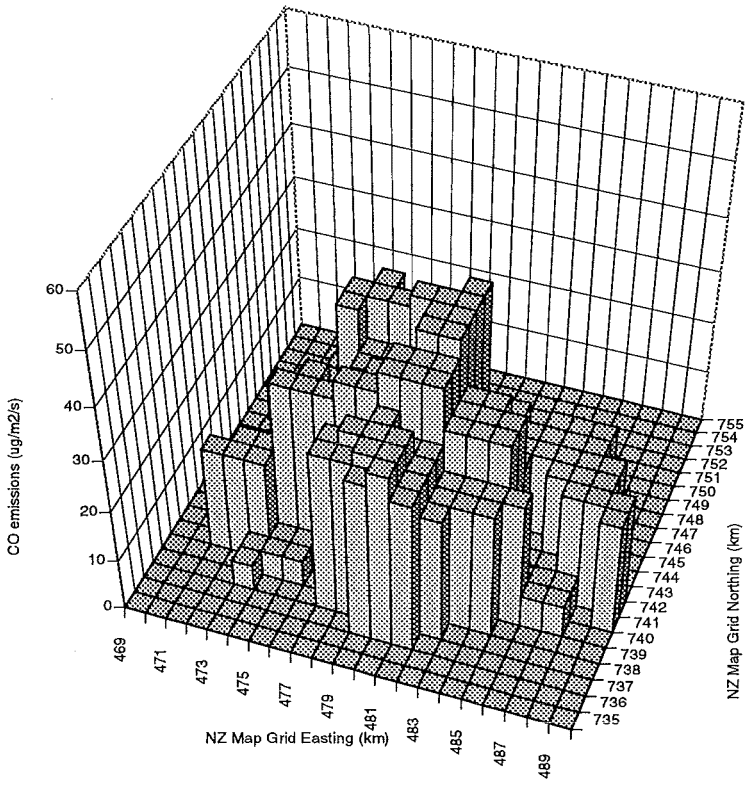

Figure B.4c Average estimated CO emissions in Christchurch from 4 pm to 10 pm local time, according to emissions inventory by Canterbury Regional Council (1997).

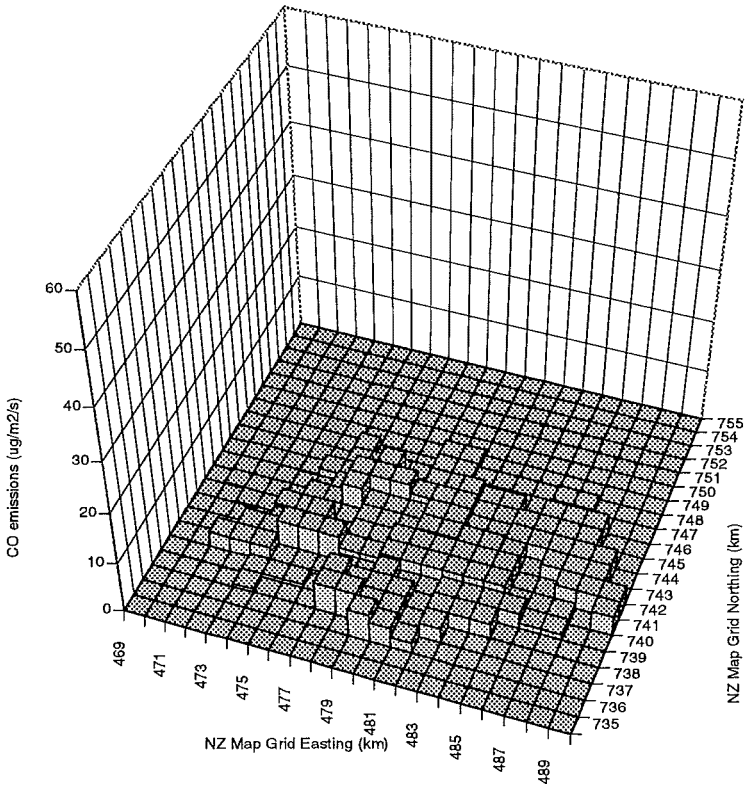

Figure B.4d Average estimated CO emissions in Christchurch from 10 pm to 6 am local time, according to emissions inventory by Canterbury Regional Council (1997).

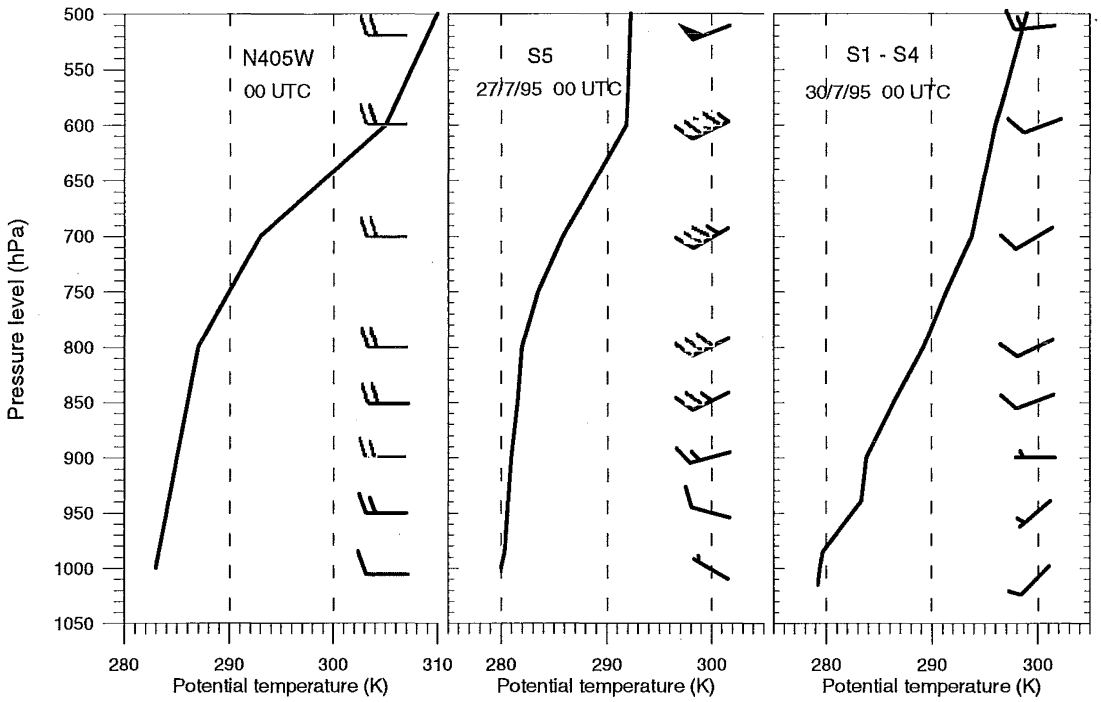

Figure B.5 Vertical profiles used to initilize simulations by N405W (left), case C2728 (centre) and case C3031 (right).